MOLECULAR AND CELLULAR FUNCTIONS OF THE ALTERNATIVELY SPLICED ISOFORMS OF GDNF RECEPTOR COMPLEX IN NEURONAL DIFFERENTIATION

ZHOU LIHAN

B.Sc. (Hons.), NUS

A THESIS SUBMITTED

FOR THE DEGREE OF DOCTOR OF PHILOSOPHY

DEPARTMENT OF BIOCHEMISTRY

NATIONAL UNIVERSITY OF SINGAPORE

2012

DECLARATION

I hereby declare that this thesis is my original work and it has been written by me in its entirety. I have duly acknowledged all the sources of information which have been used in the thesis.

This thesis has also not been submitted for any degree in any university previously.

ZHOU LIHAN

3 Dec 2012

ACKNOWLEDGEMENT

"Tell me and I forget, teach me and I may remember, involve me and I learn."

— Benjamin Franklin

Neither this thesis, nor the man I am today, would be possible without the heroic effort of Professor Too Heng-Phon, whose philosophy of mentoring is a true embodiment of the quote. Professor Too never fails to captivate, inspire and involve his students in the pursuit of scientific excellence. Working alongside with him on the bench is one of the most daunting tasks any fresh graduate can face, but also a routine one would dearly miss when leaving his lab. Professor Too and his philosophy is truly the reason that I, and the many before me, continue to pursue the fun and challenges in the arena of science.

I am also blessed to have Professor Tang Bor Luen and Professor Low Chian Ming as my thesis advisors. Special thanks for Professor Tang Bor Luen, who has been a wonderful advisor since my undergraduate days.

It was my privilege to have worked with so many dynamic and intelligent lab members over the years. My heartfelt gratitude to Dr Yoong Li Foong and Dr Wan Guoqiang, whose constant assistance and assurance helped me to survive, grow and excel in the lab. Special thanks to Zou Ruiyang and Sarah Ho Yoon Khei for being such wonderful colleagues in our pursuit of the microRNA dream. I am also grateful to Jeremy Lim Qing' En, Dr Zhou Kang, Sha Lanjie, Seow Kok Huei, Simon Zhang Congqiang, Chen Xixian, Cheng He, Wong Long Hui and Chin Meiyi for all the stimulating discussions, fun and laughter throughout the years.

This thesis, is dedicated to my parents, grandparents and my wife, who tolerated my years of absence from their lives, and supported me with unrelenting kindness, understanding and love. You are truly the safe harbour a man can ever wish for.

"For every fact there is an infinity of hypotheses."

— Robert M. Pirsig

I would also like to dedicate this thesis to those who find inspiration and use in its findings and analyses. It has been a truly enjoyable and rewarding experience making the observations, generating the hypotheses and uncovering the evidences. It is my greatest hope that these will be useful in spurring even more thoughts and hypotheses.

Table of Contents

Summary

The glial cell line-derived neurotrophic factor (GDNF) and Neurturin (NTN) are members of the GDNF family of ligands (GFLs) which have been shown to support the growth, maintenance and differentiation of both central and peripheral nervous systems. Clinical trials evaluating GDNF and NTN based gene therapy for Parkinson's disease are currently underway. These GFLs transduce signal through a multi-component receptor complex consisting of GPI anchored GDNF family receptor alpha (GFRα) and trans-membrane co-receptors RET (RE arranged during Transformation) and/or neural cell adhesion molecule (NCAM). GFRα1 and GFRα2 have been identified as the preferred receptor of GDNF and NTN respectively. Mice lacking GFRα1 and GFRα2 signaling were found to suffer from deficits in various neuronal systems, supporting the physiological role of these receptors in neuronal functions. Alternative splicing of GFRα, and RET pre-mRNA yields multiple receptor isoforms which are widely and differentially expressed in the nervous system. Our earlier work has shown that these receptor isoforms have distinct biochemical and neuritogenic functions. This thesis details the discoveries of distinct signaling pathways involved in the activation of specific proteins, mRNAs and miRNAs through combinatorial interactions of GFLs, GFRα and RET receptor isoforms and provides novel insights into the diverse functions of GFL systems.

In a widely established neuronal model PC12 cells, NTN activation of GFRα2a and GFRα2c but not GFRα2b induced biphasic ERK1/2 activation, phosphorylation of the major cAMP target CREB and neurite outgrowth. Interestingly, cAMP agonists were able to cooperate with GFRα2b to induce neurite outgrowth whereas antagonists of cAMP signaling significantly impaired GFRα2a and GFRα2c-mediated neurite outgrowth. More specifically, cAMP effector PKA but not Epac was found to mediate NTN-induced neurite outgrowth, through transcription and translation-

dependent activation of late phase ERK1/2. These results not only demonstrated the essential role of cAMP-PKA signaling in NTN-induced biphasic ERK1/2 activation and neurite outgrowth, but also suggested cAMP-PKA signaling as an underlying mechanism contributing to the differential neuritogenic activities of GFRα2 isoforms (Chapter 3).

In a separate study, we made the novel observation that NTN induced serine^{727} phosphorylation of STAT3, a classic transcription factor. Intriguingly, STAT3 phosphorylation was found to be mediated specifically by receptor isoform GFRα2c and RET9, but not the others (Chapter 4). Unexpectedly, NTN induced P-Ser-STAT3 was localized to the mitochondria but not to the nucleus. Moreover, we found Nerve Growth Factor (NGF) too induced mitochondrial but not the canonical nuclear localization of STAT3 (Chapter 5). This is in contrary to an earlier report on the nuclear functions of NGF induced P-Ser-STAT3. These mitochondrial STAT3 was further shown to be intimately involved in NTN and NGF induced neurite outgrowth. Collectively, these findings demonstrated the hitherto unrecognized role of specific ligands and receptor isoforms in activating STAT3 and the transcription independent mechanism whereby the mitochondria localized P-Ser-STAT3 mediates the neuritogenic functions of growth factors (Chapter 4 & 5).

In addition to signaling through kinases, gene regulation at transcript level is known to play a major role in mediating the neurotrophic functions of GFLs and others. A pre-requisite to accurate quantification of transcriptomic changes by high throughput methods such as real-time qPCR is data normalization using internal reference genes. Recently, some routinely used housekeeping genes such as β-actin and GAPDH were found to vary significantly across cell types and experimental conditions. To identify suitable reference genes during neuronal differentiation induced by GDNF and others, a genome-wide analysis was performed. The stability of twenty selected candidate genes was systematically evaluated with two

independent statistical approaches, geNorm and NormFinder. Interestingly, the ribosomal protein genes, RPL19 and RPL29, were identified as the most stable reference genes across six different differentiation paradigms. The combination of these two novel reference genes, but not the commonly used GAPDH, allows robust and accurate normalization of differentially expressed genes during neuronal differentiation (Chapter 6).

MicroRNA represents a unique class of non-coding genes which have been found to play critical roles in many aspects of biology. To investigate the role of microRNAs in regulating neuronal differentiation, an integrated quantitative real-time PCR based assay system was developed (Chapter 7). Using these assays, we demonstrated the involvement of two microRNAs in topological guidance of neurite outgrowth on nanostructured surfaces. Furthermore, we investigated the interplay of GDNF ligand receptor systems and microRNAs during neuronal differentiation of NTera2 neuroprogenitor cells (Chapter 8).

The findings in this thesis further highlight the diverse functions of GDNF ligand receptor system and provide novel insights into the underlying signaling mechanisms. The combinatorial interactions of GFLs, GFRα and RET receptor isoforms provides a new paradigm that allows a single ligand to exert a plethora of biological effects.

List of Figures and Tables

List of Abbreviations

cAMP	cyclic adenosine monophosphate
CREB	cAMP response element binding protein
dbcAMP	dibutyryl cyclic AMP
Epac	exchange protein directly activated by cAMP
ERK1/2	extracellular signal-regulated kinases 1 and 2
FK	forskolin
GDNF	glial cell line-derived neurotrophic factor
GFL	GDNF family ligand
GFRα1	GDNF family receptor alpha 1
GFRα2	GDNF family receptor alpha 2
GPI	glycosylphosphotidylinositol
IL6	Interleukin 6
JNK	c-Jun N-terminal kinase
MAPK	mitogen-activated protein kinase
miRNA	microRNA
NCAM	neural cell adhesion molecule
NGF	nerve growth factor
NTN	neurturin
PACAP	pituitary adenylate cyclase-activating peptide
PKA	protein kinase A
PKC	protein kinase C
p38	p38 mitogen-activated protein kinase
RA	Retinoic acid (all-trans)
RET	rearranged during transformation
RTK	receptor tyrosine kinase
siRNA	small interfering RNA
SMRT-qPCR	Stem-loop mediated reverse transcription quantitative polymerase chain reaction
mSMRT-qPCR	Modified SMRT-qPCR
STAT3	signal transducer and activator of transcription 3
ROS	reactive oxygen species

Chapter 1 Introduction

1.1 Motivations of the study

GFLs, in particular GDNF and NTN, have been shown to support a plethora of neuronal functions, including the survival, differentiation and regeneration of both neurons and glial cells (*1, 2*). Because of their potent protective and / or restorative effects on midbrain dopaminergic neurons, GDNF and NTN based gene therapies are currently in clinical trials for Parkinson's disease. Despite years of research, the molecular mechanisms underlying the diverse functions of GDNF and NTN are only beginning to be understood. It is generally accepted that GFLs activate downstream signaling by forming a multi-component ligand receptor complex consisting of the ligand, a high-affinity GFRα as well as co-receptors RET and/or NCAM (*3*). Multiple alternatively spliced isoforms of these receptors have been identified and are shown to be widely expressed in neuronal systems (*4, 5*). Our group has earlier reported that GFRα and RET isoforms have distinct biochemical properties and neuritogenic activities, which contribute to the diverse functions of GFLs (*5-7*).

This thesis further explores the emerging view that the combinatorial interactions of the multi-component ligand receptor system with multiple receptor isoforms, provide a molecular basis for the pleiotropic functions of GFLs. Using multiple cell models, we investigated the differential regulations of signaling events, at protein, mRNA and microRNA levels, by GFRα1/2 and RET receptor isoforms and examined their implications in neuronal differentiation.

1.2 Organization of the thesis

This thesis is organized into seven chapters (Chapters 3 - 8), according to the investigations of specific hypothesis and the respective findings. Chapter 3 reports that the distinct neuritogenic activities of GFRα2 isoforms may partly be attributed to the differential modulation of cAMP-PKA signaling pathway, which is required for ligand-induced neurite outgrowth through all GFRα2 isoforms. Chapter 4 reports the novel observation of NTN induced mitochondrial STAT3 phosphorylation, mediated specifically through receptor isoforms GFRα2c and RET9. Extending the work on STAT3, Chapter 5 describes the unexpected discovery that NGF induced mitochondrial but not nuclear localization of STAT3, in contrary to earlier findings on nuclear functions of NGF induced STAT3. Chapter 6 presents a workflow for the identification and validation of stable reference genes that allows accurate normalization of transcriptomic changes during neuronal differentiation induced by GDNF and others. Chapter 7 outlines the development and validation of high throughput multiplex quantitative assays for the profiling of mature human microRNAs. Using these assays, two microRNAs were found to be intimately involved in the topological guidance of neurite outgrowth on synthetic nanostructure. Lastly, Chapter 8 presents a study that demonstrates the interplay of GFL, GFRα, RET receptor isoforms and microRNA in regulating the differentiation and lineage specification of NT2 neuroprogenitor cells.

1.3 List of related publications (published, submitted and in preparation)

1. Wan G*, **Zhou L***, Lim Q, Wong YH, Too HP. (2011) Cyclic AMP signaling through PKA but not Epac is essential for neurturin-induced biphasic ERK1/2 activation and neurite outgrowths through GFRα2 isoforms. *Cell Signal* 23(11):1727-37. * Equal contributions. ***(Chapter 3)***
2. **Zhou L** and Too HP. (2012) Specific alternatively spliced isoforms of GFRα2 and RET mediate Neurturin induced mitochondrial STAT3 phosphorylation and neurite outgrowth. Manuscript under review. ***(Chapter 4)***
3. **Zhou L,** Too HP. (2011) Mitochondria STAT3 mediates NGF induced PC12 neurite outgrowth. *PLoS ONE* 6(6): e21680. ***(Chapter 5)***
4. **Zhou L,** Lim QE, Wan G, Too HP. (2010) Normalization with genes encoding ribosomal proteins but not GAPDH provides an accurate quantification of gene expressions in neuronal differentiation of PC12 cells, *BMC Genomics* 11**:**75. **(*Chapter 6)***
5. **Zhou L*,** Cheng H*, Choy WK and Too HP. (2012) MicroRNA-221 and 222 mediate nano-topological guidance of directed neurite outgrowth. Manuscript in preparation. * Equal contributions. ***(Chapter 7)***
6. **Zhou L** and Too HP. (2012) Interplay of GDNF ligand receptor system and microRNA during neuronal differentiation of Ntera 2 neuroprogenitor cells. Manuscript in preparation. ***(Chapter 8)***
7. Wan G, **Zhou L**, Too HP. (2010) Molecular neurobiology of glial cell line derived neurotrophic factor (GDNF) family of ligands and receptor complexes, *Neurogenesis, Neurodegeneration and Neuroregeneration* 201-243 ISBN: 978-81-308-0388-3 ***(Chapter 2)***

8. Ho YK, **Zhou L**, Tam KC, Too HP. (2012) Linear Polyethylenimine / DNA polyplex transfect differentiated neuronal cells with exceptionally high efficiency and low toxicity. Manuscript in preparation.
9. Lim QE, **Zhou L**, Ho YK, Wan G, Too HP. (2011) snoU6 and 5S RNAs are not reliable miRNA reference genes in neuronal differentiation. *Neuroscience* 199:32-43.
10. Zhu M, **Zhou L**, Li B, Dawood MK, Wan G, Lai CQ, Cheng H, Leong KC, Rajagopalan R, Too HP, Choi WK. (2011) Creation of nanostructures by interference lithography for modulation of cell behavior. *Nanoscale* 3:2723-2729.
11. Zhou K, **Zhou L**, Lim QE, Zou R, Stephanopoulos G, Too HP. (2011) Novel reference genes for quantifying transcriptional responses of Escherichia coli to protein overexpression by quantitative PCR. *BMC Mol Biol* 12(1):18.
12. Qian LP, **Zhou L**, Too HP, Chow GM. (2010) Gold decorated NaYF4:Yb,Er/NaYF4/silica (core/shell/shell) upconversion nanoparticles for photothermal destruction of BE(2)-C neuroblastoma cells. *J Nanopart Res* 13:499–510.
13. Dawood MK, **Zhou L**, Zheng H, Cheng H, Wan G, Rajagopalan R, Too HP, Choi WK. (2012) Nanostructured Si-Nanowire Microarrays for Enhanced-Performance Bio-analytics. *Lab Chip*, 2012, 12, 5016–5024
14. Wan G, Yang K, Lim Q, **Zhou L**, He BP, Wong HK, Too HP. (2010) Identification and validation of reference genes for expression studies in a rat model of neuropathic pain. *Biochem Biophys Res Commun* 400(4):575-80.
15. Leung A, Ho YK, Too HP, **Zhou L**, and Tam KC. (2010) Self-Assembly of Poly (L-glutamate)-b-poly(2-(diethylamino)ethyl>methacrylate) in Aqueous Solutions. *Australian Journal of Chemistry* 64(9) 1247-1255.
16. He E, Yue CY, Fritz S, **Zhou L**, Too HP, Tam KC. (2009) Polyplex formation between four-arm poly (ethylene oxide) -b-poly (2-(diethylamino) ethyl

methacrylate) and plasmid DNA in gene delivery, *J Biomed Mater Res A* 91(3):708-18.

1.4 List of Invention Disclosures

1. Analyte-specific Spatially Addressable Nanostructured Array (ASANA) – Integrated Si Nanowires with Microfluidics for Enhancement of Analytes Capture. US Provisional Application No.: 61/577,171. Inventor: Wee Kiong CHOI, Heng-Phon TOO, Raj RAJAGOPALAN, **Lihan ZHOU**, Mohammed Khalid Bin DAWOOD, Han ZHENG, He CHENG
2. TrafEn^{TM}: A Novel Reagent for Gene-Drug Therapeutics. Invention disclosure in preparation (ETPL's File Ref: BTI/Z/07248). Inventor: Yoon Khei HO, **Lihan ZHOU**, Heng-Phon TOO,

1.5 List of Awards

1. **Best Poster Award** (CPE), 2011, Singapore-MIT Alliance Annual Symposium, Singapore
2. **Best Graduate Oral Presentation Award**, 2010, Yong Loo Lin School of Medicine, National University of Singapore, Singapore
3. **Best Poster Award**, Ozbio 2010 Young Scientist Forum, Melbourne, Australia
4. **Young Scientist Fellowship,** Ozbio 2010, jointly organized by International Union of Biochemistry and Molecular Biology (IUBMB) & Federation of Asian and Oceanian Biochemists and Molecular Biologists (FAOBMB), Melbourne, Australia
5. **Best Poster Award**, 2010, 3rd Department of Biochemistry Student Symposium, Singapore
6. **Best Poster Award**, 2008, 1st Department of Biochemistry Student Symposium, Singapore

1.6 Conference Presentation

1. **Zhou L.H.** and Too H.P. Mitochondrial STAT3 mediates NGF and GDNF induced neuritogenesis, SYM-50-04, Symposium 50 - Subcellular Targeting, Ozbio 2010, Melbourne, Australia

Chapter 2 Literature Review

2.1 GDNF family of ligands (GFLs)

GDNF is the prototype of a family of structurally related molecules that are distant members of the TGFβ superfamily. GDNF was first purified from a rat glioma cell-line (B49) conditioned media, which was shown to exert potent trophic effect on cultured embryonic midbrain dopamine neurons (*8*). Subsequently, three other members NTN, Artemin (ART), and Persephin (PSP) were identified in mammals. NTN was purified from conditioned media derived from Chinese hamster ovary cells, which supported the survival of cultured superior cervical ganglion sympathetic cells (*9*). PSP was identified through homology-based PCR screening (*10*), and ART through database searches thereafter (*11*). The four GFLs were found to be conserved across a variety of vertebrates but NTN is absent in clawed frog and PSP is absent in the chicken genome (*12*). A recent in-depth search of the human genome (NCBI build 36.3) did not suggest the existence of other GFLs.

GFLs are encoded by single copy genes and are found to be expressed in many regions of the nervous system both during development and in adult stages. Functionally, these GFLs were shown to be intimately involved in the development, maturation and maintenance of a wide variety of neuronal systems (*13-16*). Multiple transcripts of GDNF (*17-23*), ART (*24*) and PSP (*25*) have been reported, the majority of which are alternatively spliced isoforms, encoding the mature forms of the GFLs with different N-terminal sequences. The expressions of some of these transcripts are tissue selective and can be specifically regulated by external stimuli (*23, 26*), with yet to be characterized mechanisms.

GFLs are produced in the form of precursors preproGFLs and further processed by proteolytic cleavages, glycosylation and disulphide linking to produce the

mature form. The four GFLs have little sequence homology but share seven conserved cysteine (Cys) residues. The monomeric structure of GFLs is composed of two β sheet fingers, a cysteine-knot core motif, and an α-helical wrist region (Figure 2.1). Functionally, these GFLs form homodimer before binding to GFRα receptors. The crystalized form of GDNF comprises an asymmetric unit of two antiparallel covalent homodimers which differ in the relative hinge angle between the "wrist" and "finger loops" within their respective monomers (*27*). While GFLs share a similar overall topology, detailed comparison of ART and GDNF homodimers revealed differences in the shape and possible flexibility of the elongated homodimer (*28*), which may have important implications in the overall structures of the ligand-receptor complex.

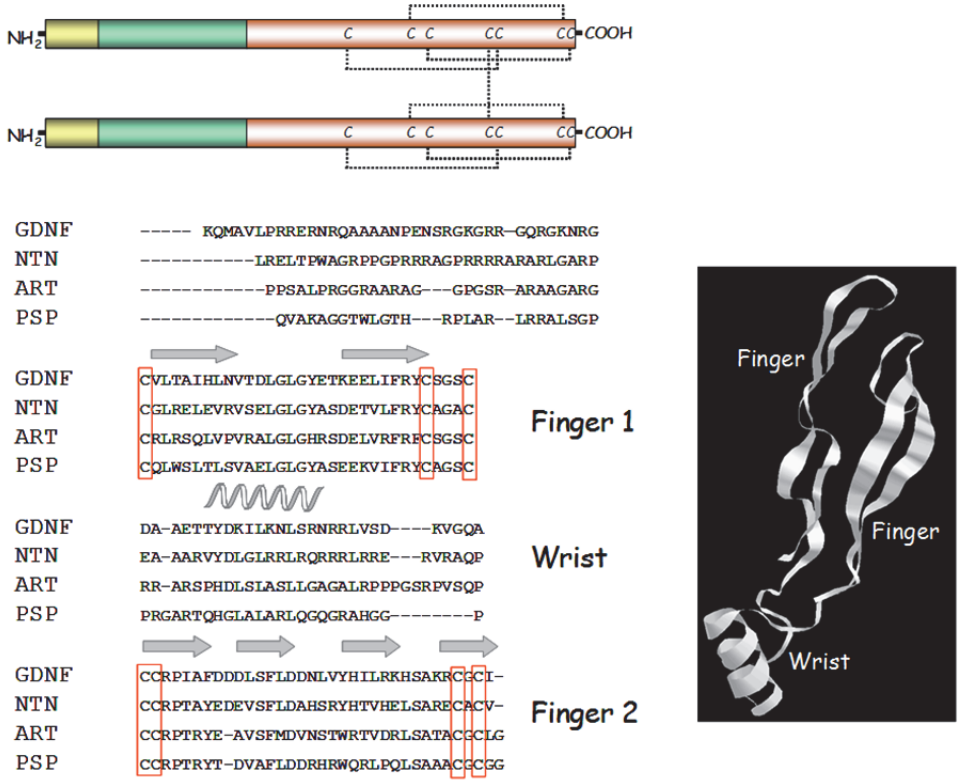

Figure 2.1 Structures of GDNF-family ligands (GFLs). A, Schematic representation of a homodimeric GFL with intra- and intermolecular disulphide bridges formed between cysteine residues designated by 'C'. B, Sequence alignment of human GFLs. The secondary-structural elements within the GFL structures are shown above the sequences by designations for alpha helices (coil) and beta strands (arrows). RasMol representation of the GDNF monomer based on coordinates described [PDB ID 1AGQ; 51]. *This figure is reproduced from Figure 1, Wan et al, Neurogenesis, Neurodegeneration and Neuroregeneration 201-243 ISBN: 978-81-308-0388-3.*

In neurons, GDNF is anterogradely transported in axons and dendrites and is implicated in neuronal plasticity (*29-33*). An important function of GFLs is to serve as target-derived innervation factors. GDNF was found to be a target-derived neurotrophic factor for nigral dopaminergic neurons and is transported to the neuron from the striatum (*34, 35*). Overexpression of GDNF exclusively in the target regions of mesencephalic neurons, particularly in the striatum, resulted in an increased number of surviving nigral dopamine neurons (*36*). In addition, NTN was reported to serve as a target-derived innervation factor for postganglionic cholinergic axons (*37*) and in the developing ciliary ganglion neurons (*38*). Furthermore, GFLs are also known to signal in an autocrine manner (*39, 40*). For instance, GDNF acts as an autocrine regulator of neuromuscular junction by promoting the insertion and stabilization of postsynaptic acetylcholine receptors (*41*).

Transgenic animal models with the disruption of the GDNF signaling pathway have been established. These early studies have failed to provide definitive evidence of a physiological neuroprotective role of GDNF in adult life. Homozygous *Gdnf* knockout mice died in the early postnatal period due to kidneys and myenteric plexus agenesis. At birth, these *Gdnf*$^{-/-}$ mice showed normal numbers of catecholaminergic neurons in the substantia nigra and locus coeruleus (*42-44*). Regional-specific knock-out of the co-receptor, RET, in dopaminergic neurons has provided conflicting results of the physiological role of this pathway in the maintenance of adult neurons. No obvious differences in the morphology or biochemical properties of the dopaminergic nigrostriatal neurons in adults of these RET-null mice as compared to controls were observed (*45*). Another report demonstrated that embryonic deletion of *RET* in catecholaminergic neurons resulted in a significant decrease of TH^+ substantia nigra neurons and striatal nerve terminals (*46*). With all these studies, the possibility of compensatory modifications masking the underlying physiologic effects of GDNF in the adult nervous system cannot be ruled out. To circumvent this

possibility, a conditional GDNF-null mouse where GDNF expression was markedly reduced in adulthood, was generated recently (*47*). These animals showed significant selective and extensive catecholaminergic neuronal death, most notably in the locus coeruleus, substantia nigra and Ventral tegmental area. Other neuronal systems, e.g, GABAergic and cholinergic pathways, appeared unaffected. These mutant mice also demonstrated progressive behavioural motor disturbances, consistent with the parallel neurochemical and histological losses. This study unequivocally indicated that GDNF is indeed required for the maintenance of catecholaminergic neurons in normal adult animals. It will be interesting to know if other GFLs and GFRα may have distinct neuroprotective roles in adult neurobiology.

2.2 GDNF family of receptors (GFRs) and co-receptors

The homodimeric GFLs activate downstream signaling by forming a multi-component ligand receptor complex consisting of a preferred high-affinity GDNF family receptor alpha (GFRα) and the co-receptor RET (REarranged during Transformation) with a proposed stoichiometry of GFL homodimer-(GFRα)2-(RET)2. Each GFL has its cognate receptor. GDNF preferentially binds to GFRα1, NTN to GFRα2, ART to GFRα3 and PSP to GFRα4. However, the multi-component receptor system shows some degree of promiscuity in their ligand specificities (Figure 2.2) (*2, 48-51*). GDNF have been reported to interact and activate GFRα2 and GFRα3 (*1*), whereas NTN and ART were shown to interact with GFRα1.

Co-receptor RET was originally identified as an oncogene activated by DNA re-arrangement in a 3T3 fibroblast cell line transfected with DNA taken from human lymphoma cells (*52, 53*). It encodes for a single-pass transmembrane receptor tyrosine kinase (RTK) with a cadherin-related motif and a cysteine-rich extracellular domain. Among all known receptor tyrosine kinase, RET is the only one which does not bind its ligands directly but requires a co-receptor (GFRα) for activation. In

addition to RET, GFLs have also been shown to signal through other co-receptors such as neural cell adhesion molecules (NCAM) (*3*) and more recently, integrin β1 (*54*). Intriguingly, GDNF induced differentiation and migration of cortical GABAergic neurons was found to be independent of both RET and NCAM, suggesting the existence of yet another signaling mechanism(s) (*55*).

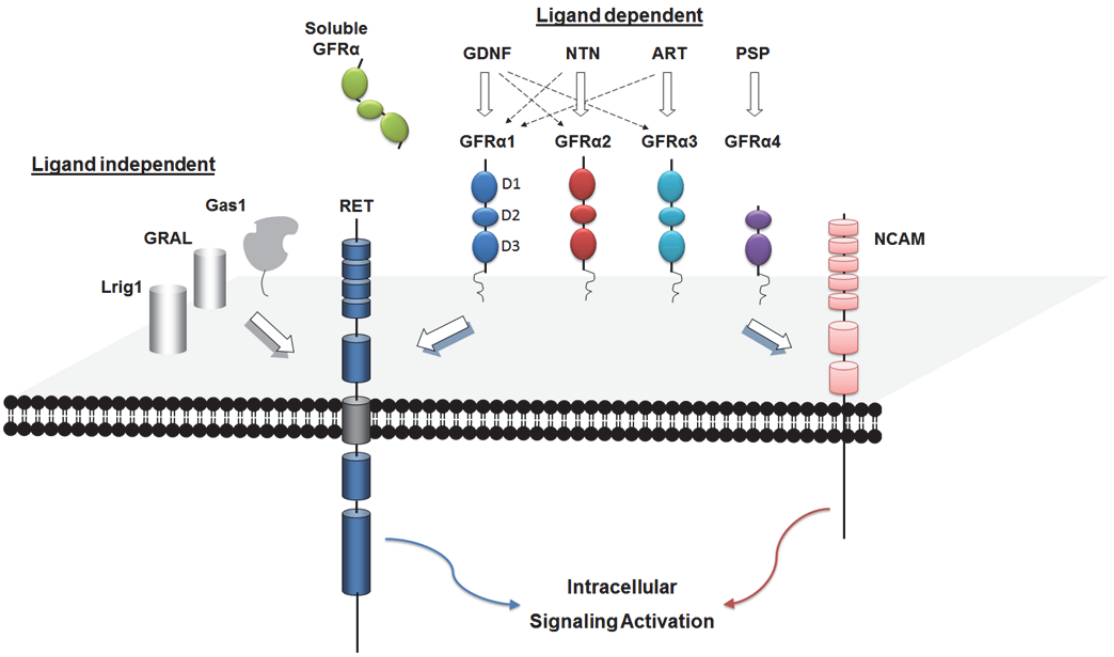

Figure 2.2 GFLs, GFRα and co-receptors interactions. Known interactions between GFLs and GFRα receptors are shown here. The arrows indicate the preferred ligand–receptor interactions and the broken arrows denote cross-talks of GFLs with non-cognate GFRα. Soluble GFRα is thought to be released through cleavage of the glycosyl-phosphotidylinositol (GPI) anchor by phospholipase or protease yet to be characterized. GFL signal is transduced through interactions of ligand bound GFRα with transmembrane co-receptor RET or NCAM. Gas 1 and Lrig interact with RET independent of ligands and regulate GDNF-GFRα-RET signaling.

Recently, distantly related GFRα-like structures have been identified in a number of proteins. Based on the conserved pattern of cysteines and other amino acid residues, GFRα-like structures are found in Gas1 (growth arrest specific 1) (*56, 57*) and GRAL (GDNF Receptor Alpha Like), a protein found in some regions of the central nervous system of unknown function (*58*). Unlike the GFRα1-4, GRAL and Gas1 function independently of GFLs. More interestingly, Gas1, as well as the leucine-rich repeats and Ig-like domain protein Lrig1 have been shown to modulate RET activity independent of ligand GDNF. Lrig1 sequesters RET from localizing to

lipid rafts whereas Gas1 recruits RET to the cholesterol rich microdomain. Interactions with the two modulators alter RET phosphorylation and downstream signaling including PI3K-AKT and MEK/MAPK activation (*59, 60*).

Structurally, GFRα is organized into three homologous cysteine-rich domains with various lengths of C-terminal extensions (*2, 61*). Domain 2 (D2) is involved in the binding of GFLs (*50, 62-64*) while Domain 3 (D3) provides a stabilizing effect. The N-terminal D1 was found to be dispensable for ligand binding and is absent in GFRα4 (*2*). However, direct chemical cross-linking showed that the residues at the distal end of the N-terminus D1 (residues 89-101 of GFRα1) contact RET at multiple sites, suggesting that D1 may modulate GFRα and co-receptor interactions (*65*). In addition, the D1 truncated mutant of GFRα1 was shown to be less biologically active compared to the full length counterpart, thus providing strong evidence for the biological relevance of the N-terminal domains.

Both GFRα1 and GFRα3 have been partially crystallized. The crystal structure of the D3 of GFRα1 was first determined and used to model the structure of D2, from which a partial structure (D2/D3) of GFRα2 was deduced (*62*). Recently, the heterotetrameric complex of GDNF dimer with two GFRα1 (D2 and D3 domains) was solved (*66*). It was found to share a similar but not identical structure with the heterotetrameric complex of ART and GFRα3 (*64*). This is consistent with the suggestion that all GFRα share similar structures but differ in the details of their ligand and co-receptor binding sites. Although the structure and function of D1 has yet to be empirically determined, it is not unreasonable to suggest that this N-terminal domain, with distinct sequences in multiple isoforms of GFRα, may play an important modulatory role in the interactions of GFRα with the different components of the receptor complexes.

In the nervous system, GFRα and RET are consistently expressed in neurons / regions where GFLs were found to serve as target innervation factors (*14, 67-77*).

RET is usually co-expressed with at least one of the GFRα, but mismatched expressions of the two components have been reported in selected brain regions (*24, 67, 71, 74, 75, 77-80*). A popular hypothesis is that these GFRα may capture diffusible GFLs and activate RET on neighboring cells in trans, in a non-cell-autonomous fashion (*81*). However, this mechanism appears to be non-essential for organogenesis and nerve regeneration in a transgenic mouse model (*82*). The expressions of RET and GFRα are developmentally regulated, with maximal expressions in early postnatal life (*67, 83-86*), consistent with its role in early development of the nervous system. Alterations in their expressions have also been observed in response to physical trauma such as nerve transection (*87, 88*), ischemia (*89-92*), excitotoxic insult (*93-96*) and epileptic seizures (*75, 96-98*), suggestive of the protective and restorative roles of GFLs signaling during nerve injuries.

2.3 Alternatively spliced isoforms of GDNF receptors

Alternative splicing is prevalent in many mammalian genomes and serves as a robust means of producing functionally diverse proteins from a single gene. In many systems, alternative spliced isoforms were shown to have distinct biochemical properties and diverse biological functions (*99*). Recent studies have found 92-94% of human genes to be alternatively spliced (*100*) and identified the central nervous system as the organ where the greatest amount of conserved splicing occurs (*101*).

Multiple alternatively spliced isoforms of GFRα1 (*73, 102, 103*), GFRα2 (*104, 105*) and GFRα4 (*61, 106, 107*) have been identified. Similarly, alternatively splicing of RET (*108, 109*) and NCAM (*110, 111*) pre-mRNA have been reported. We have since hypothesized that the spliced isoforms of GFRα, RET and NCAM may have distinct functions and their combinatorial interactions in specific cellular context could generate a myriad of biological responses. In an earlier report, ligand activation of the

GFRα2 isoforms was found to differentially regulate ERK and AKT signaling, and the expressions of early response genes. In addition, GDNF and NTN induced neurite outgrowth through GFRα2a and GFRα2c, but not GFRα2b. When co-expressed, activation of GFRα2b inhibited neurite outgrowth induced by the other GFRα2 isoforms as well as GFRα1a and Retinoic acid, through a RhoA-dependent mechanism (*6*). Likewise, the alternatively spliced isoforms of GFRα1 have been shown to exhibit distinct biochemical functions (*5, 112*). These studies strongly supported our hypothesis that GFRα receptor isoforms have distinct biochemical and neuritogenic functions.

The two major RET isoforms RET9 and RET51 differ at their C-termini (*113*). Developmentally, mice lacking RET9 showed kidney hypodysplasia and defects in enteric innervation, whereas mice lacking RET51 develop normally. Conversely, RET51 but not RET9 was shown to promote the survival and tubulogenesis of mouse inner medullary collecting duct cells (*108*), suggestive of isoform specific roles in embryo development and organogenesis. Structurally, the two RET isoforms share 16 identical tyrosine residues but RET51 contains two additional tyrosine residues in the carboxyl terminal (tyrosine 1090 and 1096). When stimulated by ligands, tyrosine 1062 in both RET isoforms can associate with Shc, FRS2 and DOK adaptors. However, adaptor protein Enigma was found to interact with RET9 but not RET51 (*114*). Furthermore, RET9 but not RET51 contains a PDZ domain binding site at its extreme C-terminus, responsible for interaction with Shank3, as well as activating sustained RAS-ERK1/2 and PI3K-AKT signaling (*115*). On the other hand, RET51-specific tyrosine 1096 can compensate for the functional capacity of tyrosine 1062 by direct association with GRB2 and downstream signaling pathways. Conversely, the presence of tyrosine 1096 also renders RET51 more susceptible to Cbl ubiquitin ligase binding and proteasome-dependent degradation (*116*). Although both RET isoforms share identical extracellular GFL and GFRα binding domains, RET9 and

RET51 seem to function as independent signaling complex in cultured sympathetic neurons and neuronal cell lines (*117, 118*).

The existence of these functionally distinct spliced variants of GDNF family ligands and receptors is suggestive of a new paradigm where a limited number of ligands and receptors generate pleiotropic effects through differential expression and combinatorial interactions of the various components.

2.4 GFL-GFRα-RET signaling and function

Upon stimulation by GFLs and GFRα, RET undergoes dimerization and trans-phosphorylation of its intracellular tyrosine residues, a process that is required for the complete activation of RET tyrosine kinase domains and downstream signaling. Autophosphorylations of RET tyrosine residues 905, 981, 1015, 1062 and 1096 were initially thought to recruit specific adaptor molecules GRB7/10 (*119, 120*), Src (*121*), PLCγ (phospholipase Cγ) (*122*), Shc (Src-homologous and collagen-like protein) (*123*) and GRB2 (*124*), respectively. With an increasing number of RET binding partners, it is now believed that each phosphotyrosine residue may serve as a competitive binding site, resulting in divergent signaling outcomes, in a cell context dependent manner.

The GFL-GFRα-RET signaling is also regulated by membrane localization of the ligand-receptor complex. Lipid rafts are plasma membrane microdomains that are enriched in cholesterol, sphingolipids and selected proteins, and have emerged as crucial membrane sub-compartments for signal transduction (*125*). Many signaling molecules including GPI-anchored receptors and dual acylated signaling intermediates such as Hedgehog and Src-family kinases (SFKs) demonstrate a high affinity for lipid rafts. In contrast, inactive RET was found to predominantly localize outside lipid raft. Upon stimulation, GFL-GFRα complex is thought to recruit RET into the lipid rafts (*126*), through a mechanism involving RET tyrosine residue Y1062 (*81*).

Localization of active GDNF signaling complex to the rafts is critical for GDNF-induced neuroblastoma cell differentiation and cerebellar granule neuron survival, which are compromised by the disruption of lipid raft signaling by either cholesterol depletion or expression of transmembrane GFRα chimera (*126*).

Furthermore, ligand stimulation has been shown to result in the internalization and endosomal localization of many RTKs, which is required in some cases for prolonged or complete activation of certain signaling pathways (*127*). GDNF stimulation has been shown to result in GFRα1 internalization, both in the presence and absence of RET, but with differences in the kinetics of internalization (*128*). In sympathetic and motor neurons, activation and internalization of the GDNF receptor complex is required for the retrograde transport of GFLs (*29, 129*). Membrane bound and internalized GDNF receptor complex were also found to result in differential signaling activation. For instance, activation of GDNF complex at distal axon led to rapid activation of both AKT and ERK1/2, whereas retrogradely transported GDNF receptor complex is responsible for activation of AKT but not ERK1/2 in the cell body. However, the mechanisms regulating the internalization and selective subcellular localizations of GFL-GFRα-RET remain to be elucidated.

2.5 Conclusion

It is evident that GFLs play important roles in many aspects of neurobiology, ranging from cell proliferation, to neuronal differentiation and maturation, as well as synaptic functions and neuronal regeneration. The diverse mechanisms underlying each of the processes will undoubtedly be highly regulated and likely to be cell context dependent. Although the existence of multiple alternatively spliced variants of the GFL, GFRα and co-receptors and their combinatorial interaction provides a molecular basis that could explain pleiotropic effects of GFLs, our current knowledge

of the biosynthesis, processing and regulation of these ligands and receptors is still limited. This complexity in GFL signaling is further increased by ligand receptor promiscuity, regulation by or cooperation with other signaling molecules, selective localization to sub-cellular compartments and the competitive interactions with myriads of adaptor molecules. Further investigations of these mechanisms will provide greater insights on the relationship between specific cellular processes, their regulatory events and the wide plethora of biological responses observed. Substantial work is required to address each hypothesis and even more to integrate these findings into systems level knowledge that explains how the various signals activated by GDNF family ligand receptors are integrated into system networks in various cellular contextual frameworks contributing to the phenotypic outcomes.

Chapter 3 Cyclic AMP signaling through PKA but not Epac is essential for neurturin-induced biphasic ERK1/2 activation and neurite outgrowths through GFRα2 isoforms

Section 3.1 Introduction

Earlier studies from our group have identified three alternatively spliced isoforms of GFRα2. These isoforms GFRα2a, 2b and 2c were subsequently shown to have distinct neuritogenic activities. Elucidating the molecular mechanisms underlying their distinct functions will provide novel insights into how NTN and GDNF may promote neurite outgrowth and identify new dimensions in signaling network interactions.

Cyclic AMP (cAMP) is an important second messenger and key regulator of neuronal functions such as survival, differentiation, regeneration and neurite guidance (*130-133*). Multiple neurotrophic factors, including GDNF, BDNF and NGF, have been reported to regulate intracellular levels of cAMP (*134*). Elevation of cAMP was shown to promote regeneration of injured axons in sciatic nerves (*135*), spinal cord neurons (*132, 136, 137*) and dorsal root ganglion (*138*). In particular, GDNF was found to elevate cAMP level to a threshold that overcame the inhibitory effect of myelin-associated inhibitory factors and induced neurite outgrowth in DRG neurons (*130*). In addition, co-administration of cAMP with neurotrophic factors has been shown to synergistically enhance axon regeneration in injured neurons (*139*). The co-operation of GDNF and dibutyryl cAMP was further found to aid in the restoration of functional motor units by embryonic stem cells in paralyzed adult rat (*140*). Although the mechanism of GDNF-cAMP synergy has yet to be characterized, GFRα2 was shown to be highly expressed in the tissues where neurite outgrowth was observed (*141, 142*), suggesting an active role of the receptor / isoforms in mediating the functional interactions between GFL and cAMP signaling.

The canonical cAMP signaling is mediated through the activation of protein kinase A (PKA). Recently, a second downstream effector of cAMP signaling,

exchange protein directly activated by cAMP (Epac), was identified (*143, 144*). Both effectors were able to mediate cAMP induced neurite extension in PC12 cells (*145, 146*) and axonal regeneration of DRG neurons (*138*). However, PKA and Epac differed in their regulation of ERK1/2 activation (*147*), which played a central role in cAMP mediated neuronal differentiation (*148-152*). Furthermore, PKA but not Epac was found to mediate cAMP-induced neuronal differentiation through CREB phosphorylation and transcriptional activation (*100, 153-155*). In view of these findings, elucidating the involvement of specific cAMP downstream effectors could provide valuable insights to the mechanism underlying the physiological interactions between cAMP and ligand activated GFRα2 isoforms.

In this study, we reported an unexpected finding of the role of cAMP signaling as an underlying mechanism contributing to the differential neuritogenic activities of GFRα2 isoforms. Interestingly, PKA but not Epac was found to be mediated biphasic ERK1/2 activation and neurite outgrowth induced by ligand stimulated GFRα2 isoforms, a hitherto unrecognized mechanism.

Section 3.2 Results

3.2.1 NTN induced CREB phosphorylation, biphasic ERK1/2 activation and neurite outgrowth through selected GFRα isoforms

In this study, PC12 cells stably expressing RET9 with either one of the alternatively spliced GFRα2 isoform, GFRα2a, GFRα2b and GFRα2c were established. The expressions of specific combinations of receptor isoforms were validated with real-time PCR (Figure 3.1A). These PC12 clones expressed similar levels of GFRα2 isoforms and RET9 and bound radiolabeled GDNF with similar affinities (*6*). The wild-type and PC12 cells carrying vector alone did not express either RET or GFRα2 isoforms and were used as controls (Figure 3.1A). Stably infected PC12 cells were then stimulated with GDNF, NTN or NGF. Interestingly,

while NGF induced extensive neurite extensions in all the PC12 cell lines, GDNF and NTN promoted neurite outgrowth only in cells expressing GFRα2a and GFRα2c but not GFRα2b (Figure 3.1B and C). This result was consistent with the previous report that GFRα2 isoforms mediated differential neuritogenic activities upon ligand stimulations (*6*) and suggested that ligand activation of GFRα2a and GFRα2c may regulate distinct signaling pathways as compared to GFRα2b.

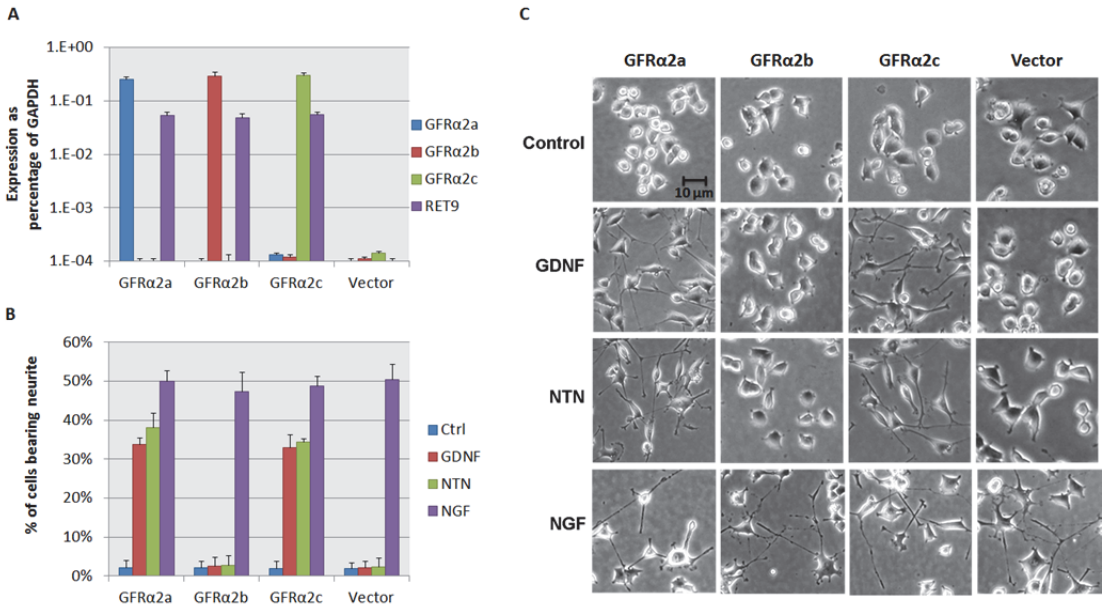

Figure 3.1 GDNF and NTN induced neurite outgrowth in PC12 cells expressing GFRα2a and GFRα2c but not GFRα2b. (A) Expression levels of RET9 and GFRα2 isoforms in wild type (WT) and stably infected PC12 cells. PC12 cells were co-infected with mouse RET9 and GFRα2 isoforms. The expression levels of RET9 and GFRα2 isoforms were quantified by real-time PCR and normalized to the expression levels of GAPDH. The results were expressed as mean ± S.E.M. (n = 3). (B) Ligand-induced neurite outgrowth in PC12 cells expressing RET9 and GFRα2 isoforms. Cells were treated with GDNF, NTN or NGF (50 ng/ml) for 48 h. Error bars indicate mean ± S.D. of quadruplicate measurements. ** $p < 0.001$, compared with non-treated cells. (C) Representative graphs of ligand-induced neurite outgrowth of PC12 cells.

To elucidate the downstream signaling pathways underlying their differential neuritogenic activities, we next investigated NTN-induced phosphorylation of CREB and ERK1/2 in PC12-GFRα2 cells over a period of 6 h (Figure 3.2). NTN stimulation of GFRα2a and GFRα2c but not GFRα2b induced CREB phosphorylation in a time-dependent manner (Figure 3.2A and B). Furthermore, NTN induced a biphasic

phosphorylation pattern of ERK1/2 in GFRα2a and GFRα2c cells, with an initial rapid phase (5 min) followed by a distinct sustained phase for at least up to 6 h (Figure 3.2A and C). In contrast, activation of ERK1/2 in NTN stimulated GFRα2b cells was transient and was dramatically reduced after 5 min (Figure 3.2A and C). These findings showed a correlation of the ligand-induced neurite outgrowth with the induction of the biphasic and sustained level of ERK1/2 activation of GFRα2a and GFRα2c.

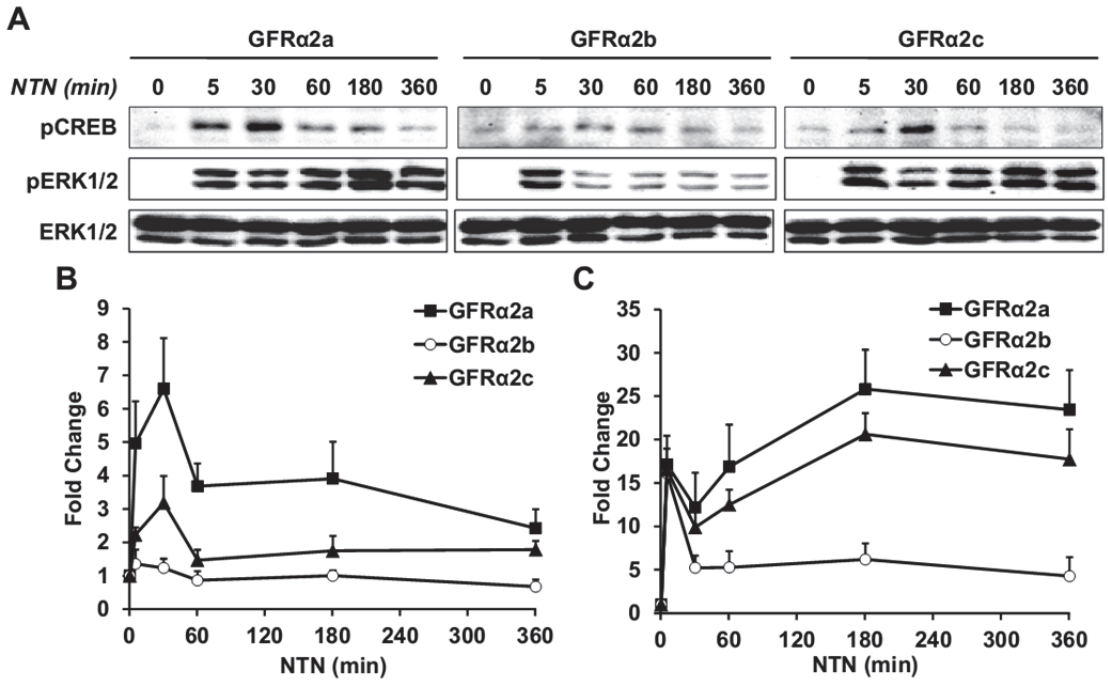

Figure 3.2 NTN promoted CREB phosphorylation and biphasic ERK1/2 activation in PC12 cells expressing GFRα2a and GFRα2c but not GFRα2b. (A) Time course of CREB and ERK1/2 phosphorylation induced by NTN. PC12 cells expressing GFRα2 isoforms were stimulated with NTN (50 ng/ml) for the indicated periods of time. Phosphorylation levels of CREB and ERK1/2 were analysed by Western blotting, the bands of expected molecular weights were presented. Blots were re-probed with total ERK1/2 antibody, serving as loading control. Fold changes of phosphorylation levels of CREB (B) and ERK1/2 (C) were quantified by densitometry and presented as Mean ± S.D. (n = 3).

3.2.2 Cyclic AMP and Protein Kinase A signaling is involved in NTN-induced neurite outgrowth

Phosphorylation of CREB is a major biochemical event downstream of cAMP signaling pathway (*153*). Importantly, cAMP signaling was found to be required for NGF-induced neurite outgrowth (*145*) and regulation of ERK1/2 activation (*147*). Since NTN stimulation of GFRα2a or GFRα2c resulted in CREB phosphorylation, we postulated that cAMP signaling may be involved in NTN induced biphasic ERK1/2 activation and neurite outgrowth in these cells. We first examined whether the distinct late phase of ERK1/2 activation was critical to GFRα2a and GFRα2c mediated neurite outgrowth. PC12-GFRα2a or GFRα2c cells were incubated with MEK inhibitor U0126 1 h before (-1 h), together (0 h), 1 h after (1 h) or 3 h (3 h) after NTN treatment. As expected, pre-incubation with U0126 (1 h before) dramatically inhibited NTN induced neurite outgrowth (Figure 3.3A). Interestingly, inhibition of the late phase of ERK1/2 by adding U0126 1 h or 3 h after NTN treatment significantly attenuate neurite outgrowth, supporting the notion that the late phase of ERK1/2 activation was required for NTN induced neurite outgrowth. Moreover, inhibiting ERK1/2 activation after 12 h of ligand stimulation failed to impair neurite outgrowth, suggestive of a restricted temporal event in the control of neuritogenic signal transduction. Interestingly, inhibition of PKA pathway with H89, a competitive inhibitor of the ATP site on the PKA catalytic subunit, was found to significantly inhibit NTN-induced ERK1/2 activation (Figure 3.3B-D) and neurite outgrowth (Figure 3.3E) in cells expressing GFRα2a or GFRα2c, suggesting the important role of cAMP pathway in mediating NTN signaling.

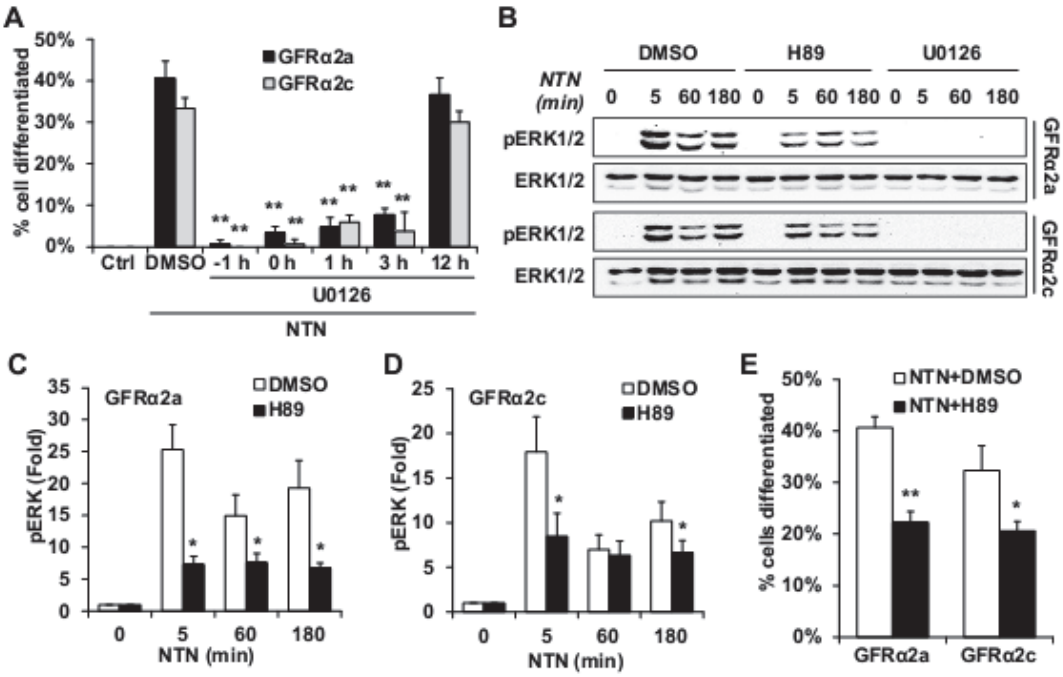

Figure 3.3 NTN-induced biphasic ERK1/2 activation and neurite outgrowth through GFRα2a and GFRα2c required cAMP-PKA signaling and *de novo* transcription and translation. (A) Effect of U0126 added at different time points on NTN-induced neurite outgrowth. Cells were incubated for 48 h from the time NTN were added. Percentage of cells differentiated was presented as Mean ± S.E.M. of at least three biological replicates. U0126 added 12 h after (*12 h*) NTN stimulation has no inhibitory effect on neurite outgrowth. ** $p < 0.001$, compared to NTN treatment without U0126. (B) Effect of H89 on NTN-induced ERK1/2 activation. Cells were stimulated with NTN (50 ng/ml) in the presence or absence of 10 μM H89 or 10 μM U0126 for the indicated periods of time. Phosphorylation levels of ERK1/2 were examined by Western blotting, the bands of expected molecular weights were presented. Fold changes of ERK1/2 phosphorylation in PC12 expressing GFRα2a (C) or GFRα2c (D) were quantified by densitometry and presented as Mean ± S.D. (n = 3). * $p < 0.05$, compared with NTN treatment without H89 at each time point. (E) Effect of H89 on NTN-induced neurite outgrowth. Cells were treated with NTN in the presence or absence of H89 for 48 h. Percentage of cells differentiated was presented as Mean ± S.E.M. of at least three biological replicates. ** $p < 0.001$, compared with NTN treatment without H89.

Since cAMP signaling has been shown to cooperate with GDNF in enhancing neuronal functions, we tested whether co-stimulation of NTN with cAMP agonist could synergistically induced neurite outgrowth. In PC12-GFRα2a and -GFRα2c cells, co-stimulation of NTN and cAMP agonist Forskolin (FK) significantly enhanced the rates of neurite outgrowth from 24 h to 72 h, compared to treatment with NTN alone (Figure 3.4). Moreover, we were interested to determine if specific downstream effector contributed to the cooperation of FK and NTN. The cAMP analogs 2-Me-

cAMP and 6-Bnz-cAMP, which have been shown to specifically activate Epac and PKA respectively in PC12 cells (*156*), were used as specific agonists in this study. Interestingly, 6-Bnz-cAMP but not 2-Me-cAMP was able to enhance NTN-induced neurite outgrowth (Figure 3.5A, B), indicating PKA but not Epac to be the downstream effector of cAMP in neurite synergy. Both 2-Me-cAMP and 6-Bnz-cAMP at 200 μM induced transient ERK1/2 activation at comparable levels (Figure 3.5C), indicating that 2-Me-cAMP was biologically active. Collectively, these findings were suggestive of the important requisite roles of cAMP-PKA signaling in biphasic and sustained ERK1/2 phosphorylation and neurite outgrowth mediated by ligand-activated GFRα2a and 2c isoforms.

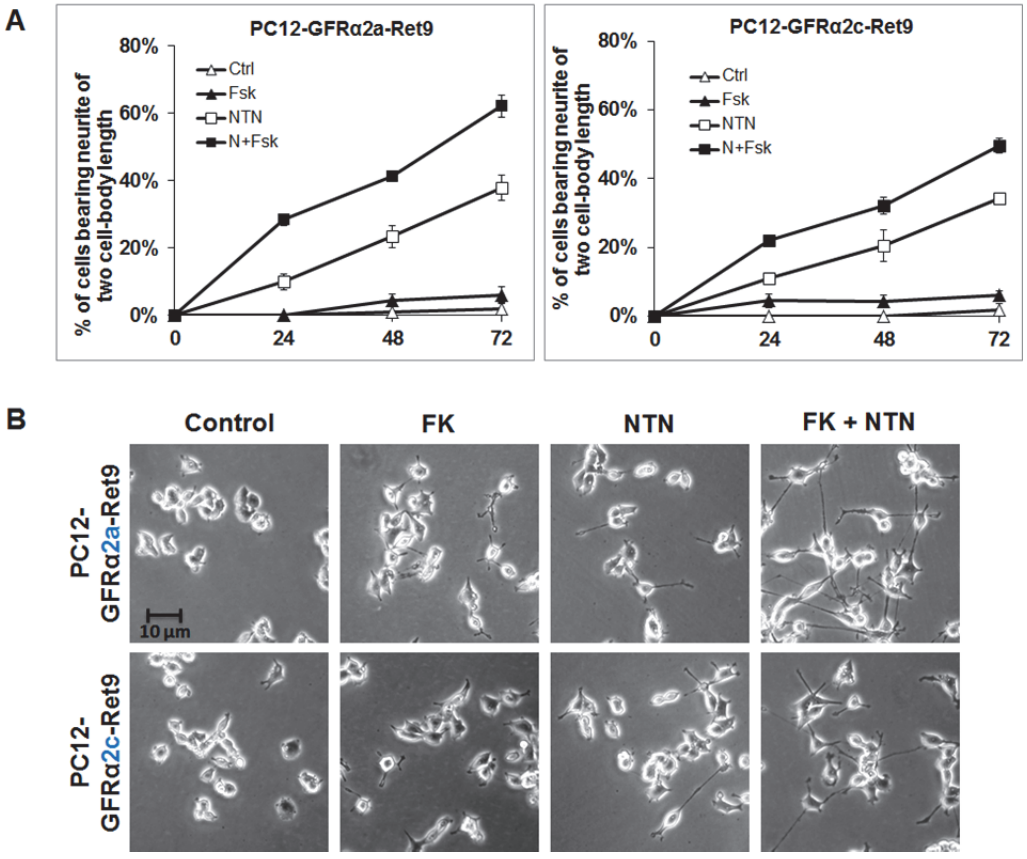

Figure 3.4 Forskolin enhances the rate of NTN induced neurite outgrowth in PC12 cells expressing GFRα2a and 2c. (A) Time course of neurite outgrowth induced by NTN and FK. PC12 cells were stimulated with NTN (50 ng/ml), FK (10 μM) or co-stimulated with both NTN and FK for 24 h, 48 h and 72 h. Percentage of differentiated cells was presented as Mean S.E.M. of at least three biological replicates. (B) Representative graphs of PC12 cells stimulated with NTN and FK for 24 h.

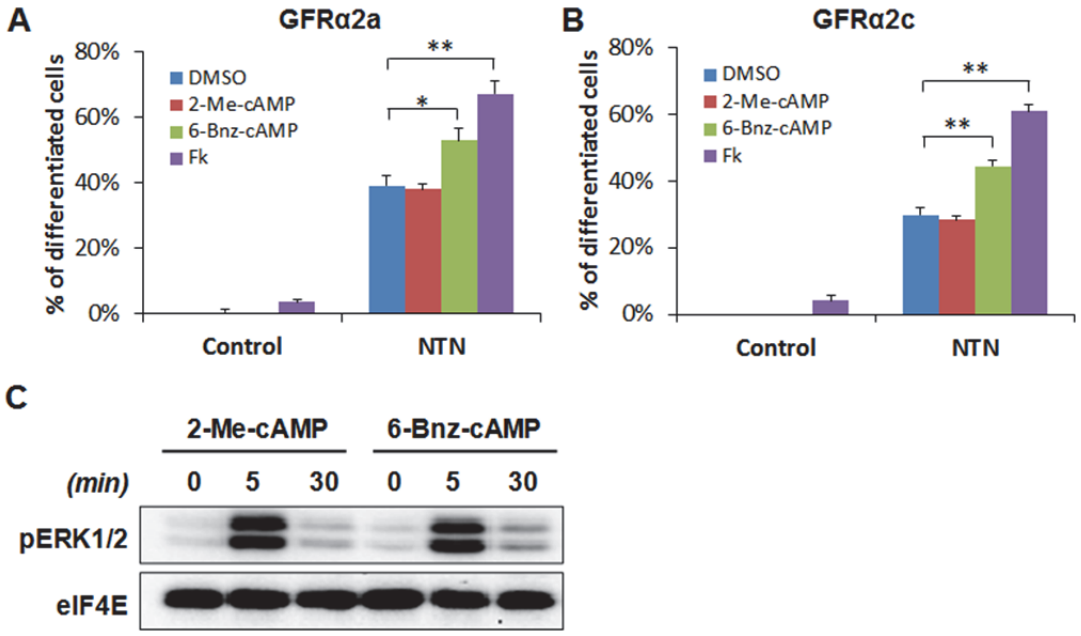

Figure 3.5 PKA but not Epac agonist enhanced NTN-induced neurite outgrowth of PC12 cells expressing GFRα2a and GFRα2c. PC12 cells expressing GFRα2a (A) or GFRα2c (B) were stimulated with 50 ng/ml NTN alone or together with DMSO, 200 μM 2-Me-cAMP, 200 μM 6-Bnz-cAMP or 10 μM FK for 48 h. Percentage of cells differentiated was presented as Mean ± S.E.M. of at least three biological replicates. * $p < 0.05$ and ** $p < 0.001$, compared to NTN alone. No differentiated cells were observed when stimulated with DMSO, 2-Me-cAMP and 6-Bnz-cAMP alone (Control). There is hence no visible bar for these conditions. (C) 2-Me-cAMP and 6-Bnz-cAMP induce transient ERK1/2 activation in PC12 cells. Cells were stimulated with 200 μM 2-Me-cAMP or 200 μM 6-Bnz-cAMP for indicated periods of time. Phosphorylation of ERK1/2 and CREB was examined by Western blotting. Blots were re-probed with eIF4E, serving as loading controls.

3.2.3 *De novo* transcription and translation is required for late phase of ERK1/2 activation and neurite outgrowth

Activation of gene transcription and regulation of protein synthesis are pivotal events to many of cAMP-mediated physiological processes (*157*). In PC12 cells expressing GFRα2a and 2c, we found that NTN stimulation promoted phosphorylation of CREB, an important transcription factor downstream of cAMP signaling, suggesting that transcriptional and translational activations may be regulated by cAMP signalling in these cells. We therefore examined whether activation of gene expressions was involved in NTN-induced sustained ERK1/2

activation and neurite outgrowth in PC12 cells expressing GFRα2a and 2c. Small molecule inhibitors Actinomycin D (ActD) and Cyclohexamide (Chx) were used to inhibit transcription and translation, respectively. ERK1/2 activation at 1 h and 6 h after NTN stimulations was significantly inhibited after pre-treatment of ActD or Chx (Figure 3.6A-C). Similarly, NTN induced neurite outgrowth was significantly impaired by these inhibitors (Figure 3.6D). These results suggested that activation of gene expressions and translation were required for both the late phase of ERK1/2 phosphorylation and neurite outgrowth induced by NTN stimulated GFRα2a and GFRα2c.

3.2.4 Cyclic AMP signaling cooperates with NTN to promote biphasic ERK1/2 activation, pERK1/2 nuclear translocation and neurite outgrowth via GFRα2b

Since GFRα2a and GFRα2c but not GFRα2b were able to activate cAMP signaling and induce neurite outgrowth, we hypothesized that exogenous activation of cAMP signaling may be able to cooperate with ligand-activated GFRα2b to promote neurite outgrowth. Indeed, while treatment of PC12 cells with various cAMP elevating agents alone (dbcAMP, FK and PACAP) only resulted in short neurite extensions, co-treatment of the agonists and GFLs induced extensive neurite outgrowth in a dose-response manner in GFRα2b expressing cells (Figure 3.7).

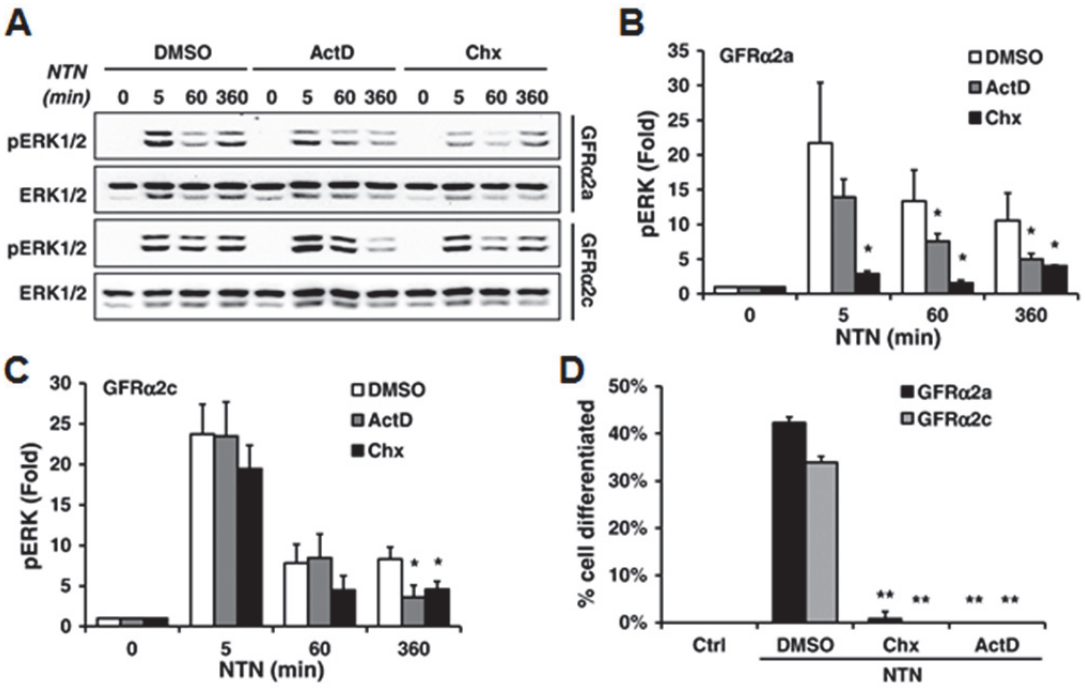

Figure 3.6 NTN-induced late phase of ERK1/2 activation and neurite outgrowth through GFRα2a and 2c required *de novo* transcription and translation. (A) Effects of ActD and Chx on NTN-induced ERK1/2 activation. Cells were stimulated with NTN in the presence or absence of 2 μg/ml ActD or 10 μg/ml Chx for the indicated periods of time. ERK1/2 phosphorylation was examined by Western blotting. Fold changes of ERK1/2 phosphorylation in PC12 expressing GFRα2a (B) or GFRα2c (C) were quantified by densitometry and presented as Mean ± S.D. (n = 3). * $p < 0.05$, compared with NTN treatment without inhibitors at each time point. (D) Effects of ActD and Chx on NTN-induced neurite outgrowth. Cells were treated with NTN in the presence or absence of inhibitors for 24 h. Percentage of cells differentiated was presented as Mean ± S.E.M. of at least three biological replicates. ** $p < 0.001$, compared with NTN treatment without inhibitors.

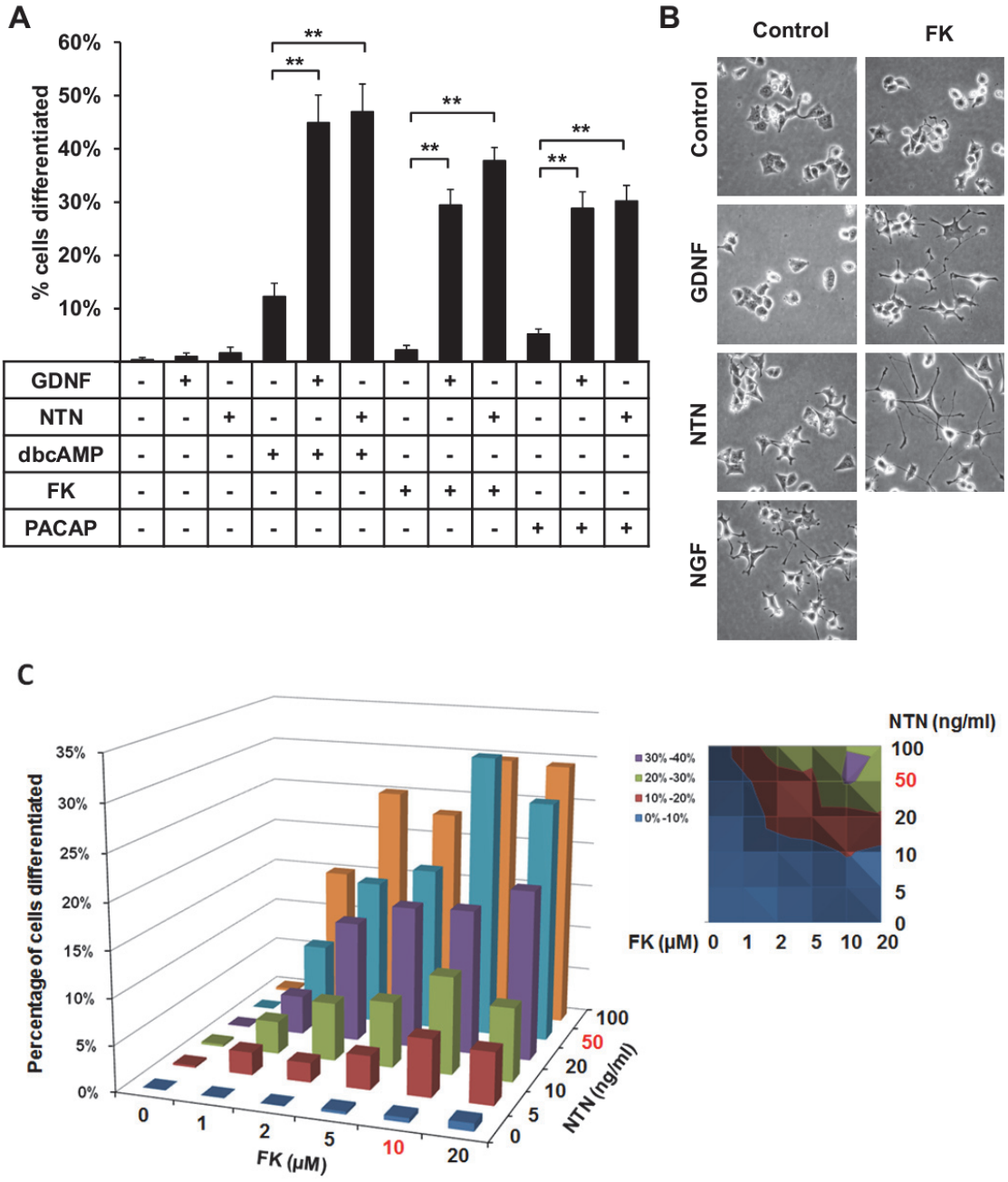

Figure 3.7 Cyclic AMP elevating agents cooperated with GDNF and NTN to induce neurite outgrowth in PC12 cells expressing GFRα2b. (A) Quantification of neurite outgrowth induced by various treatments. Cells were stimulated with GDNF or NTN (50 ng/ml) in the presence or absence of dbcAMP (100 μM), FK (10 μM) or PACAP (100 nM) for 48 h. Percentage of cells differentiated was presented as Mean ± S.E.M. of at least three biological replicates. ** $p < 0.001$, compared to dbcAMP, FK or PACAP alone. (B) Representative graphs of cells stimulated with GDNF or NTN in the presence or absence of FK for 48 h. NGF was used as positive control for induction of neurite outgrowth. (C) Dose response in NTN and FK synergy in neurite outgrowth.

As ligand-induced neurite outgrowth through GFRα2a and GFRα2c were accompanied by biphasic and sustained ERK1/2 activations (Figs. 3.2 and 3.3), we investigated if induction of neurite outgrowth by cAMP and NTN signaling through GFRα2b would also require a biphasic activation of ERK1/2. In PC12-GFRα2b cells, treatment of FK resulted in transient ERK1/2 phosphorylation, similar to the observation with NTN stimulations (Figure 3.8A). Co-treatment of cells with FK and NTN indeed promoted synergistic activation of ERK1/2 at later time points (Figure 3.8A) and resulted in a prolonged ERK1/2 phosphorylation profile. The total level of ERK1/2 was not significantly increased with FK and NTN stimulations. Furthermore, co-treatment of FK and GDNF or NTN, but not each alone, promoted nuclear translocation of activated ERK1/2 at 6 h (Figure 3.8B), a process critical for growth factor induced transcriptional activation and neuronal differentiation (*158*). These observations suggested the possibility that the late phase of ERK1/2 activation may play an essential role in neurite outgrowth induced by FK and NTN through GFRα2b. To examine this possibility, we adopted the same experimental approach described in Figure 3.3. PC12-GFRα2b cells were incubated with U0126 1 h before (-1 h), together (0 h), 1 h after (1 h) or 3 h (3 h) after the co-treatment of NTN and FK (Figure 3.8C). Pre-incubation with U0126 (1 h before) completely abolished ERK1/2 activation over 6 h period, and dramatically inhibited NTN and FK-induced neurite outgrowth (Figure 3.8D). U0126 added 1 h or 3 h after co-treatment of NTN and FK effectively inhibited ERK1/2 activation at 6 h and significantly blocked neurite outgrowth, supporting the notion that the late phase of ERK1/2 activation was also required for NTN and FK-induced neurite outgrowth. Similar to NTN activated GFRα2a and GFRα2c, inhibiting ERK1/2 activation after 12 h of ligand stimulation failed to impair neurite outgrowth, providing further evidence in support of a restricted temporal event controlling neuritogenic signal transduction.

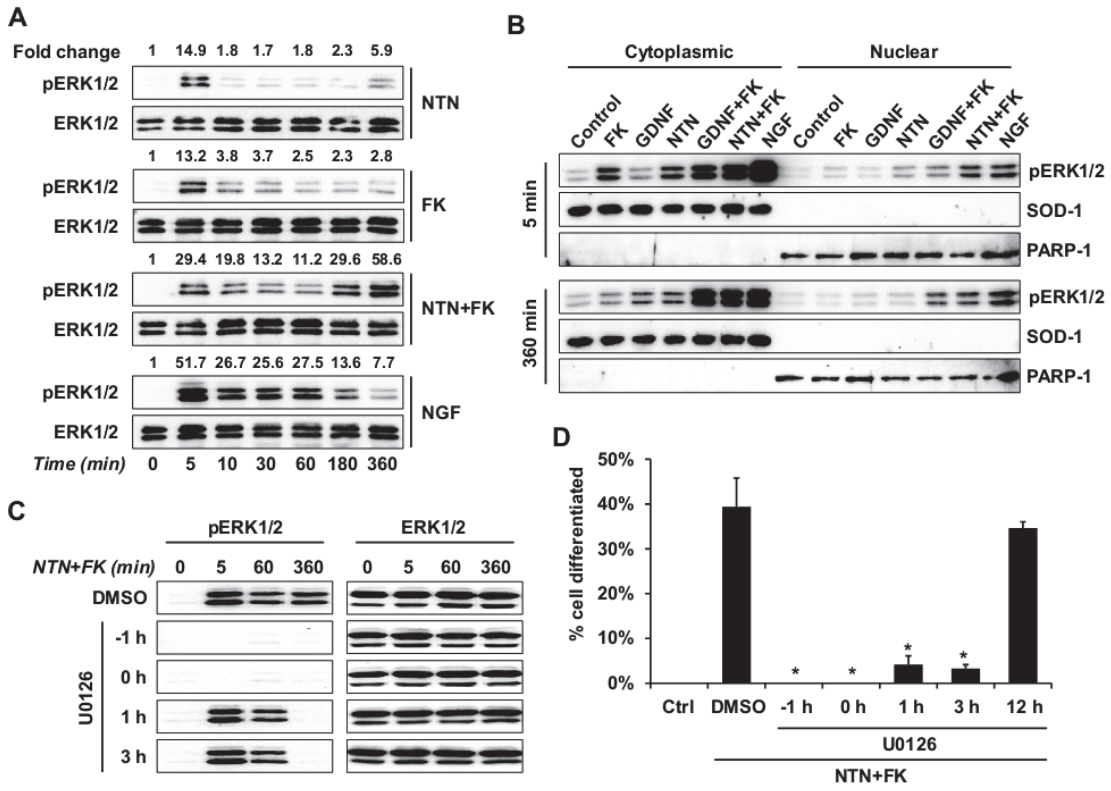

Figure 3.8 Forskolin cooperated with NTN to promote biphasic ERK1/2 activation required for pERK1/2 nuclear translocation and neurite outgrowth in PC12 cells expressing GFRα2b. (A) Biphasic ERK1/2 activation and (B) nuclear translocation of activated ERK1/2 were induced by co-treatment of NTN (50 ng/ml) with FK (10 μM). NGF was used as positive control for induction of sustained activation and nuclear translocation of ERK1/2. Phosphorylation levels of ERK1/2 were examined by Western blotting and fold changes over control were semi-quantified. SOD-1 and PARP-1 served as specific markers for cytoplasmic and nuclear proteins, respectively. The bands of expected molecular weights were presented. (C) Specific inhibition of late phase ERK1/2 activation. Cells were treated with NTN and FK for the indicated periods of time with (*U0126*) or without (*DMSO*) U0126. U0126 was added 1 h before (*-1 h*), together (*0 h*), 1 h after (*1 h*) or 3 h after (*3 h*) NTN and FK stimulations. (D) Effect of U0126 added at different time points on NTN and FK-induced neurite outgrowth. Cells were incubated for 48 h from the time NTN and FK were added and the number of cells differentiated was determined. Percentage of cells differentiated was presented as Mean ± S.E.M. of at least three biological replicates. U0126 added 12 h after (*12 h*) NTN and FK stimulation has no inhibitory effect on neurite outgrowth. * $p < 0.05$, compared to NTN and FK treatment without U0126.

3.2.5 Cooperation of cAMP signaling with NTN is mediated by PKA but not Epac

We similarly investigated the role of specific cAMP effector in mediating the cooperation of FK and NTN, using specific Epac and PKA agonist 2-Me-cAMP and 6-Bnz-cAMP. As postulated, co-treatment of NTN with 50-200 μM of 6-Bnz-cAMP significantly promoted neurite outgrowth in PC12-GFRα2b cells in a dose dependent manner (Figure 3.9A and B). In contrast, similar treatments with 2-Me-cAMP had little effects on neurite outgrowth. In agreement with the neurite outgrowth analyses, FK and 6-Bnz-cAMP but not 2-Me-cAMP cooperated with NTN to promote biphasic and sustained (up to 6 h) ERK1/2 activation (Figure 3.9C). The specific role of PKA was further supported by the observations that PKA inhibitor H89 significantly impaired both sustained ERK1/2 activation (Figure 3.9D and E) and neurite outgrowth (Figure 3.9F). These results demonstrated the involvement of PKA but not Epac in the cooperation of cAMP signaling with NTN-GFRα2b signaling to promote neurite outgrowth. Similar to GFRα2a and 2c, pre-treatment of ActD or Chx also significantly impaired ERK1/2 activation (Figure 3.10A, B) and neurite outgrowth (Figure 3.10C) induced by FK and NTN co-treatment of GFRα2b, suggesting the involvement of *de novo* transcription and translation in FK and NTN neurite synergy.

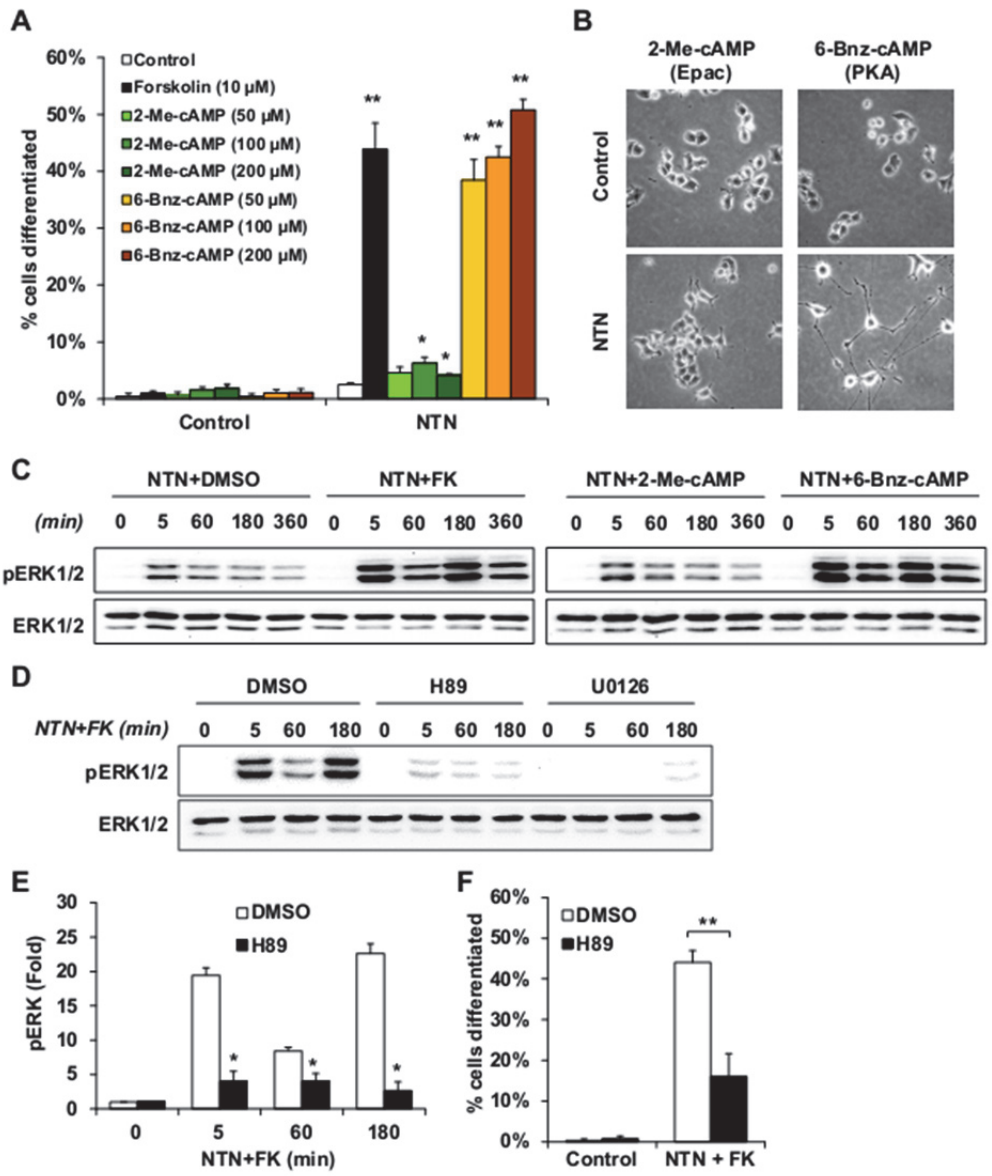

Figure 3.9 PKA but not Epac was the cAMP effector for cooperation of FK and NTN in PC12 cells expressing GFRα2b. (A) Dose dependent cooperation of 6-Bnz-cAMP but not 2-Me-cAMP with NTN to induce neurite outgrowth. Cells were co-stimulated with NTN (50 ng/ml) and the indicated concentrations of FK, 2-Me-cAMP or 6-Bnz-cAMP for 48 h. Percentage of cells differentiated was presented as Mean ± S.E.M. of at least three biological replicates. * $p < 0.05$ and ** $p < 0.001$, compared with NTN treatment alone. (B) Representative graphs of cells stimulated with NTN and 200 μM 2-Me-cAMP or 200 μM 6-Bnz-cAMP. (C) 6-Bnz-cAMP but not 2-Me-cAMP cooperated with NTN to induce biphasic and sustained ERK1/2 activation. Cells were stimulated with NTN alone or together with 10 μM FK, 200 μM 2-Me-cAMP or 200 μM 6-Bnz-cAMP for the indicated periods of time. Phosphorylation levels of ERK1/2 were analysed by Western blotting. (D) Effect of PKA inhibitor H89 on biphasic ERK1/2 activation induced by NTN and FK. Cells were co-treated with NTN and FK in the presence or absence of 10 μM H89 or 10 μM U0126 for the indicated periods of time. ERK1/2 phosphorylation was examined by Western blotting. (E) Fold changes of ERK1/2 phosphorylation were quantified by densitometry and presented as Mean ± S.D. (n = 3). * $p < 0.05$, compared with NTN and FK treatment without H89. (F) Effect of H89 on neurite outgrowth induced by NTN and FK. Cells were co-treated with NTN and FK in the presence or absence of H89 for 48 h. Percentage of cells differentiated was presented as Mean ± S.E.M. of at least three biological replicates. ** $p < 0.001$, compared with NTN and FK treatment without H89.

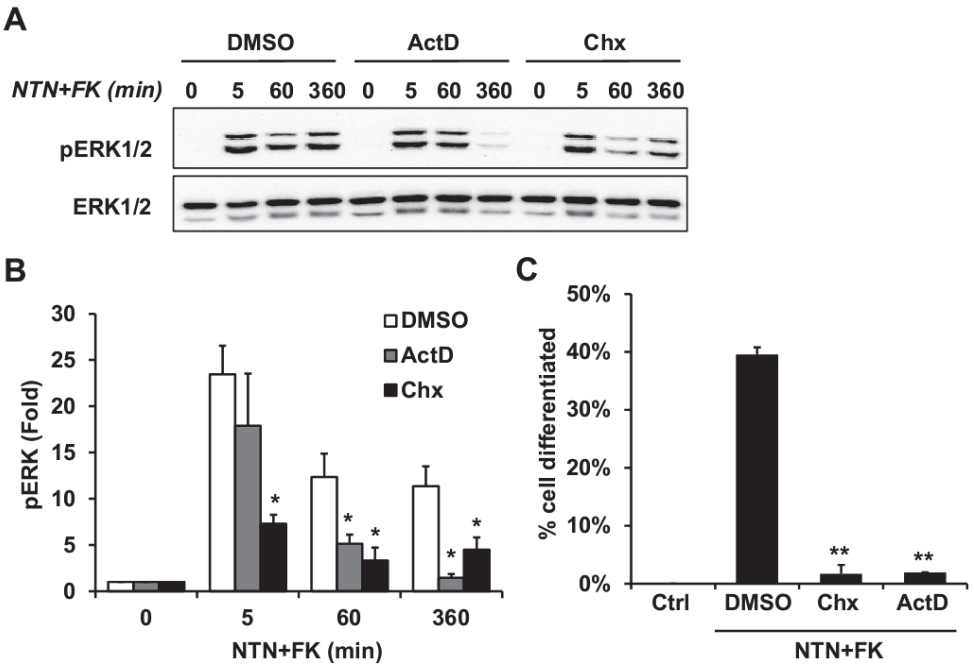

Figure 3.10 Forskolin and NTN-induced late phase of ERK1/2 activation and neurite outgrowth through GFRα2b required *de novo* transcription and translation. (A) Effect of ActD and Chx on NTN and FK-induced ERK1/2 activation. Cells were treated with 50 ng/ml NTN and FK (10 μM) in the presence or absence of 2 μg/ml ActD or 10 μg/ml Chx for the indicated periods of time. (B) Fold changes of ERK1/2 phosphorylation levels were quantified by densitometry and presented as Mean ± S.D. (n = 3). * $p < 0.05$, compared with NTN and FK treatment without inhibitors at each time point. (C) Effects of ActD and Chx on NTN and FK-induced neurite outgrowth. Cells were treated with NTN and FK in the presence or absence of inhibitors for 24 h. Percentage of cells differentiated was presented as Mean ± S.E.M. of at least three biological replicates. ** $p < 0.001$, compared with NTN and FK treatment without inhibitors.

3.2.6 Cyclic AMP and PKA signaling cooperates with NTN to promote neurite outgrowth in BE(2)-C cells

We next validated the contribution of cAMP-PKA signaling in NTN-induced neurite outgrowth in BE(2)-C, a human neuroblastoma cell line that endogenously expresses both GFRα2a and GFRα2b (*6*). We have previously shown that NTN was unable to induce significant neurite outgrowth in these cells, due to the inhibitory activity of GFRα2b (*6*). Similarly, FK, 2-Me-cAMP and 6-Bnz-cAMP also failed to promote neurite outgrowth in BE(2)-C cells. Interestingly, co-treatment of NTN with FK and 6-Bnz-cAMP but not 2-Me-cAMP resulted in extensive neurite outgrowth in BE(2)-C cells (Figure 3.11A and B), which recapitulated the specific cooperative

effect of NTN and cAMP-PKA but not Epac pathways in PC12 cells. Furthermore, we have previously shown that NTN was able to induce neurite outgrowth in BE(2)-C cells through GFRα2a, when GFRα2b was specifically knocked down (*6*). To examine if PKA signaling was involved in NTN-GFRα2a induced neurite outgrowth, BE(2)-C cells with GFRα2b knockdown were pre-treated with PKA inhibitors H89 and Rp-8-Br-cAMPS before NTN stimulation. As expected, in the absence of PKA inhibitors, NTN promoted neurite outgrowth in cells with GFRα2b knockdown (si-GFRα2b) (Figure 3.11C and D). H89 at even lowered doses resulted in significant toxicity in BE(2)-C cells, and hence was excluded from the study. U0126 and the other PKA inhibitor Rp-8-Br-cAMP significantly reduced NTN-GFRα2a induced neurite outgrowth in GFRα2b knockdown cells (Figure 3.11C and D). These findings lend further support to the idea that cAMP-PKA signaling was essential for ligand-induced neurite outgrowth through GFRα2 isoforms.

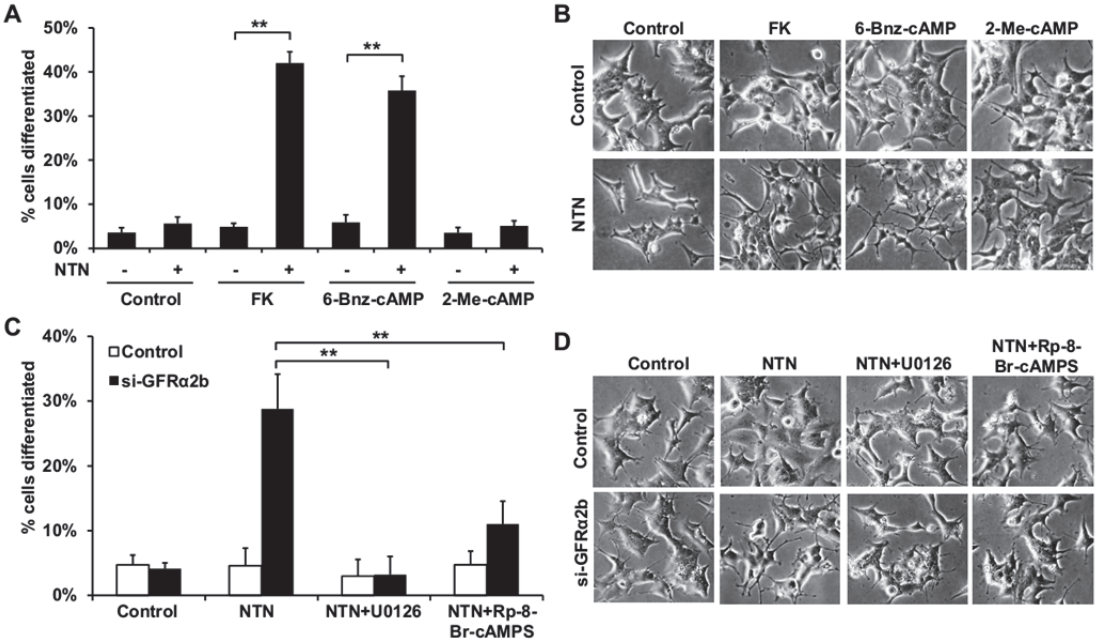

Figure 3.11 Cyclic AMP and PKA signaling was required for NTN-induce neurite outgrowth in BE(2)-C cells. (A) Quantification of neurite outgrowth induced by NTN, FK and cAMP analogs. BE(2)-C cells were treated with 10 μM FK, 200 μM 2-Me-cAMP or 200 μM 6-Bnz-cAMP in the presence or absence of 50 ng/ml NTN for 96 h. (B) Representative pictures of BE(2)-C cells stimulated with NTN, FK and cAMP analogs. (C) Quantification of neurite outgrowth induced by NTN in BE(2)-C cells with GFRα2b knockdown. BE(2)-C cells were transfected with either control or GFRα2b siRNA and treated with 50 ng/ml NTN in the presence or absence or 10 μM U0126 or 200 μM Rp-8-Br-cAMPS for 96 h. (D) Representative pictures of control and GFRα2b knockdown BE(2)-C cells stimulated by NTN with or without inhibitors. Percentage of cells differentiated was presented as Mean ± S.E.M. of at least three biological replicates. ** $p < 0.001$.

Section 3.3 Discussion

This study demonstrated the essential role of cAMP-PKA but not cAMP-Epac signaling in NTN-induced neurite outgrowth through GFRα2 isoforms (Figure 3.12). While ligand activation of GFRα2a and GFRα2c regulated PKA-dependent late phase of ERK1/2 activation and neurite outgrowth, ligand activation of GFRα2b required the cooperation of PKA agonists to promote neurite outgrowth. The functional interaction of NTN and cAMP-PKA signaling in promoting neurite outgrowth was mediated by transcription and translation-dependent late phase ERK1/2 activation. This synergistic effect of PKA agonist and NTN may extend the benefits of the use of NTN in clinical studies (*159, 160*).

Both GDNF and NTN are known to regulate neurite outgrowth through GFRα2 in various neuronal systems (*6, 161, 162*). GFRα2 is alternatively spliced into at least three isoforms (*104, 105*) and are expressed in all parts of the human nervous system examined, suggestive of their physiological relevance (*6*). Recently, we have shown that NTN induced similar rapid ERK1/2 activations in neuroblastoma cells expressing these GFRα2 isoforms but yet resulted in distinct neuritogenic outcomes (*6*). Consistent with our previous report, ligand stimulations of all three GFRα2 isoforms in PC12 cells resulted in similar early phase of ERK1/2 activation that peaked at 5 min. Interestingly, GFRα2a and GFRα2c (but not GFRα2b), were able to mediate phosphorylation of the major cAMP target CREB, a late phase of ERK1/2 activation (3-6 h) and neurite outgrowth upon ligand stimulations. This is consistent with the observations that phosphorylation of CREB and sustained activation of ERK1/2 are events necessary for neurite outgrowth in PC12 cells (*155, 163*), and suggested that such distinct signaling activation may underlie the differential neuritogenic activities of GFRα2 isoforms.

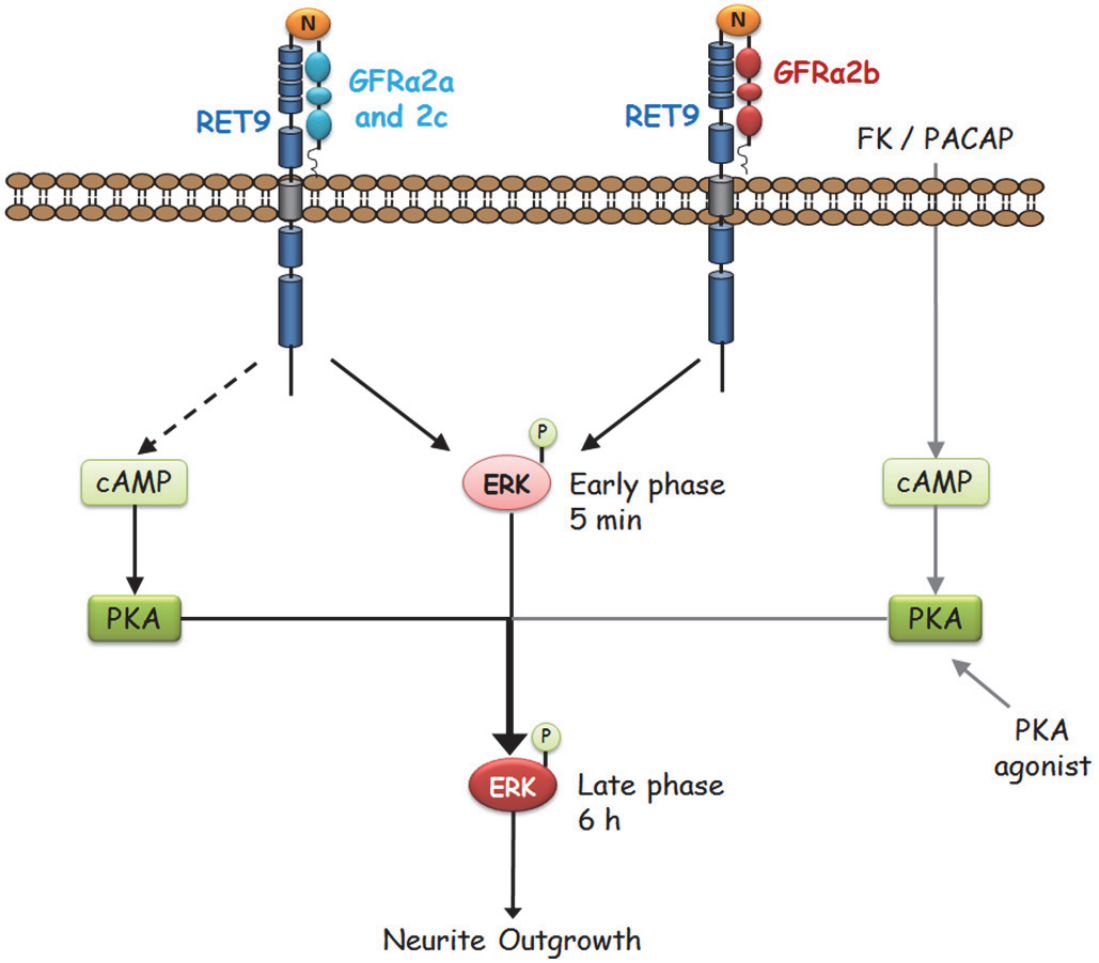

Figure 3.12 A schematic illustration of cAMP-PKA signaling in GFL-induced neurite outgrowth through GFRα2 isoforms. Upon GFL (GDNF or NTN) stimulations, GFRα2a and GFRα2c promote biphasic and sustained ERK1/2 activation and neurite outgrowth. The late phase of ERK1/2 activation is dependent on cAMP-PKA signaling and *de novo* gene expression. Ligand-activated GFRα2b only induces transient ERK1/2 activation and requires exogenous cAMP-PKA signaling to promote the late phase of ERK1/2 activation and neurite extensions.

Consistent with previous reports, activation of cAMP pathway alone failed to induce significant neurite extensions in PC12 cells (*148, 151, 164, 165*). Interestingly, GFRα2a and GFRα2c induced neurite outgrowth in PC12 cells was dependent on cAMP signaling and was enhanced by co-treatment of cAMP agonists. More importantly, while each pathway on its own failed to induce significant neurite outgrowth, the cooperation between cAMP agonists and ligand-activated GFRα2b induced extensive neurite outgrowth. This synergy between NTN and cAMP signaling

was further validated in BE(2)-C cells, which endogenously express both GFRα2a and GFRα2b. Conversely, in BE(2)-C cells with GFRα2b knocked down, NTN-induced neurite outgrowth through GFRα2a was significantly inhibited by antagonist against cAMP signaling. Taken together, these results suggest that the differential regulation of cAMP signaling may be the key event underlying the divergent neuritogenic effect of GFRα2b compared to GFRα2a and GFRα2c.

While the essential role of cAMP signaling in neurite outgrowth is well established, the specific involvement of cAMP effectors PKA or Epac is still a subject of debate. Using small molecule inhibitors, a number of studies have shown that PKA signaling is specifically required for PC12 neurite outgrowth induced by NGF (*145, 152, 165*), secretin (*149*) and panaxynol (*147*). In addition, exogenous PKA signaling is able to cooperate with non-neuritogenic stimuli (EGF and KCl) to promote neurite outgrowth in PC12 cells (*151, 154, 164*). However, recent evidence suggested that cAMP-dependent neurite outgrowth in PC12 and DRG neurons can also be mediated by Epac (*166-168*). In this study, we have provided ample evidence that favoured PKA but not Epac to be the cAMP downstream effector in promoting neurite outgrowth in ligand-activated GFRα2 isoforms. These results not only support the pivotal role of cAMP-PKA signaling in neurotrophic factor-induced neurite outgrowth, but also suggest PKA as the specific candidate therapeutic target for axonal regeneration (*134*).

Sustained activation of ERK1/2 is critical to neurite outgrowth of neuronal cells, including PC12 cells (*158*). The sustained activation is thought to result in nuclear translocation of the activated ERK1/2 (*152, 163, 169, 170*), a process important for neuronal differentiation and plasticity (*158, 171*). Consistent with these reports, NTN-induced neurite outgrowth through GFRα2 was accompanied by both activation and nuclear translocation of the late phase of ERK1/2, which was dependent on both PKA and *de novo* gene expression. Recently, thrombin stimulation of vascular

smooth muscle cells was found to exhibit a similar biphasic ERK1/2 phosphorylation and the activation of late phase ERK1/2 also required *de novo* transcription and translation (*172*). Interestingly, we found that cAMP agonist specifically regulated CREB activation, *c-fos* expression and S6 ribosomal protein phosphorylation (data not shown), consistent with the roles of PKA in mediating *de novo* RNA and protein synthesis. These findings suggest that cAMP-PKA signaling may contribute to NTN-mediated neurite outgrowth by promoting *de novo* gene expression, which is required for the late phase of ERK1/2 activation.

Structurally, GFRα2 isoforms differ at the extreme N-terminus (D1) (*2, 4*), which was shown to be dispensable for ligand binding. However, a recent study found that the distal end of the GFRα1 N-terminus (D1) interacted with RET at multiple sites, strongly support its biological relevance (*65, 173*). It is reasonable to hypothesize that the differences in the N-terminus domains in GFRα2 influence the overall conformation of the GFL-GFRα2-RET ligand-receptor complex and lead to differential activation of RET kinase domains and recruitment of distinct adaptor molecules, a possibility currently under investigation.

In conclusion, this study demonstrated an essential role of cAMP-PKA signaling in NTN-induced neurite outgrowth and suggested this to be an underlying mechanism contributing to the differential neuritogenic activities of GFRα2 isoforms. The findings on specific roles of PKA but not Epac in promoting biphasic ERK1/2 activation and neurite outgrowth provided further insights on the molecular mechanisms underlying the synergistic effects of cAMP and GDNF signaling in neuronal outgrowth.

Chapter 4 Specific alternatively spliced isoforms of GFRα2 and RET mediate Neurturin induced mitochondrial STAT3 phosphorylation and neurite outgrowth

Section 4.1 Introduction

NTN-GFRα2 signaling is crucial for neuronal development. Mice lacking NTN and GFRα2 signaling suffer from deficits in target innervations in both sympathetic (*174*) and parasympathetic neurons (*175-177*). In GFRα2 knockout mouse, NTN stimulation failed to initiate axonal outgrowth of DRG neurons, supporting the physiological role of GFRα2 in neuronal differentiation (*178*). Furthermore, NTN has also been shown to exert potent protective and / or restorative effects on midbrain dopaminergic neurons, thus leading to its clinical trial for Parkinson's disease (*159, 179*). However, the signaling network which mediates the neurotrophic functions of NTN-GFRα2 has yet to be fully elucidated.

Signal Transducer and Activator of Transcription 3 (STAT3) is a classic transcription regulator that mediates a myriad of biological functions in multiple cellular systems (*180-182*). In neuronal systems, STAT3 plays critical roles during neural development and mediates the protective and regenerative effects of multiple neurotrophic factors upon nerve injuries (*180*). The canonical pathway of STAT3 activation involves ligand induced phosphorylation of tyrosine^{705} residue (P-Tyr-STAT3), resulting in STAT3 nuclear translocation and activation of target gene transcription (*183*). STAT3 can also be phosphorylated at serine^{727} (P-Ser-STAT3), but its functional significance remains controversial. Serine phosphorylation can enhance or suppress the transcriptional activity of tyrosine phosphorylated STAT3 in a cell context dependent manner (*184-187*). More recently, STAT3 has also been shown to localize to the mitochondria and exert functions independent of its transcriptional activities (*188-191*).

Multiple reports have observed GFL independent activation of STAT3 by oncogenic RET. Depending on the type of mutations, different oncogenic RET (PTC, MEN2 or FMTC) were capable of inducing either specific tyrosine phosphorylation or dual tyrosine and serine phosphorylation of STAT3 (*192, 193*). In addition, the signaling pathways mediating oncogenic RET induced STAT3 phosphorylation vary across cell types. In ARO cells, the intrinsic kinase activity of oncogenic RET alone was found to be sufficient to induce STAT3 phosphorylation (*194*). In other cell models, combinations of JAK, Src and MAPK pathways were found to mediate STAT3 activation (*195*). Surprisingly, no report has shown the activation of STAT3 by wild type RET in a GFL dependent manner. On the contrary, GDNF was shown to suppress activation of STAT3 in models such as spermatogonial stem cells (*196*).

In this study, we tested the hypothesis that STAT3 can be activated by NTN-GFRα2 signaling and may in turn mediate the neuritogenic functions of NTN. STAT3 was found to be serine mono-phosphorylated upon NTN stimulation. The involvement of specific GFRα2 and RET isoforms in NTN induced P-Ser-STAT3 was further investigated in multiple cell models. Moreover, serine but not tyrosine dominant negative mutant of STAT3 was found to impair NTN induced neurite outgrowth. Interestingly, P-Ser-STAT3 was found to be localized to the mitochondria but not the nucleus upon NTN stimulation. The mitochondrial P-Ser-STAT3 was further shown to be intimately involved in NTN induced neurite outgrowth. To the best of our knowledge, this is the first report that demonstrated a GFL induced phosphorylation of serine residue of STAT3 through the activation of wild type GFRα and RET receptors. Our findings further illustrated the distinct functions of GFRα2 and RET isoforms and demonstrated the transcription-independent mechanism whereby mitochondria localized STAT3 mediates NTN induced neurite outgrowth.

Section 4.2 Result

4.2.1 NTN induced STAT3 phosphorylation in cortical neuron expressing multiple receptor isoforms

NTN has been reported to exert neurotrophic effects on cortical neurons (*197*), which express high levels of GFRα2 (*6*), making these neurons a suitable model to investigate NTN function and signaling. Primary cortical neurons from embryonic day 18 rat were harvested and the transcript expressions of GFRα2 and its co-receptors RET and NCAM were quantified with RT-qPCR, using GAPDH as normalizer. All three isoforms of GFRα2, GFRα2a, 2b and 2c were expressed at comparable levels in the cultured primary cortical neurons (Figure 4.1A). The co-receptor RET9 isoform was found to be expressed at slightly higher level than RET51, whereas NCAM expression was about ten-fold higher than that of RET9. NTN stimulation of cultured primary cortical neurons induced rapid phosphorylation of MAP kinase ERK. More interestingly, NTN treatment resulted in serine but not tyrosine phosphorylation of STAT3 (Figure 4.1B). These data demonstrated that STAT3 can be activated by GFL and may be mediated by distinct combinations of receptor isoforms.

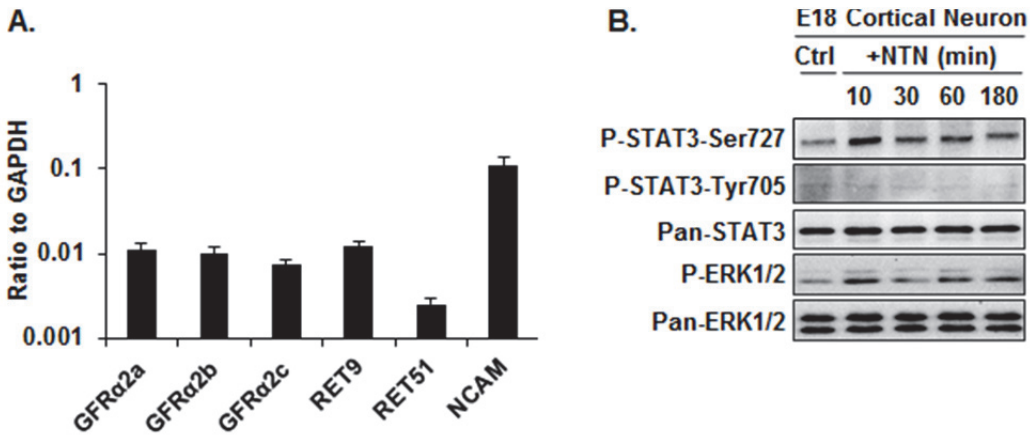

Figure 4.1 NTN induced sustained STAT3 serine^{727} but not tyrosine^{705} phosphorylation in rat embryonic cortical neurons. A. Total RNA was extracted from E18 rat embryonic cortical neurons. The transcript expressions of GFRα2, RET isoform and NCAM were quantified by RT-qPCR with standard curves. The expression copy numbers were normalized and presented as ratio to internal reference gene GAPDH. B. The isolated cortical neurons were cultured *in vitro* for 72 h before NTN stimulation (100 ng/ml) for up to 3 h. Total cell lysates were collected and the protein expression analysed by immunobloting, the bands of expected molecular weights were presented.

4.2.2 GFRα2c but not 2a or 2b mediated NTN induced STAT3 serine phosphorylation in Neuro2A cells

To test the hypothesis that NTN induced P-Ser-STAT3 is mediated through specific GFRα2 isoforms, Neuro2A cells were engineered to stably expressing either GFRα2a, 2b or 2c receptor isoforms (Figure 4.2A). Neuro2A cells endogenously express both RET and NCAM at levels comparable to that of primary cortical neurons but have negligible levels of GFRα2, making these cells an ideal model to investigate GFRα2 isoform function. These engineered Neuro2A cells were stimulated with NTN and the phosphorylation of STAT3 were measured. Consistent with the observation in primary cortical neurons, NTN did not induce tyrosine phosphorylation of STAT3 (Figure 4.2B&D). Surprisingly, NTN stimulation of GFRα2c but not 2a or 2b was found to induce sustained serine phosphorylation of STAT3 (Figure 4.2B&C), suggesting NTN activation of STAT3 was mediated by specific receptor isoform. Since STAT3 is known to mediate the neuritogenic function of neurotrophic factors, we tested if STAT3 is involved in NTN induced neurite outgrowth. Wild type and mutant STAT3 were transiently expressed in Neuro2A-GFRα2c cells using vector constructs co-expressing enhanced green florescence protein (eGFP) as a marker for gene transfer. STAT3 serine (S727A) but not tyrosine (Y705F) dominant negative mutant was found to significantly attenuate NTN induced neurite outgrowth (Figure 4.2E&F). In addition, expression of the STAT3 serine constitutive active mutant (S727E) resulted in a significant enhancement of neurite outgrowth, lending further evidence that P-Ser-STAT3 was involved in NTN induced neurite outgrowth.

4.2.3 RET but not NCAM mediated STAT3 serine phosphorylation in Neuro2A cells

Both RET and NCAM have been shown to transduce GFL signal in the presence of GFRα receptors. The involvement of these two receptors in NTN induced STAT3 phosphorylation was subsequently investigated. Neuro2A cells were transiently transfected with siRNAs targeting RET or NCAM. Transcript expressions of RET and NCAM were profiled and both siRNAs were found to specifically suppress the respective target mRNA level by more than 80% within 24 h (Figure 4.3A). Transfection of control siRNA resulted in negligible change in RET or NCAM levels. N2A-GFRα2c cells transfected with RET or NCAM siRNAs were treated with NTN and compared to control siRNA transfected cells. Upon NTN stimulation, sustained STAT3 serine phosphorylation was observed in all but RET-siRNA transfected cells (Figure 4.3B&C). Similarly, NTN induced ERK phosphorylation was also abolished by RET siRNA but not NCAM or control siRNA (Figure 4.3D&E). Furthermore, NTN induced neurite outgrowth in N2A-GFRα2c cells was attenuated by RET-siRNA but not the others (Figure 4.3F&G). Collectively, these data demonstrated that RET but not NCAM is involved in NTN induced STAT3 phosphorylation and neurite outgrowth in Neuro2A cells.

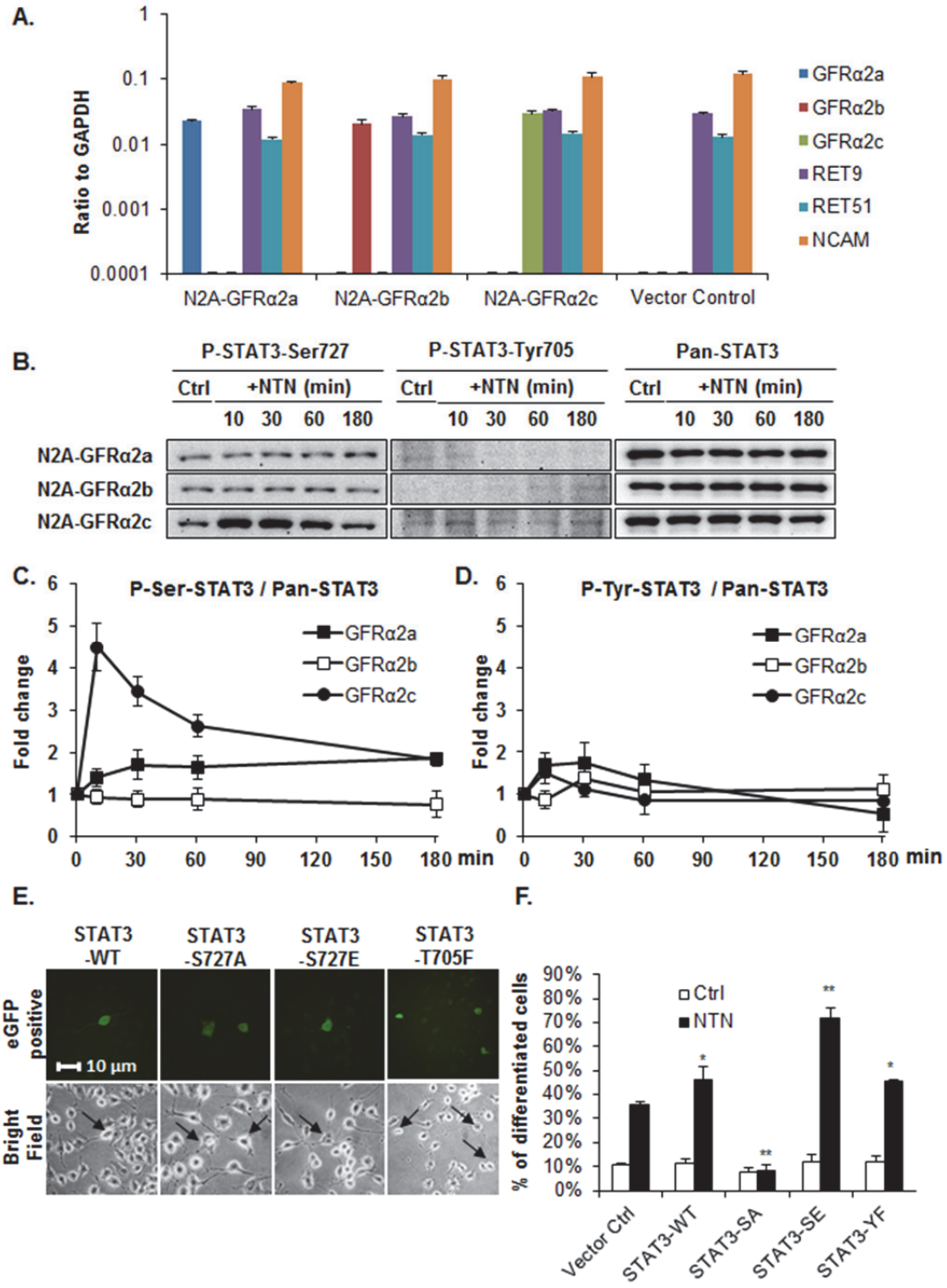

Figure 4.2 GFRα2c but not 2a or 2b mediated NTN induced STAT3 serine phosphorylation in Neuro2A cells. A. Total RNA was extracted from Neuro2A cells engineered to stably express different GFRα2 isoforms. The transcript expressions of GFRα2a, 2b, 2c, RET9, 51 and NCAM were quantified by RT-qPCR with standard curves. The expression copy numbers were normalized and presented as ratio to internal reference gene GAPDH. B. Neuro2A-GFRα2a, 2b, 2c cells were stimulated with NTN (50 ng/ml) for up to 3 h. Total cell lysates were collected and the protein expression analysed by immunobloting. C-D. NTN induced P-Ser-STAT3, P-Tyr-STAT3 were normalized to Pan-STAT3 and presented as fold change to control cells. E-F. Neuro2A-GFRα2c cells were transiently transfected with wild-type and mutant STAT3 and stimulated with NTN to induce

neurite outgrowth. More than 60 successfully transfected cells (eGFP expressing) was analysed per biological replicate per condition and the number of bearing neurite twice the cell body length was scored. Representative images are shown in E and the analysed data in F. Significant differences between the percentages of neurite bearing cells in control and STAT3 mutant expressing cells were calculated using the paired Student's t-test. A value of $p<0.05$ was considered significant (**$p<0.01$; *$p< 0.05$).

4.2.4 RET9 but not RET51 was responsible for STAT3 serine phosphorylation in PC12 cells

RET9 and RET51 are two predominant isoforms generated by alternative splicing of RET pre-mRNA. We further tested if NTN induced STAT3 phosphorylation was mediated by a particular RET isoform, using another well-established neuronal model PC12 cells. The rat pheochromocytoma PC12 cells expressed negligible amount of both GFRα2 and RET, making it a suitable model to test the combinatorial interactions of NTN and its receptor isoforms. PC12 cells were engineered to stably express combinations of GFRα2a, 2b or 2c with either RET9 or RET51. The specific expressions of the desired receptor isoform combination were confirmed by RT-qPCR (Figure 4.4A). These cells were then stimulated with NTN and STAT3 phosphorylation was monitored. Consistent with the observation in Neuro2A cells, NTN stimulation of GFRα2a or 2b expressing PC12 cells did not induce significant STAT3 phosphorylation (Figure 4.4B). Interestingly, the combinatorial interaction of GFRα2c with RET9 but not RET51 resulted in sustained STAT3 serine but not tyrosine phosphorylation (Figure 4.4B-D). Collectively, the data from Neuro2A and PC12 cells strongly supported the hypothesis that NTN activation of STAT3 was mediated by specific combinations of GFRα2 and RET receptor isoforms.

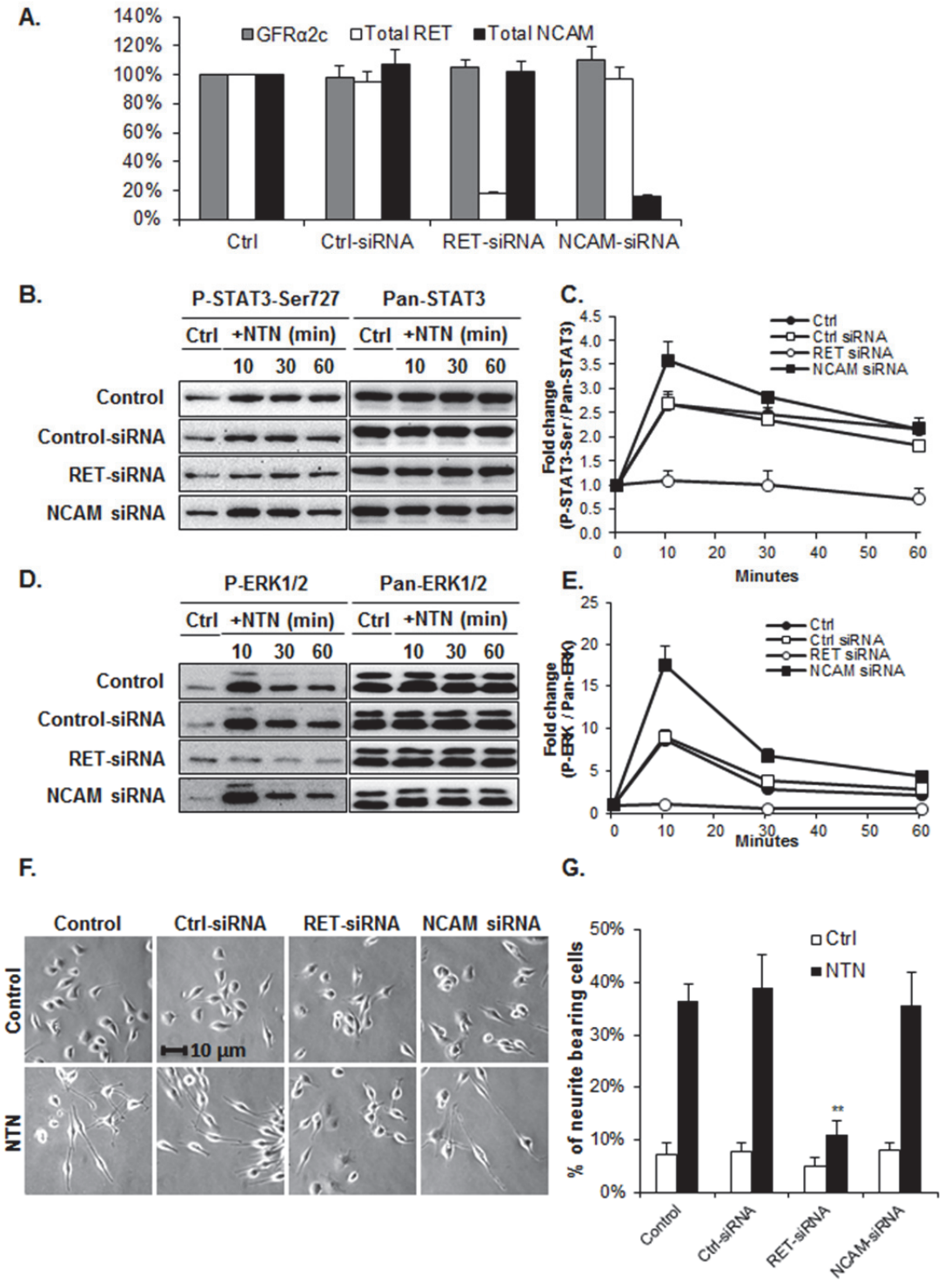

Figure 4.3 RET but not NCAM mediated NTN induced STAT3 serine phosphorylation in Neuro2A cells. A. Total RNA was extracted from Neuro2A- GFRα2c cells transiently transfected with siRNA duplex specific for RET, NCAM or control siRNA. The transcript expressions of GFRα2c, RET and NCAM quantified by RT-qPCR with standard curves and normalized by GAPDH. The effects of different siRNAs on these three genes are expressed as percentage knockdown from control cells. B-G. Neuro2A-GFRα2c transiently transfected with different siRNAs were stimulated with NTN (50 ng/ml). NTN induced P-Ser-STAT3 (B-C), P-ERK (D-E) and neurite outgrowth (F-G) were analysed. Significant differences between the percentages of neurite bearing cells in control and siRNA transfected cells were calculated using the paired Student's t-test. A value of $p<0.05$ was considered significant (**$p<0.01$; *$p<0.05$).

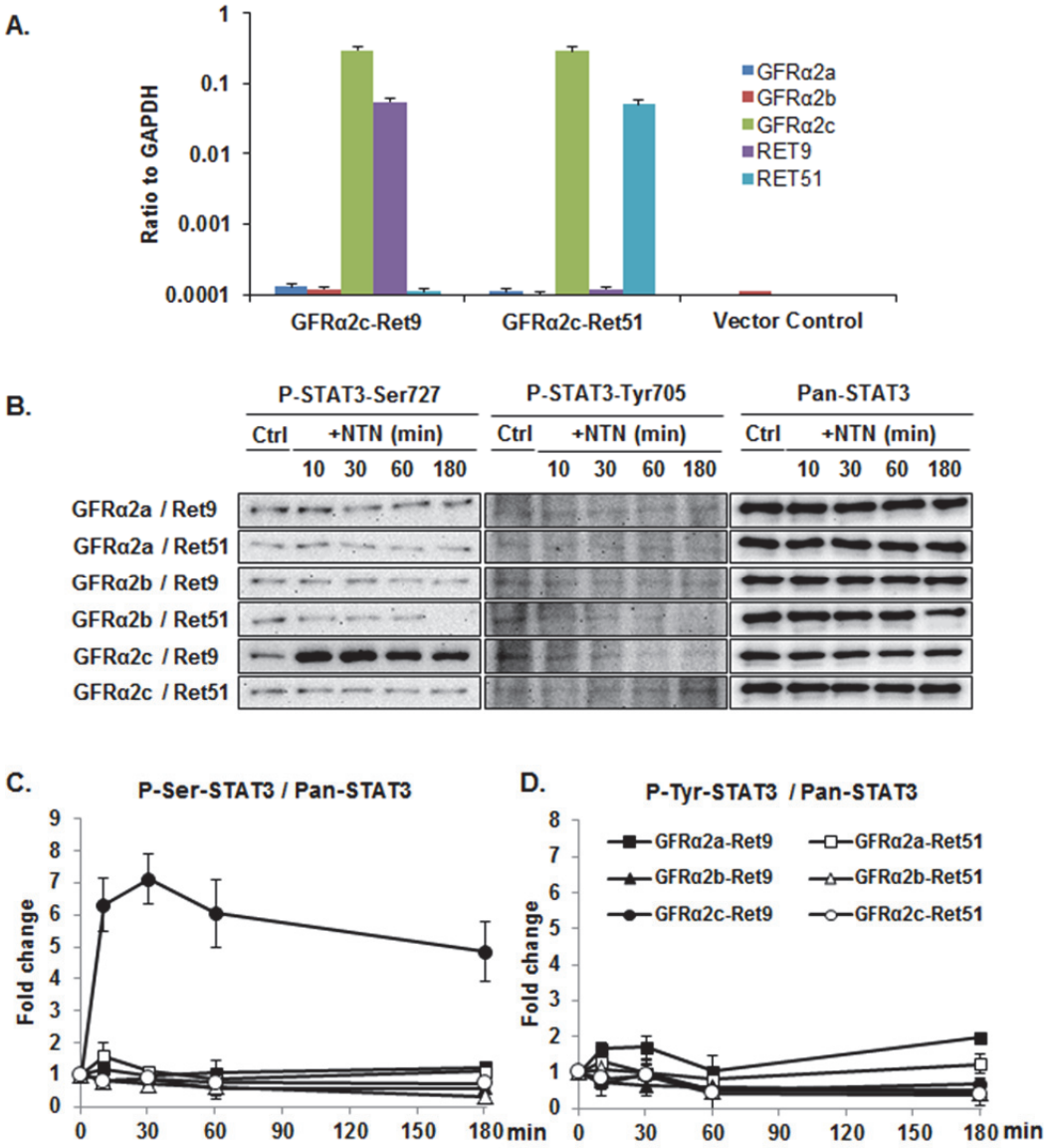

Figure 4.4 RET9 but not RET51 was responsible for NTN induced STAT3 serine phosphorylation in PC12 cells. A. Total RNA was extracted from PC12 cells engineered to stably express combinations of GFRα2 and RET isoforms. The transcript expressions of GFRα2a, 2b, 2c, RET9, 51 were quantified by RT-qPCR with standard curves. The expression copy numbers were normalized and presented as ratio to internal reference gene GAPDH. Shown here are the expression levels in vector control, GFRα2c-RET9 and GFRα2-RET51 cells. B. The engineered PC12 cells were stimulated with NTN (50 ng/ml) for up to 3 h. Total cell lysates were collected and the protein expression analysed by immunobloting. C-D. NTN induced P-Ser-STAT3, P-Tyr-STAT3 were normalized to Pan-STAT3 and presented as fold change to control cells.

4.2.5 STAT3 serine phosphorylation was regulated by Src and ERK

Multiple signaling pathways have been implicated in STAT3 serine phosphorylation. We subsequently investigated the involvement of Src, MAPKs (ERK, JNK and p38) and PKC in NTN induced STAT3 serine phosphorylation. N2A-GFRα2c and PC12-GFRα2c-RET9 cells were pretreated with established pharmacological inhibitors, and subsequently stimulated with NTN for varying periods of time. Interestingly, inhibition of Src (SU6656) and ERK (U0126) but not JNK (SP600125), p38 (SB203580) or PKC (Gö6983) was found to significantly attenuate NTN induced STAT3 serine phosphorylation, in both Neuro2A (Figure 4.5A&C) and PC12 cells (Figure 4.5B&D). Intriguingly, inhibition of Src and ERK but not JNK, p38 or PKC pathway attenuated NTN induced neurite outgrowth in Neuro2A (Figure 4.5E) and PC12 cells (Figure 4.5F). The correlation between the involvements of these pathways in NTN induced neurite outgrowth and STAT3 phosphorylation was suggestive of the role of STAT3 as a downstream mediator of neurite outgrowth.

Unexpectedly, RET9 but not RET51 was found to induce Src Y416 phosphorylation (Figure 4.6A&B) in PC12 cells. In addition, inhibition of Src attenuated RET9 mediated neurite outgrowth but not RET51 (Figure 4.6C&D). These data suggested that RET isoform involvement in specific phosphorylation of STAT3 may be explained by the differential activation of Src by RET9 but not RET51.

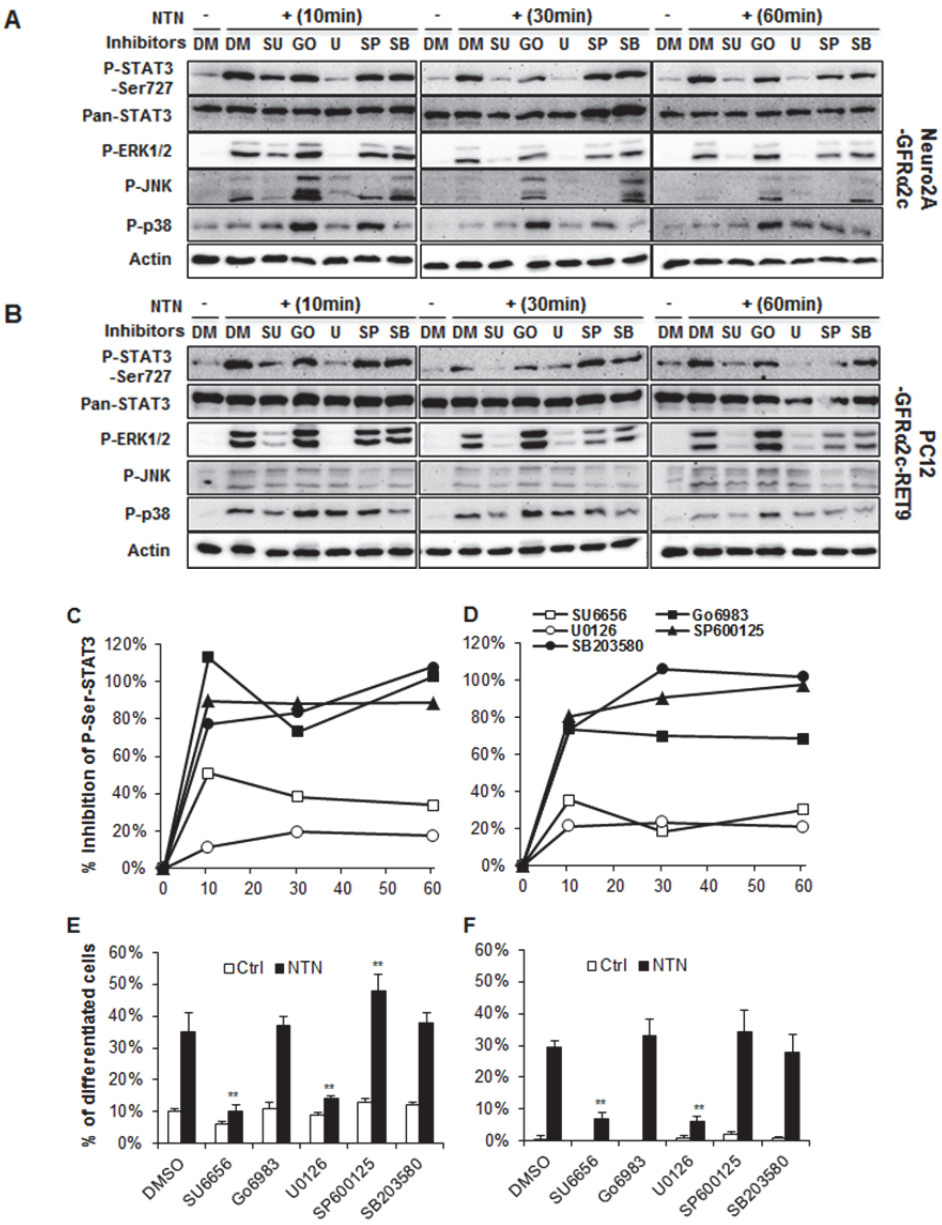

Figure 4.5 NTN induced STAT3 serine phosphorylation was regulated by Src and ERK. Neuro2A and PC12 cells were serum-deprived for 16 h and pre-treated with DMSO (DM, 0.1%, control), SU6656 (SU, 1 μM), Gö6983 (GO, 5 μM), U0126 (U, 10 μM), SP600125 (SP, 10 μM), and SB203580 (SB, 10 μM) for 1 h before stimulated with 50 ng/ml NTN in the presence of respective inhibitors. A-B. Total cell lysates were harvested from control and inhibitor treated cells after 10, 30 or 60 min of NTN stimulation and analysed by immunobloting, the bands of expected molecular weights were presented. C-D. Quantified P-Ser-STAT3 immunoblot intensity was normalized to respective Pan-STAT3 intensity. The percentage inhibition of NTN induced STAT3 serine phosphorylation by various signaling inhibitors was calculated as follows, % inhibition = (P-Ser-STAT3$_{DMSO}$ - P-Ser-STAT3$_{Inhibitor}$) / P-Ser-STAT3$_{DMSO}$ x 100%. E-F. Neuro2A and PC12 cells were stimulated with NTN for 24 and 48 h respectively in the presence of the inhibitors. The percentages of neurite bearing cells (differentiated cells) were counted to analyze the effect of various inhibitors on NTN induced neurite outgrowth. Significant differences between the percentages of differentiated cells in control and inhibitor treated cells were calculated using the paired Student's t-test. A value of $p<0.05$ was considered significant (**$p<0.01$; *$p< 0.05$).

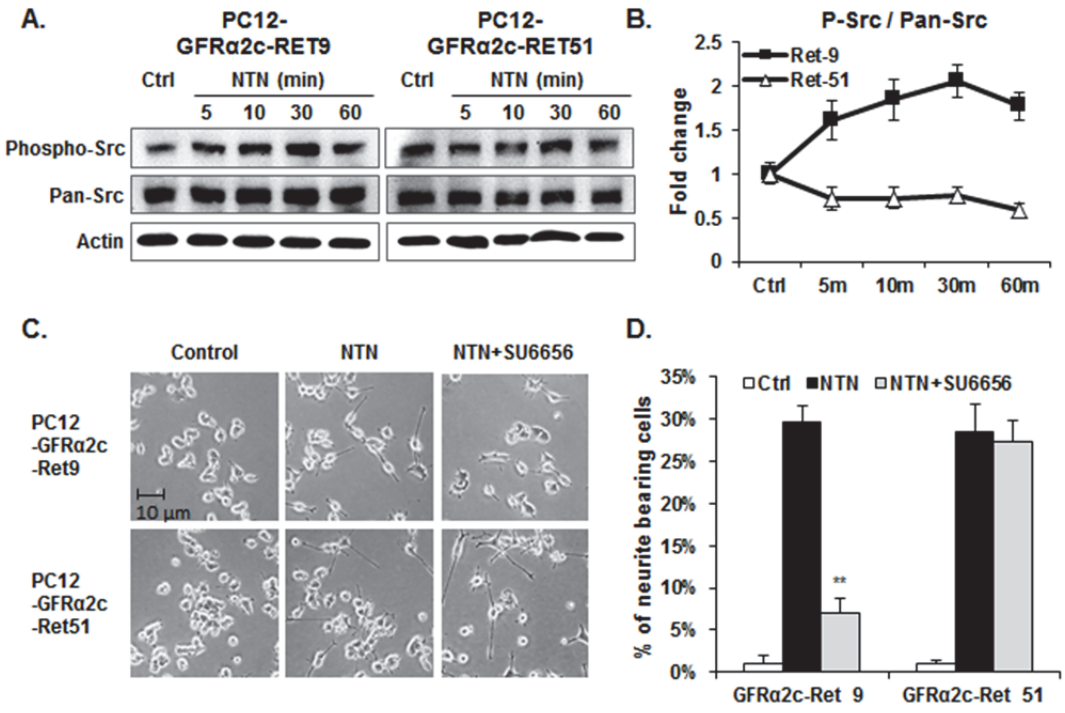

Figure 4.6 Src was involved in the neuritogenic function of RET9 but not RET51. A-B. Phosphorylation of Src was analysed in PC12-GFRα2c-RET9 and PC12-GFRα2-RET51 cells stimulated with 50 ng/ml NTN. P-Src levels were quantified and normalized to Pan-Src levels and expressed as fold change of NTN induced cells to control cells. The bands of expected molecular weights were presented. C-D. RET9 and RET51 cells were stimulated with NTN for 48 h in the presence of Src inhibitors SU6656. The percentages of neurite bearing cells (differentiated cells) were analysed. Significant differences between the percentages of differentiated RET and RET51 expressing cells were calculated using the paired Student's t-test. A value of $p<0.05$ was considered significant (**$p<0.01$).

4.2.6 NTN induced P-Ser-STAT3 was undetectable in nucleus

STAT3 is known to mediate ligand-receptor signaling through transcriptional activation of target genes. Ligand induced STAT3 nuclear translocation and its kinetics affects the temporal expressions and functions of the target genes. To test if NTN induced STAT3 phosphorylation resulted in its nuclear translocation and target gene expression, nuclear and cytosolic fractions were prepared from control and NTN stimulated PC12 cells. In addition, IL6, which has been shown to induce rapid nuclear translocation of STAT3 in PC12 cells (*198*), was used as a control. Both NTN

and IL6 induced rapid phosphorylation and increased nuclear localization of ERK (Figure 4.7A-C). Similarly, phosphorylated STAT3 was detected in nuclear fractions within 10 min of IL6 stimulation and was sustained over 6 h (Figure 4.7A, D-F). In contrast, phosphorylated STAT3 was not detectable in the nucleus in cells stimulated with NTN over the period of 6 h. Likewise, in Neuro2A cells, NTN stimulation was found to induce nuclear localization of ERK (Figure 4.8A-C) but not STAT3 (Figure 4.8A, D-F). Together, the observations suggested that NTN induced STAT3 serine phosphorylation did not result in detectable nuclear localization and may mediate NTN induced neurite outgrowth through a transcription independent mechanism.

4.2.7 STAT3 was localized to mitochondria and was serine phosphorylated upon NTN stimulation

As STAT3 has recently been shown to localize to the mitochondria, we tested the hypothesis that NTN induced P-Ser-STAT3 may be localized to the mitochondria. Cytosolic and mitochondrial fractions were isolated, using a method we have previously described, from control and NTN stimulated PC12 and Neuro2A cells. The presence of P-Ser-STAT3, as well as total STAT3, in each fraction was analysed by immunobloting. Interestingly, NTN stimulation increased the amount of P-Ser-STAT3 detected in mitochondrial fraction but not total STAT3, in PC12 (Figure 4.9A-C) and Neuro2A cells (Figure 4.10A-C). These observations suggested that STAT3 may be constitutively present in mitochondria and is serine phosphorylated upon NTN stimulation. Consistent with this suggestion is that ERK, which has been shown to phosphorylate STAT3 at serine^{727}, was robustly activated in the mitochondria upon NTN treatment (Figure 4.9 & 4.10). These observations supported the hypothesis that STAT3 may be phosphorylated in mitochondria by activated ERK or other kinases.

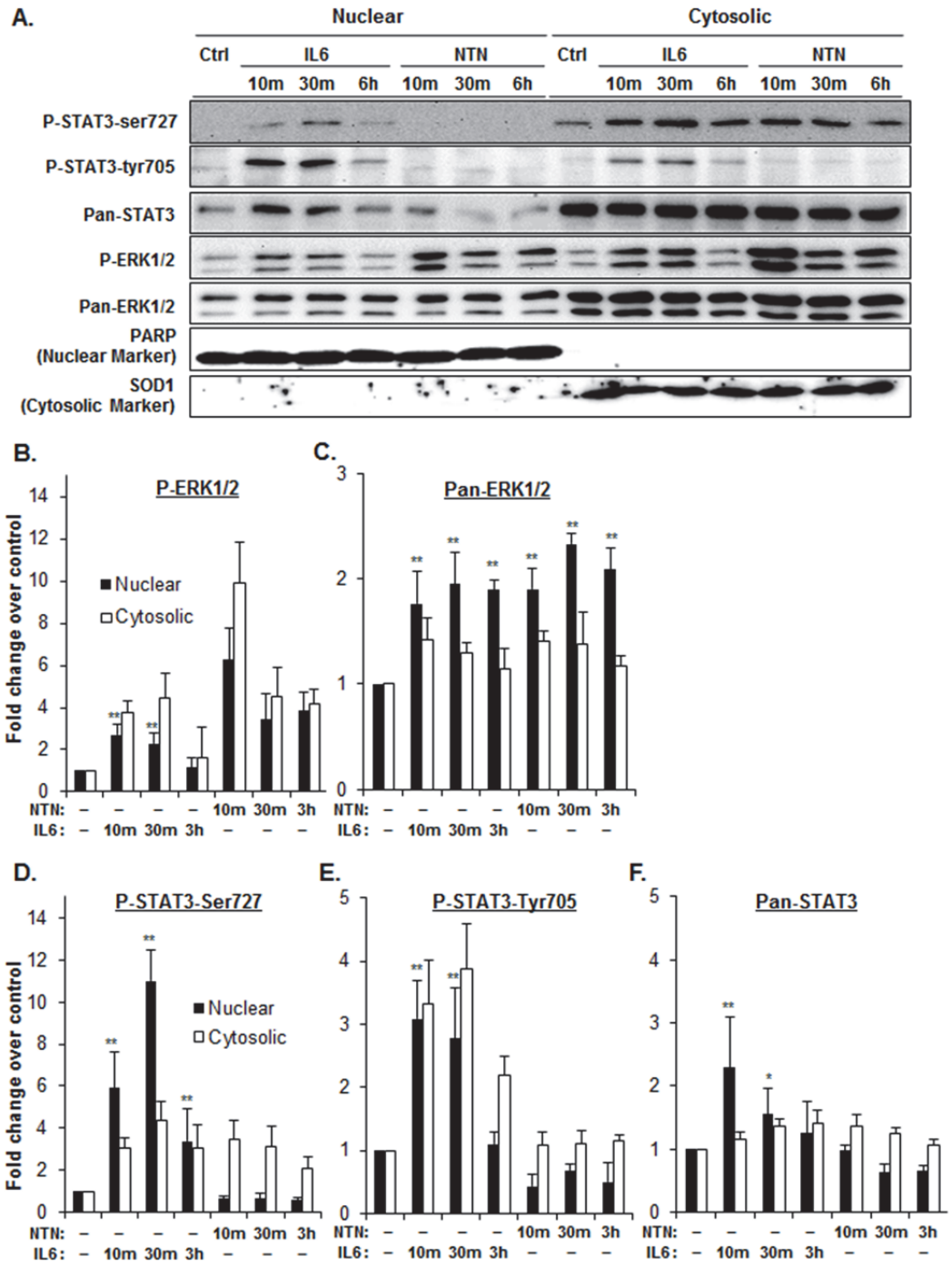

Figure 4.7 NTN did not induce STAT3 nuclear translocation in PC12 cells. PC12-GFRα2c-RET9 cells were serum-deprived for 16 h and subsequently treated with IL6 (50 ng/ml) or NTN (50 ng/ml) for 10 min, 30 min and 6 h respectively. Nuclear and cytosolic fractions were extracted and analysed by immunobloting (A). The purity of the isolated nuclear and cytosolic fractions was verified by immunobloting analysis of nuclear marker PARP and cytosolic marker SOD1. Fold changes in nuclear and cytosolic Phospho & Pan-ERK (B-C) and Phospho and Pan-STAT3 (D-F) were quantified. Nuclear proteins were normalized by PARP whereas cytosolic proteins were normalized by SOD1. The bands of expected molecular weights were presented. Significant differences in normalized nuclear levels of various proteins between control and ligand stimulated samples were calculated using the paired Student's t-test. A value of $p<0.05$ was considered significant (**$p<0.01$; *$p<0.05$).

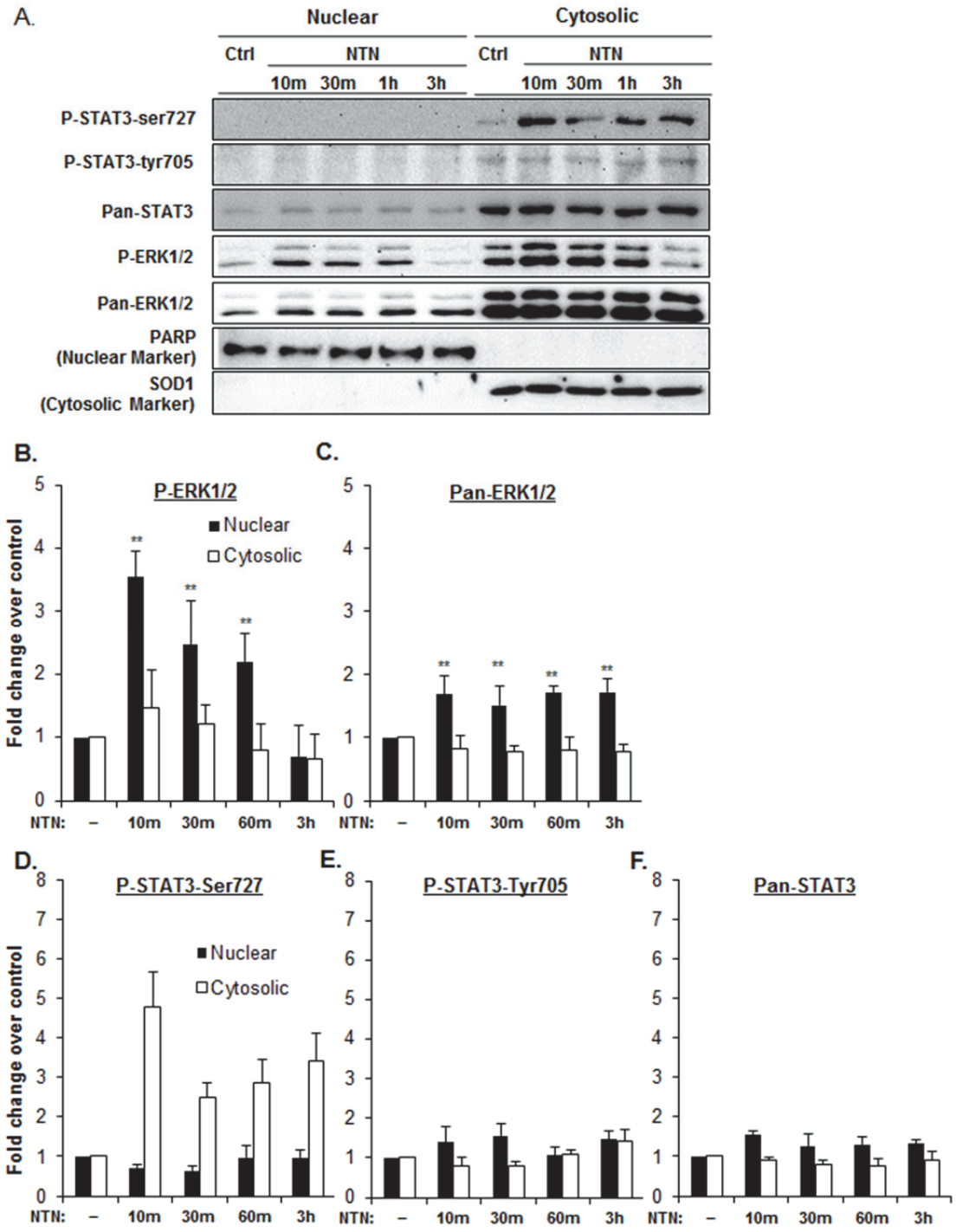

Figure 4.8 NTN did not induce STAT3 nuclear translocation in Neuro2A cells. Neuro2A-GFRα2c cells were serum-deprived for 16 h and subsequently treated with NTN (50 ng/ml) for 10 min, 30 min, 1 h and 6 h respectively. Nuclear and cytosolic fractions were extracted and analysed by immunobloting (A). The purity of the isolated nuclear and cytosolic fractions was verified by immunobloting analysis of nuclear marker PARP and cytosolic marker SOD1. Fold changes in nuclear and cytosolic Phospho & Pan-ERK (B-C) and Phospho and Pan-STAT3 (D-F) were quantified. Nuclear proteins were normalized by PARP whereas cytosolic proteins were normalized by SOD1. Significant differences in normalized nuclear levels of various proteins between control and ligand stimulated samples were calculated using the paired Student's t-test. A value of $p<0.05$ was considered significant (**$p<0.01$; *$p< 0.05$).

To test if mitochondrial P-Ser-STAT3 signal was due to contamination from the cytosol fraction, immunoblot intensity ratios of P-Ser-STAT3 to the cytosolic marker SOD1 in mitochondria and cytosol were compared as previously described (*190*). If the detected P-Ser-STAT3 in the mitochondria was due to cytosolic contamination, the ratios of P-Ser-STAT3 to SOD1 in both fractions should be similar. In PC12 cells, the intensity ratios of P-Ser-STAT3 to SOD1 in the cytosol and mitochondria at 10 min were 1.5 and 7.6 respectively (Figure 4.9). Similar observation was made in Neuro2A cells (Figure 4.10), indicating that mitochondrial P-Ser-STAT3 was not due to cytosolic contamination. In addition, the total amount of STAT3 in the mitochondria was estimated to be 11% of the cytosolic STAT3 in PC12 cells and 15% in Neuro2A cells. The ratio of mitochondrial ERK to cytosolic ERK was 22% in PC12 cells and 24% in Neuro2A cells. These data are consistent with earlier reports from both our group (*190*) and others (*188, 199*), which provided further support of the reliability of the isolation method and the approach to the study.

The presence of P-Ser-STAT3 in mitochondria was further validated by immunocytochemistry. NTN stimulation significantly increased the fluorescent intensity of P-Ser-STAT3 and its co-localization with specific mitochondria marker, Mito-Tracker, in both PC12 (*Co-localization Coefficient = 0.343*) and Neuro2A (*Co-localization Coefficient = 0.482*) cells (Figure 4.11A&C). Moreover, NTN induced P-Ser-STAT3 was also found to co-localize with GRIM-19 (Figure 4.11B&D, *Co-localization Coefficient = 0.665 & 0.797 respectively*), a known STAT3 binding partner and a component of the mitochondrial electron transport complex I (*188, 191, 200*). Consistent with the observations in cell lines, NTN induced P-Ser-STAT3 was also found to co-localize with MitoTrakcer (Figure 4.11E, *Co-localization Coefficient = 0.543*) as well as GRIM-19 (Figure 4.11F, *Co-localization Coefficient = 0.576*) in primary cortical neurons. Furthermore, the co-localization of P-Ser-STAT3 with

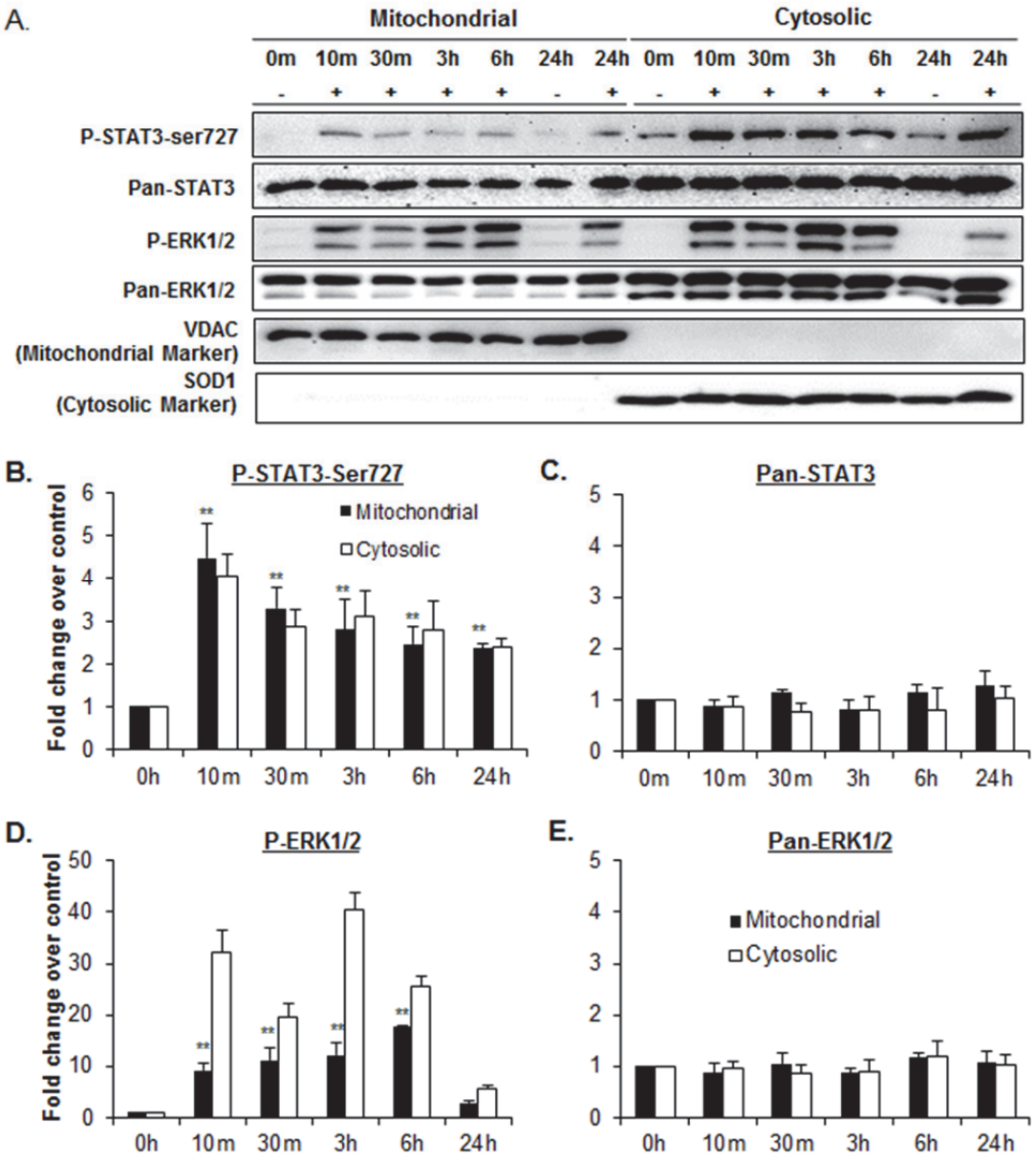

Figure 4.9 STAT3 was localized to mitochondria and was serine phosphorylated upon NTN stimulation of PC12 cells. PC12-GFRα2c-RET9 cells were serum-deprived for 16 h and subsequently treated with NTN (50 ng/ml) over 24 h. Mitochondrial and cytosolic fractions were extracted at different time points and analysed by immunobloting. The bands of expected molecular weights were presented. The purity of the isolated mitochondrial and cytosolic fractions was verified by immunobloting analysis of mitochondrial marker VDAC and cytosolic maker SOD1. Western blot images were shown in (A) and quantifications in (B-E). Mitochondrial proteins were normalized by VDAC whereas cytosolic proteins were normalized by SOD1. Significant differences in mitochondrial levels of various proteins between control and ligand stimulated samples were calculated using the paired Student's t-test. A value of $p<0.05$ was considered significant (**$p<0.01$; *$p< 0.05$).

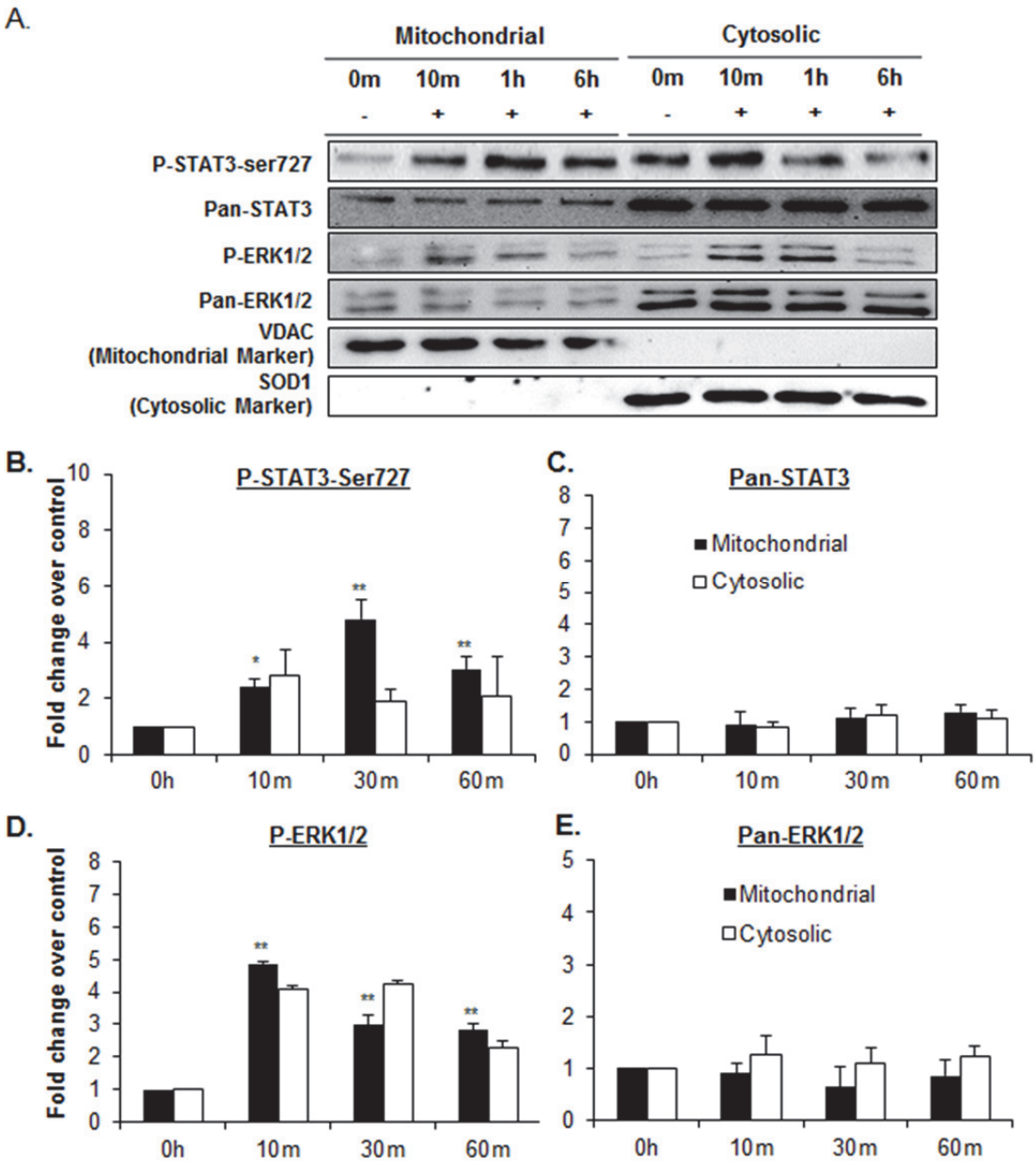

Figure 4.10 STAT3 was localized to mitochondria and was serine phosphorylated upon NTN stimulation of Neuro2A cells. Neuro2A-GFRα2c cells were serum-deprived for 16 h and subsequently treated with NTN (50 ng/ml) over 6 h. Mitochondrial and cytosolic fractions were extracted at different time points and analysed by immunobloting. The purity of the isolated mitochondrial and cytosolic fractions was verified by immunobloting analysis of mitochondrial marker VDAC and cytosolic maker SOD1. Western blot images were shown in (A) and quantifications in (B-E). Mitochondrial proteins were normalized by VDAC whereas cytosolic proteins were normalized by SOD1. Significant differences in mitochondrial levels of various proteins between control and ligand stimulated samples were calculated using the paired Student's t-test. A value of $p<0.05$ was considered significant (**$p<0.01$; *$p< 0.05$).

MitoTracker was observed not only in the cell body but also along the neurites (Figure 4.11G). Based on these observations, it is tempting to speculate that NTN may regulate local mitochondrial function along neurite and in growth cone through mitochondrial localized P-Ser-STAT3. Collectively, the data from subcellular fractionation and immunocytochemical staining provided strong evidences that P-Ser-STAT3 was localized to the mitochondria of neuronal cells upon NTN stimulation.

4.2.8 Mitochondrial STAT3 is an important mediator of NTN induced neurite outgrowth

To investigate the role of mitochondrial P-Ser-STAT3 in NTN induced neurite outgrowth, PC12-GFRα2c-RET9 cells were engineered to stably express mitochondria targeting wild type and mutant STAT3 (MTS-STAT3). These MTS-STAT3 constructs have been used successfully by both our and other groups to investigate the functions of mitochondrial STAT3 (*188-190*). The effect of different MTS-STAT3 mutants on NTN induced neurite outgrowth was studied. Remarkably, mitochondria targeted serine dominant negative mutant of STAT3 (MTS-STAT3-SA) attenuated NTN induced neurite outgrowth (Figure 4.12A-B), while the wild type (MTS-STAT3-WT) and tyrosine dominant negative mutant (MTS-STAT3-YF) slightly enhanced NTN induced neurite outgrowth. These results demonstrated the active role of mitochondrial P-Ser-STAT3 in mediating NTN induced neurite outgrowth.

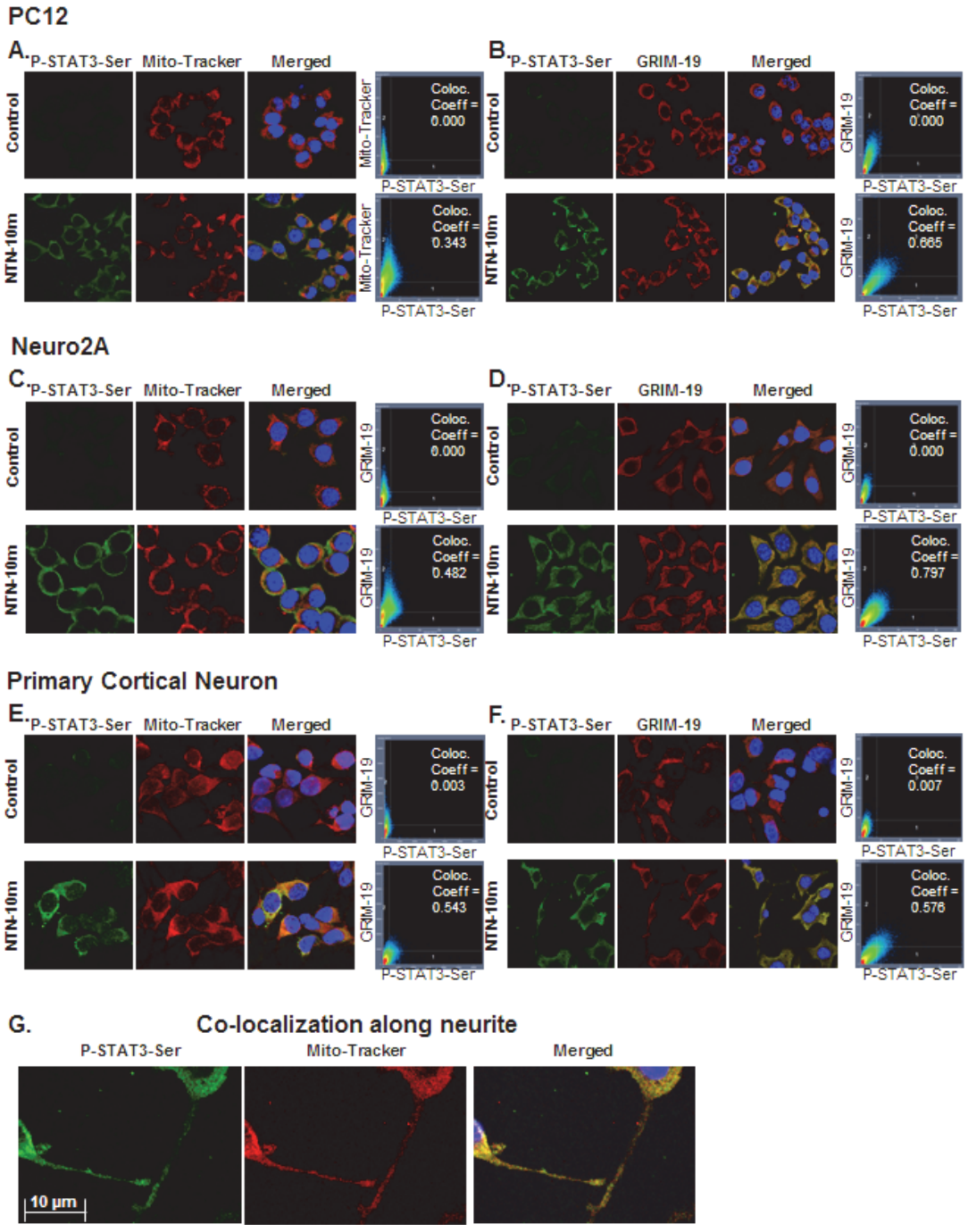

Figure 4.11 P-Ser-STAT3 was co-localized with MitoTracker and GRIM-19. NTN stimulated (10 min) PC12, Neuro2A cells and primary cortical neurons were co-stained for P-Ser-STAT3 & MitoTracker (A,C,E) or P-Ser-STAT3 & GRIM-19 (B,D,F). Confocal images of control and NTN stimulated cells of the individual and merged channels are shown. Also shown here are the intensity correlations and co-localization coefficients between P-Ser-STAT3 and MitoTracker or GRIM-19. *G.* P-Ser-STAT3 was found to co-localize with MitoTracker not only in the cell body but along the neurites in primary cortical neurons.

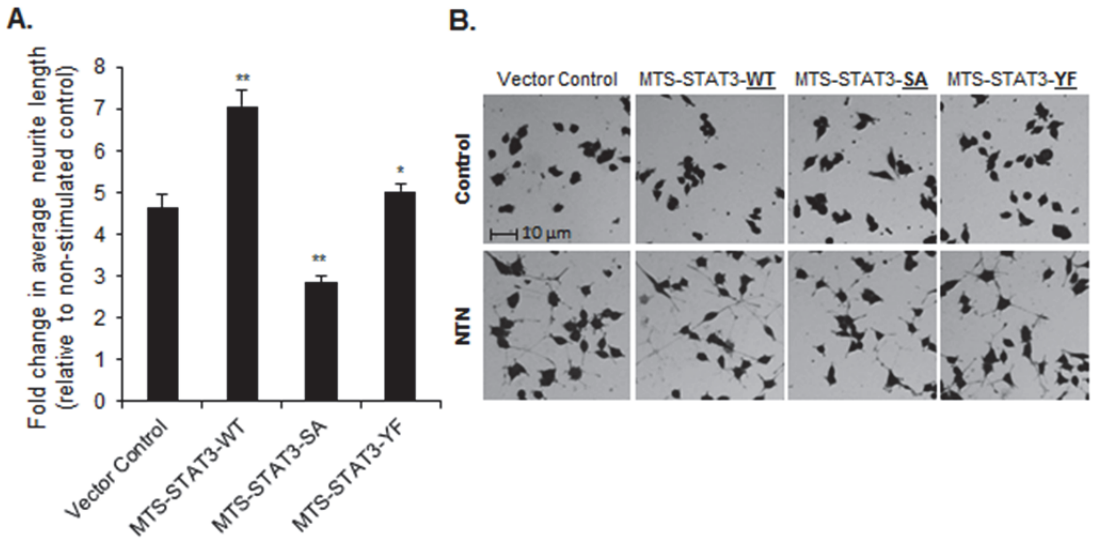

Figure 4.12 Mitochondrial STAT3 was involved in NTN induced neurite outgrowth. Control and MTS-STAT3 expressing PC12 clones were serum deprived and stimulated with 50 ng/ml NTN for 48 h. The average neurite length per cell was quantified using HCA-Vision. A. Fold changes in average neurite length in NTN treated cells over control were calculated. Significant differences between control and mutant expressing PC12 cells were calculated using the paired Student's t-test. A value of $p<0.05$ was considered significant (**$p<0.01$; *$p< 0.05$). Representative images of control and NGF treated cells are shown in B.

Section 4.3 Discussion

This study demonstrated the novel functions of alternatively spliced receptor isoform GFRα2c and RET9 in mediating NTN induced STAT3 serine phosphorylation. Unlike previous studies on oncogenic RET, this is the first report of the activation of STAT3 by a GDNF family ligand through GFRα and wild type RET. Unexpectly, P-Ser-STAT3 was found to localize to the mitochondria instead of the nucleus and mediated NTN induced neurite outgrowth independent of its transcriptional activities.

Recent study has found 92-94% of human genes to be alternatively spliced (*201*). In many systems, alternative splicing has produced multiple isoforms with distinct biochemical properties, thus allowing a single gene to exert a diverse range of biological functions (*99*). Among different tissues, it was found that the greatest amount of conserved alternative splicing occurs in the CNS (*101*). Our group has

previously identified three distinct spliced isoforms of GFRα2, the canonical receptor for NTN (*105*). The three isoforms were further shown to mediate differential signalling activation and exerted opposing neuritogenic functions. NTN activation of GFRα2b inhibited neurite outgrowth whereas GFRα2a and 2c induced neurite outgrowth (*6*). Using exon-overlapping qPCR assays that specifically detect each of the isoforms (*4*), we have shown that all three isoforms are highly expressed in the cortex (*6*), the region of the brain involved in learning complex tasks. This is consistent with the observation that GFRα2 knockout mice show significant impairment in memory tasks (*202*). Moreover, NTN has also been shown to provide both functional and structural neuroprotection for cortical neurons in mouse model of Huntington's disease (*197*). However, the signalling mechanisms underlying NTN functions in cortical neurons and the roles of different GFRα2 isoforms have yet to be thoroughly investigated.

In cultured embryonic cortical neurons, NTN stimulation resulted in rapid phosphorylation of ERK and STAT3 serine but not tyrosine residue. A classic transcription regulator, STAT3 was first discovered as a key mediator of cytokine induced inflammation and immunity (*181, 182*). Later studies have found STAT3 to regulate a much wider range of biological processes including neuritogenesis and neuroprotection (*180*). To investigate the mechanism of NTN activation of STAT3 and its role in NTN function, we engineered two well used neuronal models to express different combinations of GFRα2 and RET receptor isoforms. Intriguingly, the shortest isoform GFRα2c but not GFRα2a or 2b was able to mediate sustained STAT3 serine phosphorylation upon NTN stimulation. GFRα receptor has been partially crystallized and is thought to be structurally organized into three distinct domains (*2, 62, 66*). GFRα2c, with exon 2 and 3 deletion (*105*), differs from the other two isoforms in its N terminus domain, which has been shown to be dispensable for ligand binding (*50*). This is consistent with our earlier findings that GFL bound equally

well to all three GFRα2 isoforms in Neuro2A cells (*6*). To explain the distinct functions of these isoforms, we postulated that the N-terminal domain may be an important determinant of the overall conformation of the GFL-GFRα-RET/NCAM complex and the preferential activation of certain downstream signalling pathways. This is supported by recent findings that the N-terminal domain of GFRα1 is important for the interactions with co-receptor RET (*65*) and NCAM (*203*). Co-crystallization of the entire GFL-GFRα-RET/NCAM complexes containing different isoforms would provide the most direct means of investigating the impact of the isoform specific N-terminal domain. This is becoming increasingly feasible with the advancement in protein crystallization technologies. As an alternative means, we are currently investigating the phosphorylation patterns of co-receptor RET when coupled to different GFRα2 isoforms, in an attempt to provide further insights into their distinct biochemical properties. Nevertheless, our finding that GFRα2c but not 2a or 2b was capable to inducing STAT3 phosphorylation provided further evidence to the distinct functions of the GFRα2 receptor isoforms (*6, 204*).

In addition, ligand bound GFRα has been shown to either partner with RET or NCAM to transduce its signals. Our group has previously shown that NCAM but not RET mediated GFRα1b isoform induced glioma migration (*205*). In contrast, this study found RET but not NCAM to mediate NTN induced STAT3 phosphorylation and neurite outgrowth, albeit the significantly higher transcript expression of NCAM in Neuro2A cells. These data suggested that the selective partnering of GFRα with its co-receptors vary in a cell context dependent manner and is not determined solely by the expression levels of different co-receptors. We hypothesized that the spatial localization of GFRα, RET and NCAM on the cell membrane may vary across cell types and is currently investigating whether their partitions in- and out-side of lipid raft may play an important role. Furthermore, the alternatively spliced isoform RET9 but not RET51 was found to mediate NTN induced STAT3 phosphorylation. The two

RET tyrosine kinase isoforms share 16 identical tyrosine residues but RET51 contains two additional tyrosine residues in the carboxyl terminal (tyrosine 1090 and 1096). Mounting evidences have demonstrated the distinct functions of RET9 and 51 in different cell types. Ret9 but not Ret51 was able to promote tube formation of epithelial cells (*115*). In contrast, Ret51 but not Ret9 was found to promote the survival and tubulogenesis of mouse inner medullary collecting duct cells (*108*), suggestive of isoform-specific roles in embryo development and organogenesis. Other studies have reported RET9 and 51 to engage distinct adaptor proteins and activate different signalling pathways (*114, 116, 118*). In PC12 cells, NTN activation of RET9 but not 51 was found to induce phosphorylation of Src, an important signalling intermediate that mediated STAT3 phosphorylation, thus providing a plausible explanation for RET9 specific activation of STAT3.

To date, the functional significance of STAT3 serine phosphorylation remains controversial. It has been shown to either enhance or suppress the transcriptional activity of tyrosine phosphorylated STAT3. More recently, we and others have shown that serine mono-phosphorylated STAT3 could function independent of its transcriptional activities. The observation that NTN induced P-Ser-STAT3 did not localize to the nucleus added further evidence to this body of knowledge. Our findings that NTN induced P-Ser-STAT3 was localized to the mitochondria in both Neuro2A and PC12 cells are in congruence with our earlier report on Nerve Growth Factor (NGF) induced mitochondrial STAT3 phosphorylation (*190*). These new data suggested that the involvement of mitochondrial STAT3 in neurite outgrowth is not restricted to NGF, but a common mechanism shared by multiple neurotrophic factors. It is intriguing that P-Ser-STAT3 was localized to the mitochondria not only in the cell body but along the neurites as well. As neurite outgrowth is a dynamic and reversible process and is influenced by local mitochondrial dynamics (*206-208*), it is tempting to

speculate that mitochondrial P-Ser-STAT3 may be an important transducer of the anterograde and/or retrograde signaling of neurotrophic factors along neurites.

To the best of our knowledge, this study marked the first report of the activation of STAT3 by a ligand (NTN) activated GFRα and non-oncogenic RET receptor. It is further demonstrated that STAT3 serine phosphorylation was mediated specifically by receptor isoform GFRα2c and RET9. P-Ser-STAT3 was intimately involved in NTN induced neurite outgrowth, in a transcription independent manner, through its spatial localization to the mitochondria. Taken together, this study provided novel insights into an intriguing role of receptor isoforms in mediating NTN induced mitochondrial STAT3 and neurite outgrowth (Figure 4.13).

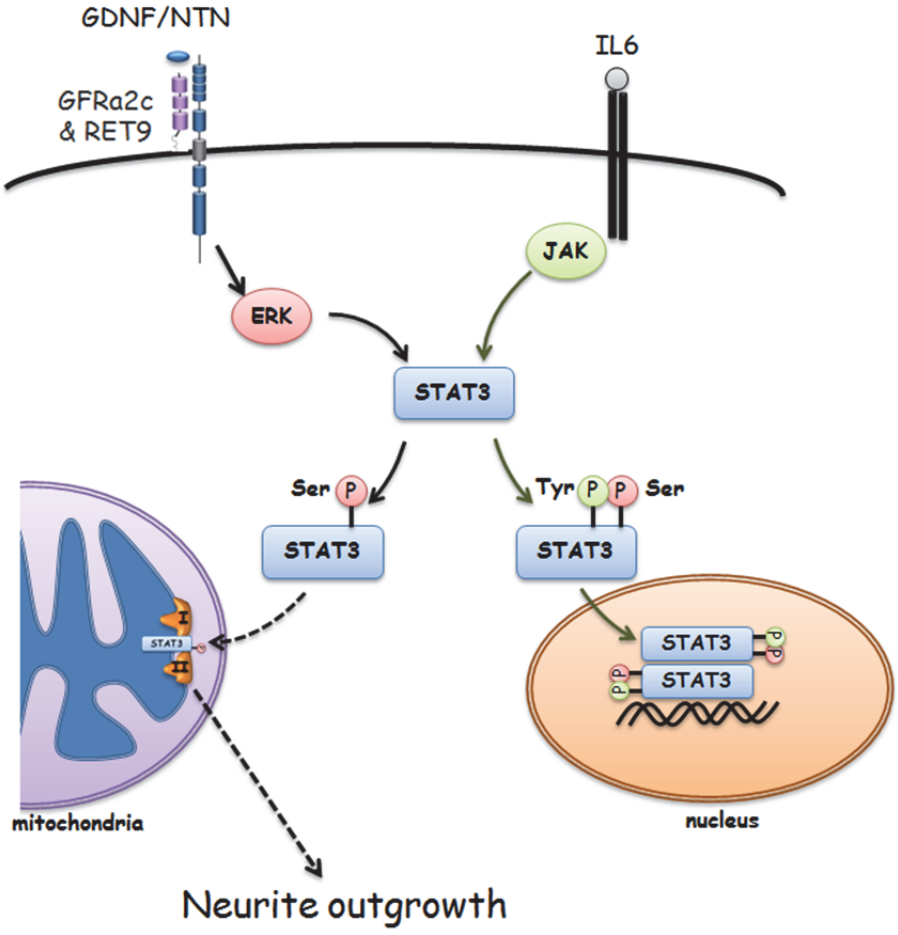

Figure 4.13 A schematic illustration of NTN activation of mitochondrial P-Ser-STAT3. NTN stimulation of GFRα2c and RET9 induced STAT3 serine^{727} phosphorylation through ERK1/2 and its mitochondrial localization. IL6 stimulation induced STAT3 tyrosine^{705} and serine^{727} dual phosphorylation and its nuclear localization. Mitochondrial P-Ser-STAT3 was found to be intimately involved in NTN induced neurite outgrowth.

Chapter 5 Mitochondrial localized STAT3 is involved in NGF induced neurite outgrowth

Section 5.1 Introduction

In literature, STAT3 have been shown to be tyrosine phosphorylated at residue 705 (P-Tyr-STAT3) by cytokines and growth factors including interleukin 6 (IL6) (*198, 209*), epidermal growth factor (EGF) (*210, 211*), and brain-derived neurotrophic factor (BDNF) (*212*). This results in the homo-dimerization and nuclear translocation of STAT3 and the subsequent activation of target gene transcription (*183*). In addition, STAT3 has also been found to be serine mono-phosphorylated upon NGF stimulation of PC12 cells, similar to that by NTN. In PC12 cells, NGF induces growth arrest and elaboration of neurite outgrowth (*213*). Interestingly, it was reported that NGF induced STAT3 nuclear localization, which in turn mediated the induction of cyclin D1 expression and growth arrest of PC12 cells. However, it is not clear whether P-Ser-STAT3 is involved in NGF induced neurite outgrowth and whether NGF too can induce mitochondrial localization of STAT3, similar to that of NTN.

In this chapter, we tested the hypothesis that P-Ser-STAT3 mediates NGF induced neurite outgrowth via a transcription-independent mechanism. Serine but not tyrosine dominant negative mutant of STAT3 was found to impair NGF induced neurite outgrowth. Surprisingly, NGF induced P-Ser-STAT3 was not detected in the nucleus, unlike the previous report (*212*). Instead, P-Ser-STAT3 was found to be localized to the mitochondria upon NGF stimulation. Using mitochondria targeted mutants, mitochondrial P-Ser-STAT3 was found to regulate NGF induced neurite outgrowth and the production of ROS. Taken together, these findings provided novel insights into an unconventional, transcription-independent mechanism whereby mitochondria localized STAT3 mediates NGF induced neurite outgrowth.

Section 5.2 Result

5.2.1 NGF induced sustained STAT3 serine but not tyrosine phosphorylation

NGF induced progressive neurite outgrowth in PC12 cells (Figure 5.1A). Within 72 h, greater than 50% of cells were found to bear neurite twice the cell body length. To gain insights into the involvement of STAT3 in this process, the phosphorylation state of STAT3 was investigated upon NGF stimulation. In agreement with previous reports (*212, 214*), STAT3 was rapidly (within 10 min) phosphorylated at serine^{727} upon NGF stimulation (Figure 5.1B). The serine^{727} residue of STAT3 remained phosphorylated over a period of 72 h. No significant increase in STAT3 tyrosine^{705} phosphorylation was observed in NGF treated PC12 cells over the period of 72 h. A concomitant activation of ERK1/2 was also observed (lower panel), consistent with the previous reports (*215, 216*). As a control, IL6 induced both tyrosine and serine phosphorylation of STAT3 in PC12 cells.

Neurotrophin receptors are expressed in cerebral cortical neuron *in vivo* (*217*) and *in vitro* (*218*). In cortical neuron, BDNF induced a transient phosphorylation of STAT3 at tyrosine^{705} and a sustained phosphorylation at serine^{727} residue (*212*). Whether NGF may similarly induce the phosphorylation of STAT3 at these sites is currently unknown. To address this possibility, primary cortical neurons were treated with NGF. Unlike BDNF (*212*), NGF induced a time dependent serine but not tyrosine phosphorylation of STAT3 in primary cortical neurons (Figure 5.1C), extending the observations found in PC12.

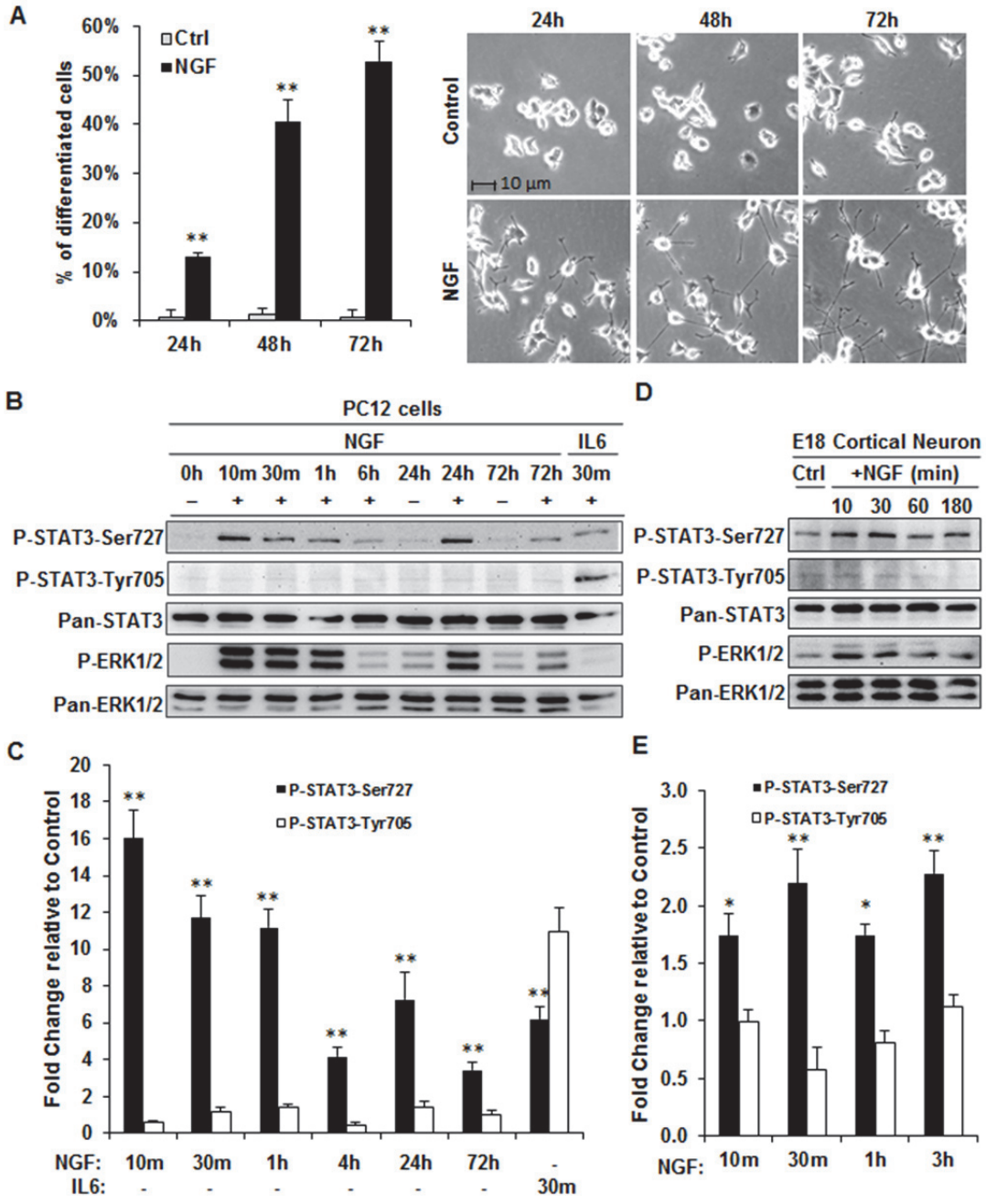

Figure 5.1 NGF induced sustained STAT3 serine^{727} but not tyrosine^{705} phosphorylation in PC12 and embryonic cortical neurons. PC12 cells were serum-deprived for 16 h and subsequently treated with NGF (50 ng/ml) for 72 h. *A.* NGF induced progressive neurite outgrowth in PC12 cells. Percentage of PC12 cells bearing neurite twice the body length (differentiated) was quantified after 24, 48 and 72 h of NGF treatment. Representative images of control and NGF treated cells are shown for each of the time point. *B.* Total cell lysates were collected over 72 h and analysed by immunobloting and quantified (*C*). NGF induced sustained STAT3 serine but not tyrosine phosphorylation over 72 h, whereas IL6 induced both STAT3 serine and tyrosine phosphorylation. *D.* Rat embryonic cortical neurons were isolated and cultured *in vitro* for 72 h before NGF stimulation (100 ng/ml) for up to 3 h. Total cell lysates were analysed and quantified (*E*). Significant differences in P-Ser or P-Tyr-STAT3 levels between ligand stimulated samples and respective controls were calculated using the paired Student's t-test. A value of $p<0.05$ was considered significant (**$p<0.01$; *$p< 0.05$).

5.2.2 STAT3 serine DN mutant impaired NGF induced neurite outgrowth

To test the hypothesis that P-Ser-STAT3 is involved in NGF induced neurite outgrowth, wild type and mutant STAT3 were transiently expressed in PC12 cells. All STAT3 constructs co-expressed enhanced green florescence protein (eGFP) which served as a marker for gene transfer. STAT3 serine (S727A) but not tyrosine (Y705F) dominant negative mutant was found to attenuate NGF induced neurite outgrowth significantly (Figure 5.2). In addition, expression of the STAT3 serine constitutive active mutant (S727E) resulted in a small but significant enhancement of NGF induced neurite outgrowth, lending further evidence that P-Ser-STAT3 was involved in neurite outgrowth.

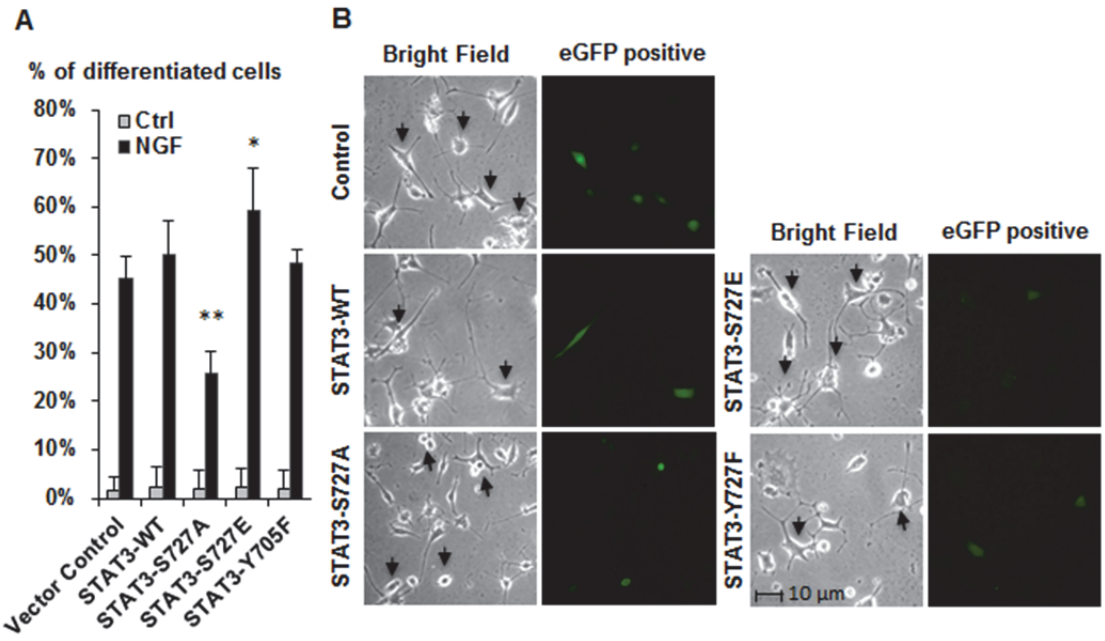

Figure 5.2 STAT3-Ser727Ala dominant negative mutant attenuated NGF induced neurite outgrowth in PC12 cells. PC12 cells were transiently infected with different STAT3 mutants using a retro-viral vector co-expressing eGFP (pQCXI-eGFP). Mutant expressing cells were identified by eGFP expression. Infected PC12 cells were serum deprived for 16 h and treated with 50 ng/ml NGF for 48 h. *A.* Neurite outgrowth from wild type and STAT3 mutants expressing PC12 cells was examined. More than 60 eGFP expressing cells were analysed per biological replicate per condition and the number of cells bearing at least one neurite twice the cell body length was scored. Significant differences between the percentages of neurite bearing cells in control and STAT3 mutant expressing cells were calculated using the paired Student's t-test. A value of $p<0.05$ was considered significant (**$p<0.01$; *$p< 0.05$). *B.* Representative bright field and florescent images of control and STAT3 mutant expressing PC12 cells 48 h after NGF treatment. Arrows in bright field images point to STAT3 mutant expressing cells identified by eGFP co-expression.

5.2.3 NGF induced P-Ser-STAT3 was undetectable in nucleus

Nuclear localization of STAT3 is known to be essential for the transcriptional activation of target genes. The temporal expressions of these target genes are likely to be influenced by the kinetics of STAT3 nuclear translocation and the duration of its presence in the nucleus. The previous report has briefly demonstrated the presence of P-Ser-STAT3 in nucleus (*212*) but it is not known if the nuclear localization of the phosphorylated STAT3 is temporally controlled. To address this, we investigated the time course of NGF induced P-Ser-STAT3 nuclear translocation. IL6, which is known to induce rapid nuclear translocation of STAT3 in PC12 cells (*219*), was used as a control. Nuclear and cytosolic fractions were prepared from PC12 cells stimulated with either IL6 or NGF and subsequently analysed (Figure 5.3A). Both IL6 and NGF induced rapid phosphorylation and increased nuclear localization of ERK (Figure 5.3B). Upon IL6 stimulation, phosphorylated STAT3 was detected in both nuclear and cytosolic fractions within 10 min and was sustained over a period of 6 h (Figure 5.3C). Contrary to the previous report (*212*), STAT3 was not detectable in the nucleus when the cells were stimulated with NGF over a period of 6 h (Figure 5.3C). This observation indicated that serine phosphorylation alone did not result in detectable nuclear localization of STAT3, suggesting that P-Ser-STAT3 may be involved in NGF induced neurite outgrowth through a transcription independent mechanism.

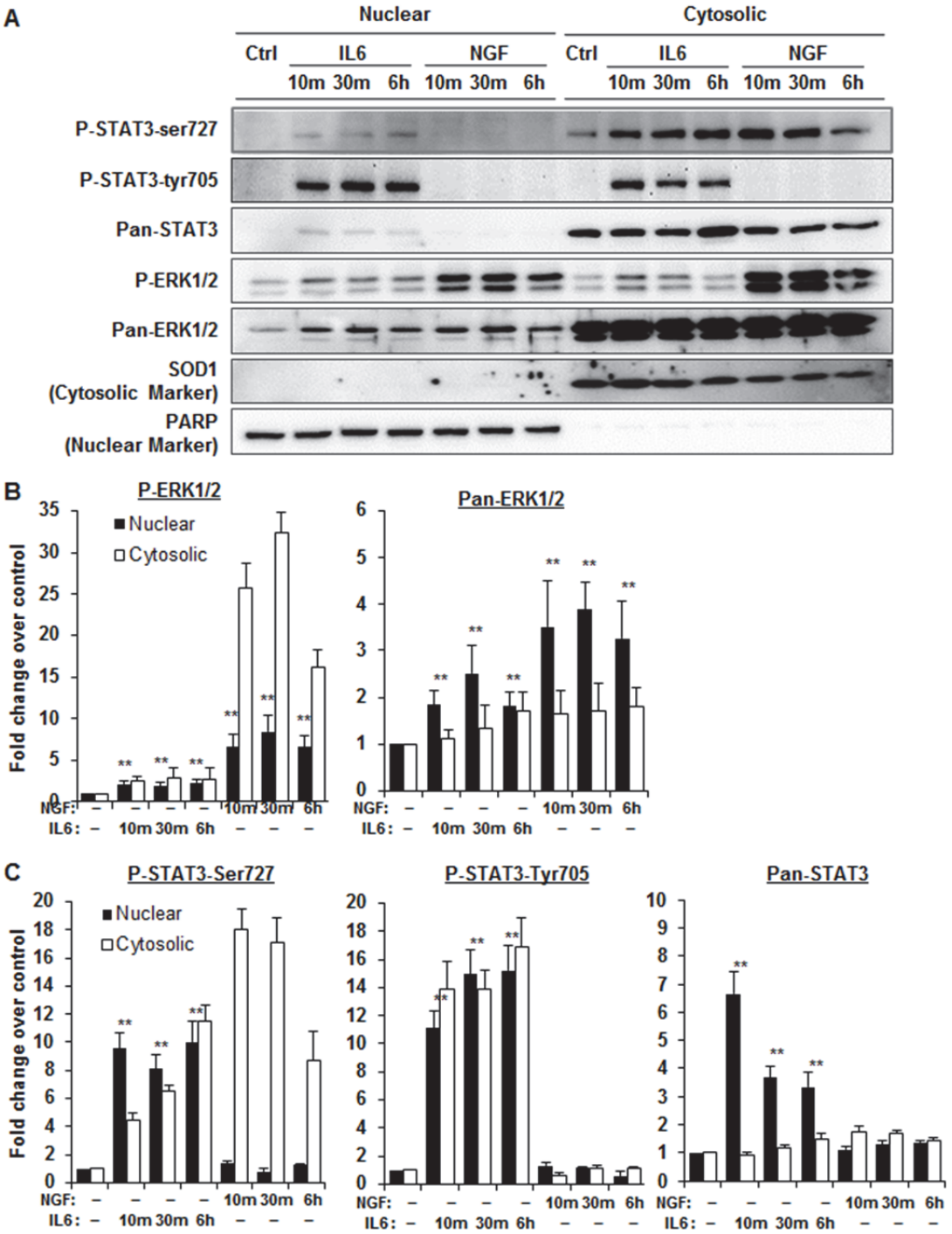

Figure 5.3 NGF did not induce STAT3 nuclear translocation. PC12 cells were serum-deprived for 16 h and subsequently treated with NGF (50 ng/ml) or IL6 (50 ng/ml) for 10 min, 30 min and 6 h respectively. Nuclear and cytosolic fractions were extracted and analysed by immunobloting. The purity of the isolated nuclear and cytosolic fractions was verified by immunobloting analysis of nuclear marker PARP and cytosolic marker SOD1. The bands of expected molecular weights were presented. Fold changes in nuclear and cytosolic Phospho & Pan-ERK (*B*) and Phospho and Pan-STAT3 (*C*) were quantified. Nuclear proteins were normalized by PARP whereas cytosolic proteins were normalized by SOD1. Significant differences in normalized nuclear levels of various proteins between control and ligand stimulated samples were calculated using the paired Student's t-test. A value of $p<0.05$ was considered significant (**$p<0.01$; *$p< 0.05$).

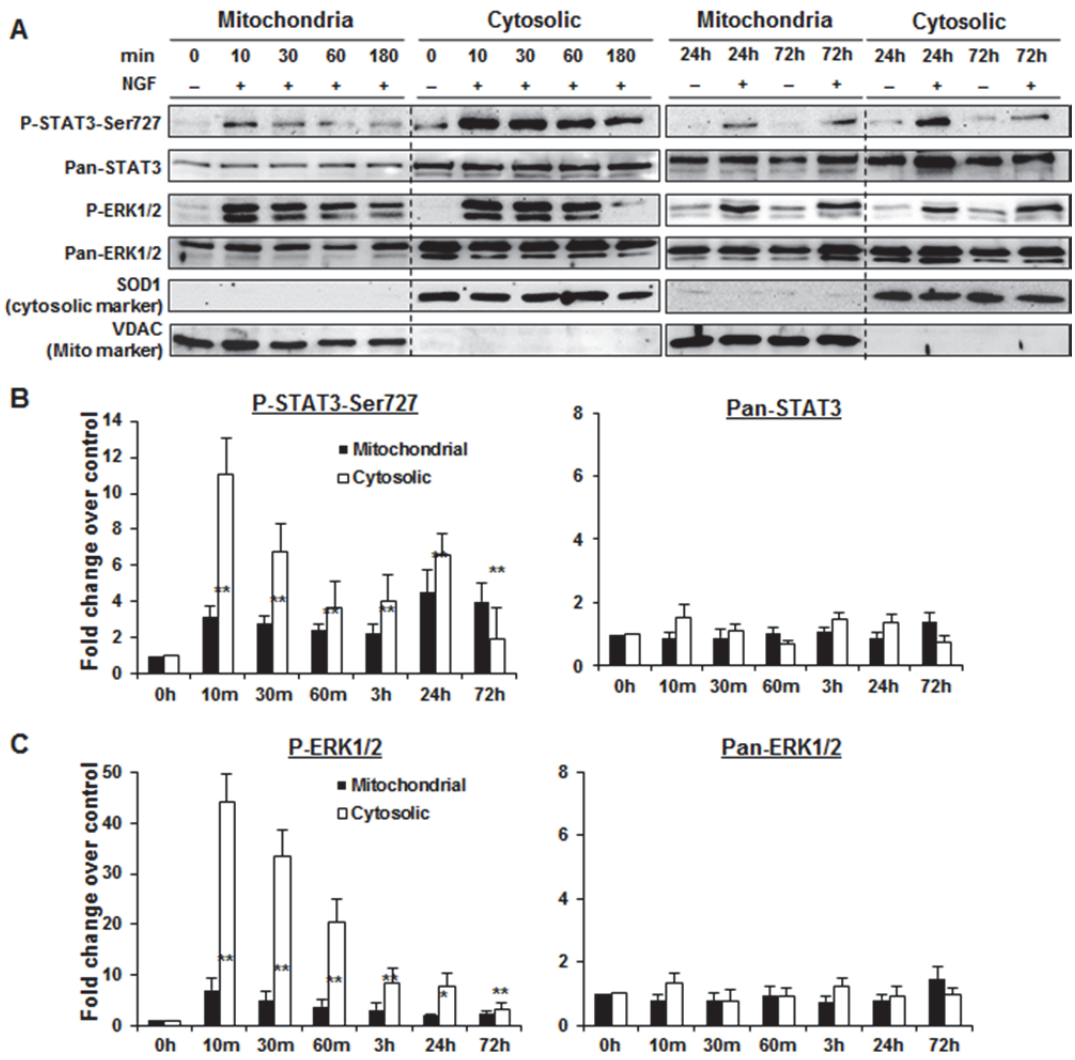

Figure 5.4 STAT3 was localized to mitochondria and was serine phosphorylated upon NGF stimulation. PC12 cells were serum-deprived for 16 h and subsequently treated with NGF (50 ng/ml) over 72 h. Mitochondrial and cytosolic fractions were extracted at different time points and analysed by immunobloting. The purity of the isolated mitochondrial and cytosolic fractions was verified by immunobloting analysis of mitochondrial marker VDAC and cytosolic maker SOD1. Western blot images were shown in (*A*) and quantifications in (*B, C*). Mitochondrial proteins were normalized by VDAC whereas cytosolic proteins were normalized by SOD1. Significant differences in mitochondrial levels of various proteins between control and ligand stimulated samples were calculated using the paired Student's t-test. A value of $p<0.05$ was considered significant (**$p<0.01$; *$p< 0.05$).

5.2.4 STAT3 was localized to mitochondria and was serine phosphorylated upon NGF stimulation

Recently, P-Ser-STAT3 was shown to be localized in the mitochondria of non-neuronal cells and regulated cellular functions independent of its transcriptional activities (*188*). We next tested the hypothesis that NGF induced P-Ser-STAT3 may similarly be localized to the mitochondria. Mitochondrial and cytosolic fractions were isolated from NGF stimulated PC12 cells and total STAT3, as well as P-Ser-STAT3, were immunoblotted. Interestingly, P-Ser-STAT3 was detected in the mitochondria fraction when the cells were stimulated with NGF as early as 10 min (Figure 5.4 A, B) and the presence of P-Ser-STAT3 was detectable over a period of 72 h.

To verify that mitochondrial P-Ser-STAT3 signal was not due to a contamination from the cytoplasm, immunoblot intensity ratios of P-Ser-STAT3 to the cytosolic marker SOD1 in mitochondria and cytosol were compared as previously described (*188*). While the intensity ratio of P-Ser-STAT3 to SOD1 in the cytosol was ~ 1.2 at 10 min, the ratio of P-Ser-STAT3 to SOD1 in the mitochondria at 10 min was ~ 8. If the detected P-Ser-STAT3 in the mitochondria was due to cytosolic contamination, the ratio of P-Ser-STAT3 to SOD1 would be ~ 1.

Since STAT3 has been shown to shuttle between nucleus and cytosol, STAT3 may similarly shuttle between mitochondria and cytoplasm. Intriguingly, total mitochondrial STAT3 was not increased by NGF stimulation, suggesting that STAT3 may be constitutively present in mitochondria. This observation suggested an intriguing possibility that STAT3 may be directly phosphorylated in the mitochondria upon NGF stimulation. Consistent with this suggestion is that ERK, which has been shown to phosphorylate STAT3 at serine^{727}, was robustly activated in the mitochondria upon NGF treatment (Figure 5.4A, C). These observations supported the hypothesis that STAT3 may be phosphorylated in mitochondria by activated ERK or other kinases.

It is of interest to note that the total amount of STAT3 in the mitochondria of PC12 cells was about 13% of cytosolic STAT3, consistent with the earlier report where mitochondrial STAT3 amounted to one-tenth of that found in the cytosol in mouse liver and heart (*188*). In addition, the amount of mitochondrial ERK in PC12 cells was about 25% of cytosolic ERK, similar to the previous report where the mitochondrial and cytosolic ERK account for 15% and 55% of total ERK in Hela cells, respectively (*220*). The agreement between our data and previous reports further supported the reliability of our method and provided indication of a possible role of mitochondrial P-Ser-STAT3 downstream of NGF.

Next, we verified the existence of P-Ser-STAT3 in the mitochondria immunocytochemically. NGF stimulation significantly increased the florescent intensity of P-Ser-STAT3 and the co-localization (*Co-localization Coefficient = 0.365*) with the specific mitochondria marker, Mito-Tracker (Figure 5.5A). Furthermore, NGF induced P-Ser-STAT3 was also found to co-localize (*Co-localization Coefficient = 0.933*) with GRIM-19 (Figure 5.5B), a known STAT3 binding partner and a component of the mitochondrial electron transport complex I (*188, 200*). To test if the mitochondrial localization of STAT3 was restricted to the transformed cell line of PC12, we extended the study to rat embryonic cortical neurons. Consistent with the observations in PC12 cells, NGF induced P-Ser-STAT3 was also found to co-localize with MitoTrakcer (Figure 5.6A, *Co-localization Coefficient = 0.463*) as well as GRIM-19 (Figure 5.6B, *Co-localization Coefficient = 0.738*) in primary cortical neurons. More intriguingly, P-Ser-STAT3 was found to co-localize with MitoTracker not only in the cell body but also along the neurites (Figure 5.6C). Since local mitochondrial function is important for growth cone activity (*221*), axonal branching (*222*), and synapse formation (*223*), it is tempting to speculate that NGF may regulate local mitochondrial function and neurite outgrowth through mitochondrial localized P-Ser-STAT3. Taken together, our data from both subcellular fractionation and

immunocytochemical staining experiments support the notion that P-Ser-STAT3 was localized to the mitochondria of neuronal cells upon NGF stimulation.

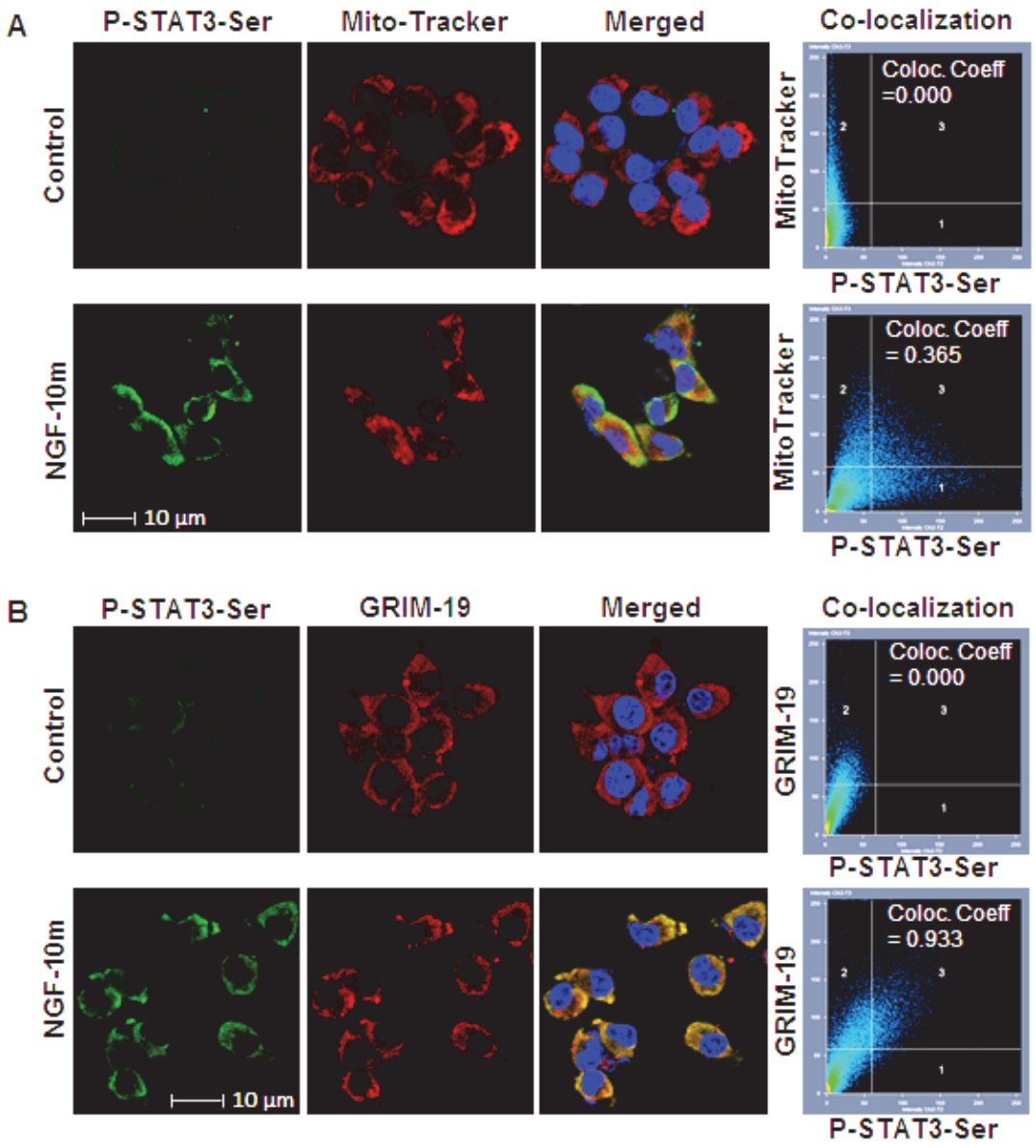

Figure 5.5 P-Ser-STAT3 was co-localized with MitoTracker and GRIM-19 in PC12 cells. NGF stimulated (10min) PC12 cells were co-stained for P-Ser-STAT3 & MitoTracker (*A*) or P-Ser-STAT3 & GRIM-19 (*B*). Confocal images of control and NGF stimulated cells of the individual and merged channels are shown. Also shown here are the intensity correlations and co-localization coefficients between P-Ser-STAT3 and MitoTracker or GRIM-19.

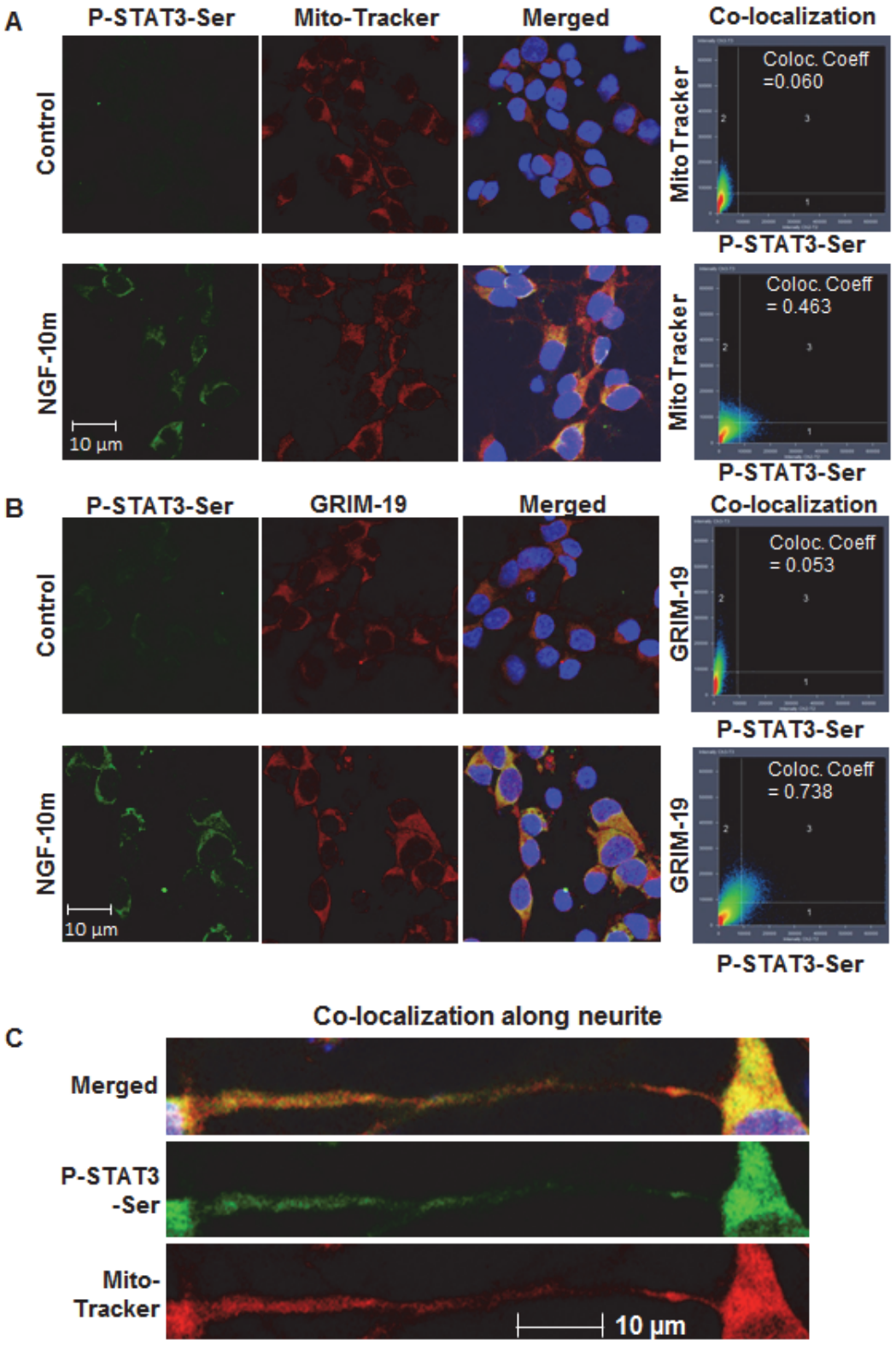

Figure 5.6 P-Ser-STAT3 was co-localized with MitoTracker and GRIM-19 in rat embryonic cortical neuron. NGF stimulated (10 min) cortical neurons were co-stained for P-Ser-STAT3 & MitoTracker (*A, C*) or P-Ser-STAT3 & GRIM-19 (*B*). Confocal images of control and NGF stimulated cells of the individual and merged channels are shown. Also shown here are the intensity correlations and co-localization coefficients between P-Ser-STAT3 and MitoTracker or GRIM-19.

5.2.5 STAT3 serine phosphorylation was temporally regulated by MAPKs and PKC

Previous report showed that inhibition of MEK-ERK pathway alone was insufficient to abolish NGF induced P-Ser-STAT3 in PC12 cells (*212*), suggesting the requirement of additional pathways for maximal STAT3 activation. To assess the possible involvement of various MAPK pathways (ERK, JNK and p38) and PKC in NGF induced STAT3 serine phosphorylation, PC12 cells were pretreated with selective pharmacological inhibitors, and subsequently stimulated with NGF for varying periods of time. Consistent with previous reports (*224, 225*), Src was found to be a crucial signaling intermediate mediating NGF activation of various MAPK pathways. Pre-treatment of PC12 cells with SU6656 substantially reduced NGF induced phosphorylation of ERK, JNK and p38. Similarly, SU6656 was able to abolish NGF induced STAT3 serine phosphorylation (Figure 5.7). Another Src inhibitor PP2 likewise abolished NGF induced P-Ser-STAT3 (data not shown). Among the three MAPKs investigated, inhibition of ERK and JNK but not p38 activation was found to attenuate STAT3 serine phosphorylation (Figure 5.7B). Phosphorylation of STAT3 serine^{727} was also inhibited by the broad spectrum protein kinase C inhibitor, Gö6983 (Figure 5.7B). Taken together, the data suggested that NGF induced P-Ser-STAT3 was temporally regulated by multiple signaling pathways including ERK, JNK and PKC. To test the possibility that ERK and JNK are involved in serine phosphorylation of mitochondrial STAT3, mitochondrial fraction was isolated from PC12 cells pre-treated with SU6656, U0126 and SP600125. All three inhibitors were found to attenuate the phosphorylation of cytosolic and mitochondria STAT3 (Figure 5.7C), indicating that pathways involving ERK, JNK and Src were indeed involved in NGF induced mitochondrial P-Ser-STAT3.

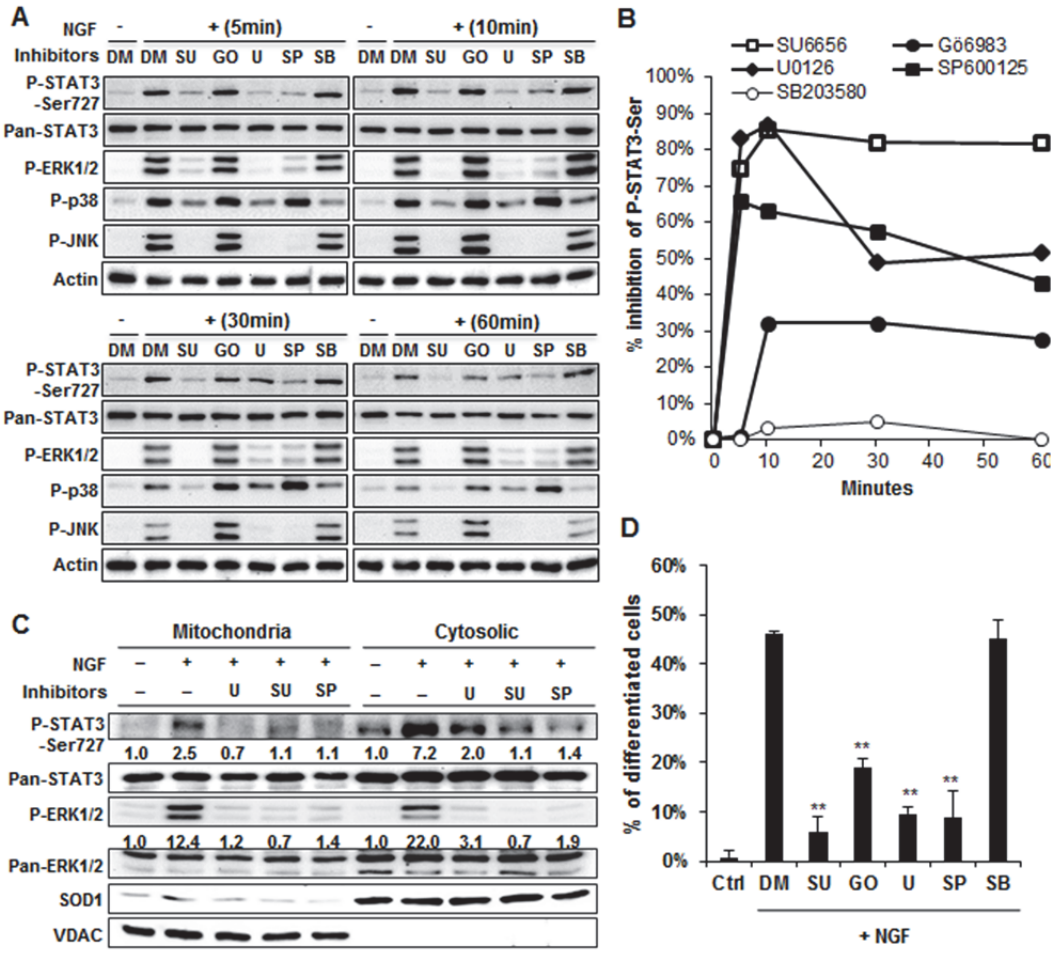

Figure 5.7 NGF induced STAT3 serine phosphorylation was temporally regulated by multiple kinases. PC12 cells were serum-deprived for 16 h and pre-treated with DMSO (DM, 0.1%, control), SU6656 (SU, 1 μM), Gö6983 (GO, 5 μM), U0126 (U, 10 μM), SP600125 (SP, 10 μM), and SB203580 (SB, 10 μM) for 1 h before stimulated with 50 ng/ml NGF in the presence of respective inhibitors. *A.* Total cell lysates were harvested from control and inhibitor treated cells after 5, 10, 30 or 60 min of NGF stimulation and analysed by immunobloting. The bands of expected molecular weights were presented. *B.* Percentage inhibition of NGF induced STAT3 serine phosphorylation by various signaling inhibitors, % inhibition = (P-Ser-$STAT3_{DMSO}$ - P-Ser-$STAT3_{Inhibitor}$) / P-Ser-$STAT3_{DMSO}$ x 100%. Quantified P-Ser-STAT3 immunoblot intensity was normalized to respective Pan-STAT3 intensity. *C.* Mitochondrial and cytosolic fractions were extracted from NGF stimulated PC12 cells (10 min) pretreated with U0126, SU6656 or SP600125, and immunoblotted. The fold changes in normalized P-Ser-STAT3 and P-ERK were quantified and shown below the blot. *D.* The effect of various inhibitors on NGF induced neurite outgrowth was quantified in PC12 cells subjected to 48 h of NGF stimulation in the presence of the inhibitors. Significant differences between the percentages of differentiated cells in control and inhibitor treated PC12 cells were calculated using the paired Student's t-test. A value of $p<0.05$ was considered significant (**$p<0.01$; *$p< 0.05$).

Intriguingly, inhibition of Src, ERK, JNK and PKC but not p38 pathway was found to attenuate NGF induced neurite outgrowth (Figure 5.7D). The correlation between the activations of these pathways in NGF induced P-Ser-STAT3 and neurite outgrowth was suggestive of STAT3 acting as a downstream effector that contributes to neurite outgrowth.

5.2.6 Mitochondrial STAT3 is an important mediator of NGF induced neurite outgrowth

To investigate the role of mitochondrial P-Ser-STAT3 in NGF induced neurite outgrowth, mitochondria targeting wild type and mutant STAT3 (MTS-STAT3) were constructed by fusing the mitochondrial targeting sequence of cytochrome c oxidase subunit VIII to the N terminus of STAT3. This sequence has been reported to target the protein of interest to the inner mitochondrial membrane (*226*), where mitochondrial STAT3 was thought to exert its function. Such MTS-STAT3 constructs have been used successfully to investigate the functions of mitochondrial STAT3 in respiration (*188*) and oncogenic transformation (*189*). Subcellular fractionation of PC12 cells stably expressing wild type and mutant MTS-STAT3 showed an over-expression of STAT3 in the mitochondrial (4-6 fold) but not in the cytosolic fraction (Figure 5.8A). NGF induced neurite outgrowth was then studied using these constructs. Remarkably, mitochondria targeted serine dominant negative mutant of STAT3 (MTS-STAT3-SA) attenuated NGF induced neurite outgrowth (Figure 5.8B, C). In contrast, wild type (MTS-STAT3-WT) and tyrosine dominant negative mutant (MTS-STAT3-YF) of STAT3 were found to enhance NGF induced neurite outgrowth. These results demonstrated the involvement of mitochondrial P-Ser-STAT3 in NGF induced neurite outgrowth.

5.2.7 NGF stimulated ROS production and the involvement of mitochondrial STAT3

NGF stimulation has previously been shown to elevate ROS level in PC12 cells, contributing to NGF induced neurite outgrowth (*227*). Recently, it was suggested that NGF may modulate ROS level in PC12 cells by regulating mitochondrial functions (*228*). Since mitochondrial P-Ser-STAT3 was reported to modulate mitochondrial electron transport activities and the rate of oxygen consumption in non-neuronal cells (*188*), we tested the hypothesis that P-Ser-STAT3 may be involved in NGF regulation of ROS level in PC12 cells. Consistent with the previous report (*227*), an increase in total intracellular ROS was observed in PC12 cells when stimulated by NGF (Figure 5.9A). As expected, pre-incubation of PC12 cells with the antioxidant N-acetylcysteine (NAC) significantly blocked NGF induced ROS production (Figure 5.9C) and attenuated NGF induced neurite outgrowth (Figure 5.9B).

NGF induced ROS production was then compared in wild type and cells stably expressing mitochondria targeted STAT3 mutants. Interestingly, we observed a significant reduction in NGF induced ROS production in cells expressing MTS-STAT3-SA mutant, and an increase in cells expressing MTS-STAT3-WT and YF mutants (Figure 5.9C, black bar). The effects of STAT3 mutants on NGF induced ROS correlated well with their effects on NGF induced neurite outgrowth (Figure 5.9C, white bar), indicative of a role of mitochondrial P-Ser-STAT3 in the regulation of NGF induced ROS production and neurite outgrowth.

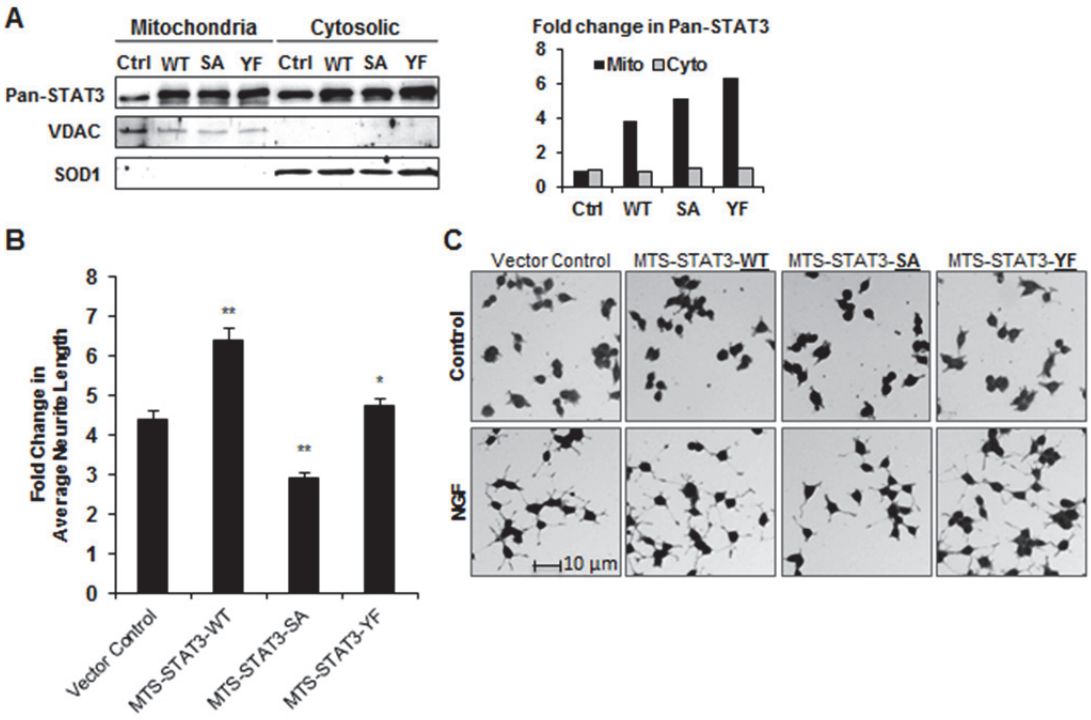

Figure 5.8 Mitochondrial STAT3 was involved in NGF induced neurite outgrowth. PC12 clones stably expressing mitochondria targeting wild type and mutant STAT3 were generated. *A.* Over-expression of STAT3 in mitochondria was verified by analyzing the level of total STAT3 in mitochondria of control and infected cells. Mitochondrial STAT3 were normalized by VDAC and cytosolic STAT3 normalized by SOD1. Fold changes in mitochondrial and cytosolic STAT3 level in infected cells over control were calculated. *B.* Control and MTS-STAT3 expressing PC12 clones were serum deprived and stimulated with 50 ng/ml NGF for 48 h. The average neurite length per cell was quantified using HCA-Vision. Fold changes in average neurite length in NGF treated cells over control were calculated for vector control PC12 cells and each of the MTS-STAT3 mutant expressing cells. Significant differences between control and mutant expressing PC12 cells were calculated using the paired Student's t-test. A value of $p<0.05$ was considered significant (**$p<0.01$; *$p< 0.05$). Representative images of control and NGF treated cells are shown in *C.*

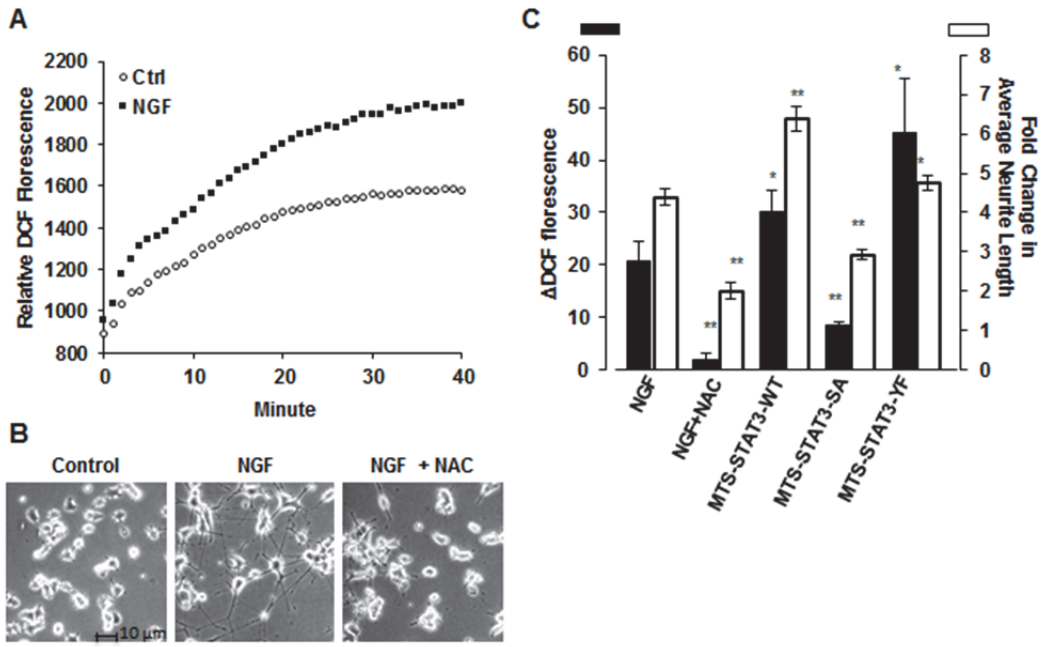

Figure 5.9 NGF induced ROS was partly mediated by mitochondrial STAT3. *A.* To quantify NGF stimulated production of ROS, PC12 cells were preloaded with DCFHDA (10 µM) for 10 min and stimulated with NGF (50 ng/ml). The florescent intensity of the oxidized product DCF was measured over the next 40 min. *B.* Representative images of control and NGF treated PC12 cells with and without NAC pre-treatment (10 mM) are shown in. *C*. The rate of ROS production in NGF treated PC12 cells was calculated using the following formula, $\Delta DCF/min=(\Delta DCF_{NGF,0\text{-}30min} - \Delta DCF_{Ctrl,0\text{-}30min}) / 30$. The rate of ROS production in PC12 cells stably expressing various MTS-STAT3 mutants was compared with that in non-simulated and NAC pre-treated vector control PC12 cells. Significant differences between the rates of ROS production were calculated using the paired Student's t-test. A value of $p<0.05$ was considered significant (**$p<0.01$; *$p< 0.05$). The effect of MTS-STAT3 mutants on rate of ROS production (black bar, primary vertical axis) was correlated with the effect on NGF induced neurite outgrowth (white bar, secondary vertical axis).

Section 5.3 Discussion

Originally identified as a key mediator of cytokine induced inflammation and immunity, STAT3 has now been shown to regulate a myriad of other biological processes. STAT3 is known to be activated by a variety of ligands involved in neurite outgrowth (*198, 209, 212, 229-232*). To date, all literature reports supporting the involvement of STAT3 in neurite outgrowth are based on observations of the effects of either P-Tyr-STAT3 or P-Tyr/Ser-STAT3 (*198, 209, 212*). The recent reports of NGF activated P-Ser-STAT3 in PC12 cells, did not demonstrate the contribution of phosphorylated serine^{727} STAT3 to neurite outgrowth (*212, 214*). This is rather surprising, as PC12 cells are commonly used as a model for neuritogenesis induced by a variety of agents, including NGF. To the best of our knowledge, this is the first report that demonstrated the involvement of P-Ser-STAT3 in neurite outgrowth and the unexpected phosphorylation on serine^{727} residue of STAT3 in mitochondria, induced by the neurotrophic factor NGF.

It is known that P-Tyr-STAT3 and P-Tyr/Ser-STAT3 translocate to the nucleus and mediate neurite outgrowth via transcriptional activation (*198, 209*). In this study, IL6 induced the efficient nuclear localization of P-Tyr/Ser-STAT3 whereas NGF induced P-Ser-STAT3 was undetectable in the nucleus even after 6 h of stimulation, an observation in contrast to the previous report (*212*). Instead, NGF was found to increase the level of P-Ser-STAT3 in mitochondria with no observable change in the total level of mitochondrial STAT3, suggesting the possibility that existing mitochondrial STAT3 may be phosphorylated directly by kinases, e.g. ERK 1/2. Such hypothesis is supported by our observation that ERK1/2 is robustly activated in mitochondria upon NGF stimulation. This is consistent with previous findings that ERK1/2 can be activated in mitochondria (*197, 233*), which in turn phosphorylated other mitochondrial proteins such as steroidogenic acute regulatory protein (*233*). However, our data does not rule out the possibility that cytosolic P-Ser-STAT3 may

be exchanged with non-phosphorylated mitochondrial STAT3 through a bi-directional trafficking mechanism. Yet it remains unclear how STAT3, which lack a putative mitochondria targeting sequence, can be translocated into the mitochondria. Binding to and translocation along with mitochondria targeting partner/s may yet be another possibility for P-Ser-STAT3 to be preferentially localized to the mitochondria. We did notice that P-Ser-STAT3 was highly co-localized with GRIM-19, a cytosolic translated component of mitochondrial complex I. Whether STAT3–GRIM-19 complex formed in the cytosol enabled STAT3 to be translocated to the mitochondria is currently under investigation.

It is increasingly recognized that mitochondria is not merely a cellular powerhouse, but a signaling hub where the bi-directional communication with the cytosolic components play an integral role in many physiological processes including neuronal survival (*234-236*). The recent evidence of mitochondria localized P-Ser-STAT3 enhancing functions of the electron transport chain(*188*) , the augmentation of oxidative phosphorylation and oxygen consumption (*189*), raised the interesting possibility that P-Ser-STAT3 may play a role in neurite outgrowth in PC12 by modifying mitochondria functions. Consistent with this hypothesis is that the over-expression of mitochondria targeted STAT3 serine dominant negative mutant (MTS-STAT3-SA) was found to attenuate NGF induced neurite outgrowth and the generation of ROS, products of the electron transport chain in mitochondria. The involvement of ROS in neurite outgrowths have been explored in both primary neurons (*237*) and cell lines (*227, 228, 238-241*). Several of these studies have shown that NGF induced neurite outgrowth in PC12 cells involves elevated ROS level (*227, 228, 240*), which may be modulated through the regulation of mitochondrial functions (*228*). In addition, ROS was recently shown to regulate F-actin dynamics in Aplysia bag cell neuron growth cone, lending further evidence that ROS participates in neuritogenesis (*237*). Similar to these reports (*227, 237-239,*

241), ROS in our study was quantified by a broad ROS sensor DCFHDA that does not discriminate different species of ROS. To unravel the precise biochemical mechanism of ROS in the regulation of neurite outgrowth, it may be necessary to take into account the different species of ROS. Whether the effect of mitochondrial P-Ser-STAT3 on ROS production directly impacts its involvement in neurite outgrowth is currently under investigation. Furthermore, it has not escaped our attention that the cytosolic P-Ser-STAT3 may also be involved in neurite outgrowth via mechanisms yet to be characterized. Nonetheless, our data demonstrated the novel and intriguing role of mitochondrial P-Ser-STAT3 in neurite outgrowth.

Depending on cell type and stimuli, multiple pathways have been implicated in the phosphorylation of serine residue of STAT3 (*186, 242, 243*). The observation that NGF induced serine phosphorylation of STAT3 in PC12 is temporally regulated by ERK, JNK and PKC pathways is novel and intriguing. The kinetics of NGF activations of these pathways is indicative of a complex network of signaling integrations and feedbacks, consistent with earlier report that NGF induced ERK and JNK pathways interact closely (*224*). In addition, NGF activation of ERK was shown to involve PKCε, a specific isoform of the PKC family (*244*). Further studies to elucidate the involvement of different PKC isoforms in STAT3 serine phosphorylation as well as their interactions with the MAPK pathways may help to delineate the biochemical mechanisms underlying the temporal regulation of NGF induced P-Ser-STAT3.

In conclusion, this study demonstrated that P-Ser-STAT3 is intimately involved in NGF induced neurite outgrowth in PC12 cells. This function is dependent on the spatial cellular organization of P-Ser-STAT3 to the mitochondria and is correlated to the regulation of ROS production. Distinct signaling mechanisms involving MAPK and PKC contribute to the phosphorylation serine^{727} residue of STAT3. Taken together, this and the previous study (chapter4) have provided novel insights into an

unconventional, transcription-independent mechanism whereby mitochondria localized STAT3 is involved in NGF and NTN induced neurite outgrowth.

Chapter 6 Normalization with genes encoding ribosomal proteins but not GAPDH provides an accurate quantification of gene expressions in neuronal differentiation of PC12 cells

Section 6.1 Introduction

During development, neurons make networks of connections with other neurons by growing axons and dendrites. These neuronal out-growths are regulated by extracellular cues such as GDNF and NGF that signal to cells resulting in phenotypic changes. A major challenge is the identification of molecular mechanisms underlying this highly complex and interactive network in terms of the functions of genes and proteins(*245*).

Currently, transcriptomic methods are widely used as an initial step in unraveling the complex signaling mechanisms underlying physiological and pathological processes and in neuronal differentiation (*246-249*). Gene microarray offers a high throughput platform for the analysis of the entire transcriptome to identify differentially expressed genes. Reverse transcription quantitative real-time PCR (RT-qPCR), with a wider dynamic range of quantification and higher assay sensitivity and precision, is often used to corroborate microarray findings (*250, 251*). Regardless of the method used, normalization, a critical process of adjusting the expression measurements between samples to compensate for various sources of variability in the assay, is essential to allow accurate comparisons of the results between different samples and conditions (*252, 253*). Normalization with internal reference gene is used to control for technical and biological variations introduced during both sample preparation and detection by RT-qPCR (*254*). It has also been shown to be suitable for the normalization of partially degraded RNA samples (*255-257*).

With nearly all normalization methods, the assumption that one or more reference genes are constitutively expressed at near-constant levels under all experimental conditions is implicit and the expression levels of all other genes in the sample are

then scaled to these reference genes accordingly. It is common to use reference genes selected from an assumed list of "housekeeping" genes (HKGs) which typically include transcripts such as GAPDH and ACTB (*253, 254, 258*). A number of studies have now shown that the expressions of these genes, in some but *not all* experimental conditions, are altered significantly (*259-262*), thus, making the choice of using these HKGs for normalization uncertain without *a priori* knowledge.

A variety of approaches have been employed to enable better selection of reference genes. One approach is the use of statistical algorithms, for example, geNorm (*258*), Best keeper (*263*), NormFinder (*264*), Global Pattern Recognition (*265*), and Equivalence tests (*266*), to evaluate the relative expression stabilities of genes from a pool of predefined lists of candidates. While this approach is certainly more robust than using the single gene methods, it too is based on potentially unfounded assumptions about which genes may be stably expressed in the conditions studied. These genes are still required to be pre-selected and incorporated into the experimental designs without any *a priori* evidence to support their use. An alternative and less biased approach is the meta-analysis of large scale gene expression profiles to identify stably expressed genes (*267-270*). A selected number of potential references genes can then be validated experimentally and the stability of expressions analysed by the above mentioned statistical algorithms in defined experimental settings.

To date, reference genes validated for neuronal differentiation studies have not been reported yet. The present study aims to identify suitable reference genes during chemically induced neuronal differentiation of PC12, a cell-line derived from a pheochromocytoma of the rat adrenal medulla. Because of its unique cellular properties, suitability for genetic and biochemical manipulations, the PC12 cell-line is widely regarded as a convenient alternative to endogenous neuronal cells, and serves as a commonly used model system for studies on neuronal differentiation

(*213, 271, 272*). For example, in response to NGF, PC12 cells stop dividing, elaborate neuronal processes, are electrically excitable, and have the potential to form synapses when co-cultured with muscle cells (*273*). Here, we measured the temporal expression of twenty novel candidate reference genes identified from microarray studies and the commonly used HKGs, ACTB and GAPDH, at various stages of PC12 differentiation. Based on two independent statistical approaches ["pairwise comparison" (*258*) and "model based variation" (*264*)], the expressions of ribosomal protein genes RPL19 and RPL29 were found to be highly stable regardless of pharmacological treatments and stages of differentiation. The combination of the two reference genes was sufficient to allow robust and accurate normalization of differentiation related genes.

Section 6.2 Result

6.2.1 Selection of candidate reference genes from microarray data

It has been suggested that suitable reference genes should be expressed in all experimental conditions and exhibit low coefficient of variation (CV) in their expressions (*269, 270, 274, 275*). In order to identify such reference genes, we first analysed the expression profiles of 21,910 genes in naïve PC12 cells and those treated with NGF or GDNF and found 8,568 genes to be expressed in all conditions (detection p values < 0.05). We then analysed the top 100 genes with the lowest CV (0.8% -1.45%) with two well accepted but different statistical approaches, "pairwise comparison" (geNorm) and "model based variation analysis" (NormFinder). The "pairwise comparison" approach assumes that a perfect pair of reference genes has a constant ratio across all experimental conditions. As such, geNorm evaluates the inter-conditional variability of the ratio between each pair of reference genes and calculates a gene stability measure M for each candidate (*258*). However, with this method, tightly co-regulated genes will appear to be stable. The second algorithm, NormFinder, was employed to safeguard against such a pitfall of misidentifying

expression invariant reference genes. This model-based variance estimation approach entails analysis of sample subgroups and calculates the variation of each candidate gene individually, based on both intra- and inter-group variation (*264*). While geNorm measures relative stability, NormFinder measures absolute stability by decomposing the variance to biological and technical elements. With this method, the expressions of co-regulated genes can be distinguished. Despite the differences in algorithms and assumptions, both statistical methods were in agreement on the identity of the twenty most stable genes (Table 6.1), most of which are novel for the purpose of normalization studies. Interestingly, thirteen of these twenty candidate reference genes were ribosomal protein genes.

6.2.2 Real-time PCR validation of novel candidate reference genes

As one of the most extensively studied models for neuronal differentiation, PC12 cells respond to a broad spectrum of pharmacological agents, which trigger a myriad of intracellular signaling pathways leading to neuronal differentiation. In order to verify the general utility of the 20 selected putative reference genes (Table 6.1) in a broader range of experimental conditions, we differentiated PC12 cells with other stimuli (Forskolin (*276*), KCl (*154*) and ROCK inhibitor Y27632 (*277*)) in addition to NGF and GDNF. GDNF was applied to PC12 cells stably expressing GDNF Family Receptor alpha 1a (GFRα1a) and co-receptor RET (either RET9 or RET51 isoforms), which are not endogenously expressed at detectable levels in PC12 cells (data not shown). The percentage of PC12 cells differentiated by the five chemical stimuli was quantified (Figure 6.1A) and the axon-like features of the extended neurite were confirmed by immunocytochemical analysis with anti-Neurofilament-200 antibody (Figure 6.1B). The extent of neurite outgrowth was highly dependent on the stimuli used. NGF and GDNF stimulation induced longer neurite outgrowths than Forskolin, KCl or Y27632. Total RNA was collected at 0.5 h, 6 h, 24 h and 72 h from control and treated cells for each stimuli, with biological triplicates, that totaled 120 samples.

Gene symbol	Definition	Mean	geNorm	Norm Finder
RPL29	Ribosomal protein L29	14.04	1	1
RPL10a	Ribosomal protein L10A	12.49	2	2
LOC292640	Vps20-associated 1 homolog	10.87	3	3
LOC498143	Similar to ribosomal protein L15	13.71	4	4
LOC317275	Similar to ribosomal protein L7-like 1	11.88	7	5
RPS15	Ribosomal protein S15	12.97	5	6
ARBP	Acidic ribosomal phosphoprotein P0	14.27	6	7
RPL14	Ribosomal protein L14	13.89	9	8
EEF1A1	Eukaryotic translation elongation factor 1 alpha 1	14.17	8	9
RPS15A	Ribosomal protein S15a	13.93	10	10
RPL18	Ribosomal protein L18	13.58	11	11
REPS1 (P)	RalBP1 associated Eps domain containing protein (predicted)	10.73	12	12
LOC363720	chromatin modifying protein 2B	10.61	14	13
CNOT8	CCR4-NOT transcription complex, subunit 8	11.00	15	14
RTCD1	RNA terminal phosphate cyclase domain 1	10.48	17	15
RPL19	Ribosomal protein L19	13.74	13	16
NDUFB6 (P)	NADH dehydrogenase (ubiquinone) 1 beta subcomplex, 6,	10.43	16	17
RPL9	Ribosomal protein L9	13.74	18	18
LOC499803	Similar to 40S ribosomal protein S3	13.76	19	19
RPL3	Ribosomal protein L3	14.03	20	20
ACTB	Actin, beta	13.85		
GAPDH	Glyceraldehyde-3-phosphate dehydrogenase	12.88		

Table 6.1 Selection of candidate reference genes from microarray data. Microarray analysis of the expression profiles of 21,910 genes in naïve PC12 cells and those treated with NGF or GDNF for 0.5 h and 72 h. Twenty candidate reference genes were selected based on pairwise comparison (geNorm) and model based variation (NormFinder) analysis of the top 100 genes with the lowest CV. The log2 transformed values of the average signal intensities among the 24 arrays were shown as Mean. Thirteen of the twenty genes were Ribosomal Protein Genes (Bold). Both ACTB and GAPDH were included for comparison but were not among the top 100 genes recommended by either statistical analysis.

We analysed the expression levels of the aforementioned twenty candidate reference genes, two most commonly used HKGs (GAPDH and ACTB), and three genes which are well known to be regulated by NGF using RT-qPCR (Figure 6.2). The expression levels of the twenty candidate reference genes and the two HKGs span three orders of magnitude. These reference genes were expressed at comparable levels or lower than the HKGs examined. For accurate determination of inter-assay variations and primer efficiencies, flanking regions of the genes (~300bp) were amplified by PCR, sub-cloned and the sequences verified. These recombinant plasmids were then linearized and served as templates to construct standard curves. All the qPCR assays showed high efficiency of amplification (>90%) and low intra- and inter-assay variations. All RNA samples showed RQI values of greater than 9, indicative of high quality and integrity (data not shown).

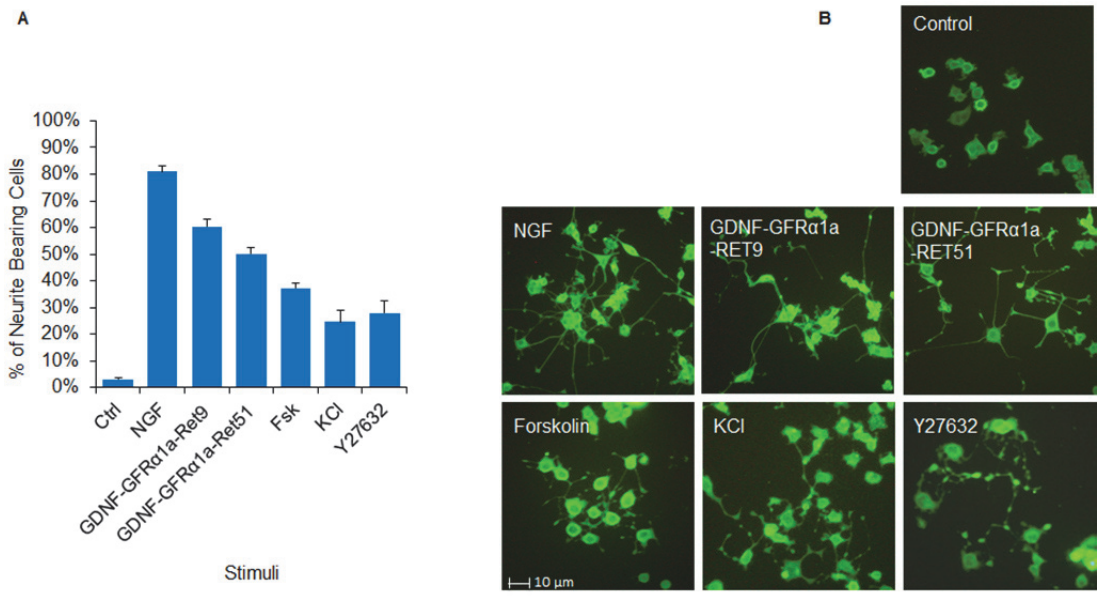

Figure 6.1 Neuronal differentiation of PC12 cells. A. Quantification of the percentage of PC12 cells bearing neurite of at least one cell body length, after 72 h of treatment with NGF (50 ng/ml), GDNF (50 ng/ml), Forskolin (10 µM), KCl (5 mM) and ROCK inhibitor Y27632 (25 µM). GDNF treatment was applied to PC12 cells stably expressing GDNF Family Receptor alpha 1a (GFRα1a) and co-receptor RET (either RET9 or RET51 isoforms), which were not endogenously expressed at detectable level in PC12 cells. All other stimulations were applied to wild type PC12 cells. B. Representative images of control and treated PC12 cells immuno-stained with anti-Neurofilament 200 antibody.

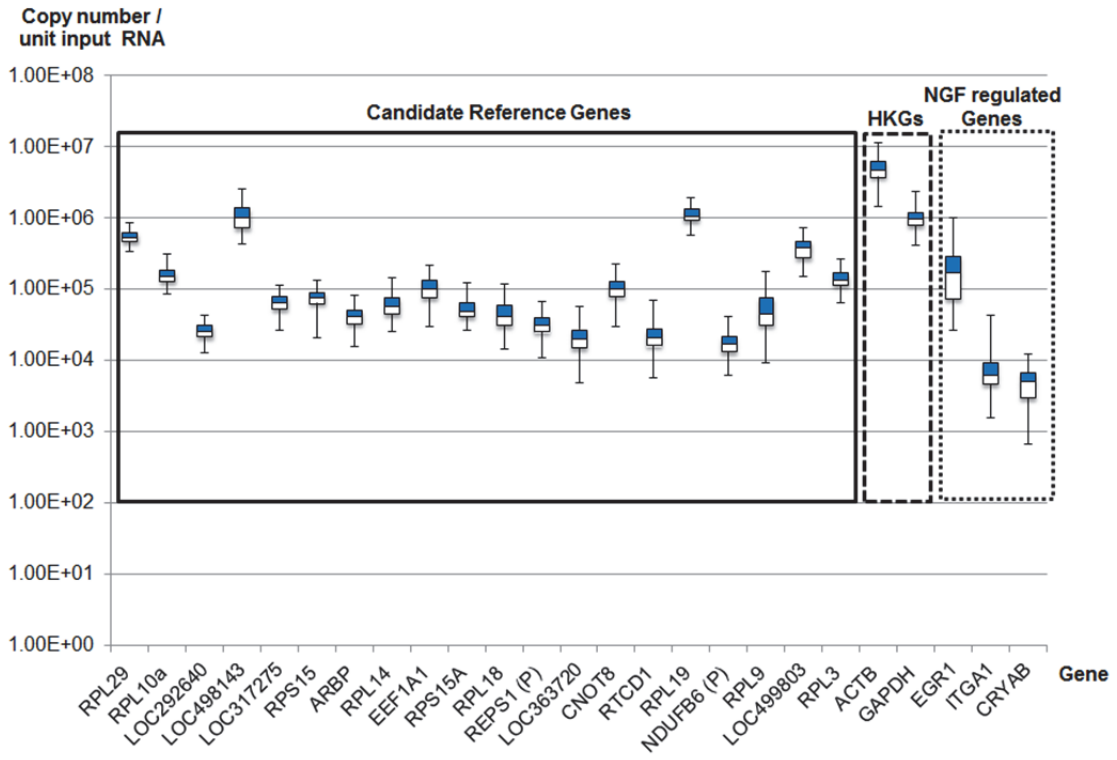

Figure 6.2 Distribution of the expression levels of genes examined. Box plot representation of the expression levels of twenty candidate reference genes (solid line), two housekeeping genes (dashed line) and three target genes (dotted line) among the 120 biological samples. The expression level of each gene was represented as the absolute copy number per unit input total RNA (0.0625µg), quantified by RT-qPCR using linearized plasmid standards.

6.2.3 Stabilities of candidate reference genes and common housekeeping genes

Using both geNorm and NormFinder, we analysed the expression stabilities of the twenty candidate reference genes and the two commonly used HKGs across all six differentiation conditions. Both statistical approaches recommended the same three ribosomal protein genes RPL19, RPL29 and RPL3 as the overall best reference genes (Figure 6.3). Pairwise variation analysis by geNorm showed that the combination of RPL19 and RPL29 is sufficiently stable (V2/3=0.107, less than the recommended cut-off of 0.15), thus excluding the need to incorporate a third reference gene RPL3 for normalization of target gene expression. Notably, neither GAPDH nor ACTB were recommended.

Further analysis of candidate gene stabilities in each treatment group (Table 6.2A) or at specific time point (Table 6.2B) revealed that the stability rankings of candidate genes do vary among different subgroups. However, with the exception of RPL29 in KCl treated samples, the two genes RPL19 and RPL29 were consistently ranked among top 5 in all subgroups. In contrast, the stability rankings of GAPDH and ACTB varied considerably among different subgroups and they were ranked among the least stable ones within the group of 22 genes in several subgroups. The data indicated that the two novel candidate genes RPL19 and RPL29 have higher expression stabilities than both GAPDH and ACTB, and may serve as better normalizers for gene expression in neuronal differentiation of PC12 cells.

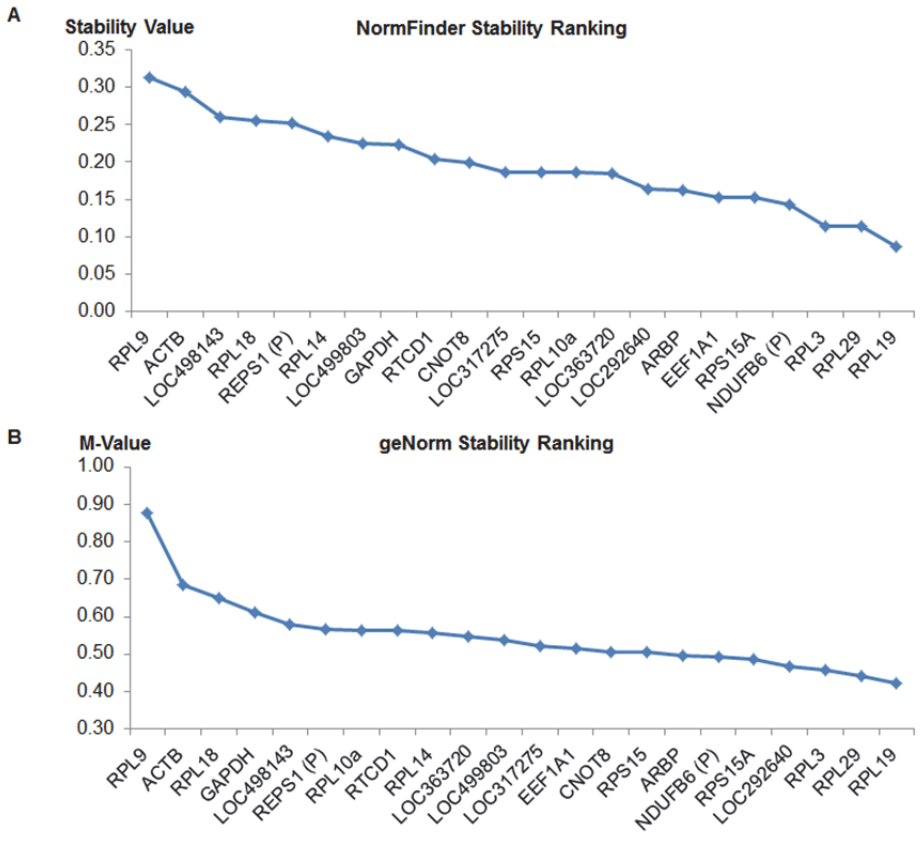

Figure 6.3 Stability analysis of candidate reference genes and housekeeping genes. Stability rankings of the twenty candidate reference genes and two most commonly used housekeeping genes ACTB and GAPDH, among all 120 biological samples, by NormFinder (A) and geNorm (B). A low 'Stability Value' or 'M-value' correlates to higher gene expression stability.

A

NGF		GDNF-GFRα1a-RET9		GDNF-GFRα1-RET51		Forskolin		KCl		Y27632	
NormFinder	geNorm	*NormFinder*	geNorm	*NormFinder*	geNorm	*NormFinder*	geNorm	*NormFinder*	geNorm	*NormFinder*	geNorm
Rpl29	Rpl10a	*Rpl3*	Rpl19	*LOC292640*	LOC292640	*Rpl19*	Rpl19	*Rpl19*	Rpl19	*Rpl29*	Rpl29
Rpl10a	Rpl29	*Rpl19*	Rpl3	*Eef1a1*	Eef1a1	*Rpl29*	Rpl29	*Reps1(p)*	Reps1(p)	*Rpl19*	Rpl19
Rpl19	Cnot8	*Rpl29*	LOC292640	*Rpl19*	Rpl19	*LOC498143*	LOC498143	*Rpl3*	LOC292640	*Rpl10a*	Rpl10a
Ndufb6(p)	Rpl19	*LOC292640*	Rpl29	*Rpl29*	Rpl29	*Rpl3*	Rps15	*LOC498143*	Rpl3	*LOC499803*	LOC292640
Cnot8	Rps15	*LOC498143*	Reps1(p)	*LOC499803*	LOC499803	*LOC363720*	Arbp	*LOC292640*	LOC498143	*LOC292640*	Reps1(p)
LOC498143	LOC292640	*Rps15a*	LOC317275	*Arbp*	Arbp	*LOC292640*	Rpl3	*Arbp*	LOC499803	*Rpl3*	Cnot8
LOC292640	LOC498143	*LOC317275*	LOC498143	*Rpl3*	Rps15	*Arbp*	LOC292640	*LOC317275*	Cnot8	*Reps1(p)*	LOC499803
Rps15	Ndufb6(p)	*Reps1(p)*	Rps15a	*Rps15*	Rpl3	*Rps15*	Cnot8	*LOC499803*	Arbp	*Cnot8*	Rpl3
Rpl3	Rtcd1	*LOC499803*	Ndufb6(p)	*Reps1(p)*	LOC317275	*LOC317275*	Reps1(p)	*Rps15*	Rps15	*Arbp*	Arbp
Rtcd1	**Actb**	*Ndufb6(p)*	LOC499803	*Ndufb6(p)*	Reps1(p)	*LOC499803*	LOC363720	***Gapdh***	**Rpl29**	*Rps15*	Rps15
Actb	Rps15a	*Cnot8*	Cnot8	*LOC498143*	Cnot8	*Reps1(p)*	LOC499803	*LOC363720*	LOC317275	*Ndufb6(p)*	LOC363720
LOC499803	LOC499803	*LOC363720*	Arbp	*LOC317275*	Ndufb6(p)	*Rtcd1*	LOC317275	*Cnot8*	Rps15a	*LOC317275*	Rpl14
Rps15a	Rpl3	*Eef1a1*	LOC363720	*Rps15a*	Rps15a	***Gapdh***	Ndufb6(p)	*Eef1a1*	LOC363720	*LOC363720*	Ndufb6(p)
Reps1(p)	Reps1(p)	*Arbp*	Rpl14	*Rpl10a*	LOC498143	*Ndufb6(p)*	Rps15a	*Rpl14*	Rpl14	*Rtcd1*	Eef1a1
Eef1a1	Arbp	*Rpl14*	Rpl18	*Cnot8*	Rtcd1	*Cnot8*	**Gapdh**	*Rpl10a*	**Gapdh**	*Eef1a1*	Rtcd1
Rpl18	Rpl18	*Rpl18*	Eef1a1	*Rtcd1*	Rpl10a	*Rpl14*	Rpl14	***Rpl29***	**Actb**	*Rps15a*	LOC317275
Arbp	LOC363720	*Rtcd1*	Rps15	*Rpl14*	Rpl14	*Eef1a1*	Rtcd1	*Rps15a*	Eef1a1	*LOC498143*	Rps15a
LOC363720	Eef1a1	*Rps15*	**Actb**	***Gapdh***	**Gapdh**	*Rps15a*	Eef1a1	*Ndufb6(p)*	Rtcd1	*Rpl14*	LOC498143
Rpl14	Rpl14	***Actb***	Rtcd1	***Actb***	**Actb**	*Rpl10a*	Rpl10a	*Rtcd1*	Ndufb6(p)	***Gapdh***	**Gapdh**
LOC317275	LOC317275	*Rpl10a*	Rpl10a	*LOC363720*	LOC363720	*Rpl18*	Rpl18	***Actb***	Rpl10a	***Actb***	**Actb**
Rpl9	Rpl9	***Gapdh***	**Gapdh**	*Rpl9*	Rpl18	***Actb***	**Actb**	*Rpl18*	Rpl18	*Rpl18*	Rpl18
Gapdh	**Gapdh**	*Rpl9*	Rpl9	*Rpl18*	Rpl9	*Rpl9*	Rpl9	*Rpl9*	Rpl9	*Rpl9*	Rpl9

B

0.5 h		6 h		24 h		72 h	
NormFinder	geNorm	*NormFinder*	geNorm	*NormFinder*	geNorm	*NormFinder*	geNorm
Rpl19	Rpl19	*Rpl19*	Rpl19	*Rpl19*	Rpl19	*Rps15a*	Rps15a
Eef1a1	Eef1a1	*Arbp*	Rpl29	*Eef1a1*	Rpl29	*Rpl29*	Rpl29
Rpl29	Arbp	*Rpl29*	Arbp	*Rpl29*	Eef1a1	*Rpl19*	Ndufb6(p)
Arbp	Rpl29	*Ndufb6(p)*	LOC292640	*Rpl3*	LOC292640	*Ndufb6(p)*	Rpl3
LOC363720	LOC363720	*LOC292640*	Rpl3	*LOC292640*	Rpl3	*Rpl3*	Rpl19
Rpl3	**Gapdh**	*Rpl3*	Ndufb6(p)	*Rps15a*	Rps15a	*LOC292640*	LOC292640
Ndufb6(p)	Rpl3	*LOC363720*	**Gapdh**	*Cnot8*	Cnot8	*Cnot8*	Cnot8
Rps15	Ndufb6(p)	***Gapdh***	Rps15	*Arbp*	Rps15	*Rpl14*	Rpl14
Gapdh	Rps15	*Eef1a1*	LOC363720	*Rps15*	Arbp	*Rtcd1*	Rtcd1
LOC292640	LOC292640	*Rps15*	LOC499803	*Ndufb6(p)*	Ndufb6(p)	*LOC317275*	LOC317275
Cnot8	Cnot8	*LOC499803*	Eef1a1	*Rpl10a*	LOC317275	*Rps15*	Rps15
LOC317275	LOC317275	*Rps15a*	Rpl10a	*LOC317275*	Rpl14	*Rpl10a*	Eef1a1
Rps15a	LOC499803	*Rpl10a*	Rps15a	*Rpl14*	LOC363720	*Arbp*	Arbp
LOC499803	Reps1(p)	*Cnot8*	Cnot8	*LOC363720*	Rpl10a	***Gapdh***	LOC499803
Rpl18	Rps15a	*Rtcd1*	Rpl18	*Reps1(p)*	LOC498143	*LOC499803*	Rpl18
Rpl14	**Actb**	*Rpl18*	Reps1(p)	*Rtcd1*	Reps1(p)	*Rpl18*	LOC498143
Rtcd1	Rpl18	*LOC317275*	LOC317275	*LOC498143*	Rtcd1	*Eef1a1*	**Gapdh**
Reps1(p)	Rpl14	*Rpl9*	Rtcd1	*Rpl18*	LOC499803	*Reps1(p)*	Rpl10a
LOC498143	Rtcd1	*LOC498143*	LOC498143	*LOC499803*	Rpl18	*LOC498143*	Reps1(p)
Actb	Rpl10a	*Reps1(p)*	Rpl9	***Actb***	**Actb**	*LOC363720*	LOC363720
Rpl10a	LOC498143	*Rpl14*	Rpl14	***Gapdh***	**Gapdh**	***Actb***	**Actb**
Rpl9	Rpl9	***Actb***	**Actb**	*Rpl9*	Rpl9	*Rpl9*	Rpl9

Table 6.2 Stability rankings of twenty candidate reference genes, ACTB and GAPDH in treatment and time-point subgroups. Stability rankings were determined by NormFinder (Italic) and geNorm, for each stimulus (Additional File 2A) or time point (Additional File 2B) subgroup. The top two candidate genes (RPL19 and RPL29) in overall ranking (Figure 4) were bolded in red and the two HKGs were bolded and highlighted in grey.

6.2.4 Comparison of the normalization factors generated by different reference gene(s)

To account for possible variations introduced during sample preparation and measurements, raw expression profiles of target genes were scaled by a normalization factor (NF) calculated based on independent measurement of one or more internal reference genes. The variation between NFs generated by different reference genes is thus directly reflective of the variation in the final target gene expression values normalized by different reference genes. We noticed that although RPL19 and RPL29 were ranked as the overall best pair of reference genes, they

were not necessarily the best pair for each treatment subgroup. To test the robustness of these two genes across different treatments, we compared the normalization factors calculated based on RPL19 and RPL29 ($NF_{RPL19/RPL29}$) to that of the most stable pair of reference genes (NF_{top2}) in each treatment subgroup. Similarly, we examined the differences between NF_{top2} and NFs calculated based on the commonly used HKGs, ACTB (NF_{ACTB}) or GAPDH (NF_{GAPDH}). The deviations of each NF from NF_{top2} are represented in Figure 6.4. The $NF_{RPL19/RPL29}$ values were found to least deviate from NF_{top2} in NGF, GDNF and KCl subgroups, and had zero deviation in Fsk and Y27632 subgroups as RPL19 and RPL29 were ranked top 2. In contrast, NF_{ACTB} and NF_{GAPDH} differed substantially from NF_{top2} in many instances, reflective of their varying stabilities across different treatments.

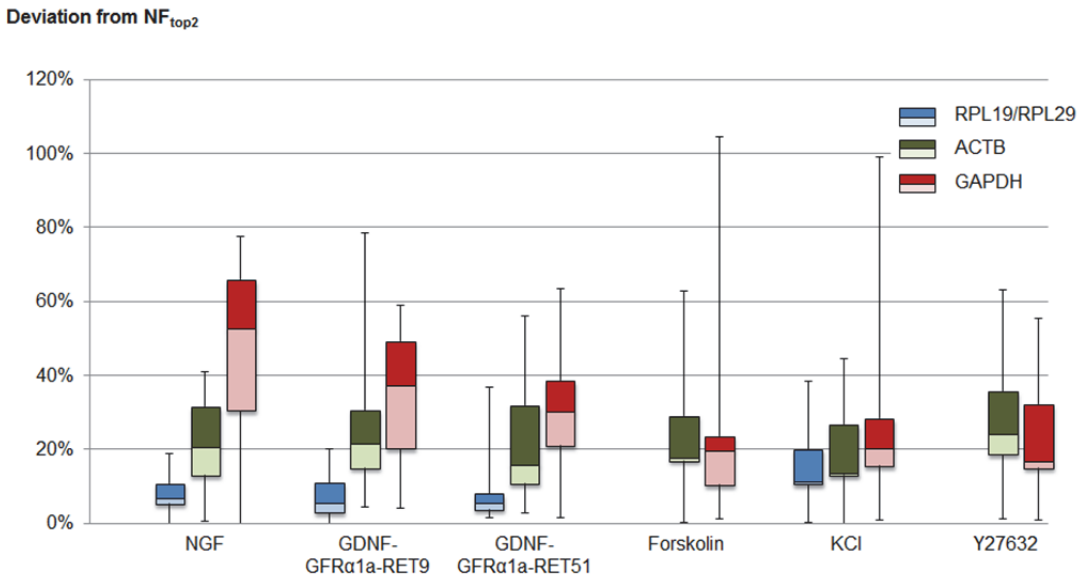

Figure 6.4 Comparison of the normalization factors calculated using different reference gene(s). Normalization factors (NFs) calculated with RPL19/RPL29, ACTB and GAPDH were compared to that calculated by the top 2 reference genes (NF_{top2}) as recommended by both NormFinder and geNorm, for each stimulus. The percentage deviations of $NF_{RPL19/RPL29}$; NF_{ACTB} ; NF_{GAPDH} from NF_{top2} ($|NF_x - NF_{top2}|/NF_{top2}$) were represented by box plot. The 25th percentile to the 75th percentile (boxes), and ranges (whiskers) were shown.

6.2.5 Effect of different reference genes on the interpretation of target gene regulation

Next, the possibility that using scaling factors of $NF_{RPL19/29}$, NF_{ACTB} or NF_{GAPDH} may substantially alter the interpretation of target gene expression regulation in NGF induced neuronal differentiation was investigated. The relative fold changes of EGR1, ITGA1 and CRYAB expressions normalized by the three NFs were compared to the values normalized by NF of the top 2 genes ($NF_{RPL29/RPL10A}$). No statistically significant differences were observed among $NF_{RPL29/RPL10A}$, $NF_{RPL19/RPL29}$, and NF_{ACTB} normalized values; whereas NF_{GAPDH} normalized fold changes were significantly different (Figure 6.5 A-C). In the case of EGR1 and ITGA1, the use of GAPDH as reference gene resulted in the underestimation of target genes expressions, leading to false negative conclusions when a two-fold cut off was applied (Figure 6.5 A-B). On the other hand, normalization by GAPDH resulted in the significant over-estimation of the down-regulation of CRYAB in NGF treated samples (Figure 6.5C).

The clearly different expression profiles of EGR1, ITGA1, and CRYAB when normalized to GAPDH raised the possibility that GAPDH expression could be regulated over the course of NGF induced differentiation. Normalization of GAPDH expression by the NF of the top 2 genes ($NF_{RPL29/RPL10A}$) and the $NF_{RPL19/RPL29}$, revealed that GAPDH expression was indeed significantly elevated (>2.5 fold at 24 h) in NGF-stimulated PC12 cells (Figure 6.6). A more detailed analysis of the kinetics of GAPDH expression over time revealed that expression of GAPDH indeed increased over a period of 28 h (data not shown). As a result, the use of GAPDH as a single, unverified reference gene would invariably lead to erroneous interpretation of target gene regulation.

Similarly, we investigated the effect of different reference gene(s) on normalized target gene expressions in GDNF, Forskolin, KCl and ROCK inhibitor Y27632 treated samples. Similar to the case of NGF treatment, with GDNF stimulated PC12-

GFRα1a/RET9 and PC12-GFRα1a/RET51 cells, normalization by GAPDH resulted in the underestimations of GDNF induced upregulation of EGR1 and ITGA1 expressions; and over-estimated CRYAB down-regulation (Figure 6.7A, B). Interestingly, normalization by ACTB was found to overestimate the expression of EGR1 and ITGA1 expressions in PC12-GFRα1a/RET51 but not RET9 cells (Figure 6.7B, 72h), highlighting the subtle differences between GFRα1a/RET9 and GFRα1a/RET51 systems.

For Forskolin and ROCK inhibitor Y23672 differentiated samples, normalization by ACTB consistently led to the over-estimations of target gene expressions (Figure 6.7C, D). Depending on the time point analysed, normalization by GAPDH was shown to result in either underestimations or overestimations of target gene expressions (Figure 6.7C, D). In KCl treated samples, no statistical significant difference was observed among $NF_{top2\ (RPL19/REPS1)}$, $NF_{RPL19/RPL29}$, NF_{ACTB} and NF_{GAPDH} normalized target gene expression, which suggested that all four were acceptable reference gene(s) for this particular experimental condition (data not shown).

It is thus evident that the stabilities of the two most commonly used HKGs, GAPDH and ACTB vary across different experimental conditions during neuronal differentiation of PC12 cells. They were acceptable reference genes under some conditions but may significantly under- or over-estimate target gene expression under others. On the contrary, the two novel candidate reference genes RPL19 and RPL29 were stably expressed among all conditions analysed and allowed accurate normalization of differentially regulated genes during PC12 differentiation. It is worthy to note that at early time points (0.5 h and 6 h), the expressions of EGR1, ITGA1 and CRYAB did not show any significant differences when scaled with either $NF_{top2,}$ $NF_{RPL19/RPL29}$, NF_{ACTB} or NF_{GAPDH} (data not shown). This is consistent with the observation that the expression of GAPDH did not change significantly at the early time points (Figure 6.6).

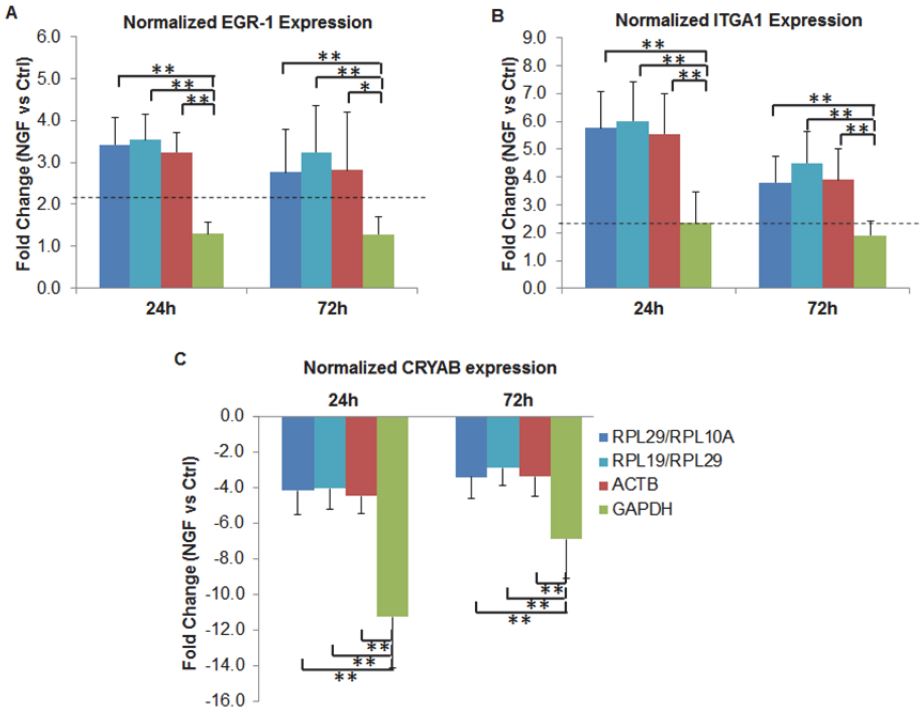

Figure 6.5 Fold changes in target gene expressions normalized using different reference gene(s). Fold changes in transcript expressions of Egr-1 (A), Integrin alpha 1, ITGA1 (B), Crystallin alpha b, CRYAB (C), in NGF treated samples relative to that of control were normalized by (1) geometric mean of RPL10a/RPL29; (2) geometric mean of RPL19/RPL29; (3) ACTB or (4) GAPDH. Normalization by GAPDH led to significant quantitative underestimations of EGR1 and ITGA1 upregulation and overestimation of CRYAB downregulation. Dotted line represents the 2-fold difference between treatment and control subjects, a cut off commonly used to distinguish significant changes from insignificant ones. Significant differences between fold changes normalized by various reference gene(s) were calculated using the paired Student's *t-test.* A value of $p<0.05$ was considered significant (**$p<0.01$; *$p< 0.05$)

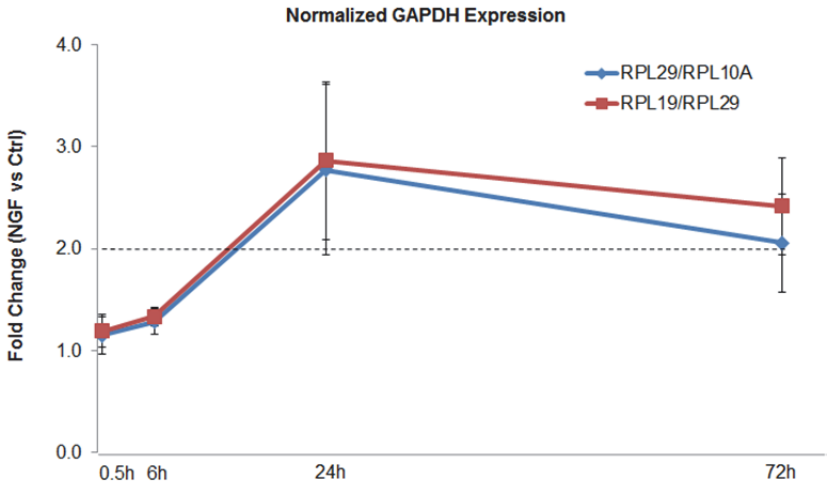

Figure 6.6 Upregulation of GAPDH transcript expression in NGF induced neuronal differentiation. Fold changes in transcript expression of GAPDH in NGF treated samples relative to that of control were normalized by (1) geometric mean of RPL10a/RPL29; or (2) geometric mean of RPL19/RPL29. Dotted line represents the 2-fold difference between treatment and control cells.

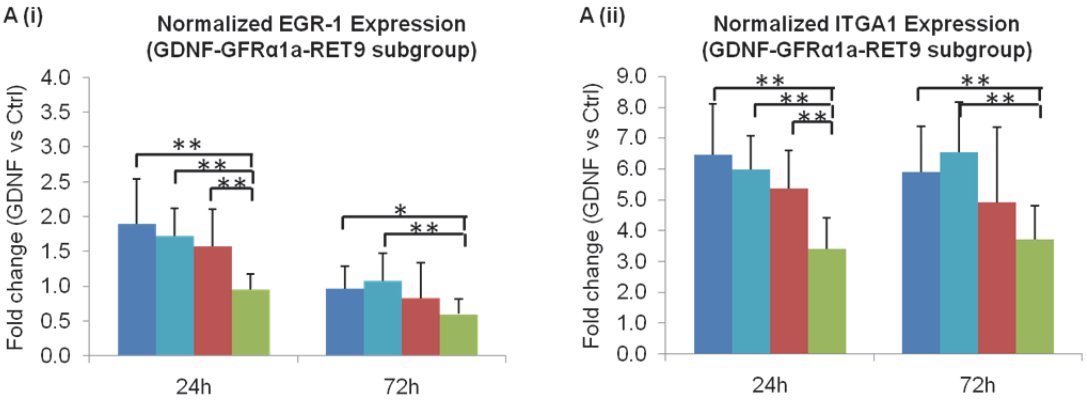
A (i)
Normalized EGR-1 Expression
(GDNF-GFRα1a-RET9 subgroup)
Fold change (GDNF vs Ctrl)
24h
72h
A (ii)
Normalized ITGA1 Expression
(GDNF-GFRα1a-RET9 subgroup)
Fold change (GDNF vs Ctrl)
24h
72h

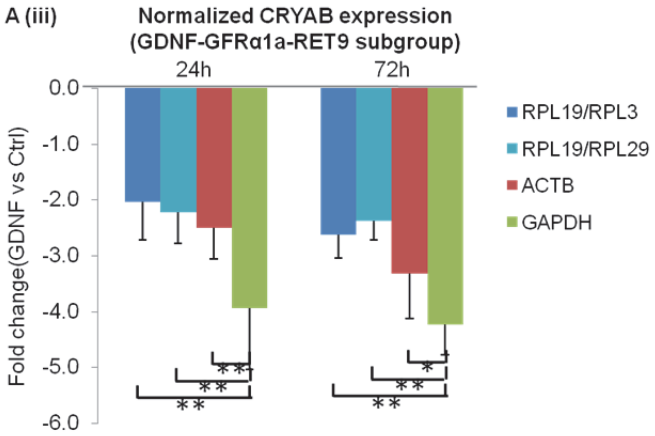
A (iii)
Normalized CRYAB expression
(GDNF-GFRα1a-RET9 subgroup)
24h
72h
Fold change(GDNF vs Ctrl)
RPL19/RPL3
RPL19/RPL29
ACTB
GAPDH

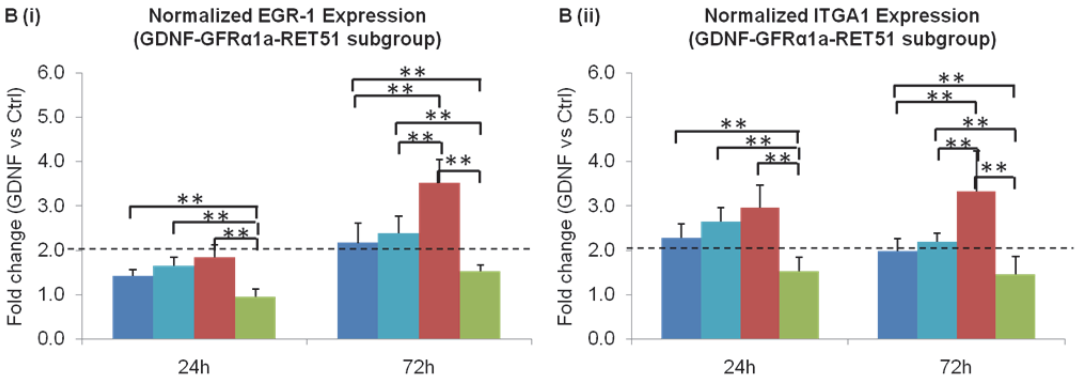
B (i)
Normalized EGR-1 Expression
(GDNF-GFRα1a-RET51 subgroup)
Fold change (GDNF vs Ctrl)
24h
72h
B (ii)
Normalized ITGA1 Expression
(GDNF-GFRα1a-RET51 subgroup)
Fold change (GDNF vs Ctrl)
24h
72h

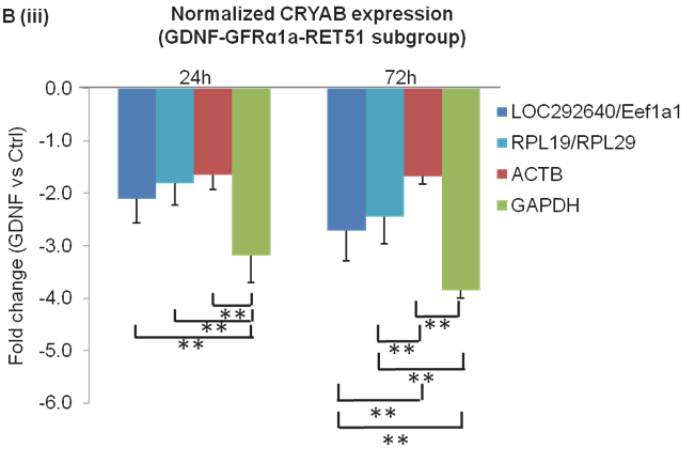
B (iii)
Normalized CRYAB expression
(GDNF-GFRα1a-RET51 subgroup)
24h
72h
Fold change (GDNF vs Ctrl)
LOC292640/Eef1a1
RPL19/RPL29
ACTB
GAPDH

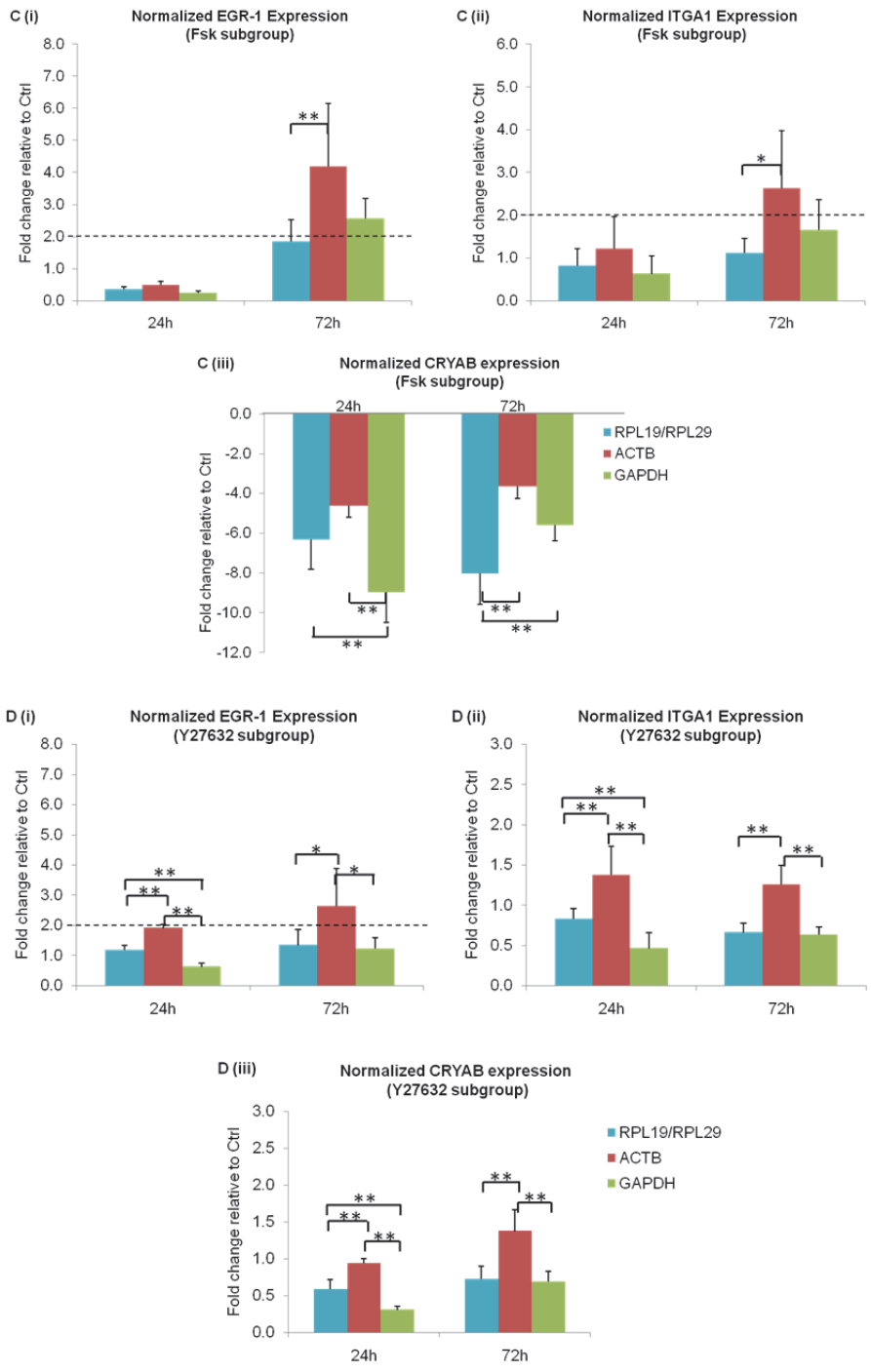

Figure 6.7 Normalized target gene expression regulation in PC12 cells differentiated with GDNF, Forskolin and Y27632. Fold changes in transcript expressions of Egr-1 (**i**), Integrin alpha 1, ITGA1 **(ii)**, and Crystallin alpha b, CRYAB (**iii**), in GDNF-GFRα1a-RET9 (**A**), GDNF-GFRα1a-RET51 (**B**), Forskolin (**C**), Y27632 (**D**) treated samples relative to that of control were normalized by geometric mean of top 2 reference genes in each subgroup; geometric mean of RPL19/RPL29; ACTB or GAPDH. Normalization by ACTB resulted in the over-estimation of target gene expression. Normalization by GAPDH led to either under- or over-estimation of target gene expression. Dotted line represents the 2-fold difference between treatment and control subjects, a cut off commonly used to distinguish significant changes from insignificant ones. Significant differences between fold changes normalized by various reference gene(s) were calculated using the paired Student's *t test.* A value of $p<0.05$ was considered significant (**$p<0.01$; *$p< 0.05$)

Section 6.3 Discussion

Twenty candidate reference genes that showed little variation but high expression in PC12 cells differentiated with NGF and GDNF were first selected from microarray datasets using two independent statistical algorithms. Together with two well-studied HKGs, the expression stabilities of these candidate reference genes were further analysed using RT-qPCR in cells differentiated with other stimuli. From these studies, unexpectedly, RPL19 and RPL29 but not the HKGs, were identified as suitable reference genes that can be used for normalization of gene expression in neuronal differentiation of PC12 induced by a variety of chemical stimuli.

Neuronal differentiation is a process where cells undergo enormous morphological changes, over a period of several days. It is accompanied by substantial biochemical changes including cell cycle exit (*278*), changes in metabolism (*279, 280*) and alteration in structural proteins (*281, 282*). Since the commonly used reference genes are mostly structural proteins or enzymes involved in metabolism, it is especially important to validate the stabilities of these genes during the process of differentiation. Many of these studies investigated gene expression changes in PC12 but few have evaluated the suitability of HKGs as normalizers in this model. Our microarray analysis revealed that a group of novel candidate genes was more stably expressed than commonly used HKGs ACTB and GAPDH, suggesting that ACTB and GAPDH may not be ideal reference genes in neuronal differentiation of PC12 cells.

In an effort to gain an insight into the temporal regulation of genes during neuronal differentiation, it is necessary that the reference genes used are stably expressed over a period of days. GAPDH and ACTB have been used for normalization in more than 90% of previous reports (*283*), often without proper validation of their stabilities. Numerous publications have reported that such HKGs can be differentially expressed under various experimental paradigms and are

therefore inappropriate for normalization (*253, 259, 260*). However, there are also recent reports that these HKGs are stably expressed and can serve as reference genes (*261, 262, 284*). Most genes, including GAPDH and ACTB, examined in this study were stable at early stages of differentiation (0.5 h or 6 h). However, as differentiation proceeded with dramatic morphological changes and concomitant biochemical changes, the instability of expressions of GAPDH and many of the genes examined was obvious. In the case of GAPDH, this instability issue correlated well with the temporal increase of expression level, which peaked at 28 h and was sustained over a period of 72 h. While GAPDH may still serve as a reference gene for PC12 cells under specific conditions, the validity of using this gene and other less stable ones should be experimentally verified. However, the two RP genes (RPL19 and RPL29) that showed good stability in expression over the period of differentiation provided an optimal pair of reference genes for the entire period of and various experimental conditions for neuronal differentiation.

Among the twenty candidate genes selected, thirteen were ribosomal protein genes, suggesting that the family of ribosomal protein genes may become yet another source of reference genes. Several recent publications have validated and recommended the use of ribosomal protein genes as reference genes (*267, 269*), while others have reported their tissue-dependent variations (*285*). A plausible explanation for such disparity is the large number of ribosomal protein genes present in mammalian systems (80 genes in human, mouse and rat genome), which may be stably or differentially expressed depending on the tissue type or experimental conditions. At present, relatively little is known about these mammalian ribosomal proteins, as compared to their bacterial and archael counterparts (*286*). While bacterial ribosomal protein genes exist largely in clusters, the mammalian RP genes are dispersed throughout the genome (*287*). Some have suggested that all of these proteins are intimately involved in ribosome production and could be co-regulated.

Depletion of a particular ribosomal protein would generally cause a reduction of all other ribosomal proteins in the same ribosome sub-unit (*288*). Other reports have shown that some ribosomal protein genes could be regulated independent of others (*289*). Recently, extra-ribosomal functions of some of these proteins have been reported (*290-293*), suggesting that they may be individually regulated. A previous study comparing random ESTs from naïve and NGF-treated PC12 cells, reported an NGF-promoted decrease in the expressions of RPL19 (*294*). However, this decrease in RPL19 was not observed in other studies using SAGE (*295*) or microarray (*246*). Similar to the latter studies, we too did not observe changes in RPL19 transcripts with NGF-treated PC12. Moreover, the SAGE study but not the microarray analysis reported a significant decrease in RPL29 expression. Using both microarray and RT-qPCR, we have also shown that RPL29 was unchanged when the cells were differentiated. The reasons for these discrepancies are unclear and may be due to the differences in methods used. We have shown here by quantitative real-time PCR that some ribosomal protein genes, RPL19 and RPL29, are highly stably expressed and are thus suitable reference genes, whereas others like RPL9 and RPL18 can vary significantly during differentiation.

Unlike some studies that attempted to identify ideal reference genes through meta-analysis of many publically available microarray data which includes a diverse range of tissue types and experimental conditions, this study was designed to specifically identify a set of suitable reference genes for PC12 cells undergoing neuronal differentiation. We have performed both the microarray analysis and RT-qPCR validation on biological samples prepared with the same techniques and reagents, thus minimizing variations introduced by differences in sample preparation methods and assay platforms. We have also systematically evaluated the effect of the use of NFs of inappropriate reference gene(s) on the expression changes of the target genes and the erroneous results they resulted in. Thus, with neuronal

differentiation of PC12 cells, scaling with the geometric means of the expressions of RPL19 and RPL29 is recommended for the accurate normalization of gene expression.

Twenty novel candidate reference genes were identified and their expression stabilities were analysed and compared to that of commonly used HKGs ACTB and GAPDH. Through this systematic study that included both microarray analysis and RT-qPCR, we have found two ribosomal protein genes RPL19, and RPL29 to be stably expressed during neuronal differentiation of PC12 cells, induced by five different chemical stimuli, over 72 h. The combination of these two novel reference genes allowed robust and accurate normalization of differentially expressed genes, regardless of stimuli and stages of differentiation. In contrast, the use of an inappropriate reference gene like GAPDH led to significant erroneous estimation of differentially expressed genes.

Chapter 7 Integration of an optimized RT-qPCR assay system for accurate quantifications of microRNAs

Section 7.1 Introduction

MicroRNAs represent a unique class of small non-coding RNAs (~22 nucleotides) that act as important post-transcriptional regulators of gene expression. The miRNA machinery has been found to regulate almost every aspect of physiological and pathological processes investigated so far. In neuronal systems, miRNAs were found to modulate various stages of nervous systems development, including neurogenesis, patterning, subtype specification and neuronal activities (*296*). For instance, miR-124a is predominantly expressed in differentiating and mature neurons (*297*), and was found to suppress the expression of a large number of non-neuronal transcripts. Our group was the first to report the regulation of miRNA precursors by GDNF and NTN activated GFRα2 in human neuroblastoma BE(2)-C cells (*298*). It is thus logical to postulate that miRNAs may in turn mediate the functions of GFLs. The differential regulations of miRNAs may provide yet another mechanism that contributes the distinct functions of GFRα and RET receptor isoforms.

Functionally, mammalian miRNAs interact with target mRNAs via partially complementary base pairing, and result predominantly in the degradation of the target mRNAs (*299*). Computational, as well as large-scale transcriptomic and proteomic analyses have revealed that each miRNA can potentially regulate hundreds of mRNAs (*300*). Conversely, each mRNA can theoretically be targeted by many miRNAs. The complexity and promiscuity of such interactions contributes to the distinct functions of single or networks of miRNAs in specific cellular contexts. Possibly as a result of this unique mechanism, miRNAs are often tightly regulated and act as a fine-tuner that modulates gene expression at a rather subtle scale.

An essential pre-requisite to understanding miRNA functions is the accurate quantification of their expressions. Currently, mature miRNAs can be detected by either direct (e.g. fluorescent, colorimetric and electrical based methods) or indirect methods such as northern blot, microarray and RT-qPCR. Among these, RT-qPCR remains to be the most sensitive and efficient means to quantify miRNA expressions. To date, a total of 1921 unique mature human miRNAs have been identified (miRBase release 18, Nov 2011), making them one of the largest classes of regulators. Because of their small size and sequence similarities, designing quantitative assays that simultaneous allow sensitive detection and specific discrimination of these miRNAs pose a major challenge to the research community. Our group has recently proposed a novel, stem-loop mediated RT-qPCR based method that allows rapid and robust quantification of miRNAs in cultured cells (*301*). Based on the principle of this method, we have further optimized the assay designs and developed an integrated system for reliable, high-throughput and multiplexed detection of mature miRNAs.

Section 7.2 Result and Discussion

7.2.1 Assay Design Workflow and Single-plex assay performance

For SMRT-qPCR based miRNA detection, the target miRNA is bound and reverse transcribed by a miRNA specific RT oligonucleotide that adopts a stable stem-loop secondary structure during RT. The resultant cDNA is then amplified by a tagged forward primer (Pf) and a hemi-nested reverse primer (Pr), where 3' nucleotides extend beyond the RT oligos (Figure 7.1). Each of the three oligos (RT, Pf and Pr) contains a 3' sequence specific to the target miRNA (MSS). The MSSs need to be optimally designed to collectively achieve maximal discrimination between target miRNA and the homologous miRNAs, without sacrificing individual assay performance. With close to 2000 annotated mature miRNA now listed in Sanger

miRBase (Release 18, Nov 2011), it is imperative to develop an efficient *in silico* assay design algorithm that replaces the laborsome manual assay design method. A semi-automated algorithm has since been developed in collaboration with MiRXES unit of the Bioprocessing Technology Institute (ASTAR), using a proprietary mathematical relationship that models the specificity of cross-hybridization between oligonucleotide based on the principles of thermodynamics. These new assays are termed mSMRT-qPCR assays.

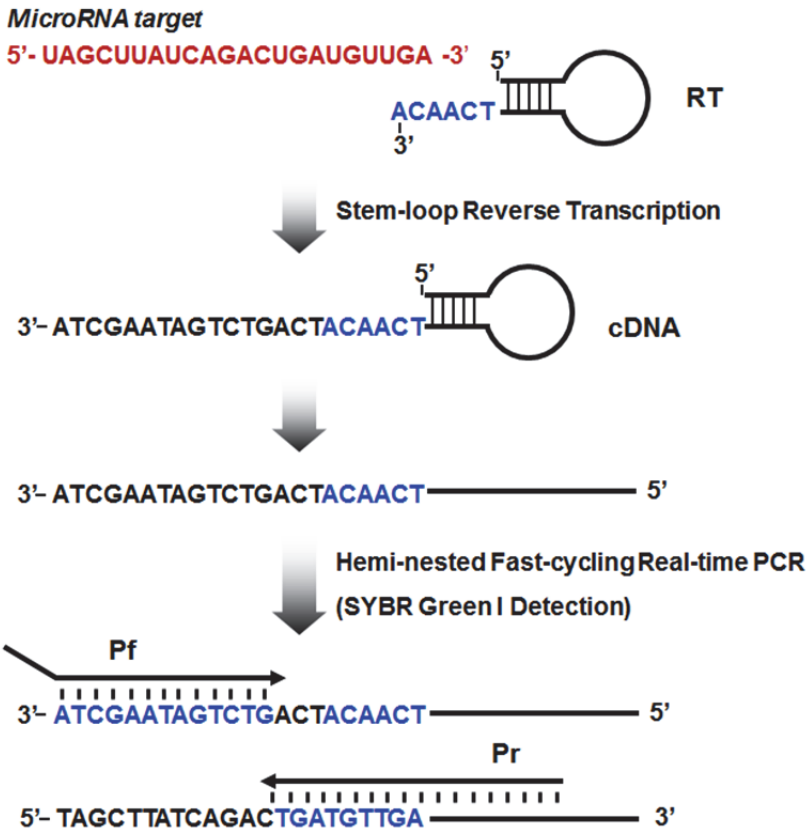

Figure 7.1 Schematics for SMRT-qPCR based miRNA detection. RT, reverse transcription primer, Pf, forward primer; Pr, reverse primer. *This figure is reproduced from Fig 1, Wan et al, RNA 2010 16: 1436-1445*

The new assay design workflow can be broadly separately into two steps (Figure 7.2): 1) Selection of MSS for Pf, Pr and RT. For each target miRNA, all possible combinations of Pf, Pr and RT MSS are generated and their performance indicators including discrimination against homologous miRNAs, PCR amplification efficiency

and primer dimer score are calculated. Several *in silico* filters based on empirical determinations are applied to shortlist up to 50 best combinations for further manual selection.

2) Optimization of stem-loop and tags sequences. Once the MSSs are selected, an optimal stem-loop sequence is calculated for the RT oligo. In addition, a 5' tag sequence is added to the Pf MSS sequence (typically around 12 nt) to increases its Tm for efficient PCR amplification. The stem-loop and tag sequences are optimized to minimize unfavourable secondary structures as well as primer-primer interactions.

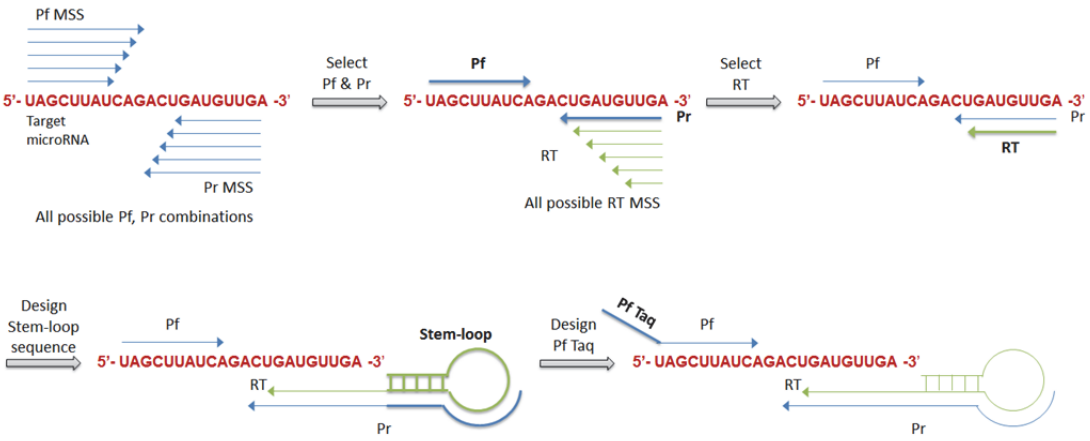

Figure 7.2 Semi-automated mSMRT-qPCR assay design algorithm and workflow

The performance of the mSMRT-qPCR single-plex assay was first evaluated using serial dilutions of synthetic DNA and RNA templates of hsa-miR-30c. Quantification of the DNA templates tests the amplification efficiency of the Pf and Pr oligos, whereas detection of the RNA templates evaluates the performance of the complete RT-PCR process. In both cases, the assay exhibited excellent linearity and wide dynamic range (7 orders of magnitude) and was able to detect as few as 100 copies (subzeptomoles) per reaction (Figure 7.3).

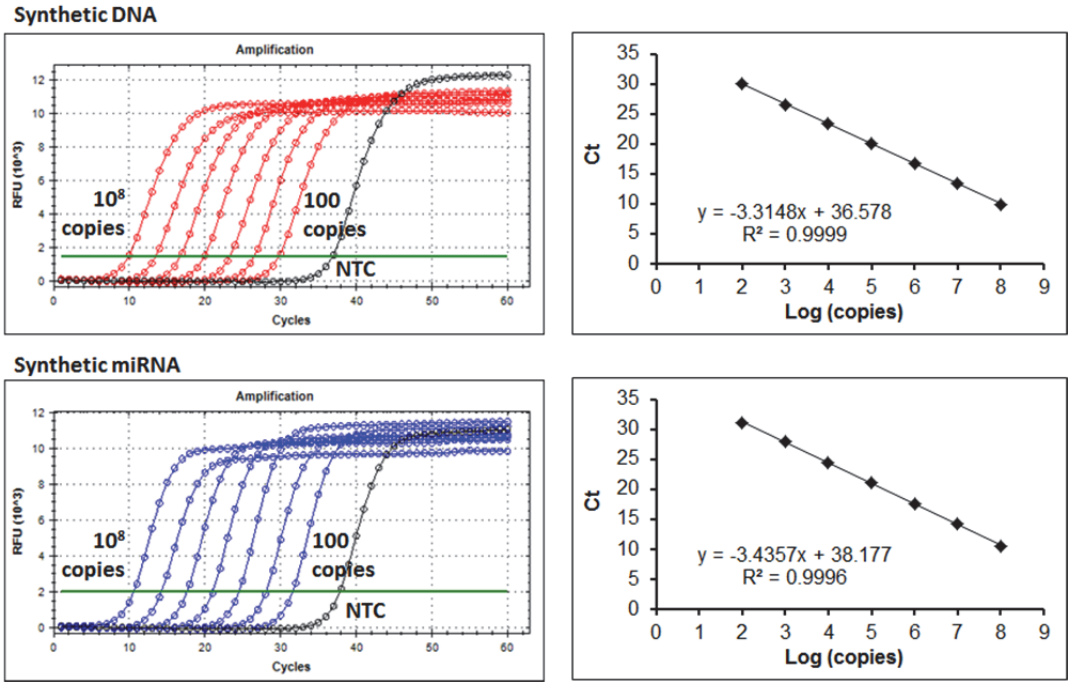

Figure 7.3. Performance of hsa-miR-30c mSMRT-qPCR assay. Synthetic cDNA and RNA of hsa-miR-30c (10^8 to 100 copies) were quantified by mSMRT-qPCR assays. Amplification curves (left) and standard curves plotted as Ct versus Log (right plot; input template per PCR reaction).

Subsequently, the performances of mSMRT-qPCR assays in detecting five randomly selected miRNAs were compared with miRNA assays from three leading commercial suppliers (ABI, Exiqon & Qiagen). All five mSMRT-qPCR assays showed comparable dynamic ranges (7 logs) and efficiencies (close to 100%) to commercial assays (Figure 7.4). However, it was noted that all five mSMRT-qPCR assays were able to detect synthetic miRNA templates with Ct values closer to the theoretical Ct (Ct of 11-12 for 10^7 copies of DNA template on Biorad CFX96 instrument), whereas assays from ABI, Qiagen and Exiqon exhibited significant delays (up to 8 cycles). The superior and consistent performances indicated that mSMRT-qPCR miRNA assays should outperform existing commercial assays as a platform technology for the quantification of miRNA.

hsa-miR-500a

UAAUCCUUGCUACCUGGGUGAGA 52% AT

	Ct (10^8)	Assay Efficiency	Sensitivity (copies)	Dynamic Range	Ct (NTC)
mSMRT-qPCR	12.5	94%	100	7	36.4
ABI	16.3	90%	100	7	N/A
Qiagen	19.8	93%	1000	6	N/A
Exiqon	15.8	95%	100	7	42.3

hsa-miR-27a*

AGGGCUUAGCUGCUUGUGAGCA 45% AT

	Ct (10^8)	Assay Efficiency	Sensitivity (copies)	Dynamic Range	Ct (NTC)
mSMRT-qPCR	12.6	93%	100	7	N/A
ABI	16.5	94%	100	7	N/A
Qiagen	18.1	95%	1000	6	N/A
Exiqon	Assay Not Avaliable				

hsa-miR-30e*

CUUUCAGUCGGAUGUUUACAGC 55% AT

	Ct (10^8)	Assay Efficiency	Sensitivity (copies)	Dynamic Range	Ct (NTC)
mSMRT-qPCR	13.1	102%	100	7	N/A
ABI	14.8	105%	100	7	N/A
Qiagen	17.2	105%	100	7	N/A
Exiqon	14.5	102%	100	7	N/A

hsa-miR-215

AUGACCUAUGAAUUGACAGAC 62% AT

	Ct (10^8)	Assay Efficiency	Sensitivity (copies)	Dynamic Range	Ct (NTC)
mSMRT-qPCR	12.8	94%	100	7	39.6
ABI	16.0	95%	100	7	N/A
Qiagen	19.5	95%	1000	6	N/A
Exiqon	15.6	94%	100	7	N/A

hsa-miR-32*

CAAUUUAGUGUGUGAUAUUU 73% AT

	Ct (10^8)	Assay Efficiency	Sensitivity (copies)	Dynamic Range	Ct (NTC)
mSMRT-qPCR	13.0	103%	100	7	34.3
ABI	21.1	107%	1000	6	N/A
Qiagen	21.2	93%	10000	5	N/A
Exiqon	Assay Not Avaliable				

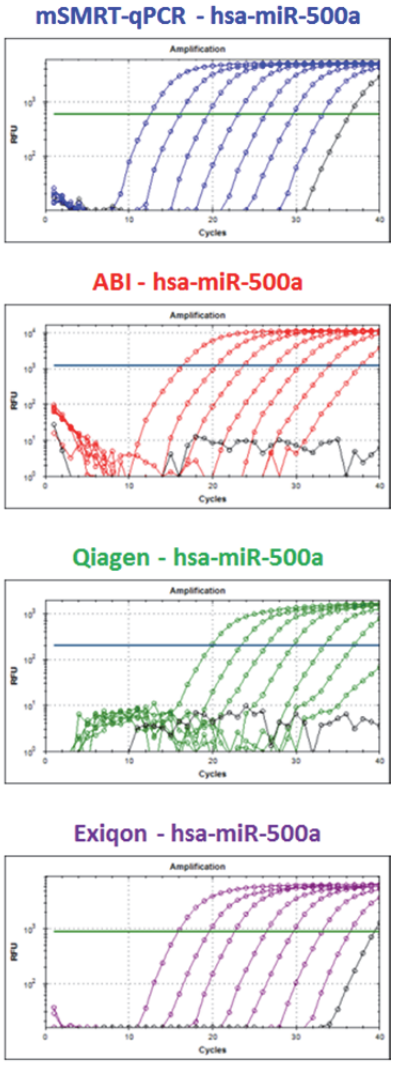

Figure 7.4 Comparison of mSMRT-qPCR miRNA assay performances with leading commercial assays. Left panel compares the performance of mSMRT-qPCR assays with the commercial assays in terms of Ct value, assay efficiency, sensitivity and dynamic range. Shown on the right panel are representative amplification curves of hsa-miR-500a of mSMRT-qPCR, ABI, Qiagen and Exiqon assays

7.2.2 Discrimination of let-7 family homologs

The ability of mSMRT-qPCR assays in discriminating highly homologous miRNA sequences was next investigated using the let-7 family of miRNAs. Several of nine let-7 family members (let-7a and let-7c, let-7a and let-7f, let-7b and let-7c, let-7b and let-7f) differ by a single nucleotide (Figure 7.5 B), making this family an excellent model to test assay discrimination. Specific assays for each let-7 miRNA were

designed. Each assay was used to detect all nine synthetic let-7 miRNAs (10^8 copies per RT) and the relative detection was compared. Depending on the positions of mismatch, discrimination of homologous family members is achieved either by RT primer, Pf primer or a combination of the two. All of the nine let-7 assays showed excellent discrimination against homologous miRNAs with less than 2% non-specific detection, except for let-7b assay with 2.2% relative detection against let-7c (Figure 7.5 A). For let-7 members that differ by 2 nucleotides or more, these assays were able to specifically detect the target miRNA with 0.1% or less cross-target amplification. These results demonstrate the robust design and performance of the mSMRT-qPCR assay in discriminating highly homologous miRNAs at levels comparable to leading commercial suppliers (*302*).

A

Relative Detection (%)		miRNA real-time RT-PCR assay								
		let-7a	let-7b	let-7c	let-7d	let-7e	let-7f	let-7g	let-7i	miR-98
Synthetic miRNA target	let-7a	100.0%	0.0%	0.1%	1.2%	0.0%	0.5%	0.0%	0.0%	0.0%
	let-7b	0.0%	100.0%	2.2%	0.0%	0.0%	0.0%	0.0%	0.0%	0.0%
	let-7c	0.8%	1.6%	100.0%	0.0%	0.0%	0.0%	0.0%	0.0%	0.0%
	let-7d	0.4%	0.0%	0.1%	100.0%	0.0%	0.0%	0.0%	0.0%	0.0%
	let-7e	0.1%	0.0%	0.0%	0.0%	100.0%	0.0%	0.0%	0.0%	0.0%
	let-7f	0.1%	0.0%	0.0%	0.0%	0.1%	100.0%	0.0%	0.0%	0.0%
	let-7g	0.0%	0.0%	0.0%	0.0%	0.0%	0.0%	100.0%	0.0%	0.0%
	let-7i	0.0%	0.0%	0.0%	0.0%	0.0%	0.0%	0.0%	100.0%	0.0%
	miR-98	0.0%	0.0%	0.0%	0.0%	0.0%	0.0%	0.0%	0.0%	100.0%

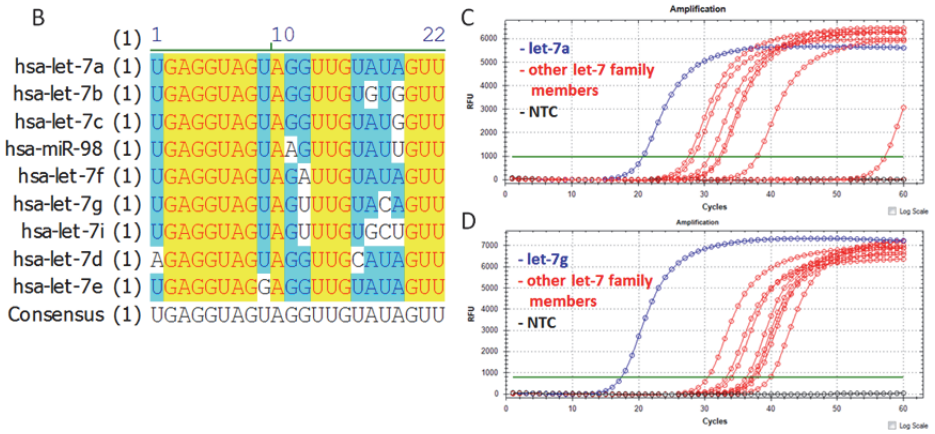

Figure 7.5 Discrimination of let-7 family homologs. A. Relative detection of target and eight other let-7 family homologs by each let-7 miRNA assays**. B.** Sequence alignment of nine let-7 family miRNAs. Several of the family members differ by a single nucleotide. **C & D.** Representative amplification curves of let-7a assay (C) and let-7g assay and (D) of the nine let-7 family miRNAs.

7.2.3 Evaluation of multiplex assay performance and pre-amplification bias

With the emerging view that miRNAs function as a network to collectively modulate target gene expression, it is often necessary to profile a large number of miRNAs on scarce samples. To reduce sample requirement, two technical approaches are applied. The first is to perform multiplex RT reactions and the second is to amplify the amount of starting targets (RNA or cDNA) using a process called pre-amplification. In this section, we compared the performances of single-plex assays with that of multiplex assays reactions with or without cDNA pre-amplification. One hundred miRNAs associated with various processes of neuronal differentiation were curated from literature and used to evaluate multiplex assay performance. *In silico* analysis using the assay design algorithm (Section 7.2.1) has predicted minimal cross-over and mis-priming among these 100 assays.

The performance of multiplex assays was first evaluated with total human RNA (Ambion). The median $\Delta Ct_{\text{multiplex - single-plex}}$ value of -0.19 with 1st and 3rd quadrants ΔCt values of -0.73 and 0.40 were observed, suggesting that multiplex assays do not significantly over- or under-estimate miRNA expressions. To evaluate the dynamic range of the multiplex method, total human RNA was diluted from 100 ng to 10 pg and subjected to single-plex or multiplex RT-qPCR. Figure 7.6 illustrates the correlation between total RNA input and the relative abundance of different miRNAs. The data are presented as correlation scatter plots with the Ct values for 100 ng RNA on the X-axis and the Ct values for 100 ng to 10 pg RNA templates on the Y-axis. If the relative efficiencies of determining miRNA concentration were maintained throughout the dilution series, the slopes of lines representing different dilutions of RNA should be or approach 1. The calculated slopes for the lines through the 100 ng to 10 pg dilution plots were very close to 1 for both single-plex and multiplex assay workflow. These data indicated that multiplex miRNA assay to 100-plex level should provide accurate relative miRNA abundance profiles even with low input RNA amount.

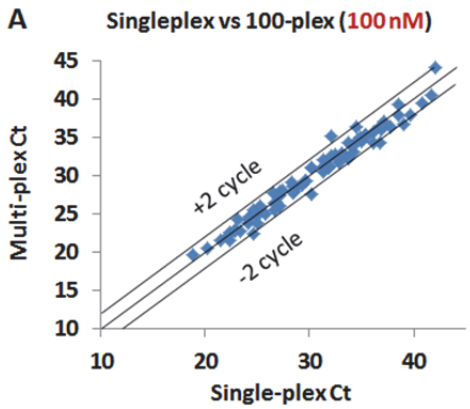

D

	Single-plex		Multiplex	
	Slope	R^2	Slope	R^2
100 ng vs 100 ng	1	1	1	1
10 ng vs 100 ng	0.96	0.99	0.95	0.98
1 ng vs 100 ng	0.98	0.97	0.96	0.96
100 pg vs 100 ng	0.96	0.94	1.03	0.94
10 pg vs 100 ng	0.97	0.92	0.88	0.8

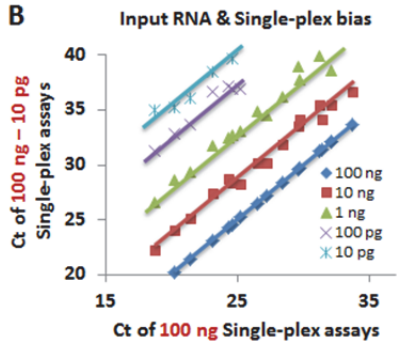

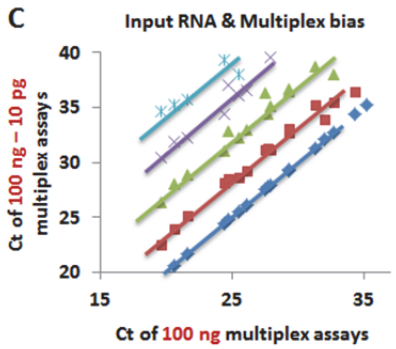

Figure 7.6 Evaluation of multiplex assay performance with total human RNA. A. Comparison of single-plex assay and 100-plex multiplex assay Ct values. Correlation scatter plots of the single-plex (**B**) and multiplex (**C**) Ct values for different miRNAs in total human RNA with 10-fold decrements in amounts. Analysis of the correlation scatter plots are shown in **D**.

The cDNA pre-amplification step was necessary to generate sufficient material from each multiplex RT reaction to allow single-plex qPCR quantifications of tens to hundreds of miRNAs. However, the presence of multiple qPCR primer pairs could potentially mis-prime non-target cDNAs, reduce assay efficiency and bias relative miRNA expression levels in the original samples. An in-depth analysis of the potential bias of a pre-amplification step was performed by comparing the miRNA expression profiles obtained with and without pre-amplification. For pre-amplification reactions, the cDNA products from the multiplex RT reactions were pre-amplified for 10 cycles (1000 fold theoretical amplification) and subsequently diluted 1000-fold. Assuming

the amplification efficiency was or close to 100%, the diluted pre-amplified samples would contain similar amount of cDNA as those without pre-amplification. A median $\Delta Ct_{\text{pre-amp - multiplex}}$ of 0.24 and median $\Delta Ct_{\text{pre-amp - single-plex}}$ of 0.04 were observed (Figure 7.7 A & B). Furthermore, the correlation scatter plots between different dilutions of RNAs undergone pre-amp assays had slopes close to 1, indicating good assay dynamic range (Figure 7.7 C). Real-time qPCR amplifications of three representative miRNAs hsa-miR-21, 103 & 518 quantified through single-plex and multiplex assay formats with or without cDNA pre-amplification were shown in Figure 7.8.

Taken together, these results indicated that the mSMRT-qPCR assay multiplex workflow with cDNA pre-amplification can provide accurate quantifications of miRNA expressions even with very low amount of input RNA.

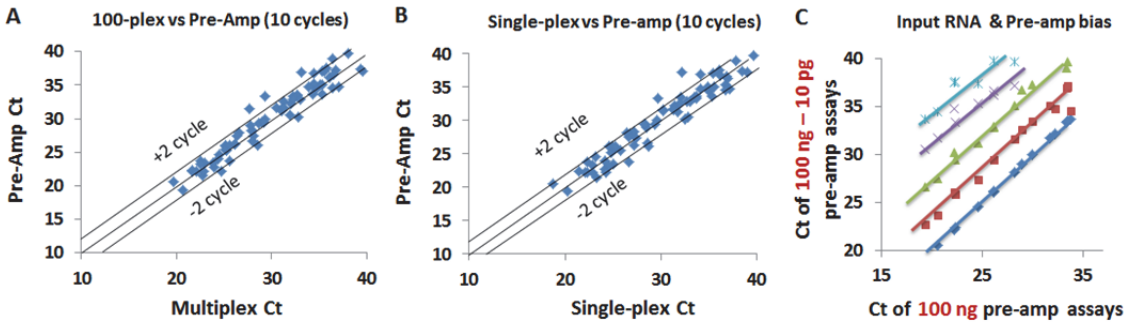

Figure 7.7 Evaluation of cDNA pre-amplification efficiency and bias with total human RNA. A & B. Comparison of pre-amplification assays vs multiplex and single-plex assay Ct values. **C.** Correlation scatter plots of the pre-amplification assay Ct values for different miRNAs in total human RNA with 10-fold decrements in amounts.

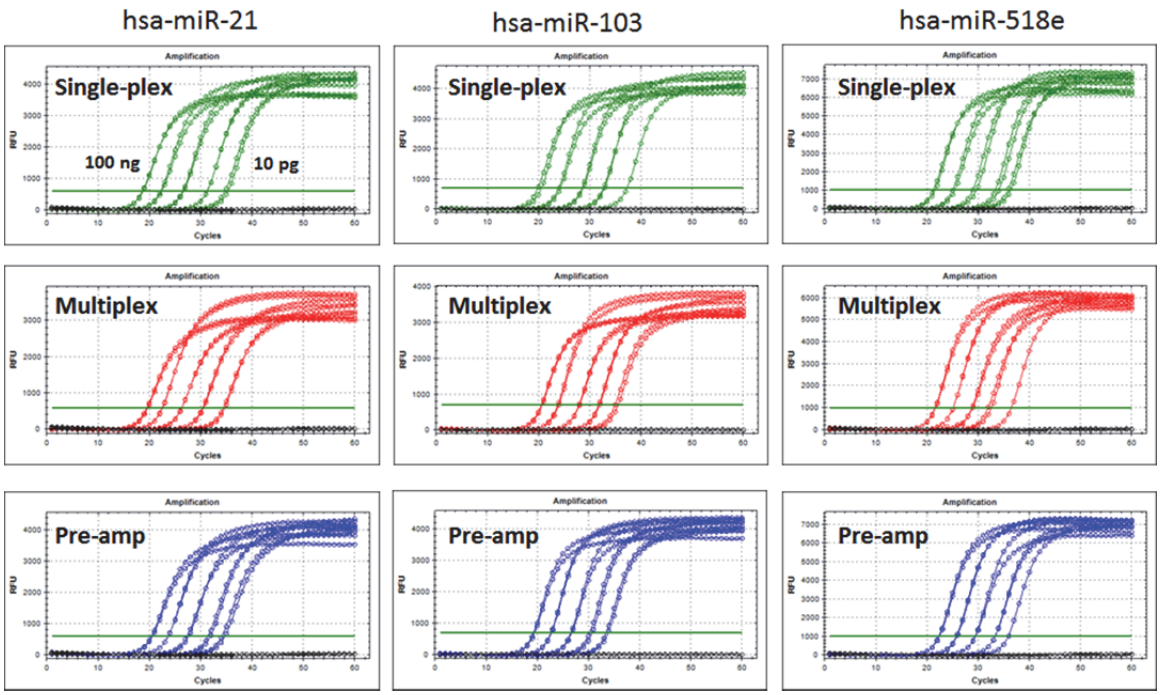

Figure 7.8 qPCR amplification curves of three representative microRNAs quantified by Single-plex, Multiplex and Pre-amp assays.

7.2.4 Application of multiplex assays in identification of miRNAs involved in topological guidance of neurite outgrowth

The correct formation of neuronal circuitry during development or upon nerve injury requires a combinations of chemical (secreted growth factors, hormones) and physical cues to guide the outgrowth and patterning of axons and dendrites from the cell soma and integrate them into a functional network. While chemo-attractants and repellents of neurite outgrowth have been extensively studied, the roles of the physical cues such as the micro- or nano-scale topologies of the local extracellular environments in directional neurite guidance are less well understood. We and others have previously reported that synthetic nano-structures are capable of directing neurite outgrowth of cultured neuronal cells (*303*). A number of mechanisms have been suggested to mediate topological guidance of neurite outgrowth, including MEK/ERK and PKA dependent inhibition of focal adhesion maturation (*304*). Since miRNAs have been found to mediate neurite outgrowth and branching, we

hypothesized that they may similarly be involved in the topological guidance of neurite outgrowth.

To investigate this hypothesis, groove like nano-structures was fabricated on polyimide substrate using nano-imprinting (Figure 7.9 A-B). When cultured PC12 cells were chemically induced to differentiate on such nano-structure, the neurites were found to extend in a direction parallel to the grooves. This is in contrast to randomized neurite outgrowth when the same cells were seeded on planar polyimide or conventional polystyrene cell culture substrate (Figure 7.9 C). We next measured the expressions of 32 neuronal miRNAs known to be involved in neurite outgrowth and morphology using multiplex mSMRT-qPCR assays. Of the nine miRNAs expressed, miR-221 and miR-222 were found to be differentially regulated on nano-structured surface when compared to planar surface, suggestive of their involvement in topological neurite guidance (Figure 7.10 A). To test the hypothesis that down-regulation of miR-221 and miR-222 was required for neurite guidance, PC12 cells were transfected with synthetic RNA mimics of miR-221 and miR-222 and induced to differentiate on nano-grooved substrate. Real-time qPCR quantification of their expression levels showed that miR-221 and miR-222 expressions were elevated by approximately 800 fold upon transfection in all conditions (Figure 7.10 B-C). It is concurrently observed that neurite outgrowth from cells transfected with miR-221 and -222 mimics were significantly less orderly when compared to that of the mock transfection control cells (Figure 7.10 D). The neurite outgrowth was tracked and their alignment to the nano-grooves were analysed by Fast Fourier Transform, a well-accepted method for the analysis of pattern regularities on spatial images (*305*). The sharp and oriented frequency pattern is reflective of the highly aligned neurite outgrowth in control cells, whereas a spherical and randomized signal spread is indicative of the less orderly neurite outgrowth in miR-221 and miR-222 mimic transfected cells (Figure 7.10 D). These data indicated that expressions of miR-221

and miR-222 mimics disrupted directed neurite outgrowth and provided strong evidence of their involvement in nano-groove mediated topological neurite guidance.

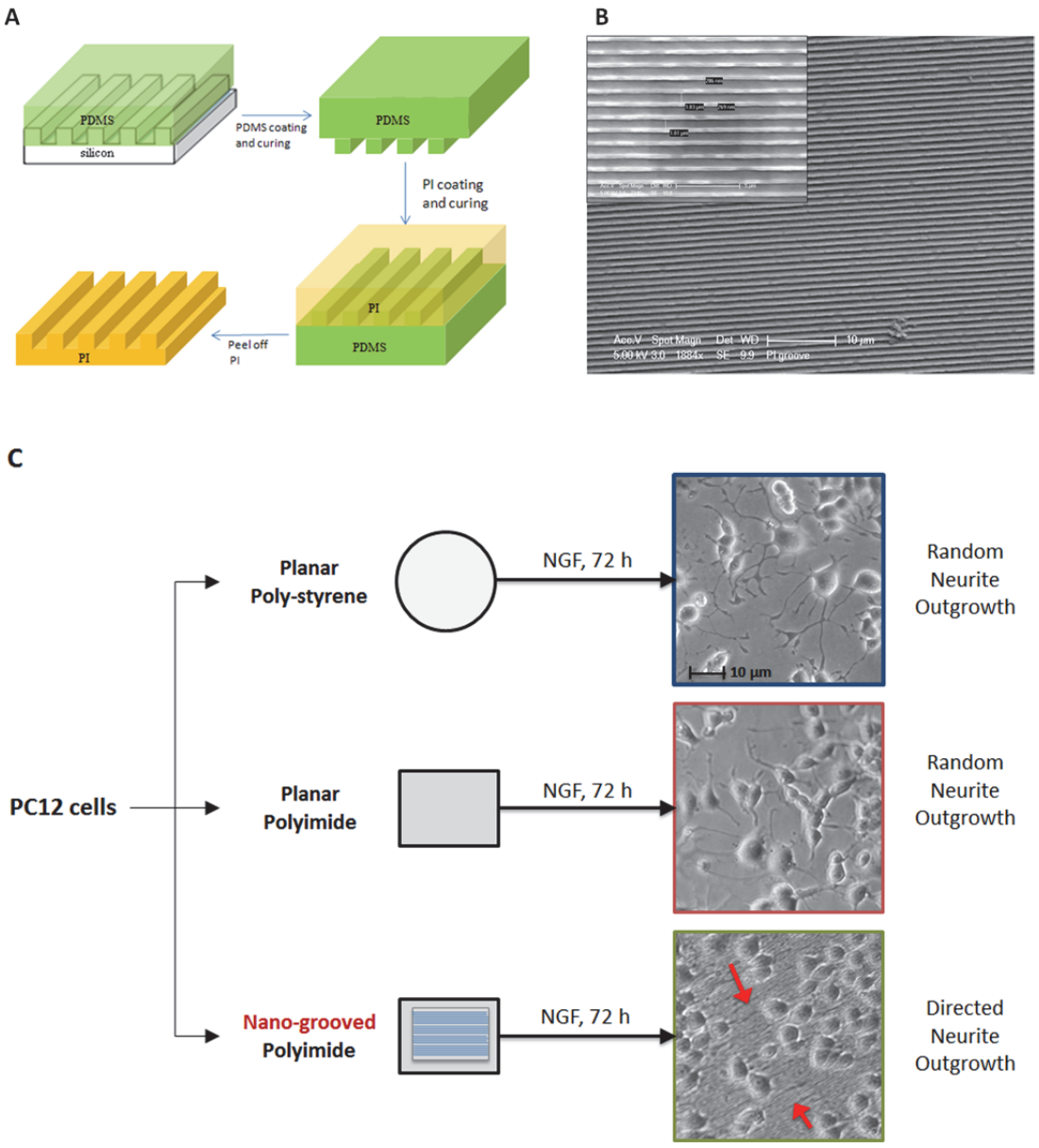

Figure 7.9 Topological guidance of NGF induced neurite outgrowth in PC12 cells. A. Schematic illustration of the fabrication of nano-grooved polyimide substrate by nano-imprinting using Si nanogroove substrate as the master. **B.** SEM image of the nano-grooved polyimide. (A & B are reproduced from Fig 2, Zhu *et al*, Nanoscale, 2011, 3, 2723–2729). **C.** PC12 cells were seeded on planar poly-styrene, planar polyimide and nano-grooved polyimide substrate and induced to differentiate with 100 ng / ml NGF for 72 h. The direction of neurite outgrowth was analysed.

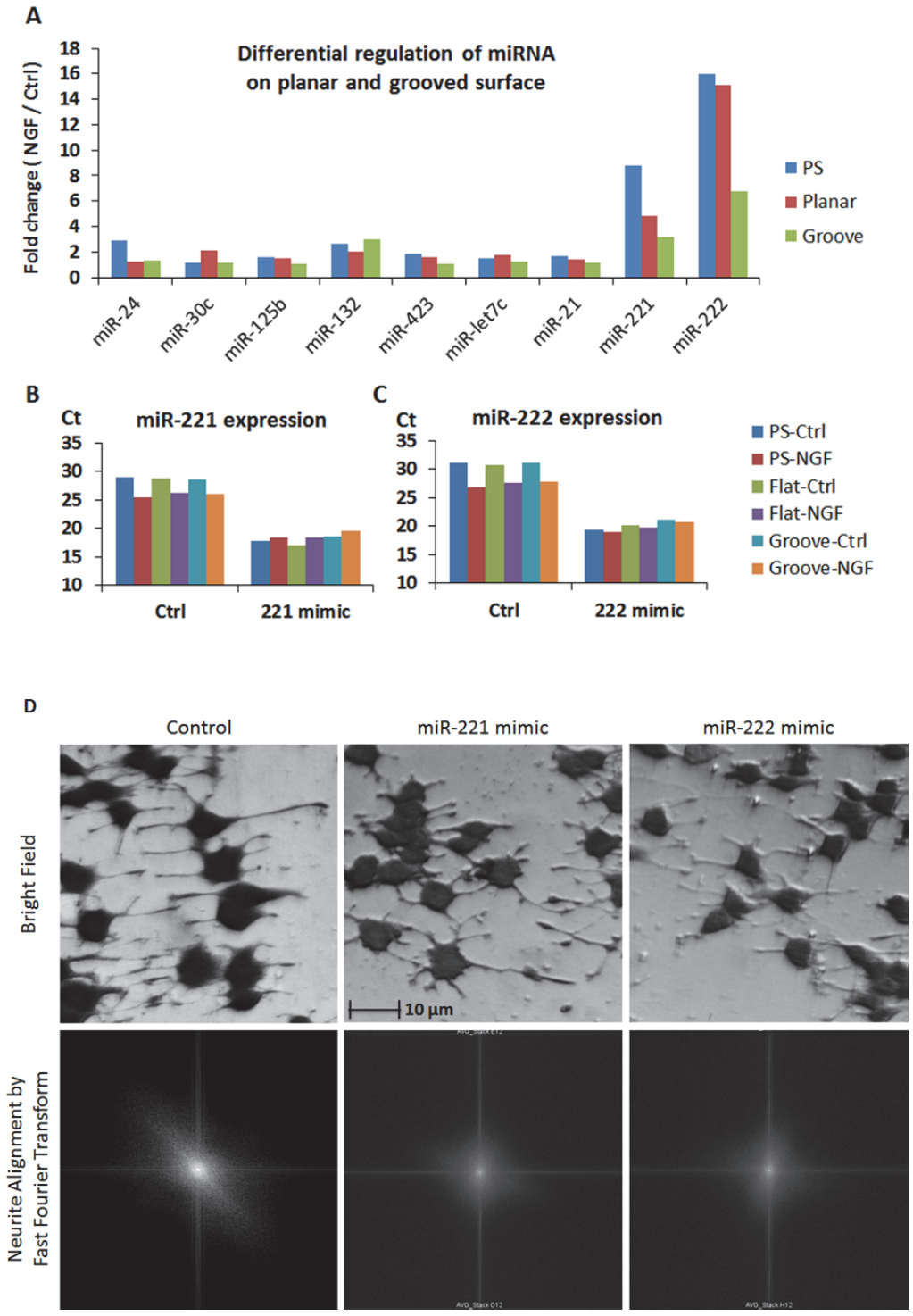

Figure 7.10 Identification of miRNAs involved in topological guidance of neurite outgrowth. A. 32 neuronal miRNAs were profiled using multiplex mSMRT-qPCR and the expressions are normalized to that of reference gene U6. Shown here are the fold change in NGF stimulated cells over control cells on three difference polystyrene (PS), planar polyimide (Planar) and nano-grooved (Groove) polyimide substrates. RNA mimics of miR-221 (**B**) and miR-222 (**C**) were transfected into PC12 cells, the expressions of the two miRNAs in control and transfected cells on different surfaces were measured. **D.** Alignment of neurite to groove nanostructures was compared in control and miR-221, -222 transfected cells. The alignment was further analysed by Fast Fourier Transform and an alignment score was calculated.

Section 7.3 Conclusion

In summary, we have developed an integrated miRNA quantification system based on the principle of SMRT-qPCR. By incorporating a mathematical relationship that determines the hybridization specificity among oligonucleotides, the assay design workflow is now semi-automated and the decision making process has become more objective. These assays allow sensitive detection of target miRNA with minimal non-specific cross-over to highly homologous sequences. In addition, it is shown that multiplexing (100-plex) at RT stage and the subsequent cDNA pre-amplification did not reduce assay efficiency or skew the expression of target miRNAs even with minute amount of input RNA (10 pg). Collectively, these data provided strong evidences that mSMRT-qPCR miRNA assays allow accurate, sensitive and specific quantification of target miRNAs to the range of sub-zeptomoles. Using these assays, we have identified two miRNAs miR-221 and miR-222 which are intimately involved in the topological guidance of NGF induced neurite outgrowth.

Chapter 8 Interplay of GFL, GFRα and microRNA in neuronal differentiation of NTera2 cells

Section 8.1 Introduction

Neurodegenerative diseases and injury related neuro-disorders are becoming increasingly prevalent in an aging population. Neural stem/progenitor cells (NSC/NPC) hold great potential for cell replacement therapies because of their distinctive capacity to both self-renew and differentiation into a wide range of specialized neuronal/glial cell types. Neuronal differentiation and lineage specification of NSC/NPC is a tightly controlled process driven by temporal regulations of cell surface receptors and transcriptional regulators, including the class of non-coding RNAs, microRNAs (miRNAs). GDNF has been shown to promote the survival and differentiation of NSC/NPC into multiple lineages including DA neurons and motor neurons (*306*). However, the precise mechanisms of GDNF function during these processes and the involvement of specific GDNF receptor isoforms (GFRα, RET or NCAM) are poorly understood. In addition, it remains to be tested if other GFLs (e.g. NTN) function similarly during NSC/NPC differentiation as ligand specificity of GFLs has been previously reported both *in vivo* and *in vitro*. Furthermore, whether GFLs could synergize with other ligands or signaling pathways such as retinoic acid to enhance survival and differentiation of NSC/NPC awaits further investigation. Understanding 1) the temporal regulations of various GDNF receptor isoforms during neuronal lineage specifications induced by multiple stimuli, and 2) the temporal and spatial activation of signaling network upon GFL stimulation will shed novel insights on the roles of GFLs and receptor systems in NSC/NPC differentiation.

MicroRNAs are increasingly recognized as an important class of regulator for neuronal differentiation (*307, 308*), acting in conjunction with other cellular regulators such as transcription factors, signaling cascades as well as epigenetic effectors.

Clusters of miRNAs have been reported to play opposing functions such as the maintenance of stem cell pluripotency and induction of differentiation. These miRNAs are temporally regulated and are often part of a complex feedback loop involving signaling molecules, transcription factors and miRNAs (*309*). In addition, several miRNAs have been shown to directly regulate the expressions of target receptor tyrosine kinases in cancer models (*310, 311*). It is thus tempting to hypothesize that GFRα and RET/NCAM isoforms expressions during NSC/NPC differentiation may similarly be controlled by miRNAs. GFL stimulation of the up-regulated receptor isoforms could in turn result in signaling activation and regulate miRNA expressions to further enhance NSC/NPC survival and differentiation into specific neuronal lineages.

The use of NSC/NPC as *in vitro* models for developmental and neurodegenerative studies and their eventual therapeutic applications has been greatly hampered by the inability of existing methods to efficiently differentiate these stem cells into a homogenous population of neuronal cells of a specific lineage. One of the key drawbacks in the existing methods may be the use of common exogenous factors to differentiate NSC/NPCs into different lineages, e.g. FGF, SHH, BDNF etc (*312*). Compare to the temporal application of combinations of exogenous factors that activate a myriad of signaling pathways, the manipulation of cell intrinsic transcriptional regulators such as TFs and miRNAs may allow a more precise and controlled differentiation of NSC/NPCs. For instance, it was reported that the expression of miR-294 induced a more homogeneous population of iPS colonies compared to its inducer cMyc (*313*). More recently, miR-93 and its family members were found to directly target TGF-b receptor II to enhance iPSC generation (*314*). However, the pre-requisite for such paradigm is the identification of unique sets of miRNAs responsible for the differentiation and maintenance of specific neuronal lineages. Since GDNF has been shown to efficiently promote differentiation of

NSC/NPC into DA or motor neurons, it is plausible to hypothesize that GDNF regulated miRNAs may serve as drivers of neuronal differentiation. To this end, the comprehensive profiling of miRNA expressions at different stages after GDNF induction will not only allow better characterization of such developmental processes, but also provide valuable insights into potential tools / methods for efficient manipulation of NSC / NPC for research and therapeutic applications.

NTera2, a human embryonal carcinoma cell line, has been shown to share similar genetic & epigenetic profiles as human embryonic stem cells. It has been used extensively as a surrogate of pluripotent ESC, to model the multistep transition from the undifferentiated neuro-progenitor state to terminally differentiated neurons (*315*). Like ESC, NT2 are capable of differentiating into multiple neuronal cell types (*316*), in a stimulus dependent manner. Retinoic acid treatment of NT2 in high density suspension culture has been shown to provide a highly reproducible model of neuronal differentiation (*317*). RA stimulated NT2 cells undergo distinct phases of precursor expansion, lineage commitment, and terminal differentiation into neurons and glial cells (*318*). Analysis has shown that, during this process, networks of neuronal genes were regulated with a temporal and spatial pattern characteristic of the neurogenesis of neuroepithelial precursors *in vivo* (*319*). Both GFRα1 and GFRα2 are expressed in NT2 cells and their expressions were regulated during NT2 differentiation induced by PA6 feeder layer (*315*) and neuro-steroid 22R-hydroxycholesterol, respectively (*320*). Furthermore, GDNF stimulation of NT2 cells were found to up-regulate p27kip1 expression and inhibit proliferation (*321*), suggestive of the intimate involvement of GDNF in NT2 differentiation.

In this chapter, we tested the hypothesis that GFRα and co-receptor RET and NCAM isoforms are differentially regulated during RA induced NT2 differentiation. These receptors in turn activate distinct signaling networks including miRNAs, in response to autocrine or exogenous GFL stimulation. Understanding the interplay

between GFLs, their receptor isoforms and miRNAs could provide novel insights into the regulatory mechanisms involved in driving NT2 differentiation and fine-tuning the lineage identity of the differentiated neurons.

Section 8.2 Result

8.2.1 Retinoic acid induced neuronal differentiation of NTera 2 neuroprogenitor cells

NT2 cells were induced to differentiate in high density suspension culture with concomitant RA treatment as previously reported. Over a period of 28 days, control NT2 cells continued to expand whereas RA treated cells ceased to proliferate and formed aggregate colonies with a surface cell density distinct from that of control cells (Figure 8.1A). When NT2 cells were transferred to adherent culture after 7 days in suspension culture, RA treated cells formed elaborate neurite outgrowth and adopt neuronal morphology over time, whereas control cells retained an epithelial-like morphology and continued to proliferate (Figure 8.1B). Quantification of the transcript expression of neuronal marker β-tubulin III showed a prominent and sustained up-regulation upon RA treatment in both suspension and adherent culture (Figure 8.1C).

Similarly, the transcript expressions of a series of neuronal lineage markers were quantified by real-time qPCR during RA induced NT2 differentiation. Among eight DA marker genes expressed, all but Otx2 were found to be significantly up-regulated upon RA stimulation, with distinct temporal profiles (Figure 8.2A). These data are consistent with earlier report where RA induced down-regulation of forebrain DA markers (Otx2 etc) and up-regulation of midbrain DA marker (En2 etc) in NT2 cells (*317*). Furthermore, it was observed that marker genes of other neuronal lineages (5-HT, glutamatergic) were concurrently up-regulated, suggesting that RA treatment resulted in a heterogeneous population of neuronal cells of multiple neuronal lineages. Collectively, these data demonstrated that RA treatment was

capable of triggering neuronal commitment of NT2 cells and their differentiation into multiple neuronal cell types, making it a suitable model to investigate the mechanisms underlying neuronal differentiation and lineage specification.

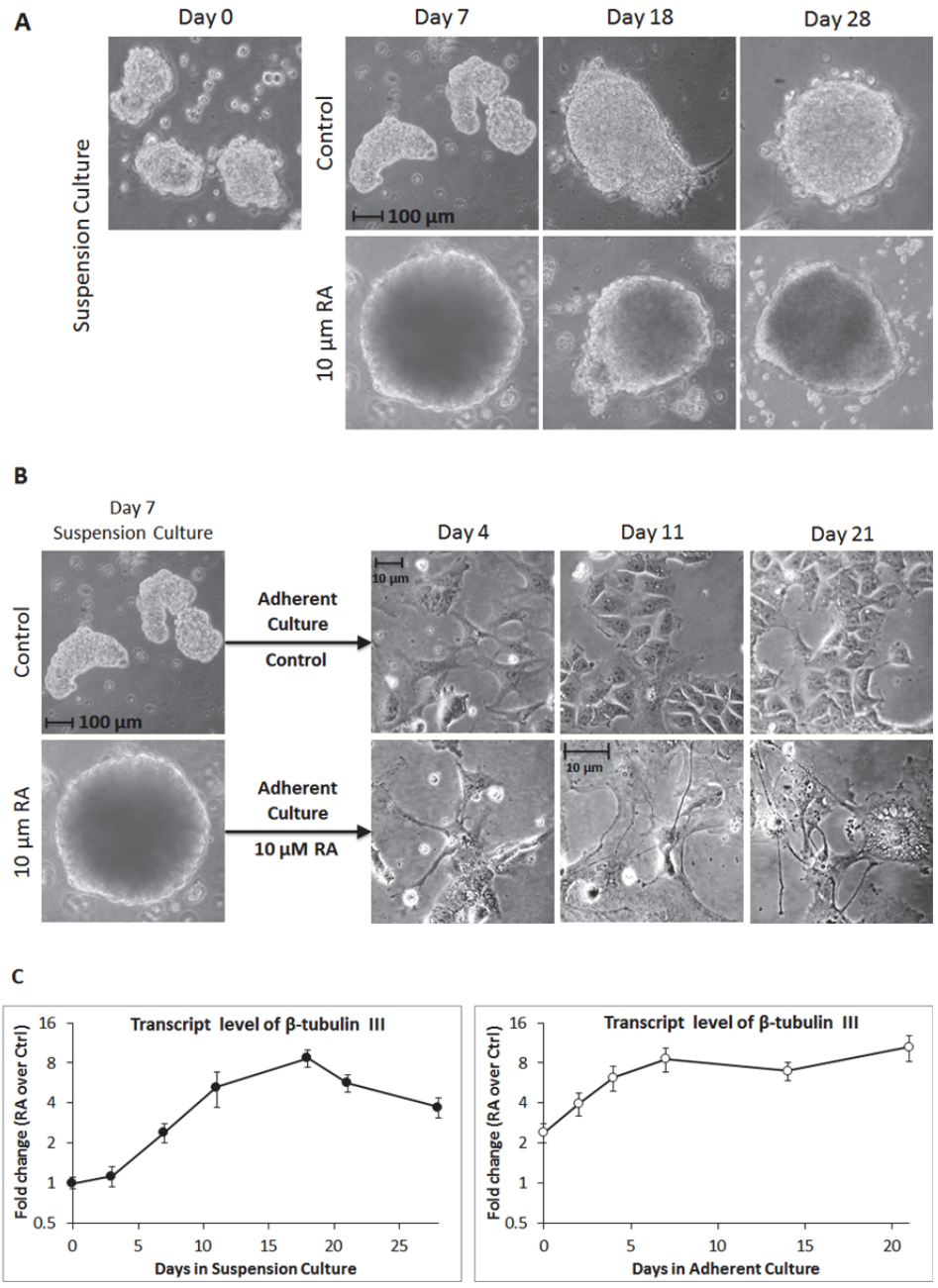

Figure 8.1 Retinoic acid induced differentiation of NT2 cells. Suspension culture of NT2 cells were incubated in growth media (DMEM + 10% FBS) or in growth media with 10 µM all-trans Retinoic acid (RA) over a period of 28 days. A. Representative images of control and RA treated NT2 cells in aggregation. B. Aggregated NT2 cells after 7 days in suspension culture were dispersed and cultured as adherent culture in control and RA containing media over 21 days. Neurite sprouting was observed in RA stimulated NT2 cells. C. Transcript level of neuronal marker β-tubulin III were quantified and normalized to reference gene GAPDH. The fold change in expression in RA treated NT2 over control cells are presented. All samples were analysed in biological triplicates with technical duplicates.

A

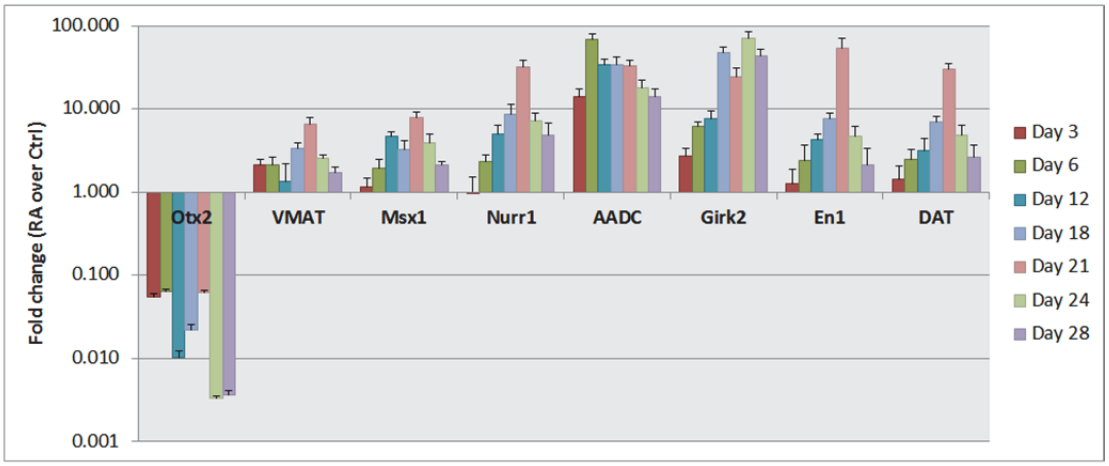

B

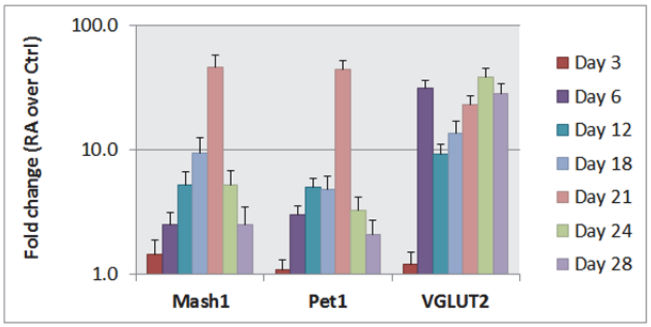

C

Gene	Neuronal Lineage	Function
AADC	DA neuron	Enzyme for carboxylation of DOPA to dopamine
DAT	DA neuron	Dapamine recycling, indicative of functional DA neuron
EN1	DA neuron	DA specific TF
GIRK	DA neuron	Potassium channel in SPnc neuron
Msx1	DA neuron	DA specific TF, induce Shh signaling
Nurr1	DA neuron	DA specific TF, induce TH, VMAT2, RET and DAT expression
Otx2	DA neuron	TF specific to forebrain DA neurons
VMAT	DA neuron	Packaging of dopamine into synaptic vesicle for exocytosis
Mash1	5-HT neuron	TF for serotoninergic differentiation
Pet1	5-HT neuron	TF for serotoninergic differentiation
VGlut2	Glutamatergic neurons	Vesicular glutamate transporter 2

Figure 8.2 Relative mRNA expressions of neuronal lineage marker genes in control and Retinoic acid treated NT2. The expressions of 8 DA marker genes and 3 other neuronal lineage markers genes were quantified in control and RA treated NT2 cells over 28 days and normalized to that of reference gene GAPDH. The fold change in the expressions of these genes in RA treated NT2 over control cells are presented (A, B). All samples were analysed in biological triplicates with technical duplicates. The functions of these genes are summarized in C.

8.2.2 Regulation of GDNF family ligand and receptors during RA induced NT2 differentiation

We next investigated the regulation of GFRα and co-receptors RET and NCAM during RA induced NT2 differentiation. Interestingly, total GFRα1, GFRα2 and NCAM were found to be up-regulated whereas total RET was initially down-regulated before gradually returning to control level (Figure 8.3A). Moreover, GFRα1, GFRα2 and NCAM showed distinct temporal profiles. Total GFRα1 and NCAM levels peaked within 6 days of RA stimulation and were sustained throughout 28 days of treatment. In contrast, total GFRα2 expression gradually increased and reached its highest level only after 21 days. The distinct regulation of these receptors was suggestive of their possible temporal involvements during RA induced neuronal differentiation. Among the receptors, total GFRα1 level was 5-10 folds higher than that of GFRα2 throughout 28 days of RA treatment. Co-receptor wise, NCAM expression was initially lower than RET in native NT2 cells but became the predominantly expressed co-receptor upon RA treatment (Figure 8.3A). The differential expressions of the two GFRα receptors and the co-receptors may result in temporal activation of distinct downstream signaling pathways during different stages of differentiation. Furthermore, it is not unreasonable to suggest that these receptors may be selectively expressed in different populations of NT2 cells and exert distinct functions in driving neuronal differentiation and lineage commitment.

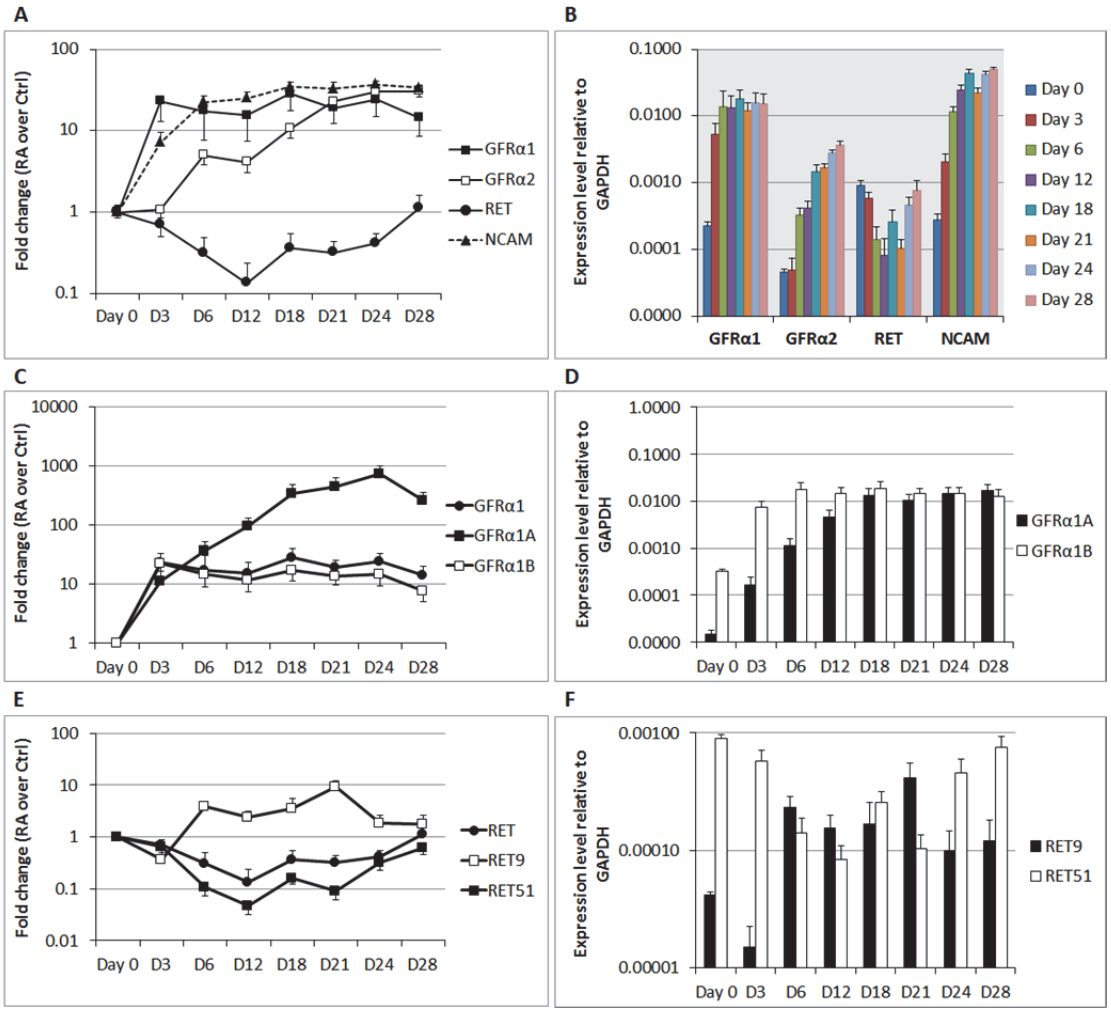

Figure 8.3 Regulation of GFRα, RET and NCAM during RA induced NT2 differentiation. The mRNA expressions of total GFRα, RET, NCAM and selected isoforms were quantified in control and RA treated NT2 cells over 28 days and normalized to GAPDH (B, D, F). The fold change in the expression of these receptors in RA treated NT2 over control cells are presented in A, C and E. All samples were analysed in biological triplicates with technical duplicates.

Since GFRα receptor isoforms have been found to have distinct biochemical and neuritogenic functions (*6, 7*), we next investigated whether these isoforms may be differentially regulated. Surprisingly, while total GFRα1 and GFRα1b up-regulation plateaued 3 days after RA stimulation, GFRα1a expression continued to increase till day 24, to a level 1000-fold higher than that in undifferentiated NT2 cells (Figure 8.3C). Prior to RA treatment, GFRα1b was the predominant isoform with an expression level more than 10-fold higher than that of GFRα1a. However, the levels

of the two isoforms became comparable after 18 days of RA treatment (Figure 8.3D). More interestingly, while the levels of total RET and isoform RET51 were down-regulated from day 6 to day 24, RET9 expression was found to be up-regulated in the same time course (Figure 8.3E). RET9, being the lesser expressed isoforms prior to RA treatment, became the predominantly expressed isoform at day 21 (Figure 8.3F). These data demonstrated that in addition to the broad regulation of GFRα and co-receptor transcript expressions, RA stimulation also induced distinct regulations of the isoform splicing.

8.2.3 GFLs stimulation differentially regulates neuronal differentiation of NT2 cells

To test whether GFL signaling can regulate neuronal differentiation of NT2, 6-day RA treated NT2 cells were stimulated with GFLs or combinations of RA and GFLs and the expressions of selected receptors and neuronal markers were compared with NT2 cells treated with RA only (Figure 8.4A). Six-day RA pre-treated NT2 cells were selected as they expressed the highest levels of GFRα1, NCAM and RET9 and significantly lower level of GFRα2 (40 fold less than GFRα1). These cells allowed the investigation of GFRα1 signaling with minimal complication by the presence of GFRα2. The effects of exogenous application of GFLs on GFRα and co-receptors were first examined (Figure 8.4B). GFL signaling was found to exert a more significant effect on the expression of RET than the rest (Figure 8.4C). Addition of GFLs, alone or in combination of RA, induced up-regulation of total as well as isoform expressions of RET, suggesting the existence of an auto feedback loop. Addition of GFLs did not alter the expressions of GFRα1 or its isoforms. In contrast, when these RA pre-treated cells were incubated with GFLs alone, GFRα1 expressions were significantly down-regulated, suggesting that RA signaling was essential for the up-regulation and maintenance of GFRα1 expression (Figure 8.4D).

We further investigated the effects of GFLs in regulating the expressions of DA marker transcripts (Figure 8.4E). Co-stimulation of GFLs with RA exerted little additional effect on the eight RA regulated genes. However, when these RA pre-treated cells were incubated with GFLs alone, all eight DA marker genes were found to be differentially regulated compared to cells which were continually treated with RA. In particular, a switch from RA to GFL signaling was found to significantly up-regulate GIRK (Figure 8.4F) and Otx expressions and down-regulate that of AADC (Figure 8.4G). Interestingly, GDNF and NTN were also found to induce differential regulations of EN1 and DAT, indicating ligand specificity in GFL regulation of DA marker genes. Taken together, these data suggested that GFLs were capable of regulating neuronal differentiation of NT2 cells and exert ligand specific effects on gene expression regulation. It is tempting to speculate that during development, RA and GFL signaling may play temporal roles in the induction and regulation of neurogenesis.

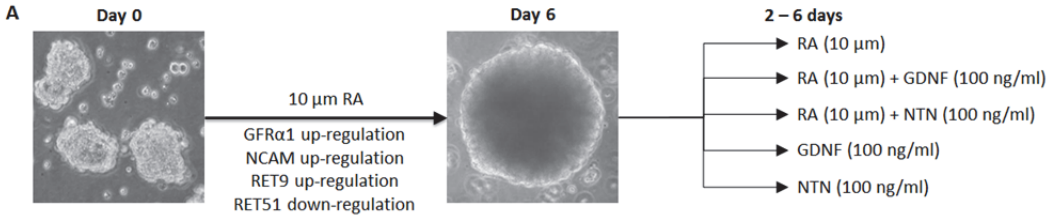

B

	RET	RET9	RET51	GFRα1	GFRα1a	GFRα1b	GFRα2	NCAM
RA	1.0 ± 0.1	1.0 ± 0.1	1.0 ± 0.2	1.0 ± 0.1	1.0 ± 0.1	1.0 ± 0.1	1.0 ± 0.1	1.0 ± 0.1
RA + GDNF	3.2 ± 0.4 **	1.0 ± 0.3	2.1 ± 0.4 **	0.9 ± 0.3	0.9 ± 0.4	1.0 ± 0.3	0.9 ± 0.3	1.3 ± 0.4
RA + NTN	1.8 ± 0.2 **	1.0 ± 0.2	1.5 ± 0.3	1.0 ± 0.3	0.7 ± 0.4	1.0 ± 0.2	0.9 ± 0.6	1.3 ± 0.3
GDNF	2.8 ± 0.3 **	0.7 ± 0.4	2.1 ± 0.5 **	0.4 ± 0.2 *	0.5 ± 0.1 **	0.5 ± 0.2 *	0.7 ± 0.3	1.5 ± 0.2 *
NTN	2.6 ± 0.5 **	3.9 ± 0.8 **	3.1 ± 1.0 **	0.3 ± 0.2 *	0.2 ± 0.1 **	0.4 ± 0.1 **	3.8 ± 1.0 *	1.5 ± 0.5

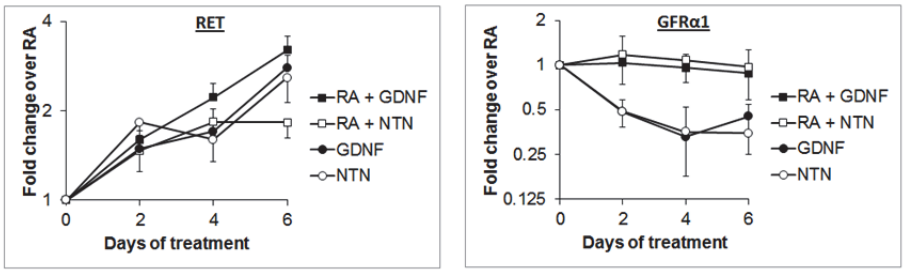

E

	EN1	DAT	GIRK	AADC	Otx	Nurr	VMAT	Msx
RA	1.0 ± 0.1	1.0 ± 0.3	1.0 ± 0.1	1.0 ± 0.1	1.0 ± 0.2	1.0 ± 0.2	1.0 ± 0.3	1.0 ± 0.1
RA + GDNF	0.7 ± 0.2	0.9 ± 0.3	0.8 ± 0.3	0.5 ± 0.3	2.2 ± 0.3 *	0.9 ± 0.4	0.9 ± 0.1	0.8 ± 0.1
RA + NTN	0.8 ± 0.1	1.0 ± 0.4	0.4 ± 0.2 *	0.8 ± 0.4	1.7 ± 0.4	0.8 ± 0.4	0.9 ± 0.5	0.7 ± 0.3
GDNF	0.5 ± 0.3 *	0.9 ± 0.5	4.9 ± 1.1 *	0.2 ± 0.1 **	12.9 ± 2.0 **	1.8 ± 0.2 **	0.6 ± 0.3	0.7 ± 0.2
NTN	4.1 ± 0.8 *	6.6 ± 1.5 *	2.5 ± 0.5 *	0.2 ± 0.1 **	6.9 ± 0.5 **	4.5 ± 0.7 *	1.9 ± 0.3 *	2.1 ± 0.3 *

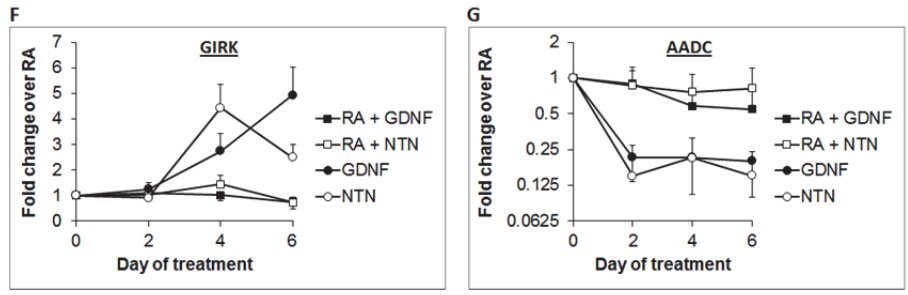

Figure 8.4 Differential regulations of GFL receptors and DA marker genes by GDNF and NTN. A. Schematics of the experiment. RA pre-treated NT2 cells (6 days) were subsequently stimulated with RA, RA + GDNF, RA + NTN, GDNF or NTN alone for 2 to 6 days. B. the effect of different ligand treatments on GFL receptor expressions over time were quantified and normalized to GAPDH. The fold changes in these genes over RA treated cells after 6 days are summarized in the table. C & D. illustrated the fold changes in total GFRa1 and RET level over 6 days of ligand treatment. E. Similarly, the effect of different ligand treatments on DA marker genes were quantified the fold changes were calculated. The fold changes in two marker genes GIRK and AADC over time are shown in F & G respectively. All samples were analysed in biological triplicates with technical duplicates. Up-regulated miRNAs were highlighted in blue and down-regulated ones in red. Significant differences between treatments were calculated using the paired Student's *t-test.* A value of $p<0.05$ was considered significant (**$p<0.01$; *$p< 0.05$)

8.2.4 Regulation of miRNA by RA and GFLs during NT2 differentiation

MicroRNAs have been shown to regulate various processes in neuronal differentiation. A list of 52 miRNAs reported to be associated with neuronal differentiation was compiled from database searches and literature curation (publications listed in PUBMED up to Nov 2011). Real-time qPCR assays were designed for these 52 miRNAs and their single-plex and multiplex performances were validated with both synthetic miRNA template and total human RNAs (Chapter 7). The expressions of these miRNAs during RA induced neuronal differentiation were profiled. Forty nine of these miRNAs were expressed in NT2 cells and their expression levels varied over 4 orders of magnitude (Figure 8.5).

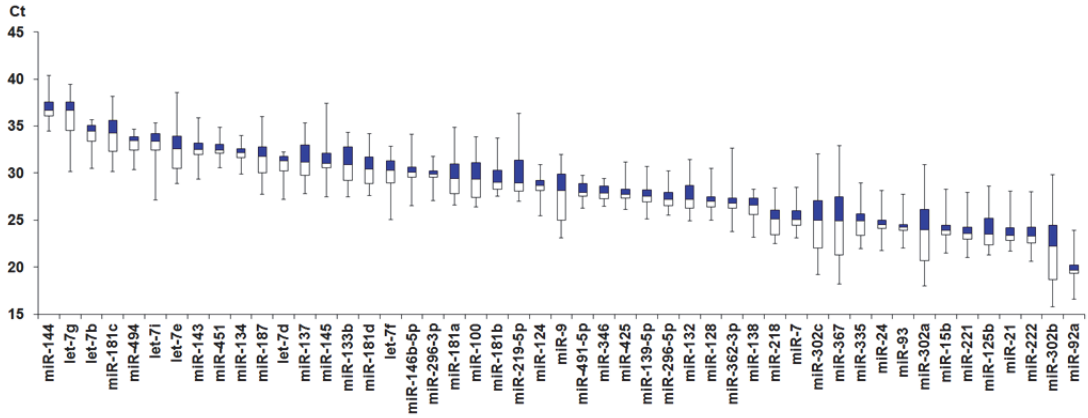

Figure 8.5 Boxplot representation of the expression levels of miRNAs examined. The expression levels (Ct values) of 49 miRNAs among control and ligand treated NT2 cells were presented in box plot.

As illustrated in Chapter 6, the use of stable reference genes is a pre-requisite to accurate profiling of transcriptomic changes. We have previously shown that commonly used housekeeping genes (GAPDH) or small RNAs (U6) were not stable during neuronal differentiation and led to over- or under-estimation of gene and miRNA expressions (*322-325*). To date, only one report has investigated the expressions of miRNAs in NT2 cells using microarray and a median centering based

global normalization strategy (*326*). For accurate normalization of the qPCR profiling results, it is thus imperative to identify and validate reference genes that are stably expressed throughout the course of NT2 differentiation, regardless of the stimuli used. To this end, seventeen of the forty nine miRNAs that exhibited low coefficient of variation (CV < 5%) during NT2 differentiation were selected as candidate reference genes. The stability of these candidate miRNAs were analysed by two statistical algorithms geNorm and NormFinder. The two algorithms consistently ranked miR-128, miR-24, miR-139-5p and miR-93 as the four most stable candidate miRNAs (Figure 8.6). Since geNorm and NormFinder were based on distinct statistical models and assumptions, an agreement between the two algorithms provided strong evidence of the stability of these four miRNAs and their suitability as reference genes. The geometric means of the four reference miRNAs were calculated and applied to normalize the expressions of the remaining miRNAs.

miRNA	NormFinder Stability Value	geNorm M-Value	Mean	STDEV	CV
miR-128	**0.050**	**0.813**	27.0	0.9	3.4%
miR-24	**0.056**	**0.847**	24.6	1.0	4.1%
miR-139-5p	**0.057**	**0.808**	27.6	1.0	3.6%
miR-93	**0.073**	**0.802**	24.3	0.9	3.7%
miR-296-3p	0.079	0.872	29.8	0.8	2.8%
miR-143	0.083	1.188	32.7	1.2	3.7%
miR-134	0.086	0.917	32.1	0.7	2.3%
miR-15b	0.093	0.941	24.0	1.1	4.7%
miR-491-5p	0.094	0.874	28.1	0.8	2.9%
miR-451	0.125	1.018	32.5	0.9	2.7%
miR-494	0.156	1.255	33.1	1.1	3.4%
miR-21	0.156	0.944	23.5	1.1	4.6%
miR-124	0.162	1.066	28.6	1.0	3.4%
miR-7	0.164	1.08	25.2	1.2	4.6%
miR-138	0.189	1.199	26.4	1.2	4.7%
let-7d	0.211	1.553	30.9	1.5	4.9%
let-7b	0.221	1.413	34.1	1.3	3.9%

Figure 8.6 Stability analysis of candidate miRNA reference genes. Seventeen miRNAs with CV < 5% were selected as candidate reference genes. The stability of these miRNAs in ligand induced NT2 differentiation was analysed and ranked by two statistical algorithms NormFinder and geNorm. A lower 'Stability Value' or "M-Value" correlates to higher expression stability. The top four candidate miRNAs with the highest stability value or M-value are highlighted in red.

Among the remaining 45 miRNAs, 41 were found to have their expressions altered by 2 fold or more, with 29 up-regulated miRNAs and 12 down-regulated ones. Interestingly, these miRNAs were shown to have distinct temporal profiles during the course of RA induced differentiation (Figure 8.7A-B). For instance, miR-219-5p was immediately and robustly up-regulated upon RA treatment but gradually returned to a level slightly above control after 25 days. In contrast, the expression of let-7b increased only after 15 days. Among the down-regulated miRNAs, miR-367 expression was immediately and robustly down-regulated (>100 fold) throughout the course of differentiation. MicroRNA-222 on the other hand, showed a transient up-regulation in its expression before being down-regulated. Furthermore, members of the same miRNA family were found to be co-regulated. Members of let-7, miR-302 and miR-181 family shared similar temporal profiles with some variations in their relative fold changes at each time point.

Since GFL signaling was shown to differentially regulate DA marker genes, we hypothesized that GFL stimulation may also result in miRNA regulation distinct from RA treatment. Seventeen miRNAs were found to be differentially regulated when RA pre-treated NT2 cells were switched from RA treatment to GFLs or combinations of GFLs and RA (Figure 8.8). Surprisingly, a group of miRNAs including let-7 family members, miR-9, miR-137 and miR-335 were found to be up-regulated when stimulated with GFLs alone but were down-regulated when stimulated with GFLs and RA. Another 10 miRNAs were shown to be down-regulated upon GFLs treatment regardless of the presence of RA. These results showed that GFLs were capable of triggering differential miRNA regulation in neuronal differentiation of NT2 cells. In addition, GFLs signaling can also act in conjunction with RA signaling to induce opposing miRNA expression changes in a miRNA specific manner. Together, these data highlighted the diverse functions of GFL signaling but the underlying mechanism remains to be investigated.

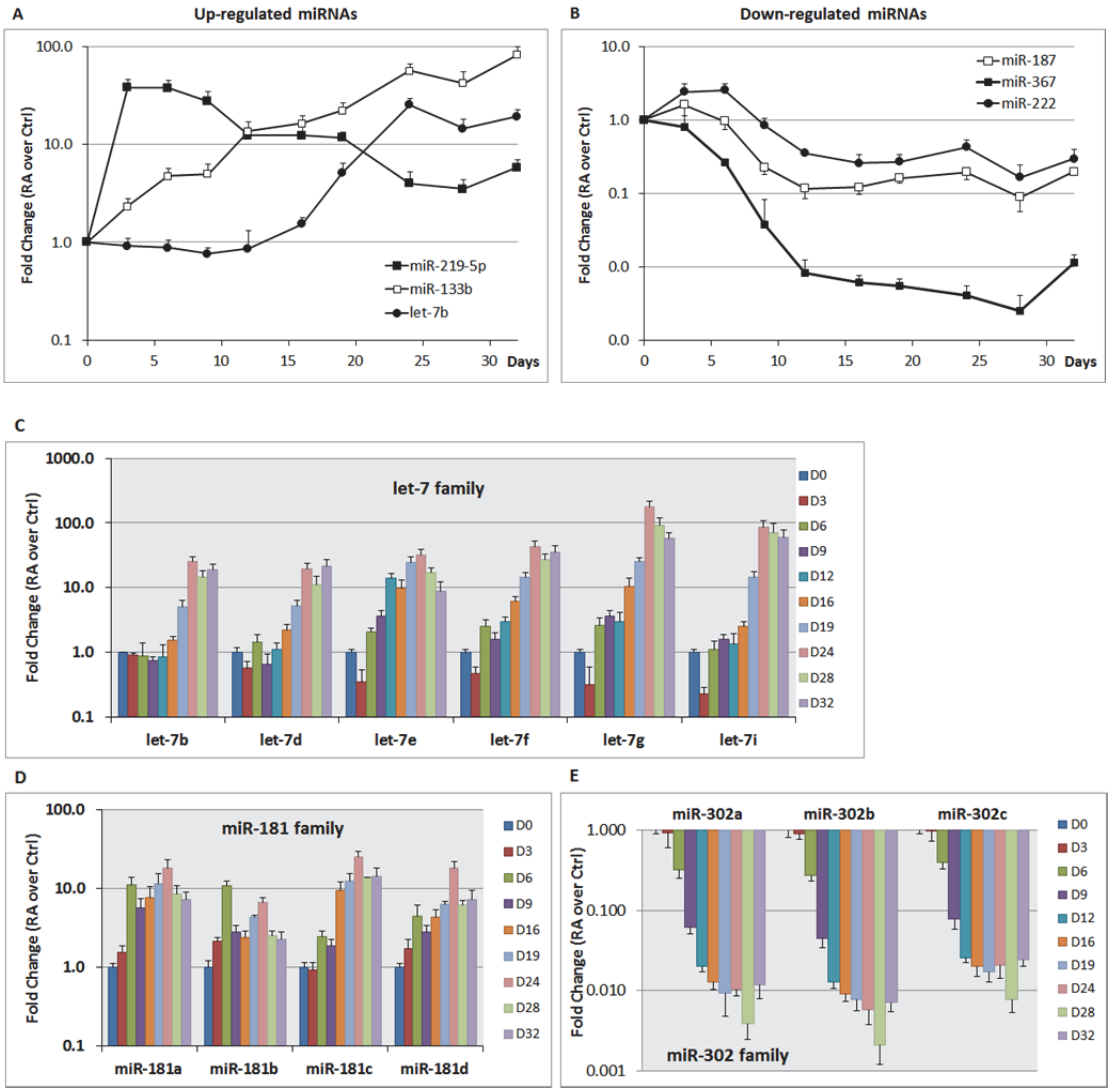

Figure 8.7 Regulation of neuronal miRNAs during RA induced NT2 differentiation. The expressions of neuronal miRNAs were quantified in control and RA treated NT2 cells over 32 days and normalized to the geometric means of three validated reference gene miR-128, miR-24 and miR-139-5p. A & B showed distinct up- and down-regulations of selected miRNAs, respectively. Retinoic acid regulations of various members of let-7 family, miR-181 family and miR-302 family were shown in C-E. All samples were analysed in biological triplicates with technical duplicates. All samples were analysed in biological triplicates with technical duplicates.

	let-7b	let-7f	let-7g	let-7i	miR-9	miR-137	miR-335
RA	1.0 ± 0.1	1.0 ± 0.1	1.0 ± 0.1	1.0 ± 0.1	1.0 ± 0.2	1.0 ± 0.1	1.0 ± 0.1
RA + GDNF	-1.6 ± 0.2	-2.2 ± 0.3 *	-1.6 ± 0.2	-2.2 ± 0.1**	-3.4 ± 0.5 **	-3.0 ± 0.4 *	-3.7 ± 0.3 **
RA + NTN	-1.1 ± 0.3	-1.5 ± 0.4	-1.4 ± 0.3	-1.5 ± 0.3	-2.0 ± 0.3 *	-1.9 ± 0.4	-2.0 ± 0.2 **
GDNF	2.3 ± 0.2 **	2.1 ± 0.2 **	2.5 ± 0.4 *	3.2 ± 0.4 **	3.2 ± 0.6 *	3.8 ± 0.7 *	2.3 ± 0.4 *
NTN	1.4 ± 0.3	1.1 ± 0.2	1.5 ± 0.5	1.5 ± 0.4	1.4 ± 0.4	2.1 ± 0.2 **	-1.2 ± 0.1

	miR-7	miR-15b	miR-100	miR-124	miR-218	miR-187	miR-302a	miR-302b	miR-302c	miR-367
RA	1.0 ± 0.1	1.0 ± 0.1	1.0 ± 0.1	1.0 ± 0.1	1.0 ± 0.2	1.0 ± 0.1	1.0 ± 0.1	1.0 ± 0.2	1.0 ± 0.1	1.0 ± 0.1
RA + GDNF	-2.5 ± 0.5 *	-2.8 ± 0.4 *	-2.5 ± 0.3 **	-2.6 ± 0.3 **	-2.7 ± 0.4 *	-2.0 ± 0.1	-2.1 ± 0.3 *	-2.5 ± 0.2 **	-2.4 ± 0.3 **	-3.7 ± 0.6 *
RA + NTN	-1.5 ± 0.4	-1.9 ± 0.6	-1.7 ± 0.3	-2.0 ± 0.2 **	-1.7 ± 0.2	-1.6 ± 0.4	-2.1 ± 0.1 **	-2.3 ± 0.3 *	-1.8 ± 0.4	-3.3 ± 0.5 *
GDNF	1.6 ± 0.8	1.5 ± 0.5	1.8 ± 0.2	-1.3 ± 0.3	1.7 ± 0.4	-1.5 ± 0.2	-1.4 ± 0.3	-1.6 ± 0.4	-1.1 ± 0.2	-1.4 ± 0.2
NTN	-1.1 ± 0.5	-1.3 ± 0.3	-1.1 ± 0.1	-2.1 ± 0.2 **	-1.2 ± 0.3	-2.7 ± 0.3 **	-2.2 ± 0.2 **	-2.2 ± 0.3 *	-1.6 ± 0.1	-2.3 ± 0.3 *

Figure 8.8 Differential regulations of miRNAs by GDNF and NTN. RA pre-treated NT2 cells (6 days) were subsequently stimulated with RA, RA + GDNF, RA + NTN, GDNF or NTN alone for 6 days. The expressions of neuronal miRNAs were quantified and normalized to the geometric means of three validated reference gene miR-128, miR-24 and miR-139-5p. The fold changes of miRNAs in cells treated with RA+GFL or GFL alone over that in RA treated cells were summarized in the table. All samples were analysed in biological triplicates with technical duplicates. Up-regulated miRNAs were highlighted in blue and down-regulated ones in red. Significant differences between treatments were calculated using the paired Student's *t-test.* A value of $p<0.05$ was considered significant (**$p<0.01$; *$p< 0.05$)

Section 8.3 Discussion

In this study, we established human NTera 2 cells as a model to investigate the regulations and functions of GFRα and co-receptor isoforms in differentiation and maturation of neural progenitor cells into lineage specific neurons. Both GFRα1 and GFRα2, as well as the co-receptors RET and NCAM were endogenously expressed in NT2 cells and were differentially regulated by RA treatment, with distinct temporal profiles. More interestingly, RA stimulation induced distinct regulations of GFRα1 and RET isoforms, making NT2 a suitable model to investigate the mechanisms regulating alternative splicing of receptor isoforms. GFL signaling mediated by one or more receptor isoforms, in turn regulated the expressions of DA marker genes and miRNAs.

NT2 cell line is a well characterized "surrogate" stem cell model for the study of neurogenesis *in vitro*. Comparing to hESC, NT2 cells can be easily and rapidly propagated, without feeder cells or defined media. Nonetheless, NT2 cells were

found to share highly similar genetic and epigenetic profiles with hESC and the ability to generate cells from all three germ layers. NT2 cells have been extensively used to study cell cycle regulation, neuronal differentiation and lineage specification including that of DA and motor neurons (*327-329*). Despite dozen of studies on NT2 differentiation into DA neurons, little is known about the involvement and functions of GFLs, which are known to have potent neurotrophic effects on DA neurons and are undergoing clinical trials for Parkinson's disease. Although GDNF has been shown to inhibit NT2 proliferation through RET mediated p27 up-regulation (*321*), it is not known if GDNF and NTN are involved in other aspects of NT2 differentiation and if specific GFRα receptors or isoforms are involved.

To this end, we selected retinoic acid treatment in high density suspension culture as our initial model of differentiation. Comparing to other differentiation paradigms including feeder cells, feeder layer conditioned media, or defined media with multiple growth factors, the RA protocol offers a simple but highly efficient and reproducible model of neuronal differentiation. Importantly, the use of RA, a well-established transcriptional regulator, as the sole inducer of differentiation reduced the signaling complexity that may complicate the investigation of GFL signaling.

We first examined the expressions of GFRα and co-receptors during the course of RA induced NT2 differentiation. Unlike the qualitative evidences from earlier publications (*315, 320*), the total and isoform specific expressions of these receptors were quantitatively measured using qPCR assays capable of discriminating isoforms by several orders of magnitude. Using these assays, we made a number of novel observations on the transcriptional regulation of GFRα and the co-receptors. All four genes examined, GFRα1, GFRα2, RET and NCAM, were robustly regulated upon RA treatment, with distinct temporal profiles, suggestive of their stage dependent functions during the course of NT2 differentiation. Moreover, we observed differential regulation of receptor isoforms. GFRα1a showed a more sustained up-regulation

than GFRα1b, with a fold change 2 orders of magnitude higher than GFRα1b. More intriguingly, the two RET isoforms were found to be regulated with opposing trends. Total RET and RET51 were robustly down-regulated while RET9 was selectively up-regulated during the same time course.

Furthermore, we noted a gradual change in the relative expressions of the four receptors and their isoforms. NCAM had a lower expression than RET in undifferentiated NT2 cells, but became the predominantly expressed co-receptor upon RA stimulation. GFRα1a expression was twenty fold lower than GFRα1b in undifferentiated NT2 cells but reached a level comparable to GFRα1b 18 days after RA treatment. It is not clear if the changes in the relative expressions will alter the partnering of GFRα with RET and NCAM and the formation of the ligand-receptor complex. There is currently no consensus on whether GFRα interacts with RET and NCAM in a selective or competitive manner. To this end, the gradual change in relative expressions of these receptors in RA treated NT2 could provide a suitable model to examine the interactions of GFRα with the co-receptors. We are also aware that RA treatment of NT2 cells results in a heterogeneous population of neurons and glial cells. The four genes (GFRα1, GFRα2, RET and NCAM) may be selectively expressed on different types of cells.

Exogenous application of GFLs after RA treatment was found to regulate the expressions of DA marker genes and miRNAs. Interestingly, a switch to GFL signaling after 6 days of RA treatment upregulated the expression of Nurr1, a transcription factor required for the acquisition of midbrain dopaminergic (mDA) phenotype, including the expressions of DA genes such as TH, VMAT2 and DAT (*330, 331*). These data suggested that temporal applications of RA and GFLs may increase the lineage commitment towards mDA neurons after RA induction of neuronal differentiation. The choice of adding GFLs after 6 days of RA treatment was made based on knowledge of their receptor expressions. A more thorough

investigation is currently underway to examine the temporal functions of GFLs in the presence of distinct profiles of GFRα1, GFRα2 and co-receptors during RA induced NT2 differentiation. In addition to gaining a better understanding of GFL signaling, the data will also be useful in designing a more focused differentiation paradigm in driving DA differentiation of neuro-precursor cells.

The expressions of numerous miRNAs were investigated during RA induced NT2 differentiation and upon addition of GFLs. Instead of carrying out a large scale, genome wide profiling of miRNA expressions using sequencing or microarray, we chose to quantify a more focused panel of curated miRNAs known to be associated with neuronal differentiation in various cell models. The aim is to better understand the roles of these neuronal miRNAs instead of embarking on another cataloging effort. As a result, 41 of the 52 curated miRNAs were found to be robustly regulated during NT2 differentiation. For accurate quantifications of such expression changes, a suitable panel of reference miRNAs stably expressed throughout the course of NT2 differentiation was validated, using two independent statistical approaches. After normalization, we made a series of interesting observations on the distinct temporal regulations of neuronal miRNAs (family). The functions of these miRNAs at different stages of NT2 differentiation and their regulations of the expressions of neuronal marker genes as well as GFRα and co-receptors are currently being investigated. We hypothesize that some of these miRNAs may act as key drivers of neuronal differentiation and lineage commitment. These miRNAs may be used, either alone or in combinations with ligands and other cell intrinsic regulators, to provide a more precise and controlled process of lineage specific neuronal differentiation.

In summary, this chapter detailed a preliminary study on the regulations and functions of GFL signaling and miRNAs in neuronal differentiation of NT2 cells. RA treatment of NT2 cells was established as a suitable model to investigate the interplay between GFL, GFRα and miRNAs in neuronal differentiation. We have

made a series of novel observations that allowed the proposal and investigation of many new hypotheses. Further studies will not only shed insights into the mechanisms underlying the diverse functions of GFLs and their receptor isoforms, but provide a new paradigm where ligand, receptor and miRNA act in synergy to drive and regulate neurogenesis.

Chapter 9 Conclusion and Future Studies

9.1 Conclusion

This thesis investigated the hypotheses that combinatorial interactions of GFL, GFRα and co-receptor isoforms contribute to the diverse functions of GFL systems through activations of distinct signaling pathways involving proteins, mRNAs and miRNAs. GFRα2a and GFRα2c but not GFRα2b were found to induce biphasic ERK1/2 activation and neurite outgrowth. Inhibition of cAMP-PKA signaling significantly impaired GFRα2a and GFRα2c mediated late phase ERK1/2 and neurite outgrowth. Conversely, cAMP agonists synergized with GFRα2b to activate late phase ERK1/2 and induce neurite outgrowth. Collectively, these data demonstrated the essential role of cAMP-PKA signaling in GFL function and suggested it as an underlying mechanism contributing to the differential neuritogenic activities of GFRα2 isoforms. In a separate study, GFRα2c but not GFRα2a or GFRα2b was found to induce serine^{727} phosphorylation of STAT3 in cultured neuronal cells and primary cortical neurons. With respect to co-receptors, STAT3 activation was mediated specifically by RET9 but not RET51 or NCAM. Unexpectedly, NTN induced phosphorylated STAT3 was localized to the mitochondria, instead of the nucleus. Mitochondrial P-Ser-STAT3 was further shown to mediate the neuritogenic functions of NTN via a transcription independent mechanism. Together with earlier publications from our group, we have now demonstrated that each of the GFRα2 isoforms has distinct functions and induces differential signaling activation. These data provided further evidence to support the emerging view that combinatorial interactions of GFL, GFRα and co-receptor isoforms provide a new paradigm that allows a single ligand to exert a plethora of biological effects. It is intriguing to note that NGF through TrkA similarly induced serine^{727} phosphorylation of STAT3 and enhancing mitochondria

localization, suggestive of a hitherto unrecognized mechanism of some growth factors involved in neurite outgrowths.

A substantial portion of this thesis was dedicated to the development and validation of methods and tools essential for the investigation of transcriptomic changes. Selection and validation of reference genes is a crucial but often overlooked process during qPCR based transcriptomic profiling. Our group has repeatedly shown, in multiple cell models from mammalian cells to bacteria that commonly used housekeeping genes can vary significantly and lead to false interpretations of target gene expression. In this thesis, we have presented a validated workflow for the identification and validation of stable reference genes, which allowed accurate quantifications of mRNA and miRNA expression changes during neuronal differentiation. Furthermore, we have developed and optimized an integrated system for reliable and high-throughput multiplex detection of mature miRNAs, based on the stem-loop RT-qPCR method that our group has previously reported. These new assays are able to quantify target miRNAs at sub-zeptomole range and have excellent discrimination against highly homologous miRNA sequences. A comparison with leading commercial reagents showed that these assays have comparable if not more superior performances. Using these assays, two miRNAs miR-221 and miR-222 were found to be intimately involved in topological guidance of neurite outgrowth.

Equipped with the knowledge of GFRα isoform function and a validated transcriptomic profiling workflow, we investigated the regulations and functions of GFRα and co-receptor isoforms during RA induced NT2 differentiation. We made a series of novel observations on the distinct and temporal regulations of GFRα and co-receptor isoform expression. Exogenous applications of GFLs were further shown to regulate the expressions of DA marker genes and miRNAs.

Taken together, the work presented in this thesis has provided novel insights into the mechanisms underlying the diverse functions of GDNF family of ligands and receptor isoforms. More importantly, our findings and analyses have allowed the proposal of new hypotheses, the investigation of which will continue to advance our understanding of the molecular and cellular functions of GFLs and their receptor isoforms, and how a single ligand-receptor system could exert a plethora of functions in neurogenesis and beyond.

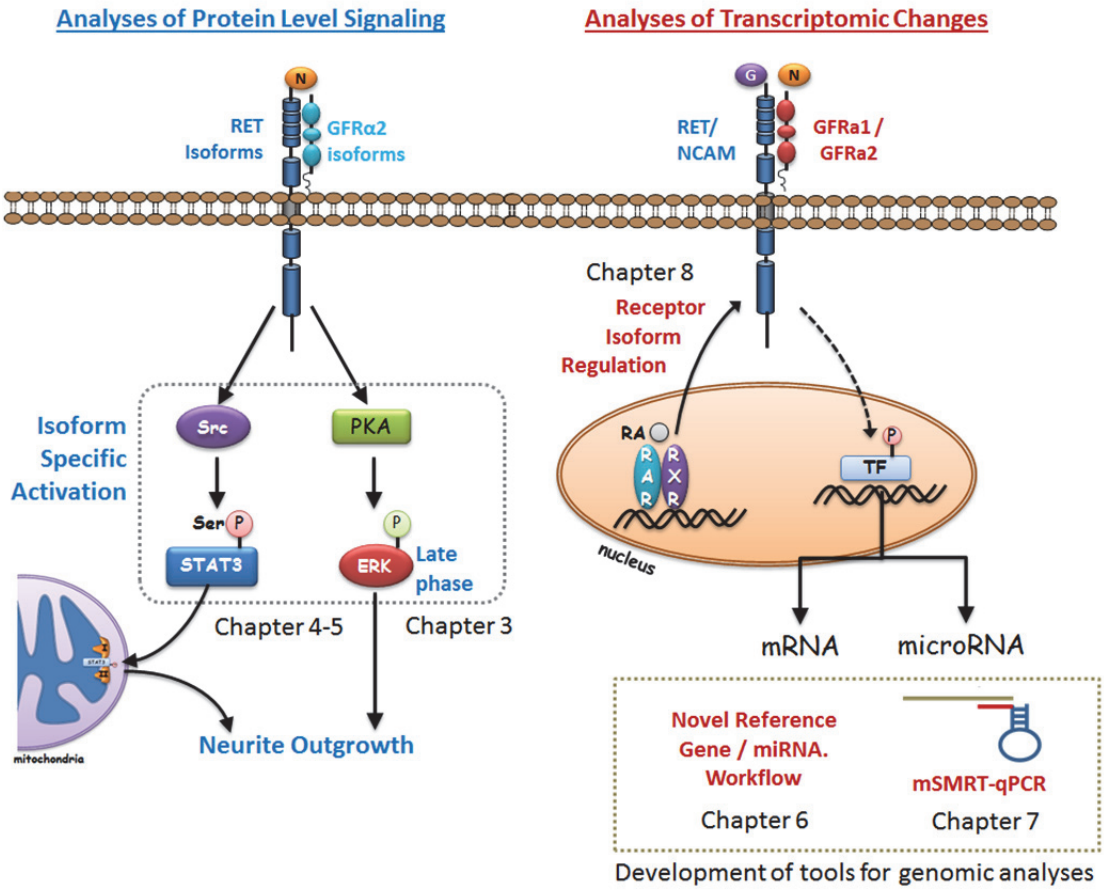

Figure 9.1 A schematic diagram summarizing the main findings in this thesis. This thesis can be broadly divided into two main sections: 1) the investigation of GFL and receptor mediated protein level signaling (Chapter 3-5), and 2) the development of genomic analyses tools and the investigation of transcriptomic regulation involving and induced by GFL and receptor complex (Chapter 6-8).

9.2 Future Studies

9.2.1 Crystal structure of ligand receptor complex & phosphorylation pattern of co-receptors

It is now clear that GFRα receptor isoforms have distinct properties and the combinatorial interactions of GFRα and co-receptor isoforms could mediate diverse functions of GDNF and NTN. However, it remains to be understood how these GFRα isoforms induce differential signaling activation, through the same co-receptor. Structurally, GFRα1 and GFRα2 isoforms differ at the extreme N-terminus (D1 or D1/D2), which was shown to be dispensable for ligand binding. Interestingly, a recent study found that residues 89-101 at the distal end of the N-terminus (D1) of GFRα1 interacted with RET at multiple sites, strongly support its biological relevance. We hypothesize that the differences in the N-terminus domains in GFRα1 and GFRα2 influence the overall conformation of the GFL-GFRα-RET/NCAM ligand-receptor complex and lead to differential activation of RET/NCAM kinase domains. However, to date, only partial structure of GFRα1 (D2 & 3) has been crystallized. It will be valuable to determine the structures of full-length GFRα1 and GFRα2 isoforms, preferably in the heterotetrameric complex form with GFLs and co-receptors.

The activation of RET and NCAM kinase domains is the first step in transducing the signal of GFLs and GFRα isoforms. We hypothesize that GFRα isoforms activate distinct signaling networks by differential phosphorylation of RET and NCAM kinase domain residues and subsequent recruitment of specific adaptor molecules. To this end, the analyses of RET and NCAM phosphorylation patterns, when bound by different GFRα isoforms, will provide useful information in deciphering the mechanisms involved in downstream signaling events. Recent advance in high throughput analyses of phospho-residues in large membrane receptors has

suggested mass spectrometry as a suitable technology in determining co-receptor phosphorylation patterns.

9.2.2 Role of GFL and GFRα in regulation of mitochondrial function and the impact on neurodegenerative diseases

Our findings on NTN induced STAT3 phosphorylation and its mitochondrial localization suggested a unique signaling network involving GFL, receptor isoforms and mitochondria. While we have established Src as the mechanism underlying RET9 specific STAT3 phosphorylation, the activation STAT3 by GFRα2c but not GFRα2a remains to be explained. Preliminary data has suggested that although GFRα2a and GFRα2c activate many similar signaling pathways, they differ in the temporal requirement in ligand stimulation. A transient stimulation of GFRα2a (1h) by GFLs was sufficient to induce neurite outgrowth, but a prolonged stimulation (12-24h) of GFRα2c is required to achieve the same phenotype (unpublished data). Further investigation of the temporal activation of various adaptor molecules and the magnitude of activation by GFRα2 isoforms may provide valuable insights into the selective activation of STAT3 by GFRα2c.

More importantly, these data have established a link between GFLs and mitochondrial function. Mitochondrial abnormalities have been reported in multiple neurodegenerative diseases, including Parkinson's, Alzheimer's, and Huntington's diseases. Much evidence has suggested the involvement of mitochondrial dysfunction and oxidative stress in the pathogenesis of these disorders. Recently, mitochondrial STAT3 have been shown to modulate the functions of the electron transport chain and oxidative respiration. It is plausible to investigate if the activation of mitochondrial STAT3 is one of the mechanisms mediating the protective and restorative effects of GFLs on DA neurons in PD. In addition, it is also of great

interest to investigate if GFLs and receptor isoforms can regulate the functions of other mitochondrial proteins.

9.2.3 Regulation and function of GFRα and co-receptor isoforms in neurogenesis

GFRα and co-receptor isoforms were found to be robustly regulated during the course of NT2 differentiation. Ligand stimulation of these receptors in turn regulated the expressions of neuronal genes and miRNAs. The next step is to understand the mechanisms underlying the distinct regulation of receptor expression and isoform splicing. The immediate candidates include RA regulated transcription factors and miRNAs. In addition, the distinct temporal profiles of different GFRα and co-receptor isoforms are suggestive of their roles at different phases of neuronal differentiation and lineage commitment. Further investigations will provide novel insights of their stage dependent functions. Moreover, as RA induction of NT2 differentiation generates a heterogeneous population of neurons and glial cells, it should be investigated if GFRα and co-receptor isoforms are selectively expressed on different types of cells. To examine their spatial localization, it is imperative to develop and optimize new antibodies or *in situ* hybridization probes which allow sensitive and specific detection of each isoform in cells and tissues.

9.2.4 Functions of miRNA in GFL signaling and neurogenesis

It is now well accepted that miRNAs play important regulatory roles during neurogenesis. Our group was the first to investigate the regulation of both precursor and mature miRNAs by GFLs. With an optimized mSMRT-qPCR miRNA assay system, large numbers of annotated and novel miRNAs can be efficiently and accurately profiled. For instance, several dozens of miRNAs were found to be regulated by RA or GFLs in NT2 cells, some of which displayed distinct temporal

profiles that correlated with the regulation of DA and receptor transcript expressions. The reciprocal relationship between the regulated miRNAs and mRNAs can be investigated through *in silico* target prediction and empirical functional studies using siRNA or shRNA based mimic and inhibitors of target miRNAs. Knowledge of the regulations and functions of these miRNAs will allow the development of novel differentiation protocols driven by combinations of miRNAs, transcription factors and ligand.

Chapter 10 Materials and Methods

10.1 Ligands and Chemicals

Human recombinant GDNF, NTN, mouse recombinant NGF and IL6 were purchased from Peprotech (Rocky Hill, NJ). The following chemicals were purchased from Sigma Aldrich (Saint Louis, MO): Polybrene, Forskolin (FK), Dibutyryl cyclic AMP (dbcAMP), Pituitary adenylate cyclase-activating peptide (PACAP), H89, Actinomycin D (ActD) and Cyclohexamide (Chx). MEK inhibitor U0126 was from Promega (Madison, WI). 8-p-chlorophenylthio-2'-O-methyl-cAMP (2-Me-cAMP), N6-Benzoyl-cAMP (6-Bnz-cAMP) and Rp-8-Br-cAMPS were from Biolog (Bremen, Germany). Antibiotics G418 and hygromycin B were from PAA (Austria) and Invitrogen (Carlsbad, CA), respectively. Primary antibodies against Phospho-CREB (#9191, MW: 43 kDa), Phospho-STAT3-ser727 (#9134, MW: 86 kDa), Pan-STAT3 (#9132, MW: 79 & 86 kDa), Phospho-ERK1/2 (#9101, MW: 42, 44), Pan-ERK1/2 (#9102, MW: 42, 44), PARP (#9542, MW: 89, 116), VDAC (#4866, MW: 32 kDa) were purchased from Cell Signaling Technologies (Danvers, MA). Antibodies against phospho-STAT3-tyr705 (sc-8059, Santa Cruz, MW: 79 & 86 kDa) and SOD1 (sc-11407, Santa Cruz, MW: 23 kDa) were purchased from Santa Cruz. Antibody against Flag-tag (F1804) was purchased from Sigma Aldrich. Secondary antibodies conjugated with horseradish peroxidase (HRP) were from Pierce (Rockford, IL).

10.2 Cloning and Vector Construction

Construction of retroviral vectors containing wild type and mutant STAT3 - Modified pXJ-40 vectors containing cDNAs for wild type and three mutant forms of STAT3a (Ser727Ala, Ser727Glu, Tyr705Phe) were kindly provided by Dr Cao Xinming (Institute of Molecular and Cellular Biology, Singapore). These wild type and

mutant STAT3a constructs were sub-cloned into a modified murine retroviral pQCXI vector (Clontech, Mountain View, CA) that harbors an eGFP-coding sequence under the control of an internal ribosomal entry site (pQCXI-eGFP). To create mitochondria targeted STAT3 constructs, the mitochondrial targeting sequence (MTS, from cytochrome c oxidase subunit VIII) was first cloned by polymerase chain reaction (PCR). The MTS sequence was fused to the 5' of wild type and mutant STAT3a by assembly PCR and subcloned into the retroviral pQCXI-P vector containing puromycin resistance gene as selection marker.

10.3 Cell Culture

Culture of neuronal cell lines - The murine neuroblastoma cell line Neuro2A cells (American Type Culture Collection; catalog # CCL-131), human neuroblastoma BE(2)-C (ATCC catalog # CRL-2268) and human embryonal carcinoma NTERA-2 cl.D1 cells (ATCC catalog # CRL-1973) were grown in DMEM (Sigma, St. Louis, MO) supplemented with 10% heat-inactivated fetal bovine serum (FBS; Sigma), 100 units/ml penicillin (Pan Biotech, Germany) and 100 µg/ml streptomycin (Pan Biotech), at 37°C in a humidified atmosphere with 5% CO2. The rat pheochromocytoma cell line PC12 cells (American Type Culture Collection; catalog # CRL-1721) were grown in DMEM (Sigma, St. Louis, MO) supplemented 10% heat-inactivated FBS, 5% Horse Serum (HS, Hyclone, Logan, UT), 100 units/ml penicillin and 100 µg/ml streptomycin.

Primary Culture - Rat primary cortical neurons were isolated from embryonic day 18 (E18) rat embryos, as described previously [29]. Briefly, the cortices were dissected and dissociated in Hank's balanced salt solution (Sigma), and plated on poly-D-lysine (Sigma) coated culture plates in Minimal essential medium (MEM, Sigma) supplemented with glucose (0.6% wt/vol, Sigma) and 10% FBS. After 24 h, MEM

was replaced by Neurobasal medium (Invitrogen, Carlsbad, CA) containing B27 supplement (Invitrogen), 2 mM glutamine (Invitrogen), 100 units/ml penicillin and 100 µg/ml streptomycin and continued to culture for 48 h at 37 °C in a humidified atmosphere with 5% CO2. On DIV 3 (3 days *in vitro*), primary cortical neurons were washed once with Neurobasal medium without B27 and kept in the same medium for 3 h before stimulated with 100 ng/ml NTN. All procedures were performed according to the guidelines issued by the National University of Singapore Institutional Animal Care & Use Committee (IACUC). This study was approved under a broader project titled “Mechanism elucidation and application of global Transcriptional Machinery Engineering (gTME) to the modulation of the isoprenoid pathway for biosynthesis of pharmaceutical” and given the animal work permits (072/09).

Transient Transfection of Neuro2A Cells - The wild-type and mutant STAT3 – eGFP co-expression constructs were transiently transfected into Neuro2A cells using Transfectin (BioRad) at a ratio of 8 µl Transfectin to 4 µg cDNA per 100,000 cells. Neuro2A cells were incubated with the transfection mixture for 12 h and allowed to recover for 24 h in complete medium before experimentation. Successfully transfected cells were identified through eGFP expression. For knockdown experiments, small interfering RNA (siRNA) duplexes for murine RET (sc-36405) and NCAM (sc-36017) were purchased from Santa Cruz. Briefly, subconfluent cells (50–80%) were transfected with siRNA duplexes (40 nM) using Transfectin (Bio-Rad) for 24 h. Cells were serum deprived for 12 – 16 h before stimulation with 50 ng/ml NTN to induce signaling activation and neurite outgrowth.

Stable Transfection of Neuro2A and retroviral Infection of PC12 Cells – The establishment of Neuro2A cells stably expressing GFRα2 isoforms has been described previously [12]. Retroviral vector pQCXIN (Clontech, Palo Alto, CA) carrying neomycin resistance gene was used to clone the open reading frames (ORFs) of mouse GFRα2a (GenBank accession number: AF079108), GFRα2b

(GenBank accession number: AF079107) and GFRα2c (GenBank accession number: AF002701). Retroviral vector pQCXIH (Clontech) carrying hygromycin B resistance gene was used to clone mouse ORF of RET9 (GenBank accession number: AY326397) and RET51 (GenBank accession number: AF209436). Retroviral pQCXI-P vector carrying puromycin resistance gene was used to clone MTS-STAT3 constructs. Plat-E cells were transfected with these retroviral vectors using FuGene 6 (Roche, Germany). Active retroviruses were collected from supernatants and used to infect PC12 cells in the presence of 8 μg/ml of polybrene. PC12 cells were first infected with combinations of pQCXIN and pQCXIH vectors and selected over 2 month in complete medium supplemented with 0.4 mg/ml G418 and 0.1 mg/ml hygromycin B. The selected PC12 cells were then infected with retroviruses carrying different MTS-STAT3 mutants and further selected over 2 months with 2 μg/ml Puromycin (Sigma). These engineered PC12 cells were shown to stably overexpress wild type and mutant MTS-STAT3 in the mitochondrial but not in the cytosolic fraction.

Knockdown of GFRα2b in BE(2)-C Cells - Small interfering RNA (siRNA) duplexes (Invitrogen) with target sequence: TCTTCTTCTTTCTAGGTGAGGA were used to specifically knockdown GFRα2b in BE(2)-C cells as previously described [12]. Briefly, subconfluent cells (50–80%) were transfected with siRNA duplexes (20 nM) using Transfectin (Bio-Rad) for 24 h. Cells were pre-treated with 10 μM U0126 or 200 μM Rp-8-Br-cAMPS for 1 h before stimulation with 50 ng/ml NTN.

Differentiation and assessment of neurite outgrowth – Neuro2A cells were seeded on 12-well cell culture plates (NUNC, Finland) in DMEM supplemented with 10% FBS overnight. Upon attachment, the cells were serum deprived (DMEM supplemented with 1% FBS) for 12-16 h. Control and transfected cells were then treated with 50 ng/ml NTN for 24 h to induce neurite outgrowth. For transient STAT3 mutant expression experiments, infected cells were identified by eGFP expression and those eGFP positive cells bearing at least one neurite with the length equivalent

to two cell-body length were scored. More than 60 eGFP positive cells from three biological replicates were counted. Stably infected PC12 cells were seeded on poly-D-lysine coated 12-well cell culture plates overnight in DMEM supplemented with 10% FBS and 5% HS. Upon attachment, the cells were serum starved (DMEM supplemented with 0.5% FBS and 0.25%HS) for 12 - 16 h. The cells were then treated with 50 ng/ml NTN for 24 - 72 h to induce neurite outgrowth. For inhibitor studies in both cells, serum deprived cells were pre-treated with selected pharmacological inhibitors for 1 h before NTN stimulation. After 24 to 72 h, the cells bearing at least one neurite with the length equivalent to two cell-body length were scored. More than 300 cells from three biological replicates were counted to obtain the mean and standard deviation. Significance differences between stimulated and control samples were calculated using Students t-test. A value of $p < 0.05$ was considered significant. For studies of mitochondria targeted STAT3 mutants, NTN induced neurite outgrowth in PC12 clones stably expressing different mutants were analysed using HCA-Vision (CSIRO, AU). Briefly, control and NTN treated PC12 cells were fixed with 4% paraformaldehyde (PFA; BDH Laboratory, UK). The cell bodies and neurites were stained with Imperial Stain (Pierce) and the nuclei with 1 µg/ml Hoescht 33342 (Sigma). All images of control and NTN treated cells were acquired with identical imaging parameters using a Zeiss Axio Observer Z1 Inverted Microscope (Carl Zeiss, Germany). The images were batch analysed using HCA-Vision through a 3-step analysis including Neuron Body Detection, Neurite Detection and Neurite Analysis, with identical parameters. Significant differences in neurite outgrowth between wild type and STAT3 mutant expressing PC12 cells were calculated using the paired Student's t-test. A value of $p<0.05$ was considered significant (**$p<0.01$; *$p< 0.05$).

Ligand stimulation and inhibitor studies – For cAMP study (chapter 3), PC12 and BE(2)-C cells were initially seeded in growth medium for 24-48 h, and serum was

depleted (0.5% FBS) for another 16 h. Cells were then stimulated with individual or combinations of the following chemicals: 50 ng/ml GDNF, NTN or NGF, 10 μM Forskolin (FK), 100 μM dbcAMP, 100 nM PACAP, 50 μM, 100 μM or 200 μM of 2-Me-cAMP or 6-Bnz-cAMP in serum-depleted DMEM for 48 h or 96 h for PC12 or BE(2)-C cells, respectively. For inhibitor studies, cells were pre-treated for 1 h with the following chemicals before ligand stimulations: 10 μM U0126, 10 μM H89, 200 μM Rp-8-Br-cAMPS, 2 μg/ml ActD or 10 μg/ml Chx. Cells were then incubated with inhibitors and ligands for 24 h, 48 h or 96 h for neurite outgrowth analyses. To inhibit ERK1/2 activation at different time points after ligand stimulations, PC12 cells were treated with ligands (NTN and/or FK) for 0, 1 or 3 h followed by co-treatment with ligands and 10 μM U0126 for 48 h. For STAT3 study (chapter 4 & 5): Neuro2A and PC12 cells were first serum starved in DMEM with 1/20 of original serum content (0.5% FBS for Neuro2A and 0.25% HS, 0.5% FBS for PC12) for 12 – 16 h. Cells were pre-treated with U0126 (Promega), SP600125 (Tocris, Bristol, UK), SB203580 (Tocris), PP2 (Tocris), SU6656 (Sigma), or Gö6983 (Sigma) for 1 h before ligand stimulation (50 ng/ml of NTN or IL6) in the presence of these inhibitors.

Measurement of intracellular reactive oxygen species - PC12 cells were seeded overnight in Poly-D-Lysine coated 96-well plate (NUNC) and serum-starved in DMEM lacking phenol red (Sigma) supplemented with 0.25% HS and 0.5% FBS for 12–16 h. Prior to NGF stimulation, cells were loaded with 5 μg/ml 2',7'-dichlorofluorescein diacetate (DCFHDA, Sigma) for 10 min at 37 °C in the dark and washed once with DMEM lacking phenol red. The DCF fluorescence intensity upon NGF stimulation was measured by a SpectraMax GerminiXS spectrometer (Molecular Device, Sunnyvale, CA) with an excitation wavelength of 485 nm and emission wavelength of 525 nm, over the period of 40 min.

10.4 Analysis of gene expression (mRNA & miRNA)

RNA Extraction and Reverse Transcription - Total RNA from primary neurons or cultured cells was isolated using TRI-Reagent (Sigma) according to manufacturer's instruction. The integrity of isolated total RNA was validated by denaturing agarose gel electrophoresis and the concentration measured by Nanodrop 2000 (Thermo Scientific). For transcriptomic profiling of mRNA, 2 µg of total RNA were reverse transcribed using ImPromII reverse transcriptase (Promega) and 0.5 µg random hexamer for 60 min at 42°C according to manufacturer's instruction. The reaction was terminated by heating at 70°C for 5 min. For transcriptomic profiling of miRNA, up to 100 ng of total RNA were reverse transcribed using ImPromII reverse transcriptase (Promega) and 100 nM of single-plex or multiplex stem-looped RT oligos for 30 min at 42°C followed by heat inactivation at 70°C for 5 min.

Primers and qPCR - Real-time qPCR using SYBR Green I was performed on the CFX96 (Biorad, Hercules, CA) in a total volume of 25 µl in 1× XtensaMix-SGTM (BioWORKS, Singapore), containing 2.5 mM $MgCl_2$, 200 nM of primers and 0.5 U of KlearTaq DNA polymerase (KBiosciences, UK). Real-time qPCR for mRNA was carried out after an initial denaturation for 10 min at 95°C followed by 40 cycles of 30 s denaturation at 95°C, 30 s annealing at 60°C and 30 s extension at 72°C. Real-time qPCR for microRNA was carried out with an initial denaturation for 10 min at 95°C followed by 40 cycles of 10 s denaturation at 95°C and 30 s annealing and extension at 60°C. Melt curve analyses were performed at the end of reaction to verify the identity of the products. The threshold cycles (Ct) were calculated using the CFX manager v1.6 (Biorad). All real-time PCR quantification was carried out simultaneously with linearized plasmid standards and non-template controls.

Primer Design and Plasmid Standards for mRNA - The Genbank accession for each target gene was retrieved from the Illumina microarray probe set and compared

to the NCBI RefSeq database (Release 16; http://www.ncbi.nlm.nih.gov). Transcript splicing sites were retrieved from Ensembl (http://www.ensembl.org). Where more than one transcript matched the probe, the sequences were aligned and the primers were designed to amplify the consensus region. Vector NTI Advance 10 was used to design two sets of primers for each target gene. The first set of primers generates an amplicon of ~300 bp and is used as a template for RT-qPCR of the targeted gene. The template was subcloned into pGEMT-easy (Promega) vector as previously described [54]. The second set of primers was used for RT-qPCR and was designed to amplify a ~100 bp region within the ~300 bp template. Both primer sets were exon spanning to avoid amplification from genomic sequences. Where possible, primers for RT-qPCR were designed to target the same exons used in the Illumina Expression BeadChip. All primer sequences were evaluated for possible false priming to known rat sequences using the NCBI BLAST tool (http://blast.ncbi.nlm.nih.gov/). All products generated after amplifications were verified by gel-electrophoresis and DNA sequencing.

Assays for mature miRNA - The designs of mSMRT-qPCR microRNA assays are properties of Exploit Technologies Private Limited (Biopolis, Singapore). The research use of these assays is governed by the End User License Agreement. Examples of mSMRT-qPCR assay are as follows:

microRNA	Stem-loop RT Primer	qPCR Primer Pair
hsa-miR-221	AGAGGTTTGCCTCTGAAACCCAGC	Pf: TCCCTCCCAGCTACATTGTCT Pr: GCCTCTGAAACCCAGCA
hsa-miR-222	CGTGCTTCCGCACGACCCAGTA	Pf: ACACAAGGAACCAGCTACATCTG Pr: CGCACGACCCAGTAGC
hsa-miR-335	GACCCAGGCGGGTCACATTTTTCGT	Pf: ATCACACCTCCGTCAAGAGCAA Pr: CAGGCGGGTCACATTTTTCGTT

Gene expression stability analysis - Gene expression stability was analysed using two publicly available software tools, geNorm (http://medgen.ugent.be/ genorm/) and NormFinder (http://www.mdl.dk/), according to authors' instruction.

List of qPCR primers for mRNA

Gene	Species	Forward Primer	Reverse Primer
GDNF family			
GDNF	mmu,rno	TGAAGTTATGGGATGTCGTGG	TTGGAGTCACTGGTCAGCG
GFRα1a	mmu,rno	CATATCAGATGTTTTCCAGCA	TGGT(A/G)CAGGGGGTGATGTAGG
GFRα1b	mmu,rno	CAGTCCCGTTCATATCAGTGGA	TGGT(A/G)CAGGGGGTGATGTAGG
GFRα1-GPI	mmu,rno	GCCAGCCAGAGTCAAGGTCT	GCCAATCAGTCCCGAGTAGG
GFRα2a	mmu	GCCTCTTCTTCTTTTTAGACGAA	TGTCGTTCAGGTTGCAGGCCT
GFRα2b	mmu	GCCTCTTCTTCTTTTTAGGTGAG	TGTCGTTCAGGTTGCAGGCCT
GFRα2c	mmu	GCCTCTTCTTCTTTTTAGGGACA	TGTCGTTCAGGTTGCAGGCCT
GFRα2-GPI	mmu,rno	TGTCATCACCACCTGCACATC	AGGCCAAGGTCA(C/G)CATCAGG
RET9	mmu,rno	CCCCTGGTGGACTGTAACA	GTAAATGCATGTGAAATTCTACC
RET51	mmu,rno	CCCCTGGTGGACTGTAACA	TCGGCTCTCGTGAGTGGTA
RET-TK2	mmu,rno	TCAATCAGAGCCTGGACCATA	GGAGGAAGA(C/T)GGTGAGCA
NCAM	mmu,rno	TGTCAAGTGGCAGGAGATGC	GGCGTTGTAGATGGTGAGGGT
GDNF	hsa	TCACTGACTTGGGTCTGGG	TCAAAGGCGATGGGTCTGC
GFRα1a	hsa	CATATCAGATGTTTTTCAGCAAGTGGA	CAGACATCGTTGGACACGCT
GFRα1b	hsa	TGGTCCCATTCATATCAGTGGA	CAGACATCGTTGGACACGCT
GFRα2-GPI	hsa	CAGTGACAGTACCAGCTTGGG	AAGGCCTGTTTCAGCATCAG
RET9	hsa	GGATTGAAAACAAACTCTATGGTAGA	AGGAAGGATAGTGCARAGGGGAC
RET51	hsa	AAACAAACTCTATGGCATGTCAGAC	CGCTGAGGGTGAAAGCATC
NCAM	hsa	CAGCAGCGGATCTCAGTGGT	CATCACACACAATCACGGCA
Neuronal Markers			
VMAT	hsa	TGGATTCGTCAATGATGCCT	CAGAAGGACCTATAGCATACCC
TH	hsa	GTGCTAAACCTGCTCTTCTC	GCTTCAAACGTCTCAAACAC
AADC	hsa	CAATCTCTTAGAAGTCGGTCCT	AATCTGCAAACTCCACTCCA
Msx1	hsa	AGACGCAGGTGAAGATATGG	ATCTTCAGCTTCTCCAGCTC
En1	hsa	GCCAAGATCAAGAAAGCCAC	TACTCGCTCTCGTCTTTGTC
EN2	hsa	CCGGCGTGGGTCTACTGTA	GGCCGCTTGTCCTCTTTGTT
Girk2	hsa	CATGATTGAGTGAAGCCACC	AGGACGTTAGTCATGGATTCTG
Otx2	hsa	GTACCCAGACATCTTCATGC	GATTCTTAAACCATACCTGCACC
Mash1	hsa	TCTTCGCCCGAACTGATGC	CAAAGCCCAGGTTGACCAACT
Pet1	hsa	CACGGCGAGTTCAAGCTCA	TTGCCATGCACCTTGCTCA
Gata2	hsa	GCAACCCCTACTATGCCAACC	CAGTGGCGTCTTGGAGAAG
SERT	hsa	ATTTTTGGGGGAATCCCGCTC	GCAGATGGCATAACCAATCCCT
HB9	hsa	TGCCTAAGATGCCCGACTT	AGCTGCTGGCTGGTGAAG
Islet1	hsa	AAGGACAAGAAGCGAAGCAT	TTCCTGTCATCCCCTGGATA
Olig2	hsa	AGCTCCTCAAATCGCATCC	ATAGTCGTCGCAGCTTTCG
VGLUT1	hsa	TTTTCTGGGGCTACATTGTCAC	ACTCCGTTCTAAGGGTGGGG
VGLUT2	hsa	TCATCACTCAGATTCCGGGAG	CACACCCTCAACAAGTCCCTG
GAPDH	hsa	AAACCTGCCAAATATGATGAC	ACCTGGTGCTCAGTGTAG

Candidate reference genes			
RPL29	mmu, rno	ACAGAAATGGCATCAAGAAACCC	TCTTGTTGTGCTTCTTGGCAAA
RPL10a	mmu, rno	GGTGGCCAAAGTGGATGAGG	CATCGGTCATCTTCACGTGG
LOC292640	mmu, rno	GTCCACAGACTGTCCCAGCCAT	AGCCCGAGCAAAGTCCTCTG
LOC498143	mmu, rno	ACCAGCTGAAATTTGCCCGA	GTGGAATCTTCACCAACCCA
LOC317275	mmu, rno	CCGTCATGCTACCAAGAATAGAGTG	TCTAGTTGAGCTGCCGGATGAG
RPS15	mmu, rno	TTCACCTACCGTGGCGTGGA	TGAGTGCTGCTTCCTCCGCA
ARBP	mmu, rno	GGTCCTGGCTTTGTCTGTGG	CAGCCGCAAATGCAGATGGA
RPL14	mmu, rno	GCCAAGATGACAGATTTTGATCG	GAGAGCAGCTCTCTGGAGTTTCTTC
EEF1A1	mmu, rno	GATGCTGCCATTGTTGACAT	TGTCTGCCTCATGTCACGAA
RPS15A	mmu, rno	TCAACAACGCGGAGAAGAGG	CACCAATGTAGCCATGCTTCATC
RPL18	mmu, rno	AAGGGCCGAGAGGTGTACCGACACT	TCGAACTTCCGGCCCTTGGA
REPS1	mmu, rno	ACGCAATAAGGAGACCAACA	TCCAGTTGAACTTCCAGGGA
LOC363720	mmu, rno	AAAGCCAGGACATCGTGAATCA	AGCAGATGGCAAACTTCTGGC
CNOT8	mmu, rno	CCCTTCTGGAATCAACACGT	GAACTGCAGCCCTGAGTTGG
RTCD1	mmu, rno	ACGGGACCAGTCACACTCCA	GGCATCTTCCTCCTCTTCTG
RPL19	mmu, rno	ACCTGGATGCGAAGGATGAG	ACCTTCAGGTACAGGCTGTG
NDUFB6	mmu, rno	CTGGAGCGATTCTGGAATAACTTTT	GGTATGATCACATGGGAAACAGTGA
RPL9	mmu, rno	TATCAGGAAGTTTTTGGATGGCATC	TCAGGATCTTGTTTCTGAAGCTAGG
LOC499803	mmu, rno	CCTGGGACCCAAGCGGTAAGAT	ATGGGGGTGGTGGGCAAGAT
RPL3	mmu, rno	TGGGCAAGATGAGATGATTGACGTC	GGGTCTTTCGGGGCAGCTTCTTT
ACTB	mmu, rno	GCTATGAGCTGCCTGACGGT	GTTTCATGGATGCCACAGGA
GAPDH	mmu, rno	ACCACGAGAAATATGACAACTCCC	CCAAAGTTGTCATGGATGACC
EGR1	mmu, rno	AAGGGGAGCCGAGCGAACAA	GATAACTTGTCTCCACCAGCGCC
ITGA1	mmu, rno	GTCTGAGGTTCTCAAAAGAGGCAC	TCACTTGACTCAGGTCGGAAGG
CRYAB	mmu, rno	TGCGGGCACCTAGCTGGATT	CCTCTGGAGAGAAGTGCTTCACG

RNA Purification and cDNA Preparation for microarray - Total RNA from PC12 cells was prepared using TRIzol reagent (Invitrogen, CA) according to manufacturer's instruction. Total RNA was collected from samples in quadruplicate at each treatment time point and the integrity of the RNA validated by denaturing agarose gel electrophoresis and using the StdSens analysis chip on the Experion Automated Electrophoresis System (BioRad, CA) according to manufacturer's instructions. The Experion Automated Electrophoresis System assigns a RQI to each RNA electropherogram which ranges from 10 (intact RNA) to 1 (completely degraded RNA). RNA concentration was quantified using a NanoDrop ND-1000 spectrophotometer (Thermo Scientific, Wilmington, DE), and the 260/280 and

260/230 ratios were examined for protein and solvent contamination. Five micrograms of total RNA were reverse transcribed in a total volume of 20 µl containing 400 U of ImpromII and 0.5 µg of random hexamer (Promega, Madison, WI) for 60 min at 42°C according to the manufacturer's instructions. The reaction was terminated by heating at 70°C for 5 min, and the cDNA was diluted 1:20 for quantitative real-time PCR.

Microarray - PC12 cells were seeded on 25cm^2 flask in complete medium and subsequently incubated for 12 h in serum free DMEM. The cells were then treated with GDNF (50 ng/ml) or NGF (50 ng/ml) for 0.5 h or 72 h in duplicates. Total RNA was isolated, quantified and integrity verified before it was amplified using Ambion Illumina RNA Amplification kit (Ambion, TX, USA). Briefly, total RNA (500 ng) was reverse transcribed by ArrayScript in the presence of T7 Oligo(dT) primer. Second strand of the cDNA was synthesized by DNA polymerase at 16°C for 2 h. The cDNA was purified and *in vitro* transcribed with T7 RNA polymerase and biotin-NTPs. Biotin-labeled cRNA samples were purified and quantified by ND-1000 spectrophotometer (NanoDrop, Fisher Thermo, DE, USA). Each cRNA (750 ng) was hybridized to RatRef-12 Expression BeadChip (Illumina, San Diego, CA, USA) containing 22,523 probes for a total of 21,910 rat genes selected primarily from the NCBI RefSeq database (Release 16) according to instruction provided by Experienced User Card (11286340 Rev A, Illumina). After hybridization, washing and blocking, the BeadChip was incubated with Streptavidin-Cy3 solution (Amersham Biosciences, Piscataway, NJ, USA). Fluorescent signals were obtained from scans on the high resolution Illumina BeadArray reader, using a two-channel, 0.8 µm resolution confocal laser scanner. The Illumina BeadStudio software (Version 2.0) was used to extract fluorescence intensities and the raw fluorescent data was background subtracted and used for analysis. Background is defined as the average signal intensity estimated from the negative control bead types. Outliers are removed

using the median absolute deviation method. Detection p-values produced by the BeadStudio software were corrected for multiple hypothesis testing.

10.5 Analysis of protein expression

Western blot analysis - Primary cortical neurons or cultured neuronal cells were washed once with PBS and subsequently lysed in lysis buffer containing 2% (w/v) SDS. Protein concentrations were quantified using the microBCA assay (Pierce, Rockford, IL). The protein samples were separated by SDS-PAGE gel and incubated with respective primary antibodies over night at 4°C and subsequently with corresponding secondary antibodies for 2 h at 37°C. The protein bands were developed with Immobilon Western Chemilum HRP Substrate (Millipore, Billerica, MA) on ChemiDoc XRS system (Biorad). The band intensities were quantified with Quantity One 1-D Analysis software v4 (Biorad).

Preparation of nuclear and cytosolic extracts - The nuclear and cytosolic extracts were prepared using NE-PER® Nuclear and Cytoplasmic Extraction Reagents (Pierce), according to manufacturer's instruction. Briefly, PC12 and Neuro2A cells were washed twice with ice-cold PBS and harvested by gentle scraping. Cells were pelleted by centrifugation at 500 x g for 5 min, resuspended in ice cold CER I and incubated on ice for 10 min. The cells were then lysed by addition of ice cold CER II and centrifuged for 5 min at 16,000 x g to separate the cytosolic fraction (supernatant) from the nucleus (pellet). The pellet was resuspended in ice cold NER and incubated on ice for 40 min with occasional vortexing (15 s after every 10 min of incubation). The nuclear extracts (supernatant) were separated from the debris by centrifugation at 16,000g for 10 min.

Preparation of mitochondrial and cytosolic extracts – Mitochondrial and cytosolic extracts were prepared from PC12 and Neuro2A cells using differential centrifugation,

as previously described [29]. Briefly, the cells were washed twice with ice-cold phosphate buffer saline (PBS) and harvested by gentle scraping. Cells were pelleted by centrifugation at 500 x g for 5 min and resuspended in ice cold mitochondria extraction buffer (50 mM HEPES pH 7.4, 68 mM sucrose, 200 mM D-mannitol, 50 mM KCl, 2 mM MgCl2, 5 mM EDTA, 10 µg/ml aprotinin, 2 µg/ml pepstatin A, 10 µg/ml leupeptin, 50 mM NaF, 0.5 mM sodium vanadate, 20 mM glycerol phosphate) and incubated on ice for 15 min to allow swelling. The cells were dounce homogenized with 60 strokes. The unbroken cells and nuclei were removed by centrifugation at 800 x g for 10 min at 4°C. The supernatants were further centrifuged at 10,000 x g for 30 min at 4°C to obtain the crude mitochondrial fraction. The resulting supernatants were collected as the cytosolic extracts and the crude mitochondrial pellet was washed once with extraction buffer and collected by centrifugation at 10,000 x g for 30 min at 4°C.

Immunocytochemistry - Control and NTN treated Neuro2A, PC12 Cells and rat embryonic cortical neurons were fixed with 4% paraformaldehyde in PBS for 15 min at 37°C, subsequently permeabilized in 0.5% Triton-X100 / PBS and blocked with normal goat serum (1:10; Dako, Glostrup, Denmark) in 0.5% Triton X-100 / PBS for 45 min at 37°C. The cells were then incubated with primary antibodies against Phospho-STAT3-ser727 (CST #9134, 1:100 dilution) or GRIM-19 (Invitrogen #438900, 1:100 dilution) in 0.3% Triton X-100 / 1% BSA / PBS overnight at 4°C and washed three times in PBS. Subsequently, the cells were incubated with goat anti-rabbit or goat anti-mouse fluorescent secondary antibody (Alexa Fluor 488 / 596; Invitrogen, CA) diluted 1:400 in 0.3% Triton X-100 / 1% BSA / PBS for 2h at 37°C. The cells were washed three times in PBS and mounted. For Mitotracker labeling, live Neuro2A or PC12 cells were pre-incubated with 200 nM MitoTracker® Red CMXRos (Invitrogen M7512) for 10 min before NTN stimulation. Image acquisition was performed using the Zeiss LSM710 with Axio Observer.Z1 confocal microscope

equipped with fluorescence detection (Oberkochen, Germany). Images of control and NTN stimulated samples were taken with identical laser and optical settings. Colocalization coefficients between P-Ser-STAT3 and MitoTracker or P-Ser-STAT3 and GRIM-19 were analysed with Zeiss ZEN software (v2010).

Bibliography

1. R. H. Baloh, H. Enomoto, E. M. Johnson, Jr., J. Milbrandt, The GDNF family ligands and receptors - implications for neural development. *Curr Opin Neurobiol* **10**, 103 (Feb, 2000).
2. M. S. Airaksinen, A. Titievsky, M. Saarma, GDNF family neurotrophic factor signaling: four masters, one servant? *Mol Cell Neurosci* **13**, 313 (May, 1999).
3. G. Paratcha, F. Ledda, GDNF and GFRalpha: a versatile molecular complex for developing neurons. *Trends Neurosci* **31**, 384 (Aug, 2008).
4. H. P. Too, Real time PCR quantification of GFRalpha-2 alternatively spliced isoforms in murine brain and peripheral tissues. *Brain research. Molecular brain research* **114**, 146 (Jun 10, 2003).
5. L. F. Yoong, Z. N. Peng, G. Wan, H. P. Too, Tissue expression of alternatively spliced GFRalpha1, NCAM and RET isoforms and the distinct functional consequence of ligand-induced activation of GFRalpha1 isoforms. *Brain research. Molecular brain research* **139**, 1 (Sep 13, 2005).
6. L. F. Yoong, H. P. Too, Glial cell line-derived neurotrophic factor and neurturin inhibit neurite outgrowth and activate RhoA through GFR alpha 2b, an alternatively spliced isoform of GFR alpha 2. *J Neurosci* **27**, 5603 (May 23, 2007).
7. L. F. Yoong, G. Wan, H. P. Too, GDNF-induced cell signaling and neurite outgrowths are differentially mediated by GFRalpha1 isoforms. *Mol Cell Neurosci* **41**, 464 (Aug, 2009).
8. L. F. Lin, D. H. Doherty, J. D. Lile, S. Bektesh, F. Collins, GDNF: a glial cell line-derived neurotrophic factor for midbrain dopaminergic neurons. *Science* **260**, 1130 (May 21, 1993).
9. P. T. Kotzbauer *et al.*, Neurturin, a relative of glial-cell-line-derived neurotrophic factor. *Nature* **384**, 467 (Dec 5, 1996).
10. J. Milbrandt *et al.*, Persephin, a novel neurotrophic factor related to GDNF and neurturin. *Neuron* **20**, 245 (Feb, 1998).
11. R. H. Baloh *et al.*, Artemin, a novel member of the GDNF ligand family, supports peripheral and central neurons and signals through the GFRalpha3-RET receptor complex. *Neuron* **21**, 1291 (Dec, 1998).
12. M. S. Airaksinen, L. Holm, T. Hatinen, Evolution of the GDNF family ligands and receptors. *Brain Behav Evol* **68**, 181 (2006).
13. M. Del Fiacco *et al.*, Topographical localization of glial cell line-derived neurotrophic factor in the human brain stem: an immunohistochemical study of prenatal, neonatal and adult brains. *J Chem Neuroanat* **23**, 29 (Jan, 2002).
14. M. Quartu *et al.*, Tissue distribution of Ret, GFRalpha-1, GFRalpha-2 and GFRalpha-3 receptors in the human brainstem at fetal, neonatal and adult age. *Brain Res* **1173**, 36 (Oct 10, 2007).
15. M. Quartu *et al.*, Neurturin, persephin, and artemin in the human pre- and full-term newborn and adult hippocampus and fascia dentata. *Brain Res* **1041**, 157 (Apr 18, 2005).
16. A. Saavedra, G. Baltazar, E. P. Duarte, Driving GDNF expression: the green and the red traffic lights. *Prog Neurobiol* **86**, 186 (Nov, 2008).
17. N. Cristina, C. Chatellard-Causse, M. Manier, C. Feuerstein, GDNF: existence of a second transcript in the brain. *Brain research. Molecular brain research* **32**, 354 (Sep, 1995).

18. L. Grimm *et al.*, Analysis of the human GDNF gene reveals an inducible promoter, three exons, a triplet repeat within the 3'-UTR and alternative splice products. *Hum Mol Genet* **7**, 1873 (Nov, 1998).
19. D. G. Schaar *et al.*, Multiple astrocyte transcripts encode nigral trophic factors in rat and human. *Exp Neurol* **130**, 387 (Dec, 1994).
20. J. E. Springer *et al.*, cDNA sequence and differential mRNA regulation of two forms of glial cell line-derived neurotrophic factor in Schwann cells and rat skeletal muscle. *Exp Neurol* **131**, 47 (Jan, 1995).
21. C. Suter-Crazzolara, K. Unsicker, GDNF is expressed in two forms in many tissues outside the CNS. *Neuroreport* **5**, 2486 (Dec 20, 1994).
22. M. Tanaka, S. Ito, K. Kiuchi, Novel alternative promoters of mouse glial cell line-derived neurotrophic factor gene. *Biochim Biophys Acta* **1494**, 63 (Nov 15, 2000).
23. T. Tanaka *et al.*, Identification of a novel GDNF mRNA induced by LPS in immune cell lines. *Neurosci Res* **61**, 11 (May, 2008).
24. S. Masure *et al.*, Molecular cloning, expression and tissue distribution of glial-cell-line-derived neurotrophic factor family receptor alpha-3 (GFRalpha-3). *Eur J Biochem* **251**, 622 (Feb 1, 1998).
25. J. Jaszai *et al.*, GDNF-related factor persephin is widely distributed throughout the nervous system. *J Neurosci Res* **53**, 494 (Aug 15, 1998).
26. C. M. Backman *et al.*, Gene expression patterns for GDNF and its receptors in the human putamen affected by Parkinson's disease: a real-time PCR study. *Mol Cell Endocrinol* **252**, 160 (Jun 27, 2006).
27. C. Eigenbrot, N. Gerber, X-ray structure of glial cell-derived neurotrophic factor at 1.9 A resolution and implications for receptor binding. *Nat Struct Biol* **4**, 435 (Jun, 1997).
28. L. Silvian *et al.*, Artemin crystal structure reveals insights into heparan sulfate binding. *Biochemistry* **45**, 6801 (Jun 6, 2006).
29. M. Coulpier, C. F. Ibanez, Retrograde propagation of GDNF-mediated signals in sympathetic neurons. *Mol Cell Neurosci* **27**, 132 (Oct, 2004).
30. K. Ohta, T. Inokuchi, E. Gen, J. Chang, Ultrastructural study of anterograde transport of glial cell line-derived neurotrophic factor from dorsal root ganglion neurons of rats towards the nerve terminal. *Cells Tissues Organs* **169**, 410 (2001).
31. H. B. Rind, C. S. von Bartheld, Anterograde axonal transport of internalized GDNF in sensory and motor neurons. *Neuroreport* **13**, 659 (Apr 16, 2002).
32. F. D. Russell, K. Koishi, Y. Jiang, I. S. McLennan, Anterograde axonal transport of glial cell line-derived neurotrophic factor and its receptors in rat hypoglossal nerve. *Neuroscience* **97**, 575 (2000).
33. C. S. von Bartheld, X. Wang, R. Butowt, Anterograde axonal transport, transcytosis, and recycling of neurotrophic factors: the concept of trophic currencies in neural networks. *Mol Neurobiol* **24**, 1 (Aug-Dec, 2001).
34. P. Barroso-Chinea *et al.*, Striatal expression of GDNF and differential vulnerability of midbrain dopaminergic cells. *The European journal of neuroscience* **21**, 1815 (Apr, 2005).
35. A. Tomac *et al.*, Retrograde axonal transport of glial cell line-derived neurotrophic factor in the adult nigrostriatal system suggests a trophic role in the adult. *Proc Natl Acad Sci U S A* **92**, 8274 (Aug 29, 1995).
36. R. E. Burke, GDNF as a candidate striatal target-derived neurotrophic factor for the development of substantia nigra dopamine neurons. *J Neural Transm Suppl*, 41 (2006).
37. P. Hiltunen *et al.*, Initial characterization of GDNF-family receptor GFRα4-deficient mice. *Soc Neurosci Abstr* **27**, Progr no 364.31 (2001).

38. E. Hashino *et al.*, GDNF and neurturin are target-derived factors essential for cranial parasympathetic neuron development. *Development* **128**, 3773 (Oct, 2001).
39. J. A. Davies, C. B. Millar, E. M. Johnson, Jr., J. Milbrandt, Neurturin: an autocrine regulator of renal collecting duct development. *Dev Genet* **24**, 284 (1999).
40. H. Song, A. Moon, Glial cell-derived neurotrophic factor (GDNF) promotes low-grade Hs683 glioma cell migration through JNK, ERK-1/2 and p38 MAPK signaling pathways. *Neurosci Res* **56**, 29 (Sep, 2006).
41. L. X. Yang, P. G. Nelson, Glia cell line-derived neurotrophic factor regulates the distribution of acetylcholine receptors in mouse primary skeletal muscle cells. *Neuroscience* **128**, 497 (2004).
42. M. W. Moore *et al.*, Renal and neuronal abnormalities in mice lacking GDNF. *Nature* **382**, 76 (Jul 4, 1996).
43. J. G. Pichel *et al.*, Defects in enteric innervation and kidney development in mice lacking GDNF. *Nature* **382**, 73 (Jul 4, 1996).
44. M. P. Sanchez *et al.*, Renal agenesis and the absence of enteric neurons in mice lacking GDNF. *Nature* **382**, 70 (Jul 4, 1996).
45. S. Jain *et al.*, RET is dispensable for maintenance of midbrain dopaminergic neurons in adult mice. *J Neurosci* **26**, 11230 (Oct 25, 2006).
46. E. R. Kramer *et al.*, Absence of Ret signaling in mice causes progressive and late degeneration of the nigrostriatal system. *PLoS Biol* **5**, e39 (Mar, 2007).
47. A. Pascual *et al.*, Absolute requirement of GDNF for adult catecholaminergic neuron survival. *Nat Neurosci* **11**, 755 (Jul, 2008).
48. M. Cik *et al.*, Binding of GDNF and neurturin to human GDNF family receptor alpha 1 and 2. Influence of cRET and cooperative interactions. *J Biol Chem* **275**, 27505 (Sep 8, 2000).
49. B. A. Horger *et al.*, Neurturin exerts potent actions on survival and function of midbrain dopaminergic neurons. *J Neurosci* **18**, 4929 (Jul 1, 1998).
50. R. P. Scott, C. F. Ibanez, Determinants of ligand binding specificity in the glial cell line-derived neurotrophic factor family receptor alpha S. *J Biol Chem* **276**, 1450 (Jan 12, 2001).
51. L. C. Wang, A. Shih, J. Hongo, B. Devaux, M. Hynes, Broad specificity of GDNF family receptors GFRalpha1 and GFRalpha2 for GDNF and NTN in neurons and transfected cells. *J Neurosci Res* **61**, 1 (Jul 1, 2000).
52. P. Runeberg-Roos, M. Saarma, Neurotrophic factor receptor RET: structure, cell biology, and inherited diseases. *Ann Med* **39**, 572 (2007).
53. M. Takahashi, Structure and expression of the ret transforming gene. *IARC Sci Publ*, 189 (1988).
54. J. P. Cao *et al.*, Integrin beta1 is involved in the signaling of glial cell line-derived neurotrophic factor. *J Comp Neurol* **509**, 203 (Jul 10, 2008).
55. E. Pozas, C. F. Ibanez, GDNF and GFRalpha1 promote differentiation and tangential migration of cortical GABAergic neurons. *Neuron* **45**, 701 (Mar 3, 2005).
56. J. R. Cabrera *et al.*, Gas1 is related to the glial cell-derived neurotrophic factor family receptors alpha and regulates Ret signaling. *J Biol Chem* **281**, 14330 (May 19, 2006).
57. O. Schueler-Furman, E. Glick, J. Segovia, M. Linial, Is GAS1 a co-receptor for the GDNF family of ligands? *Trends Pharmacol Sci* **27**, 72 (Feb, 2006).
58. Z. Li *et al.*, Identification, expression and functional characterization of the GRAL gene. *J Neurochem* **95**, 361 (Oct, 2005).
59. F. Ledda, O. Bieraugel, S. S. Fard, M. Vilar, G. Paratcha, Lrig1 is an endogenous inhibitor of Ret receptor tyrosine kinase activation, downstream signaling, and biological responses to GDNF. *J Neurosci* **28**, 39 (Jan 2, 2008).

60. M. A. Lopez-Ramirez, G. Dominguez-Monzon, P. Vergara, J. Segovia, Gas1 reduces Ret tyrosine 1062 phosphorylation and alters GDNF-mediated intracellular signaling. *Int J Dev Neurosci* **26**, 497 (Aug, 2008).
61. M. Lindahl *et al.*, Human glial cell line-derived neurotrophic factor receptor alpha 4 is the receptor for persephin and is predominantly expressed in normal and malignant thyroid medullary cells. *J Biol Chem* **276**, 9344 (Mar 23, 2001).
62. V. M. Leppanen *et al.*, The structure of GFRalpha1 domain 3 reveals new insights into GDNF binding and RET activation. *EMBO J* **23**, 1452 (Apr 7, 2004).
63. L. M. Wang *et al.*, A structure-function analysis of glial cell-line-derived neurotrophic factor receptor alpha1. *Protein Pept Lett* **10**, 61 (Feb, 2003).
64. X. Wang, R. H. Baloh, J. Milbrandt, K. C. Garcia, Structure of artemin complexed with its receptor GFRalpha3: convergent recognition of glial cell line-derived neurotrophic factors. *Structure* **14**, 1083 (Jun, 2006).
65. A. Amoresano *et al.*, Direct interactions among Ret, GDNF and GFRalpha1 molecules reveal new insights into the assembly of a functional three-protein complex. *Cell Signal* **17**, 717 (Jun, 2005).
66. V. Parkash *et al.*, The structure of the glial cell line-derived neurotrophic factor-coreceptor complex: insights into RET signaling and heparin binding. *J Biol Chem* **283**, 35164 (Dec 12, 2008).
67. T. C. Burazin, A. L. Gundlach, Localization of GDNF/neurturin receptor (c-ret, GFRalpha-1 and alpha-2) mRNAs in postnatal rat brain: differential regional and temporal expression in hippocampus, cortex and cerebellum. *Brain research. Molecular brain research* **73**, 151 (Nov 10, 1999).
68. G. W. Glazner, X. Mu, J. E. Springer, Localization of glial cell line-derived neurotrophic factor receptor alpha and c-ret mRNA in rat central nervous system. *J Comp Neurol* **391**, 42 (Feb 2, 1998).
69. J. P. Golden *et al.*, Expression of neurturin, GDNF, and their receptors in the adult mouse CNS. *J Comp Neurol* **398**, 139 (Aug 17, 1998).
70. S. Homma *et al.*, Differential expression of the GDNF family receptors RET and GFRalpha1, 2, and 4 in subsets of motoneurons: a relationship between motoneuron birthdate and receptor expression. *J Comp Neurol* **456**, 245 (Feb 10, 2003).
71. S. Masure *et al.*, Enovin, a member of the glial cell-line-derived neurotrophic factor (GDNF) family with growth promoting activity on neuronal cells. Existence and tissue-specific expression of different splice variants. *Eur J Biochem* **266**, 892 (Dec, 1999).
72. C. A. Nosrat, A. Tomac, B. J. Hoffer, L. Olson, Cellular and developmental patterns of expression of Ret and glial cell line-derived neurotrophic factor receptor alpha mRNAs. *Exp Brain Res* **115**, 410 (Jul, 1997).
73. M. Sanicola *et al.*, Glial cell line-derived neurotrophic factor-dependent RET activation can be mediated by two different cell-surface accessory proteins. *Proc Natl Acad Sci U S A* **94**, 6238 (Jun 10, 1997).
74. J. J. Treanor *et al.*, Characterization of a multicomponent receptor for GDNF. *Nature* **382**, 80 (Jul 4, 1996).
75. M. Trupp, N. Belluardo, H. Funakoshi, C. F. Ibanez, Complementary and overlapping expression of glial cell line-derived neurotrophic factor (GDNF), c-ret proto-oncogene, and GDNF receptor-alpha indicates multiple mechanisms of trophic actions in the adult rat CNS. *J Neurosci* **17**, 3554 (May 15, 1997).
76. J. Widenfalk *et al.*, Neurturin and glial cell line-derived neurotrophic factor receptor-beta (GDNFR-beta), novel proteins related to GDNF and GDNFR-alpha with specific cellular patterns of expression suggesting roles in the developing and adult nervous system and in peripheral organs. *J Neurosci* **17**, 8506 (Nov 1, 1997).

77. C. A. Worby *et al.*, Identification and characterization of GFRalpha-3, a novel Co-receptor belonging to the glial cell line-derived neurotrophic receptor family. *J Biol Chem* **273**, 3502 (Feb 6, 1998).
78. T. C. Burazin, A. L. Gundlach, Up-regulation of GDNFR-alpha and c-ret mRNA in facial motor neurons following facial nerve injury in the rat. *Brain research. Molecular brain research* **55**, 331 (Apr, 1998).
79. C. W. Ehrenfels, P. J. Carmillo, O. Orozco, R. L. Cate, M. Sanicola, Perturbation of RET signaling in the embryonic kidney. *Dev Genet* **24**, 263 (1999).
80. D. S. Worley *et al.*, Developmental regulation of GDNF response and receptor expression in the enteric nervous system. *Development* **127**, 4383 (Oct, 2000).
81. G. Paratcha *et al.*, Released GFRalpha1 potentiates downstream signaling, neuronal survival, and differentiation via a novel mechanism of recruitment of c-Ret to lipid rafts. *Neuron* **29**, 171 (Jan, 2001).
82. H. Enomoto, Regulation of neural development by glial cell line-derived neurotrophic factor family ligands. *Anat Sci Int* **80**, 42 (Mar, 2005).
83. J. Cho, N. G. Kholodilov, R. E. Burke, Patterns of developmental mRNA expression of neurturin and GFRalpha2 in the rat striatum and substantia nigra do not suggest a role in the regulation of natural cell death in dopamine neurons. *Brain Res Dev Brain Res* **148**, 143 (Jan 31, 2004).
84. J. Cho, O. Yarygina, T. F. Oo, N. G. Kholodilov, R. E. Burke, Glial cell line-derived neurotrophic factor receptor GFRalpha1 is expressed in the rat striatum during postnatal development. *Brain research. Molecular brain research* **127**, 96 (Aug 23, 2004).
85. T. Lenhard, C. Suter-Crazzolara, Developmental expression of GDNF, neurturin and their receptors in rat hippocampus. *Neuroreport* **9**, 2927 (Sep 14, 1998).
86. J. Zhang, E. J. Huang, Dynamic expression of neurotrophic factor receptors in postnatal spinal motoneurons and in mouse model of ALS. *J Neurobiol* **66**, 882 (Jul, 2006).
87. H. Hammarberg, F. Piehl, M. Risling, S. Cullheim, Differential regulation of trophic factor receptor mRNAs in spinal motoneurons after sciatic nerve transection and ventral root avulsion in the rat. *J Comp Neurol* **426**, 587 (Oct 30, 2000).
88. H. Tsujino *et al.*, Discordant expression of c-Ret and glial cell line-derived neurotrophic factor receptor alpha-1 mRNAs in response to motor nerve injury in neonate rats. *Brain research. Molecular brain research* **70**, 298 (Jul 5, 1999).
89. A. Arvidsson, Z. Kokaia, M. S. Airaksinen, M. Saarma, O. Lindvall, Stroke induces widespread changes of gene expression for glial cell line-derived neurotrophic factor family receptors in the adult rat brain. *Neuroscience* **106**, 27 (2001).
90. K. Horinouchi *et al.*, Functional recovery and expression of GDNF seen in photochemically induced cerebral infarction. *Int J Neurosci* **117**, 315 (Mar, 2007).
91. H. Miyazaki, K. Nagashima, Y. Okuma, Y. Nomura, Expression of Ret receptor tyrosine kinase after transient forebrain ischemia is modulated by glial cell line-derived neurotrophic factor in rat hippocampus. *Neurosci Lett* **318**, 1 (Jan 18, 2002).
92. A. Sarabi *et al.*, Differential expression of the cell line-derived neurotrophic factor (GDNF) receptor GFRalpha1 in heterozygous Gfralpha1 null-mutant mice after stroke. *Neurosci Lett* **341**, 241 (May 8, 2003).
93. Q. Cheng, V. Di Liberto, G. Caniglia, G. Mudo, Time-course of GDNF and its receptor expression after brain injury in the rat. *Neurosci Lett* **439**, 24 (Jul 4, 2008).
94. S. H. Lee *et al.*, Sustained activation of Akt by melatonin contributes to the protection against kainic acid-induced neuronal death in hippocampus. *J Pineal Res* **40**, 79 (Jan, 2006).

95. S. Marco *et al.*, Excitatory amino acids differentially regulate the expression of GDNF, neurturin, and their receptors in the adult rat striatum. *Exp Neurol* **174**, 243 (Apr, 2002).
96. M. Reeben, A. Laurikainen, J. O. Hiltunen, E. Castren, M. Saarma, The messenger RNAs for both glial cell line-derived neurotrophic factor receptors, c-ret and GDNFRalpha, are induced in the rat brain in response to kainate-induced excitation. *Neuroscience* **83**, 151 (Mar, 1998).
97. A. C. Chen *et al.*, Regulation of GFRalpha-1 and GFRalpha-2 mRNAs in rat brain by electroconvulsive seizure. *Synapse* **39**, 42 (Jan, 2001).
98. X. Gao, J. Wang, X. Wei, [Expressions of GDNF, GDNFR alpha and Ret proteins in the brain of rats with seizures induced by pilocarpine]. *Beijing Da Xue Xue Bao* **35**, 296 (Jun 18, 2003).
99. C. J. Lee, K. Irizarry, Alternative splicing in the nervous system: an emerging source of diversity and regulation. *Biological psychiatry* **54**, 771 (Oct 15, 2003).
100. H. Maruoka *et al.*, Dibutyryl-cAMP up-regulates nur77 expression via histone modification during neurite outgrowth in PC12 cells. *J Biochem* **148**, 93 (2010).
101. Z. Kan, P. W. Garrett-Engele, J. M. Johnson, J. C. Castle, Evolutionarily conserved and diverged alternative splicing events show different expression and functional profiles. *Nucleic Acids Res* **33**, 5659 (2005).
102. S. E. Shefelbine *et al.*, Mutational analysis of the GDNF/RET-GDNFR alpha signaling complex in a kindred with vesicoureteral reflux. *Hum Genet* **102**, 474 (Apr, 1998).
103. B. K. Dey, Y. W. Wong, H. P. Too, Cloning of a novel murine isoform of the glial cell line-derived neurotrophic factor receptor. *Neuroreport* **9**, 37 (Jan 5, 1998).
104. N. F. Dolatshad, A. T. Silva, M. J. Saffrey, Identification of GFR alpha-2 isoforms in myenteric plexus of postnatal and adult rat intestine. *Brain research. Molecular brain research* **107**, 32 (Oct 30, 2002).
105. Y. W. Wong, H. P. Too, Identification of mammalian GFRalpha-2 splice isoforms. *NeuroReport* **9**, 3767 (Dec 1, 1998).
106. M. Lindahl, T. Timmusk, J. Rossi, M. Saarma, M. S. Airaksinen, Expression and alternative splicing of mouse Gfra4 suggest roles in endocrine cell development. *Mol Cell Neurosci* **15**, 522 (Jun, 2000).
107. S. Masure *et al.*, Mammalian GFRalpha -4, a divergent member of the GFRalpha family of coreceptors for glial cell line-derived neurotrophic factor family ligands, is a receptor for the neurotrophic factor persephin. *J Biol Chem* **275**, 39427 (Dec 15, 2000).
108. D. C. Lee, K. W. Chan, S. Y. Chan, RET receptor tyrosine kinase isoforms in kidney function and disease. *Oncogene* **21**, 5582 (Aug 15, 2002).
109. M. J. Lorenzo *et al.*, RET alternate splicing influences the interaction of activated RET with the SH2 and PTB domains of Shc, and the SH2 domain of Grb2. *Oncogene* **14**, 763 (Feb 20, 1997).
110. B. Buttner, W. Reutter, R. Horstkorte, Cytoplasmic domain of NCAM 180 reduces NCAM-mediated neurite outgrowth. *J Neurosci Res* **75**, 854 (Mar 15, 2004).
111. G. K. Povlsen, D. K. Ditlevsen, V. Berezin, E. Bock, Intracellular signaling by the neural cell adhesion molecule. *Neurochem Res* **28**, 127 (Jan, 2003).
112. N. Charlet-Berguerand *et al.*, Expression of GFRalpha1 receptor splicing variants with different biochemical properties is modulated during kidney development. *Cell Signal* **16**, 1425 (Dec, 2004).
113. T. Tahira, Y. Ishizaka, F. Itoh, T. Sugimura, M. Nagao, Characterization of ret proto-oncogene mRNAs encoding two isoforms of the protein product in a human neuroblastoma cell line. *Oncogene* **5**, 97 (Jan, 1990).

114. M. G. Borrello *et al.*, Differential interaction of Enigma protein with the two RET isoforms. *Biochem Biophys Res Commun* **296**, 515 (Aug 23, 2002).
115. G. Schuetz *et al.*, The neuronal scaffold protein Shank3 mediates signaling and biological function of the receptor tyrosine kinase Ret in epithelial cells. *J Cell Biol* **167**, 945 (Dec 6, 2004).
116. R. P. Scott, S. Eketjall, H. Aineskog, C. F. Ibanez, Distinct turnover of alternatively spliced isoforms of the RET kinase receptor mediated by differential recruitment of the Cbl ubiquitin ligase. *J Biol Chem* **280**, 13442 (Apr 8, 2005).
117. R. H. Lee, W. L. Wong, C. H. Chan, S. Y. Chan, Differential effects of glial cell line-derived neurotrophic factor and neurturin in RET/GFRalpha1-expressing cells. *J Neurosci Res* **83**, 80 (Jan, 2006).
118. B. A. Tsui-Pierchala, R. C. Ahrens, R. J. Crowder, J. Milbrandt, E. M. Johnson, Jr., The long and short isoforms of Ret function as independent signaling complexes. *J Biol Chem* **277**, 34618 (Sep 13, 2002).
119. K. Durick, R. Y. Wu, G. N. Gill, S. S. Taylor, Mitogenic signaling by Ret/ptc2 requires association with enigma via a LIM domain. *J Biol Chem* **271**, 12691 (May 31, 1996).
120. A. Pandey, X. Liu, J. E. Dixon, P. P. Di Fiore, V. M. Dixit, Direct association between the Ret receptor tyrosine kinase and the Src homology 2-containing adapter protein Grb7. *J Biol Chem* **271**, 10607 (May 3, 1996).
121. M. Encinas, R. J. Crowder, J. Milbrandt, E. M. Johnson, Jr., Tyrosine 981, a novel ret autophosphorylation site, binds c-Src to mediate neuronal survival. *J Biol Chem* **279**, 18262 (Apr 30, 2004).
122. M. G. Borrello *et al.*, The full oncogenic activity of Ret/ptc2 depends on tyrosine 539, a docking site for phospholipase Cgamma. *Mol Cell Biol* **16**, 2151 (May, 1996).
123. E. Arighi *et al.*, Identification of Shc docking site on Ret tyrosine kinase. *Oncogene* **14**, 773 (Feb 20, 1997).
124. L. Alberti *et al.*, Grb2 binding to the different isoforms of Ret tyrosine kinase. *Oncogene* **17**, 1079 (Sep 3, 1998).
125. K. Simons, D. Toomre, Lipid rafts and signal transduction. *Nat Rev Mol Cell Biol* **1**, 31 (Oct, 2000).
126. M. G. Tansey, R. H. Baloh, J. Milbrandt, E. M. Johnson, Jr., GFRalpha-mediated localization of RET to lipid rafts is required for effective downstream signaling, differentiation, and neuronal survival. *Neuron* **25**, 611 (Mar, 2000).
127. M. A. Barbieri, T. P. Ramkumar, S. Fernadez-Pol, P. I. Chen, P. D. Stahl, Receptor tyrosine kinase signaling and trafficking--paradigms revisited. *Curr Top Microbiol Immunol* **286**, 1 (2004).
128. P. Vieira, J. Thomas-Crusells, A. Vieira, Internalization of glial cell-derived neurotrophic factor receptor GFR alpha 1 in the absence of the ret tyrosine kinase coreceptor. *Cell Mol Neurobiol* **23**, 43 (Feb, 2003).
129. M. L. Leitner *et al.*, Analysis of the retrograde transport of glial cell line-derived neurotrophic factor (GDNF), neurturin, and persephin suggests that in vivo signaling for the GDNF family is GFRalpha coreceptor-specific. *J Neurosci* **19**, 9322 (Nov 1, 1999).
130. T. Fujioka, A. Fujioka, R. S. Duman, Activation of cAMP signaling facilitates the morphological maturation of newborn neurons in adult hippocampus. *J Neurosci* **24**, 319 (Jan 14, 2004).
131. S. S. Hannila, M. T. Filbin, The role of cyclic AMP signaling in promoting axonal regeneration after spinal cord injury. *Exp Neurol* **209**, 321 (Feb, 2008).
132. S. Neumann, F. Bradke, M. Tessier-Lavigne, A. I. Basbaum, Regeneration of sensory axons within the injured spinal cord induced by intraganglionic cAMP elevation. *Neuron* **34**, 885 (Jun 13, 2002).

133. R. E. Rydel, L. A. Greene, cAMP analogs promote survival and neurite outgrowth in cultures of rat sympathetic and sensory neurons independently of nerve growth factor. *Proc Natl Acad Sci U S A* **85**, 1257 (Feb, 1988).
134. Q. Cui, Actions of neurotrophic factors and their signaling pathways in neuronal survival and axonal regeneration. *Mol Neurobiol* **33**, 155 (Apr, 2006).
135. S. L. Kilmer, R. C. Carlsen, Forskolin activation of adenylate cyclase in vivo stimulates nerve regeneration. *Nature* **307**, 455 (Feb 2-8, 1984).
136. D. Cai *et al.*, Neuronal cyclic AMP controls the developmental loss in ability of axons to regenerate. *J Neurosci* **21**, 4731 (Jul 1, 2001).
137. J. Qiu *et al.*, Spinal axon regeneration induced by elevation of cyclic AMP. *Neuron* **34**, 895 (Jun 13, 2002).
138. D. Cai, Y. Shen, M. De Bellard, S. Tang, M. T. Filbin, Prior exposure to neurotrophins blocks inhibition of axonal regeneration by MAG and myelin via a cAMP-dependent mechanism. *Neuron* **22**, 89 (Jan, 1999).
139. P. Lu, H. Yang, L. L. Jones, M. T. Filbin, M. H. Tuszynski, Combinatorial therapy with neurotrophins and cAMP promotes axonal regeneration beyond sites of spinal cord injury. *J Neurosci* **24**, 6402 (Jul 14, 2004).
140. D. M. Deshpande *et al.*, Recovery from paralysis in adult rats using embryonic stem cells. *Ann Neurol* **60**, 32 (Jul, 2006).
141. D. L. Bennett *et al.*, The glial cell line-derived neurotrophic factor family receptor components are differentially regulated within sensory neurons after nerve injury. *J Neurosci* **20**, 427 (Jan 1, 2000).
142. A. Mikaels, J. Livet, H. Westphal, O. De Lapeyriere, P. Ernfors, A dynamic regulation of GDNF-family receptors correlates with a specific trophic dependency of cranial motor neuron subpopulations during development. *The European journal of neuroscience* **12**, 446 (Feb, 2000).
143. J. L. Bos, Epac proteins: multi-purpose cAMP targets. *Trends Biochem Sci* **31**, 680 (Dec, 2006).
144. X. Cheng, Z. Ji, T. Tsalkova, F. Mei, Epac and PKA: a tale of two intracellular cAMP receptors. *Acta Biochim Biophys Sin (Shanghai)* **40**, 651 (Jul, 2008).
145. M. C. Chen *et al.*, Involvement of cAMP in nerve growth factor-triggered p35/Cdk5 activation and differentiation in PC12 cells. *Am J Physiol Cell Physiol* **299**, C516 (Aug, 2010).
146. S. Kiermayer *et al.*, Epac activation converts cAMP from a proliferative into a differentiation signal in PC12 cells. *Mol Biol Cell* **16**, 5639 (Dec, 2005).
147. Z. Wang *et al.*, Rap1-mediated activation of extracellular signal-regulated kinases by cyclic AMP is dependent on the mode of Rap1 activation. *Mol Cell Biol* **26**, 2130 (Mar, 2006).
148. M. Frodin, P. Peraldi, E. Van Obberghen, Cyclic AMP activates the mitogen-activated protein kinase cascade in PC12 cells. *J Biol Chem* **269**, 6207 (Feb 25, 1994).
149. H. S. Kim *et al.*, Secretin induces neurite outgrowth of PC12 through cAMP-mitogen-activated protein kinase pathway. *Exp Mol Med* **38**, 85 (Feb 28, 2006).
150. T. K. Monaghan, C. J. Mackenzie, R. Plevin, E. M. Lutz, PACAP-38 induces neuronal differentiation of human SH-SY5Y neuroblastoma cells via cAMP-mediated activation of ERK and p38 MAP kinases. *J Neurochem* **104**, 74 (Jan, 2008).
151. H. Yao *et al.*, Cyclic adenosine monophosphate can convert epidermal growth factor into a differentiating factor in neuronal cells. *J Biol Chem* **270**, 20748 (Sep 1, 1995).
152. H. Yao, R. D. York, A. Misra-Press, D. W. Carr, P. J. Stork, The cyclic adenosine monophosphate-dependent protein kinase (PKA) is required for the sustained activation of mitogen-activated kinases and gene expression by nerve growth factor. *J Biol Chem* **273**, 8240 (Apr 3, 1998).

153. G. A. Gonzalez *et al.*, A cluster of phosphorylation sites on the cyclic AMP-regulated nuclear factor CREB predicted by its sequence. *Nature* **337**, 749 (Feb 23, 1989).
154. M. D. Mark, Y. Liu, S. T. Wong, T. R. Hinds, D. R. Storm, Stimulation of neurite outgrowth in PC12 cells by EGF and KCl depolarization: a Ca(2+)-independent phenomenon. *J Cell Biol* **130**, 701 (Aug, 1995).
155. H. C. Cheng, H. M. Shih, Y. Chern, Essential role of cAMP-response element-binding protein activation by A2A adenosine receptors in rescuing the nerve growth factor-induced neurite outgrowth impaired by blockage of the MAPK cascade. *J Biol Chem* **277**, 33930 (Sep 13, 2002).
156. A. E. Christensen *et al.*, cAMP analog mapping of Epac1 and cAMP kinase. Discriminating analogs demonstrate that Epac and cAMP kinase act synergistically to promote PC-12 cell neurite extension. *J Biol Chem* **278**, 35394 (Sep 12, 2003).
157. M. Montminy, Transcriptional regulation by cyclic AMP. *Annu Rev Biochem* **66**, 807 (1997).
158. C. J. Marshall, Specificity of receptor tyrosine kinase signaling: transient versus sustained extracellular signal-regulated kinase activation. *Cell* **80**, 179 (Jan 27, 1995).
159. W. J. Marks, Jr. *et al.*, Gene delivery of AAV2-neurturin for Parkinson's disease: a double-blind, randomised, controlled trial. *Lancet Neurol* **9**, 1164 (Dec, 2010).
160. W. J. Marks, Jr. *et al.*, Safety and tolerability of intraputaminal delivery of CERE-120 (adeno-associated virus serotype 2-neurturin) to patients with idiopathic Parkinson's disease: an open-label, phase I trial. *Lancet Neurol* **7**, 400 (May, 2008).
161. K. B. Zihlmann *et al.*, The GDNF family members neurturin, artemin and persephin promote the morphological differentiation of cultured ventral mesencephalic dopaminergic neurons. *Brain Res Bull* **68**, 42 (Dec 15, 2005).
162. Y. Wanigasekara, J. R. Keast, Neurturin has multiple neurotrophic effects on adult rat sacral parasympathetic ganglion neurons. *The European journal of neuroscience* **22**, 595 (Aug, 2005).
163. S. Traverse, N. Gomez, H. Paterson, C. Marshall, P. Cohen, Sustained activation of the mitogen-activated protein (MAP) kinase cascade may be required for differentiation of PC12 cells. Comparison of the effects of nerve growth factor and epidermal growth factor. *Biochem J* **288 (Pt 2)**, 351 (Dec 1, 1992).
164. M. D. Hilborn, S. G. Rane, J. D. Pollock, EGF in combination with depolarization or cAMP produces morphological but not physiological differentiation in PC12 cells. *J Neurosci Res* **47**, 16 (Jan 1, 1997).
165. C. Richter-Landsberg, B. Jastorff, The role of cAMP in nerve growth factor-promoted neurite outgrowth in PC12 cells. *J Cell Biol* **102**, 821 (Mar, 1986).
166. A. J. Murray, D. A. Shewan, Epac mediates cyclic AMP-dependent axon growth, guidance and regeneration. *Mol Cell Neurosci* **38**, 578 (Aug, 2008).
167. M. J. Gerdin, L. E. Eiden, Regulation of PC12 cell differentiation by cAMP signaling to ERK independent of PKA: do all the connections add up? *Sci STKE* **2007**, pe15 (Apr 17, 2007).
168. G. X. Shi, H. Rehmann, D. A. Andres, A Novel Cyclic AMP-Dependent Epac-Rit Signaling Pathway Contributes to PACAP38-Mediated Neuronal Differentiation. *Mol Cell Biol* **26**, 9136 (2006).
169. S. Traverse *et al.*, EGF triggers neuronal differentiation of PC12 cells that overexpress the EGF receptor. *Curr Biol* **4**, 694 (Aug 1, 1994).
170. Horgan, A., Examining the mechanism of Erk nuclear translocation using green fluorescent protein. *Exp Cell Res* **285**, 208 (2003).
171. M. J. Robinson, S. A. Stippec, E. Goldsmith, M. A. White, M. H. Cobb, A constitutively active and nuclear form of the MAP kinase ERK2 is sufficient for neurite outgrowth and cell transformation. *Curr Biol* **8**, 1141 (Oct 22, 1998).

172. A. P. Sastre, S. Grossmann, H. P. Reusch, M. Schaefer, Requirement of an intermediate gene expression for biphasic ERK1/2 activation in thrombin-stimulated vascular smooth muscle cells. *J Biol Chem* **283**, 25871 (Sep 19, 2008).
173. H. Virtanen *et al.*, The first cysteine-rich domain of the receptor GFRalpha1 stabilizes the binding of GDNF. *Biochem J* **387**, 817 (May 1, 2005).
174. F. Karim, H. J. Hu, H. Adwanikar, D. Kaplan, R. W. t. Gereau, Impaired inflammatory pain and thermal hyperalgesia in mice expressing neuron-specific dominant negative mitogen activated protein kinase kinase (MEK). *Molecular pain* **2**, 2 (2006).
175. J. Rossi *et al.*, Alimentary tract innervation deficits and dysfunction in mice lacking GDNF family receptor alpha2. *The Journal of clinical investigation* **112**, 707 (Sep, 2003).
176. H. Yan, J. R. Keast, Neurturin regulates postnatal differentiation of parasympathetic pelvic ganglion neurons, initial axonal projections, and maintenance of terminal fields in male urogenital organs. *J Comp Neurol* **507**, 1169 (Mar 10, 2008).
177. Y. Wanigasekara, M. S. Airaksinen, R. O. Heuckeroth, J. Milbrandt, J. R. Keast, Neurturin signalling via GFRalpha2 is essential for innervation of glandular but not muscle targets of sacral parasympathetic ganglion neurons. *Mol Cell Neurosci* **25**, 288 (Feb, 2004).
178. M. Paveliev, M. S. Airaksinen, M. Saarma, GDNF family ligands activate multiple events during axonal growth in mature sensory neurons. *Mol Cell Neurosci* **25**, 453 (Mar, 2004).
179. R. T. Bartus *et al.*, Properly scaled and targeted AAV2-NRTN (neurturin) to the substantia nigra is safe, effective and causes no weight loss: support for nigral targeting in Parkinson's disease. *Neurobiol Dis* **44**, 38 (Oct, 2011).
180. S. Dziennis, N. J. Alkayed, Role of signal transducer and activator of transcription 3 in neuronal survival and regeneration. *Rev Neurosci* **19**, 341 (2008).
181. E. Devarajan, S. Huang, STAT3 as a central regulator of tumor metastases. *Curr Mol Med* **9**, 626 (Jun, 2009).
182. H. Yu, D. Pardoll, R. Jove, STATs in cancer inflammation and immunity: a leading role for STAT3. *Nature Reviews Cancer* **9**, 798 (2009).
183. N. C. Reich, L. Liu, Tracking STAT nuclear traffic. *Nature Reviews Immunology* **6**, 602 (2006).
184. N. Jain, T. Zhang, W. H. Kee, W. Li, X. Cao, Protein kinase C delta associates with and phosphorylates Stat3 in an interleukin-6-dependent manner. *J Biol Chem* **274**, 24392 (Aug 20, 1999).
185. K. Yokogami, S. Wakisaka, J. Avruch, S. A. Reeves, Serine phosphorylation and maximal activation of STAT3 during CNTF signaling is mediated by the rapamycin target mTOR. *Curr Biol* **10**, 47 (Jan 13, 2000).
186. C. P. Lim, X. Cao, Serine phosphorylation and negative regulation of Stat3 by JNK. *J Biol Chem* **274**, 31055 (Oct 22, 1999).
187. J. Chung, E. Uchida, T. C. Grammer, J. Blenis, STAT3 serine phosphorylation by ERK-dependent and -independent pathways negatively modulates its tyrosine phosphorylation. *Mol Cell Biol* **17**, 6508 (Nov, 1997).
188. J. Wegrzyn *et al.*, Function of mitochondrial Stat3 in cellular respiration. *Science* **323**, 793 (Feb 6, 2009).
189. D. J. Gough *et al.*, Mitochondrial STAT3 Supports Ras-Dependent Oncogenic Transformation. *Science* **324**, 1713 (2009).
190. L. Zhou, H. P. Too, Mitochondrial localized STAT3 is involved in NGF induced neurite outgrowth. *PLoS ONE* **6**, e21680 (2011).
191. N. Shulga, J. G. Pastorino, GRIM-19 Mediated Translocation of STAT3 to Mitochondria is Necessary for TNF Induced Necroptosis. *J Cell Sci*, (Mar 5, 2012).

192. J. J. Schuringa *et al.*, MEN2A-RET-induced cellular transformation by activation of STAT3. *Oncogene* **20**, 5350 (Aug 30, 2001).
193. I. Plaza-Menacho *et al.*, Ras/ERK1/2-mediated STAT3 Ser727 phosphorylation by familial medullary thyroid carcinoma-associated RET mutants induces full activation of STAT3 and is required for c-fos promoter activation, cell mitogenicity, and transformation. *J Biol Chem* **282**, 6415 (Mar 2, 2007).
194. J. H. Hwang *et al.*, Activation of signal transducer and activator of transcription 3 by oncogenic RET/PTC (rearranged in transformation/papillary thyroid carcinoma) tyrosine kinase: roles in specific gene regulation and cellular transformation. *Mol Endocrinol* **17**, 1155 (Jun, 2003).
195. I. Plaza Menacho *et al.*, RET-familial medullary thyroid carcinoma mutants Y791F and S891A activate a Src/JAK/STAT3 pathway, independent of glial cell line-derived neurotrophic factor. *Cancer Res* **65**, 1729 (Mar 1, 2005).
196. A. V. Kaucher, M. J. Oatley, J. M. Oatley, NEUROG3 Is a Critical Downstream Effector for STAT3-Regulated Differentiation of Mammalian Stem and Progenitor Spermatogonia. *Biology of reproduction*, (Feb 29, 2012).
197. S. Ramaswamy *et al.*, Intrastriatal CERE-120 (AAV-Neurturin) protects striatal and cortical neurons and delays motor deficits in a transgenic mouse model of Huntington's disease. *Neurobiol Dis* **34**, 40 (Apr, 2009).
198. Y. Y. Wu, R. A. Bradshaw, Activation of the Stat3 signaling pathway is required for differentiation by interleukin-6 in PC12-E2 cells. *J Biol Chem* **275**, 2147 (Jan 21, 2000).
199. J. A. Bauer *et al.*, A New Paradigm for MAPK: Structural Interactions of hERK1 with Mitochondria in HeLa Cells. *PLoS ONE* **4**, e7541 (2009).
200. C. Lufei *et al.*, GRIM-19, a death-regulatory gene product, suppresses Stat3 activity via functional interaction. *EMBO J* **22**, 1325 (Mar 17, 2003).
201. E. T. Wang *et al.*, Alternative isoform regulation in human tissue transcriptomes. *Nature* **456**, 470 (Nov 27, 2008).
202. V. Voikar, J. Rossi, H. Rauvala, M. S. Airaksinen, Impaired behavioural flexibility and memory in mice lacking GDNF family receptor alpha2. *The European journal of neuroscience* **20**, 308 (Jul, 2004).
203. D. Sjostrand, J. Carlsson, G. Paratcha, B. Persson, C. F. Ibanez, Disruption of the GDNF binding site in NCAM dissociates ligand binding and homophilic cell adhesion. *J Biol Chem* **282**, 12734 (Apr 27, 2007).
204. G. Wan, L. Zhou, Q. Lim, Y. H. Wong, H. P. Too, Cyclic AMP signalling through PKA but not Epac is essential for neurturin-induced biphasic ERK1/2 activation and neurite outgrowths through GFRalpha2 isoforms. *Cell Signal* **23**, 1727 (Nov, 2011).
205. G. Wan, H. P. Too, A specific isoform of glial cell line-derived neurotrophic factor family receptor alpha 1 regulates RhoA expression and glioma cell migration. *J Neurochem* **115**, 759 (Nov, 2010).
206. P. J. Hollenbeck, W. M. Saxton, The axonal transport of mitochondria. *J Cell Sci* **118**, 5411 (Dec 1, 2005).
207. G. Ruthel, P. J. Hollenbeck, Response of mitochondrial traffic to axon determination and differential branch growth. *J Neurosci* **23**, 8618 (Sep 17, 2003).
208. J. Verburg, P. J. Hollenbeck, Mitochondrial membrane potential in axons increases with local nerve growth factor or semaphorin signaling. *J Neurosci* **28**, 8306 (Aug 13, 2008).
209. Y. Zorina, R. Iyengar, K. D. Bromberg, Cannabinoid 1 Receptor and Interleukin-6 Receptor Together Induce Integration of Protein Kinase and Transcription Factor Signaling to Trigger Neurite Outgrowth. *Journal of Biological Chemistry* **285**, 1358 (2009).

210. C. S. Shi, Pyk2 Amplifies Epidermal Growth Factor and c-Src-induced Stat3 Activation. *Journal of Biological Chemistry* **279**, 17224 (2004).
211. K. M. Quesnelle, A. L. Boehm, J. R. Grandis, STAT-mediated EGFR signaling in cancer. *Journal of Cellular Biochemistry* **102**, 311 (2007).
212. Y. P. Ng, STAT3 as a Downstream Mediator of Trk Signaling and Functions. *Journal of Biological Chemistry* **281**, 15636 (2006).
213. D. Vaudry, P. J. Stork, P. Lazarovici, L. E. Eiden, Signaling pathways for PC12 cell differentiation: making the right connections. *Science* **296**, 1648 (May 31, 2002).
214. C. Miranda *et al.*, Role of STAT3 in In Vitro Transformation Triggered by TRK Oncogenes. *PLoS ONE* **5**, e9446 (2010).
215. S. Sasagawa, Y. Ozaki, K. Fujita, S. Kuroda, Prediction and validation of the distinct dynamics of transient and sustained ERK activation. *Nat Cell Biol* **7**, 365 (Apr, 2005).
216. A. von Kriegsheim *et al.*, Cell fate decisions are specified by the dynamic ERK interactome. *Nat Cell Biol* **11**, 1458 (Dec, 2009).
217. M. W. Miller, F. A. Pitts, Neurotrophin receptors in the somatosensory cortex of the mature rat: co-localization of p75, trk, isoforms and c-neu. *Brain Res* **852**, 355 (Jan 10, 2000).
218. J. Johansson, E. Formaggio, G. Fumagalli, C. Chiamulera, Choline up-regulates BDNF and down-regulates TrkB neurotrophin receptor in rat cortical cell culture. *NeuroReport* **20**, 828 (2009).
219. Y. Y. Wu, R. A. Bradshaw, Induction of neurite outgrowth by interleukin-6 is accompanied by activation of Stat3 signaling pathway in a variant PC12 cell (E2) line. *J Biol Chem* **271**, 13023 (May 31, 1996).
220. S. Galli *et al.*, A New Paradigm for MAPK: Structural Interactions of hERK1 with Mitochondria in HeLa Cells. *PLoS ONE* **4**, e7541 (2009).
221. A. Ludwig *et al.*, Neurturin evokes MAPK-dependent upregulation of Egr4 and KCC2 in developing neurons. *Neural plasticity* **2011**, 1 (2011).
222. P. C. Holm, P. Akerud, J. Wagner, E. Arenas, Neurturin is a neuritogenic but not a survival factor for developing and adult central noradrenergic neurons. *J Neurochem* **81**, 1318 (Jun, 2002).
223. J. P. Golden, J. Milbrandt, E. M. Johnson, Jr., Neurturin and persephin promote the survival of embryonic basal forebrain cholinergic neurons in vitro. *Exp Neurol* **184**, 447 (Nov, 2003).
224. P. H. Tso, C. J. Morris, L. Y. Yung, N. Y. Ip, Y. H. Wong, Multiple Gi proteins participate in nerve growth factor-induced activation of c-Jun N-terminal kinases in PC12 cells. *Neurochem Res* **34**, 1101 (Jun, 2009).
225. L. Y. Yung *et al.*, Nerve growth factor-induced stimulation of p38 mitogen-activated protein kinase in PC12 cells is partially mediated via Gi/o proteins. *Cellular Signalling* **20**, 1538 (2008).
226. R. Rizzuto, A. W. Simpson, M. Brini, T. Pozzan, Rapid changes of mitochondrial Ca2+ revealed by specifically targeted recombinant aequorin. *Nature* **358**, 325 (Jul 23, 1992).
227. K. Suzukawa *et al.*, Nerve growth factor-induced neuronal differentiation requires generation of Rac1-regulated reactive oxygen species. *J Biol Chem* **275**, 13175 (May 5, 2000).
228. S. Cassano *et al.*, Reactive oxygen species, Ki-Ras, and mitochondrial superoxide dismutase cooperate in nerve growth factor-induced differentiation of PC12 cells. *J Biol Chem* **285**, 24141 (Jul 30, 2010).
229. W.-F. Lin *et al.*, SH2B1β enhances fibroblast growth factor 1 (FGF1)-induced neurite outgrowth through MEK-ERK1/2-STAT3-Egr1 pathway. *Cellular Signalling* **21**, 1060 (2009).

230. R. Y. Liu, W. D. Snider, Different signaling pathways mediate regenerative versus developmental sensory axon growth. *J Neurosci* **21**, RC164 (Sep 1, 2001).
231. J. C. He, The G o/i-coupled Cannabinoid Receptor-mediated Neurite Outgrowth Involves Rap Regulation of Src and Stat3. *Journal of Biological Chemistry* **280**, 33426 (2005).
232. A. Fricker, C. Rios, L. Devi, I. Gomes, Serotonin receptor activation leads to neurite outgrowth and neuronal survival. *Molecular Brain Research* **138**, 228 (2005).
233. C. Poderoso *et al.*, A Mitochondrial Kinase Complex Is Essential to Mediate an ERK1/2-Dependent Phosphorylation of a Key Regulatory Protein in Steroid Biosynthesis. *PLoS ONE* **3**, e1443 (2008).
234. J. Lee, S. Sharma, J. Kim, R. J. Ferrante, H. Ryu, Mitochondrial nuclear receptors and transcription factors: Who's minding the cell? *Journal of Neuroscience Research* **86**, 961 (2008).
235. H. M. McBride, M. Neuspiel, S. Wasiak, Mitochondria: More Than Just a Powerhouse. *Current Biology* **16**, R551 (2006).
236. M. Salvi, A. M. Brunati, A. Toninello, Tyrosine phosphorylation in mitochondria: A new frontier in mitochondrial signaling☆. *Free Radical Biology and Medicine* **38**, 1267 (2005).
237. V. Munnamalai, D. M. Suter, Reactive oxygen species regulate F-actin dynamics in neuronal growth cones and neurite outgrowth. *Journal of Neurochemistry* **108**, 644 (2009).
238. J. Y. Min *et al.*, Staurosporin induces neurite outgrowth through ROS generation in HN33 hippocampal cell lines. *Journal of Neural Transmission* **113**, 1821 (2006).
239. E. Kotakenara, K. Saida, Characterization of CoCl2-induced reactive oxygen species (ROS): Inductions of neurite outgrowth and endothelin-2/vasoactive intestinal contractor in PC12 cells by CoCl2 are ROS dependent, but those by MnCl2 are not. *Neuroscience Letters* **422**, 223 (2007).
240. R. Gopalakrishna, U. Gundimeda, J. E. Schiffman, T. H. McNeill, A direct redox regulation of protein kinase C isoenzymes mediates oxidant-induced neuritogenesis in PC12 cells. *J Biol Chem* **283**, 14430 (May 23, 2008).
241. H. Wu *et al.*, Docosahexaenoic acid induces ERK1/2 activation and neuritogenesis via intracellular reactive oxygen species production in human neuroblastoma SH-SY5Y cells. *Biochimica et Biophysica Acta (BBA) - Molecular and Cell Biology of Lipids* **1791**, 8 (2009).
242. M. Kuroki, J. T. O'Flaherty, Extracellular signal-regulated protein kinase (ERK)-dependent and ERK-independent pathways target STAT3 on serine-727 in human neutrophils stimulated by chemotactic factors and cytokines. *Biochem J* **341 (Pt 3)**, 691 (Aug 1, 1999).
243. T. Decker, P. Kovarik, Serine phosphorylation of STATs. *Oncogene* **19**, 2628 (May 15, 2000).
244. C. Brodie *et al.*, Protein kinase C-epsilon plays a role in neurite outgrowth in response to epidermal growth factor and nerve growth factor in PC12 cells. *Cell Growth Differ* **10**, 183 (Mar, 1999).
245. Z. Qiu, A. Ghosh, A brief history of neuronal gene expression: regulatory mechanisms and cellular consequences. *Neuron* **60**, 449 (Nov 6, 2008).
246. T. F. Dijkmans *et al.*, Temporal and functional dynamics of the transcriptome during nerve growth factor-induced differentiation. *J Neurochem* **105**, 2388 (Apr 9, 2008).
247. C. Perez-Iratxeta *et al.*, Study of stem cell function using microarray experiments. *FEBS Lett* **579**, 1795 (Mar 21, 2005).
248. D. R. Rhodes, A. M. Chinnaiyan, Integrative analysis of the cancer transcriptome. *Nat Genet* **37 Suppl**, S31 (Jun, 2005).

249. T. M. Preuss, M. Caceres, M. C. Oldham, D. H. Geschwind, Human brain evolution: insights from microarrays. *Nature reviews* **5**, 850 (Nov, 2004).
250. M. S. Rajeevan, D. G. Ranamukhaarachchi, S. D. Vernon, E. R. Unger, Use of real-time quantitative PCR to validate the results of cDNA array and differential display PCR technologies. *Methods* **25**, 443 (Dec, 2001).
251. R. F. Chuaqui *et al.*, Post-analysis follow-up and validation of microarray experiments. *Nat Genet* **32 Suppl**, 509 (Dec, 2002).
252. J. H. Do, D. K. Choi, Normalization of microarray data: single-labeled and dual-labeled arrays. *Mol Cells* **22**, 254 (Dec 31, 2006).
253. J. Huggett, K. Dheda, S. Bustin, A. Zumla, Real-time RT-PCR normalisation; strategies and considerations. *Genes and immunity* **6**, 279 (Jun, 2005).
254. O. Thellin *et al.*, Housekeeping genes as internal standards: use and limits. *Journal of biotechnology* **75**, 291 (Oct 8, 1999).
255. J. Antonov *et al.*, Reliable gene expression measurements from degraded RNA by quantitative real-time PCR depend on short amplicons and a proper normalization. *Laboratory investigation; a journal of technical methods and pathology* **85**, 1040 (Aug, 2005).
256. S. Fleige, M. W. Pfaffl, RNA integrity and the effect on the real-time qRT-PCR performance. *Molecular aspects of medicine* **27**, 126 (Apr-Jun, 2006).
257. S. Fleige *et al.*, Comparison of relative mRNA quantification models and the impact of RNA integrity in quantitative real-time RT-PCR. *Biotechnology letters* **28**, 1601 (Oct, 2006).
258. J. Vandesompele *et al.*, Accurate normalization of real-time quantitative RT-PCR data by geometric averaging of multiple internal control genes. *Genome Biol* **3**, RESEARCH0034 (Jun 18, 2002).
259. S. Waxman, E. Wurmbach, De-regulation of common housekeeping genes in hepatocellular carcinoma. *BMC Genomics* **8**, 243 (2007).
260. M. Jung *et al.*, In search of suitable reference genes for gene expression studies of human renal cell carcinoma by real-time PCR. *BMC molecular biology* **8**, 47 (2007).
261. H. Rhinn *et al.*, Housekeeping while brain's storming Validation of normalizing factors for gene expression studies in a murine model of traumatic brain injury. *BMC molecular biology* **9**, 62 (2008).
262. G. Spinsanti *et al.*, Selection of reference genes for quantitative RT-PCR studies in striped dolphin (Stenella coeruleoalba) skin biopsies. *BMC molecular biology* **7**, 32 (2006).
263. M. W. Pfaffl, A. Tichopad, C. Prgomet, T. P. Neuvians, Determination of stable housekeeping genes, differentially regulated target genes and sample integrity: BestKeeper--Excel-based tool using pair-wise correlations. *Biotechnology letters* **26**, 509 (Mar, 2004).
264. C. L. Andersen, J. L. Jensen, T. F. Orntoft, Normalization of real-time quantitative reverse transcription-PCR data: a model-based variance estimation approach to identify genes suited for normalization, applied to bladder and colon cancer data sets. *Cancer Res* **64**, 5245 (Aug 1, 2004).
265. S. Akilesh, D. J. Shaffer, D. Roopenian, Customized molecular phenotyping by quantitative gene expression and pattern recognition analysis. *Genome Res* **13**, 1719 (Jul, 2003).
266. F. Haller *et al.*, Equivalence test in quantitative reverse transcription polymerase chain reaction: confirmation of reference genes suitable for normalization. *Analytical biochemistry* **335**, 1 (Dec 1, 2004).
267. V. Popovici *et al.*, Selecting control genes for RT-QPCR using public microarray data. *BMC bioinformatics* **10**, 42 (2009).

268. S. Lee, M. Jo, J. Lee, S. S. Koh, S. Kim, Identification of novel universal housekeeping genes by statistical analysis of microarray data. *Journal of biochemistry and molecular biology* **40**, 226 (Mar 31, 2007).
269. H. J. de Jonge *et al.*, Evidence based selection of housekeeping genes. *PLoS ONE* **2**, e898 (2007).
270. M. J. Kwon *et al.*, Identification of novel reference genes using multiplatform expression data and their validation for quantitative gene expression analysis. *PLoS ONE* **4**, e6162 (2009).
271. A. Ravni *et al.*, The neurotrophic effects of PACAP in PC12 cells: control by multiple transduction pathways. *Journal of neurochemistry* **98**, 321 (Jul, 2006).
272. A. Levi, S. Biocca, A. Cattaneo, P. Calissano, The mode of action of nerve growth factor in PC12 cells. *Mol Neurobiol* **2**, 201 (Fall, 1988).
273. K. Fujita, P. Lazarovici, G. Guroff, Regulation of the differentiation of PC12 pheochromocytoma cells. *Environmental health perspectives* **80**, 127 (Mar, 1989).
274. M. Sysi-Aho, M. Katajamaa, L. Yetukuri, M. Oresic, Normalization method for metabolomics data using optimal selection of multiple internal standards. *BMC bioinformatics* **8**, 93 (2007).
275. W. Wu *et al.*, Comparison of normalization methods for CodeLink Bioarray data. *BMC bioinformatics* **6**, 309 (2005).
276. A. Ravni *et al.*, A cAMP-dependent, protein kinase A-independent signaling pathway mediating neuritogenesis through Egr1 in PC12 cells. *Molecular pharmacology* **73**, 1688 (Jun, 2008).
277. E. Pacary, E. Petit, M. Bernaudin, Concomitant inhibition of prolyl hydroxylases and ROCK initiates differentiation of mesenchymal stem cells and PC12 towards the neuronal lineage. *Biochem Biophys Res Commun* **377**, 400 (Dec 12, 2008).
278. P. K. Politis, D. Thomaidou, R. Matsas, Coordination of cell cycle exit and differentiation of neuronal progenitors. *Cell Cycle* **7**, 691 (Mar 15, 2008).
279. J. Burkhalter, H. Fiumelli, I. Allaman, J. Y. Chatton, J. L. Martin, Brain-derived neurotrophic factor stimulates energy metabolism in developing cortical neurons. *J Neurosci* **23**, 8212 (Sep 10, 2003).
280. S. R. Salton, Neurotrophins, growth-factor-regulated genes and the control of energy balance. *The Mount Sinai journal of medicine, New York* **70**, 93 (Mar, 2003).
281. J. S. da Silva, C. G. Dotti, Breaking the neuronal sphere: regulation of the actin cytoskeleton in neuritogenesis. *Nat Rev Neurosci* **3**, 694 (Sep, 2002).
282. C. W. Pak, K. C. Flynn, J. R. Bamburg, Actin-binding proteins take the reins in growth cones. *Nat Rev Neurosci* **9**, 136 (Feb, 2008).
283. T. Suzuki, P. J. Higgins, D. R. Crawford, Control selection for RNA quantitation. *Biotechniques* **29**, 332 (Aug, 2000).
284. N. Silver, S. Best, J. Jiang, S. L. Thein, Selection of housekeeping genes for gene expression studies in human reticulocytes using real-time PCR. *BMC molecular biology* **7**, 33 (2006).
285. L. Thorrez *et al.*, Using ribosomal protein genes as reference: a tale of caution. *PLoS ONE* **3**, e1854 (2008).
286. D. L. Lafontaine, D. Tollervey, The function and synthesis of ribosomes. *Nat Rev Mol Cell Biol* **2**, 514 (Jul, 2001).
287. N. Kenmochi *et al.*, A map of 75 human ribosomal protein genes. *Genome Res* **8**, 509 (May, 1998).
288. S. Robledo *et al.*, The role of human ribosomal proteins in the maturation of rRNA and ribosome production. *Rna* **14**, 1918 (Sep, 2008).

289. D. Faliks, O. Meyuhas, Coordinate regulation of ribosomal protein mRNA level in regenerating rat liver. Study with the corresponding mouse cloned cDNAs. *Nucleic Acids Res* **10**, 789 (Feb 11, 1982).
290. C. B. Kirn-Safran, S. Dayal, P. A. Martin-DeLeon, D. D. Carson, Cloning, expression, and chromosome mapping of the murine Hip/Rpl29 gene. *Genomics* **68**, 210 (Sep 1, 2000).
291. M. Wanzel *et al.*, A ribosomal protein L23-nucleophosmin circuit coordinates Miz1 function with cell growth. *Nat Cell Biol* **10**, 1051 (Aug 1, 2008).
292. H. He, Y. Sun, Ribosomal protein S27L is a direct p53 target that regulates apoptosis. *Oncogene* **26**, 2707 (Apr 26, 2007).
293. Y. J. Jeon *et al.*, Ribosomal protein S6 is a selective mediator of TRAIL-apoptotic signaling. *Oncogene* **27**, 4344 (Jul 17, 2008).
294. N. H. Lee *et al.*, Comparative expressed-sequence-tag analysis of differential gene expression profiles in PC-12 cells before and after nerve growth factor treatment. *Proc Natl Acad Sci U S A* **92**, 8303 (Aug 29, 1995).
295. J. M. Angelastro *et al.*, Identification of diverse nerve growth factor-regulated genes by serial analysis of gene expression (SAGE) profiling. *Proc Natl Acad Sci U S A* **97**, 10424 (Sep 12, 2000).
296. M. Coolen, L. Bally-Cuif, MicroRNAs in brain development and physiology. *Curr Opin Neurobiol* **19**, 461 (Oct, 2009).
297. J. Krutzfeldt *et al.*, Silencing of microRNAs in vivo with 'antagomirs'. *Nature* **438**, 685 (Dec 1, 2005).
298. L. F. Yoong, G. Wan, H. P. Too, Glial cell-line derived neurotrophic factor and neurturin regulate the expressions of distinct miRNA precursors through the activation of GFRalpha2. *J Neurochem* **98**, 1149 (Aug, 2006).
299. H. Guo, N. T. Ingolia, J. S. Weissman, D. P. Bartel, Mammalian microRNAs predominantly act to decrease target mRNA levels. *Nature* **466**, 835 (Aug 12, 2010).
300. A. Muniategui, J. Pey, F. Planes, A. Rubio, Joint analysis of miRNA and mRNA expression data. *Briefings in bioinformatics*, (Jun 12, 2012).
301. G. Wan, Q. E. Lim, H. P. Too, High-performance quantification of mature microRNAs by real-time RT-PCR using deoxyuridine-incorporated oligonucleotides and hemi-nested primers. *Rna* **16**, 1436 (Jul, 2010).
302. C. Chen *et al.*, Real-time quantification of microRNAs by stem-loop RT-PCR. *Nucleic Acids Res* **33**, e179 (2005).
303. M. Zhu *et al.*, Creation of nanostructures by interference lithography for modulation of cell behavior. *Nanoscale* **3**, 2723 (Jul, 2011).
304. A. Ferrari, P. Faraci, M. Cecchini, F. Beltram, The effect of alternative neuronal differentiation pathways on PC12 cell adhesion and neurite alignment to nanogratings. *Biomaterials* **31**, 2565 (Mar, 2010).
305. L. J. Millet, M. B. Collens, G. L. Perry, R. Bashir, Pattern analysis and spatial distribution of neurons in culture. *Integrative biology : quantitative biosciences from nano to macro* **3**, 1167 (Dec, 2011).
306. M. Denham, M. Dottori, Signals Involved in Neural Differentiation of Human Embryonic Stem Cells. *Neurosignals* **17**, 234 (2009).
307. F. B. Gao, Context-dependent functions of specific microRNAs in neuronal development. *Neural Dev* **5**, 25 (2010).
308. Y. Shi *et al.*, MicroRNA regulation of neural stem cells and neurogenesis. *J Neurosci* **30**, 14931 (Nov 10, 2010).
309. N. J. Martinez, R. I. Gregory, MicroRNA gene regulatory pathways in the establishment and maintenance of ESC identity. *Cell Stem Cell* **7**, 31 (Jul 2, 2010).

310. G. Mudduluru *et al.*, Regulation of Axl receptor tyrosine kinase expression by miR-34a and miR-199a/b in solid cancer. *Oncogene*, (2011).
311. C. Oneyama *et al.*, MicroRNA-mediated downregulation of mTOR/FGFR3 controls tumor growth induced by Src-related oncogenic pathways. *Oncogene*, (2011).
312. T. Barberi *et al.*, Neural subtype specification of fertilization and nuclear transfer embryonic stem cells and application in parkinsonian mice. *Nature Biotechnology* **21**, 1200 (2003).
313. R. L. Judson, J. E. Babiarz, M. Venere, R. Blelloch, Embryonic stem cell–specific microRNAs promote induced pluripotency. *Nature Biotechnology* **27**, 459 (2009).
314. Z. Li, C. S. Yang, K. Nakashima, T. M. Rana, Small RNA-mediated regulation of iPS cell generation. *EMBO J* **30**, 823 (Mar 2, 2011).
315. C. M. Schwartz *et al.*, NTera2: a model system to study dopaminergic differentiation of human embryonic stem cells. *Stem Cells Dev* **14**, 517 (Oct, 2005).
316. I. Damjanov, R. K. Clark, P. W. Andrews, Cytoskeleton of human embryonal carcinoma cells. *Cell differentiation* **15**, 133 (Dec, 1984).
317. D. E. Coyle, J. Li, M. Baccei, Regional differentiation of retinoic acid-induced human pluripotent embryonic carcinoma stem cell neurons. *PLoS ONE* **6**, e16174 (2011).
318. S. A. Przyborski, I. E. Morton, A. Wood, P. W. Andrews, Developmental regulation of neurogenesis in the pluripotent human embryonal carcinoma cell line NTERA-2. *The European journal of neuroscience* **12**, 3521 (Oct, 2000).
319. S. J. Pleasure, V. M. Lee, NTera 2 cells: a human cell line which displays characteristics expected of a human committed neuronal progenitor cell. *J Neurosci Res* **35**, 585 (Aug 15, 1993).
320. Z. X. Yao *et al.*, 22R-Hydroxycholesterol induces differentiation of human NT2 precursor (Ntera2/D1 teratocarcinoma) cells. *Neuroscience* **148**, 441 (Aug 24, 2007).
321. G. Baldassarre *et al.*, Glial cell line-derived neurotrophic factor induces proliferative inhibition of NT2/D1 cells through RET-mediated up-regulation of the cyclin-dependent kinase inhibitor p27(kip1). *Oncogene* **21**, 1739 (Mar 7, 2002).
322. L. Zhou, Q. E. Lim, G. Wan, H. P. Too, Normalization with genes encoding ribosomal proteins but not GAPDH provides an accurate quantification of gene expressions in neuronal differentiation of PC12 cells. *BMC Genomics* **11**, 75 (2010).
323. G. Wan *et al.*, Identification and validation of reference genes for expression studies in a rat model of neuropathic pain. *Biochem Biophys Res Commun* **400**, 575 (Oct 1, 2010).
324. K. Zhou *et al.*, Novel reference genes for quantifying transcriptional responses of Escherichia coli to protein overexpression by quantitative PCR. *BMC molecular biology* **12**, 18 (2011).
325. Q. E. Lim, L. Zhou, Y. K. Ho, G. Wan, H. P. Too, snoU6 and 5S RNAs are not reliable miRNA reference genes in neuronal differentiation. *Neuroscience* **199**, 32 (Dec 29, 2011).
326. B. Smith *et al.*, Large-scale expression analysis reveals distinct microRNA profiles at different stages of human neurodevelopment. *PLoS ONE* **5**, e11109 (2010).
327. C. M. Schwartz, Derivation, Enrichment and Characterization of Dopaminergic Neurons from Pluripotent Stem Cells. *PhD Thesis*, (2010).
328. P. Grzegorz, Differentiation of human teratocarcinoma cell line into motor neurons: investigation of cellular phenotype in vitro and in transplantation studies. *PhD Thesis*, (2009).
329. I. E. Misiuta, Characterization of the Dopaminergic Potential of the Human NTera2/D1 (NT2) Cell Line In Vitro. *PhD Thesis*, (2005).
330. A. Wallen *et al.*, Fate of mesencephalic AHD2-expressing dopamine progenitor cells in NURR1 mutant mice. *Exp Cell Res* **253**, 737 (Dec 15, 1999).

331. A. A. Wallen *et al.*, Orphan nuclear receptor Nurr1 is essential for Ret expression in midbrain dopamine neurons and in the brain stem. *Mol Cell Neurosci* **18**, 649 (Dec, 2001).